Double-Edged Sword of Viscoelasticity in Self-Healing Conductive Composites

DISSERTATION

zur Erlangung des akademischen Grades eines Doktors der Naturwissenschaften

(Dr. rer. nat.)

in der Bayreuther Graduiertenschule für Mathematik und Naturwissenschaften

(BayNAT)

der Universität Bayreuth

vorgelegt von

Pavel Milkin

Aus Krasny Jar, Astrachaner Gebiet, Russland

Bayreuth, 2024

The preparation of this doctoral thesis started in November 2020 and was finished in August 2024 under the supervision of Prof. Leonid Ionov. It was made in the Biofabrication group at the University of Bayreuth.

This is a full reprint of the thesis submitted to obtain the academic degree of Doctor of Natural Sciences (Dr. rer. nat.) and approved by the Bayreuth Graduate School of Mathematical and Natural Sciences (BayNAT) of the University of Bayreuth.

Form of the dissertation: Cumulative dissertation

Date of submission: 03.09.2024

Admission by executive board: 11.09.2024

Date of defence: 16.05.2025

Acting director: Prof. Dr. Jürgen Köhler

Doctoral committee:

Prof. Dr. Leonid Ionov (reviewer)

Prof. Dr. Anayancy Osorio-Madrazo (reviewer)

Prof. Dr. Johannes Brendel (chair)

Prof. Dr. Markus Retsch

(additional reviewers: Prof. Dr. Manfred Wilhelm and Prof. Dr. André Gröschel)

Table of Contents

Summary

The e-waste problem is a significant global issue, characterized by the rapid accumulation of discarded electronic devices, which contain hazardous substances that pose severe environmental and health risks if not properly managed[1]. The improper disposal of e-waste can lead to contamination of soil and water, causing long-term ecological damage and health issues. Self-healing materials offer a promising solution to mitigate the e-waste crisis. These materials can autonomously repair damage, thereby extending the lifespan of electronic devices and reducing the need for frequent replacements. By incorporating self-healing properties into electronics, the durability and reliability of devices can be enhanced and lead to a substantial reduction in e-waste generation. Additionally, self-healing materials can integrate other beneficial properties such as biodegradability and biocompatibility, further contributing to environmentally friendly electronic products. A typical approach to creating self-healing electronics involves the combination of a self-healing polymer matrix and functional fillers to form a composite material. However, there is still a lack of comprehensive data on the interactions between self-healing polymers and functional fillers, which is crucial for optimizing the performance and self-healing efficiency of these composites.

The aim of this work is to investigate thoroughly the electromechanical dynamics trends and applicability limits of conductive self-healing composites based on self-healing viscoelastic liquid and carbon fillers for soft wearable electronics. It is envisioned that the healing of these composites is not autonomous[2], as can be found in literature, and it is still necessary to understand the healing conditions and the best performance. The novelty of this work is the qualitative and quantitative evaluation of self-healing polymer – carbon filler interaction and approaching their performance and self-healing limits.

The work includes a thorough investigation of PDMS-carbon based self-healing conductive composites dynamics through mechanical spectroscopy and electromechanical characterization and projecting obtained knowledge on the real device. The influence of varying polymer relaxation time and filler aspect ratio on self-healing properties has been discussed and explored through mechanical spectroscopy, electrical impedance spectroscopy, and different rheology techniques. The wearable strain sensor was fabricated based on investigated self-healing composites and demonstrated the applicability of the material as well as its practical limitations.

Overall, in this work, it was shown, that in order to obtain the high self-healing ability of the material, the polymer flowability and particle mobility (weak particle network) should not be compromised,

though it could lead to low conductivity. To obtain high conductivity, a strong filler network must be created, but then the mobility of the polymer chains and particles, and as a consequence the healing, will be limited. Thus, it is a double-edged sword working with self-healing viscoelastic blends: either we sacrifice mechanical and healing properties or electrical. The fabricated wearable strain sensor confirmed the aforementioned conclusions.

Zusammenfassung

Das Problem des Elektroschrotts ist ein bedeutendes globales Problem, welches durch die rasche Anhäufung ausrangierter elektronischer Geräte verursacht wird. Diese Geräte enthalten gefährliche Stoffe, die bei unsachgemäßer Entsorgung schwere Umwelt- und Gesundheitsrisiken darstellen. Die unsachgemäße Entsorgung von Elektroschrott kann zu einer Verunreinigung von Boden und Wasser führen und langfristige ökologische Schäden und Gesundheitsprobleme verursachen. Selbstheilende Materialien bieten eine vielversprechende Lösung zur Entschärfung der E-Müll-Krise. Diese Materialien können Schäden selbstständig reparieren, wodurch sich die Lebensdauer elektronischer Geräte verlängert, und die Notwendigkeit eines häufigen Austauschs reduziert. Durch die Einbindung selbstheilender Eigenschaften in die Elektronik können die Haltbarkeit und Zuverlässigkeit von Geräten erhöht und die Erzeugung von Elektroschrott erheblich reduziert werden. Darüber hinaus können selbstheilende Materialien auch andere vorteilhafte Eigenschaften wie biologische Abbaubarkeit und Biokompatibilität aufweisen, was einen weiteren Beitrag zu umweltfreundlichen Elektronikprodukten leistet. Ein typischer Ansatz zur Herstellung selbstheilender Elektronik besteht in der Kombination einer selbstheilenden Polymermatrix mit funktionellen Füllstoffen zu einem Verbundmaterial. Es mangelt jedoch noch an umfassenden Daten über die Wechselwirkungen zwischen selbstheilenden Polymeren und funktionellen Füllstoffen, die für die Optimierung der Leistung und der Selbstheilungseffizienz dieser Verbundwerkstoffe von entscheidender Bedeutung sind.

Das Ziel dieser Arbeit ist es, die elektromechanischen Dynamiktrends und die Grenzen der Anwendbarkeit von leitfähigen selbstheilenden Verbundwerkstoffen auf der Grundlage einer selbstheilenden viskoelastischen Flüssigkeit und eines Kohlenstofffüllstoffs für weiche tragbare Elektronik gründlich zu untersuchen. Es wird davon ausgegangen, dass die Heilung dieser Verbundwerkstoffe nicht autonom erfolgt, wie in der Literatur zu lesen ist, und es ist immer noch notwendig, die Heilungsbedingungen und die beste Leistung zu verstehen. Die Neuheit dieser Arbeit besteht in der qualitativen und quantitativen Bewertung der Wechselwirkung zwischen selbstheilendem Polymer und Kohlenstofffüllstoff und in der Annäherung an ihre Leistung und Selbstheilungsgrenzen.

Die Arbeit umfasst eine gründliche Untersuchung der Dynamik von selbstheilenden leitfähigen Verbundwerkstoffen auf PDMS-Kohlenstoffbasis durch mechanische Spektroskopie und elektromechanische Charakterisierung sowie die Projektion der gewonnenen Erkenntnisse auf das

reale Gerät. Der Einfluss der unterschiedlichen Polymerrelaxationszeit und des Füllstoff-Seitenverhältnisses auf die Selbstheilungseigenschaften wurde diskutiert und durch mechanische Spektroskopie, elektrische Impedanzspektroskopie und verschiedene rheologische Techniken untersucht. Der tragbare Dehnungssensor wurde auf der Grundlage der untersuchten selbstheilenden Verbundwerkstoffe hergestellt und demonstrierte die Anwendbarkeit des Materials sowie seine praktischen Grenzen.

Insgesamt konnte in dieser Arbeit gezeigt werden, dass für eine hohe Selbstheilungsfähigkeit des Materials die Fließfähigkeit des Polymers und die Partikelmobilität (schwaches Partikelnetzwerk) nicht beeinträchtigt werden sollten, die Leitfähigkeit jedoch gering sein wird. Um eine hohe Leitfähigkeit zu erreichen, muss ein starkes Füllstoffnetzwerk geschaffen werden, was jedoch die Mobilität der Polymerketten und Partikel und folglich die Heilung eingeschränkt. Die Arbeit mit selbstheilenden viskoelastischen Mischungen ist also ein zweischneidiges Schwert: Entweder wir opfern die mechanischen und heilenden Eigenschaften oder die elektrischen. Der hergestellte tragbare Dehnungssensor bestätigt die oben genannten Schlussfolgerungen.

1. Introduction

Electrical and Electronic Equipment (EEE) is increasingly in demand in today's society, driven by higher industrialization and population growth. However, such electronics have a short life span due to failure caused by mechanical or electrical stress. Repairing of such electronics is difficult and/or expensive. In the end, we have E-waste generation, which grows annually. In fact, by the end of 2022, there were at least 347 million tons of unrecycled E-waste[3]. It results in non-degradable polymers and toxic metals contamination, loss of valuable materials (copper, silver, gold, palladium), and climate change due to the production of new electronics.

And that is where the topic of self-healing comes to the stage. To find a solution to the problem, scientists often turn to different sources of inspiration. For instance, biological systems have the powerful ability to self-heal; wound healing of animals[4] or succulent plant self-sealing[5]. Or filmmakers represent their dreams of self-regeneration mechanisms in their works. Getting inspired, scientists came up with the idea of using self-healing polymers and their composites to create self-maintaining electronic devices.

1.1. Self-healing electronics

All electronic devices contain three main components: insulator, conductor, and semiconductor[6] (Figure 1). All these three components should be self-healable in order to fabricate a self-repairing device. The functionality is provided by a filler (on top or inside of a polymer matrix) or by lack of it (in the case of an insulator). The dynamic crosslinking of polymer is responsible for material self-healing. In the ideal case, the unexpected damage should be healed autonomously no matter the size of the damage, recovering the electrical functionality with time. The perfect polymer for this should combine properties of elastomer since material can be subjected to significant wear and tear over time, and large toughness to have tolerance to damages or small cracks.

Each of these components has its own challenges. For insulators usually bare self-healing polymer is used for gate dielectrics[7] or circuit board substrates. The polymer contains plenty of hydrophilic bonds (hydrogen bonds, or ligand-metal interaction). As a result, the polymer tends to adsorb moisture, leading to modulus drop[8] and instability under high electric fields. Conductors contain a lot of conductive fillers, providing an electric current path. They are typically used as wires[9] or electrodes, for instance, in Triboelectric Nanogenerators (TENGs)[10]. After mechanical damage, the healing matrix recovers to its initial state, but the filler network, due to lack of autonomous mobility, does not change both electrical and mechanical characteristics. Semiconductors, typically applied in organic

field-effect transistors (OFET) devices, usually are used as a thin layer (<100 nm). Therefore, it is extremely challenging to align damaged areas, which results in deterioration of charge transport. Using semiconductive polymers is difficult as well since most of them are semicrystalline with high glass transition temperature and their property recovery requires additional solvent or thermal annealing[11]. Though, recently there have been attempts to fabricate autonomous self-healing transistors with healing all three mentioned components of a device by combining semiconductive polymer in an insulating supramolecular self-healing matrix with conductive vapor deposited metal cluster[12]. Thus, the moisture-insensitive molecular design of the polymer and filler network is an important focal point for self-healing electronics research. Additionally, the mobility of polymer chains, polymer segments, and particles in the damaged area is crucial to investigate.

By fabrication devices, other challenges begin to emerge. The fabrication of self-healing materials is incompatible with existing electronic technologies. Small feature sizes are still difficult to produce. Therefore, there is a need for photo patternable self-healing materials. The characteristics of self-healing conductors and semiconductors are still non-comparable with traditional electronics. The healing process is still relatively slow and mostly non-autonomous. Mechanics of autonomous self-healing in composite materials are understudied containing scare rheological data. Moreover, if the size of the damaged area is larger than the thickness of the healing layer, efficient healing is very challenging.

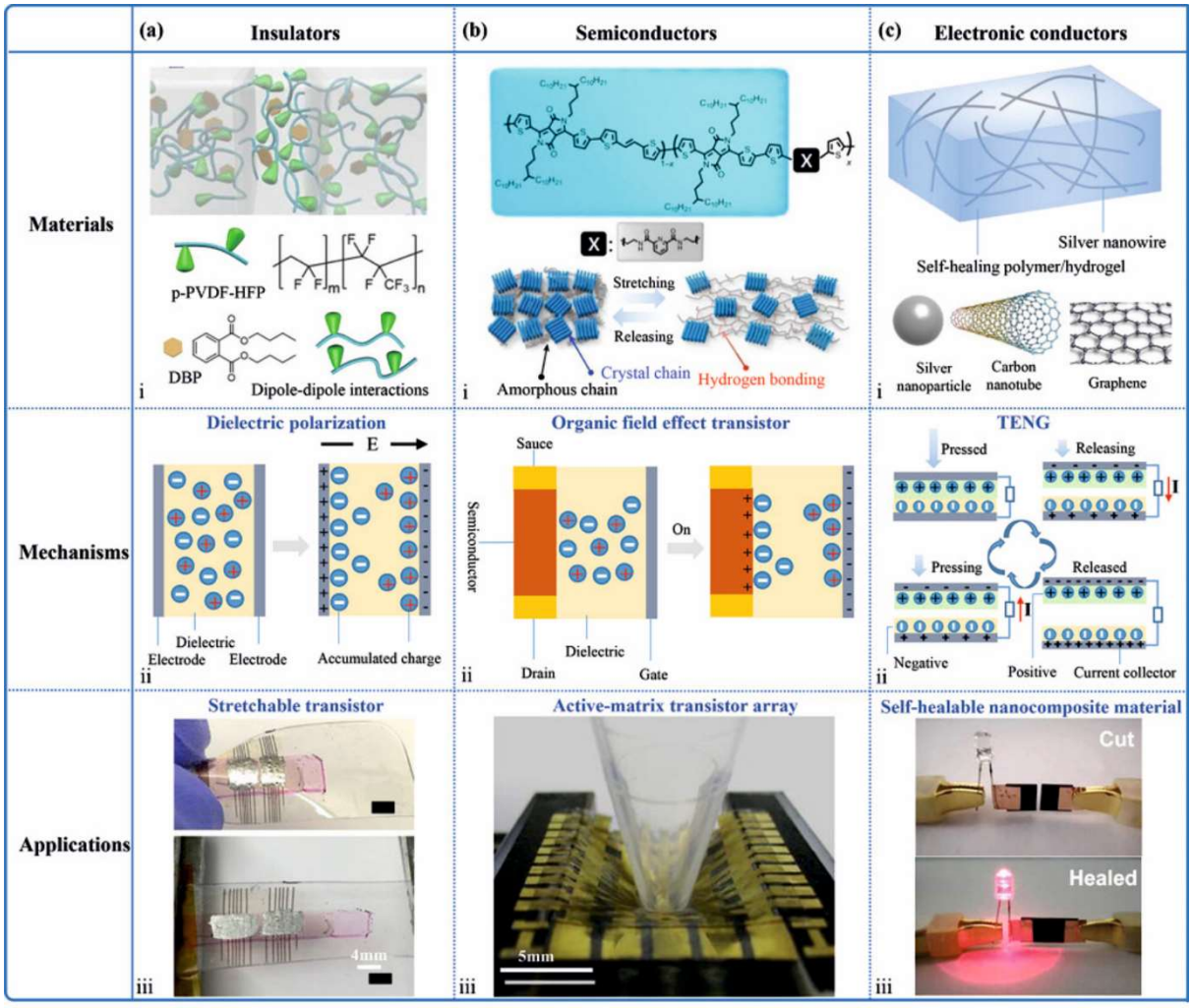

Figure 1. Materials, working mechanisms, and applications of self-healing materials in soft electronics. a) Insulators composed of polymers are used as dielectric layers in OFETs, and their dielectric polarization mechanisms are described. b) Semiconductors composed of conjugated polymers are used to construct OFETs, and the working mechanism of OFET is introduced. c) Electronic conductors are usually composed of conductive nanoparticle-polymer composite systems, and their working mechanism for TENG application is sketched[6]. Copyrights 2023, Wiley-VCH GmbH.

1.2. Self-healing chemistry

1.2.1. Self-healing bonds

Self- healing is possible due to the healing abilities of polymer matrix. The polymer should meet two main requirements: 1) low glass transition temperature to maintain chain and segmental mobility; 2) Dynamic interactions – the interaction with activation energy lower than conventional covalent bonds

(E_a<100 kJ/mol), which can be broken and easily restored either autonomous or with some external stimuli (Figure 2 a-b)[13]. The dynamic interactions can be divided into two main groups: noncovalent and covalent bonds (Figure 2c). Noncovalent bonding includes ionic, hydrogen, Van der Waals, π-π, and metal-ligand interactions. Among dynamic covalent bonding, one can highlight C-C (Diels-Alder reaction), C-N (urea/imine exchange, aminal and amide formation), C-O (ester and acetal formation), C-S (thioacetal and thiazolidine exchange), B-O (boronic ester exchange), S-S (disulfide exchange) bonds[14].

The activation energy defines the dissociation time, in other words lifetime of dynamic bonds. In the case if $E_a < RT \ln N_x$, where N_x is the average number of polymer segments between dynamic bonds (stickers), the bonds dissociate much faster than the chain with N_x segments relaxes (the polymer follows Rouse dynamics), and it cares no interest. When $RT \ln N_x < E_a < 2RT\ln N_x$, or the difference between E_{diss}-E_{accoc} ~ several RT, the dissociation of bonds is longer than chain relaxation time but shorter than diffusion time to find another sticker. This regime is called dissociative exchange. It is an example of almost all hydrogen bonds, Diels-Alder reaction, and urethane/urea dissociation. At the associative exchange, when $E_a > 2RT\ln N_x$, the exchange is completely controlled by dissociation time. The exchange takes place only in contact of nonbonded species with one of the associating groups or in contact between two pairs of dynamic bonds. Such mechanism is also called hopping. The mechanism is typical for transamination, imine exchange, transesterification, boronic ester exchange, etc[13].

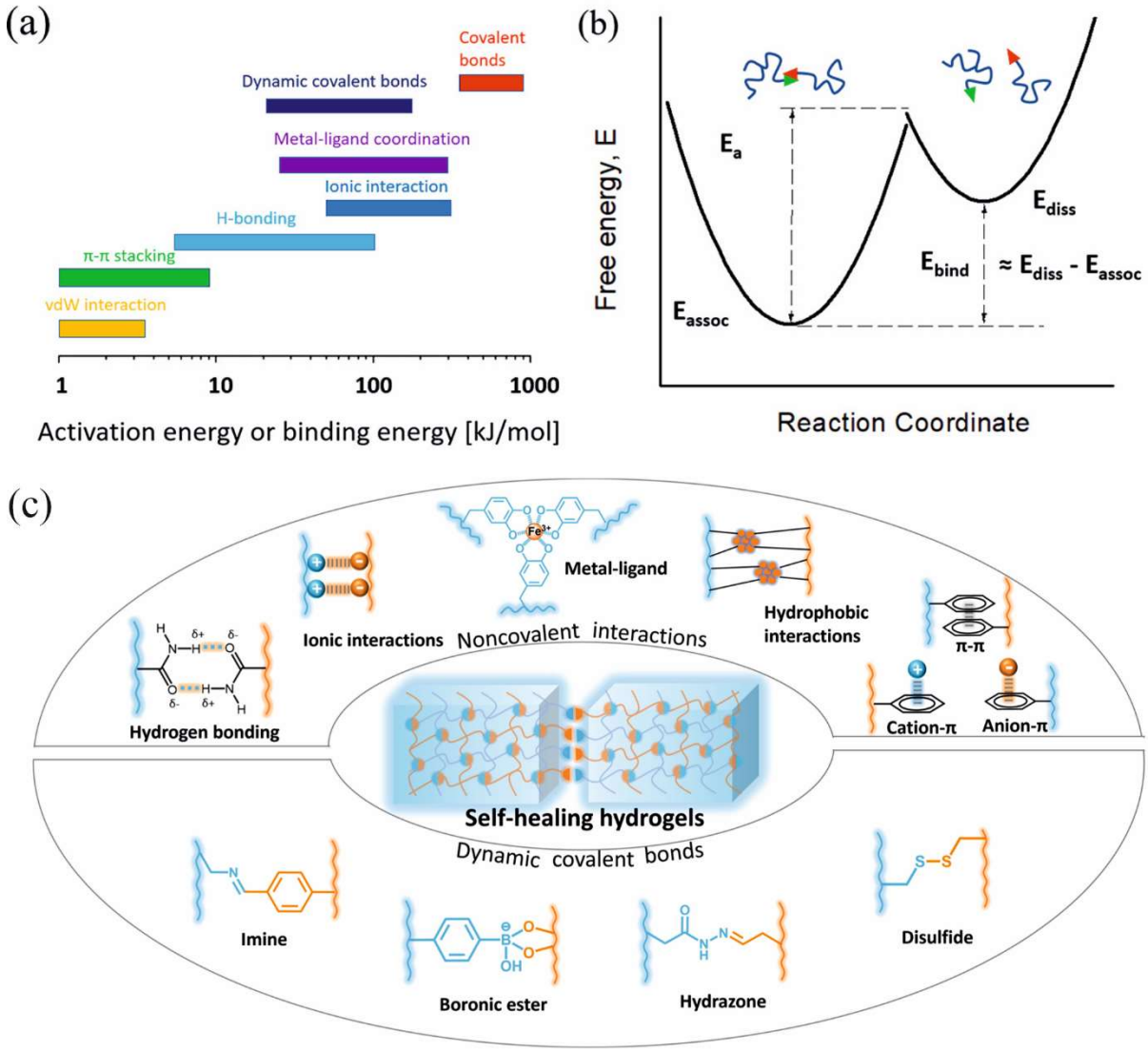

Figure 2. (a) Activation energy of dissociation and binding energy for various types of bonds and interactions. (b) Schematics of free energies of the associated and dissociated states of reversible bonds[13]. Copyrights 2021, American Chemical Society; (c) different types of dynamic covalent and noncovalent bonds[14]. Copyrights 2023, KeAi.

Dynamic crosslinking of short polymers increases their effective molecular weight, and such polymer can be expressed as an entangled solution of long chains in its own monomer. The concentration φ of long polymer chains in such a solution can be estimated by the value of the plateau of shear modulus G_N^0 in comparison to the plateau of high molecular polymer melt. The plateau modulus is equal to

$$G_N^0 \approx \frac{kT}{b^3 N_{em}} \varphi^{\frac{7}{3}}$$

where T – temperature, k – Bolzman constant, N_{em} – number of Kuhn monomers in an entanglement strand in the melt, b – length of monomer[15]. The concentration value is indirect parameter to estimate the dissociation time of stickers.

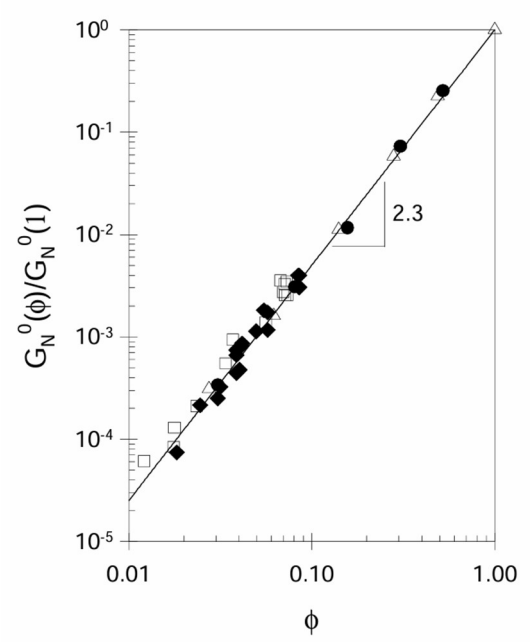

Figure 3. The ratio of plateau modulus of a high molecular weight polymer in theta solution to the plateau value of high molecular polymer melt[15].

1.2.2. PDMS-based self-healing polymers

The PDMS has a huge interest among self-healing polymers since it possesses the lowest glass transition temperature $T_g \approx -150°C$[16], providing amorphousness and large chain and segmental mobility at room temperature. By itself PDMS does not possess any strong dynamic interaction and healing can occur only through self-diffusion or entanglements formation. Functionalization with stickers can be made by modification of terminal groups. It can be different bipyridine – metal complexes with Eu^{3+} [17], Fe^{2+} or Zn^{2+} [7], boroxine[18, 19], imine[20], and disulfide bonds[21]. Due to the large mobility of chains in the PDMS-based self-healing polymers, they recover faster and demonstrate higher stretchability.

Although the healing ability of PDMS-based self-healing polymers is high, on another hand, the dynamic bonds are labile which affects mechanical properties: poorer mechanical strength, and lower Young modulus. The stronger metal-ligand coordination-based stickers minimize this problem, providing tough and rigid self-healing materials[22].

PDMS-based self-healing composites have been developed for various applications, including all three necessary components for electronic devices: insulators, semiconductors, and conductors. For instance, PDMS composites are used as high-voltage insulators in outdoor power transmission lines, where they could replace conventional ceramic insulators[23]. As semiconductors, PDMS-based self-healing dielectric elastomers cross-linked through metal-ligand coordination have been integrated into organic field-effect transistors (OFETs), demonstrating increased dielectric constants and stable electrical performance under strain[7].

As for conductors, PDMS composites embedded with liquid metal droplets[24] or multiwalled carbon nanotubes (MWCNTs)[25] exhibit high electrical conductivity and self-healing capabilities, making them suitable for applications in flexible electronics and wearable devices. Or MXene-based composite strain sensors were fabricated for the detection of various body signals[26].

The data about dynamic bonds for pure PDMS polymers is possible to find in literature and the relation of Young modulus to chain relaxation time for different kinds of bonds is illustrated in Figure 4. There is no pronounced trend, and one can only say that the Young modulus is defined by the effective molecular weight, which depends on the dynamic crosslinking points density. The chain relaxation time depends on the type of bond at the same distance between crosslinking points However, in most of the cases there is no comprehensive investigation of molecular dynamics in such a system, and collecting the rheological data is challenging. In most cases, researchers demonstrate self-healing abilities by cutting and bringing two pieces together, applying random force, which cannot be called “self-healing”.

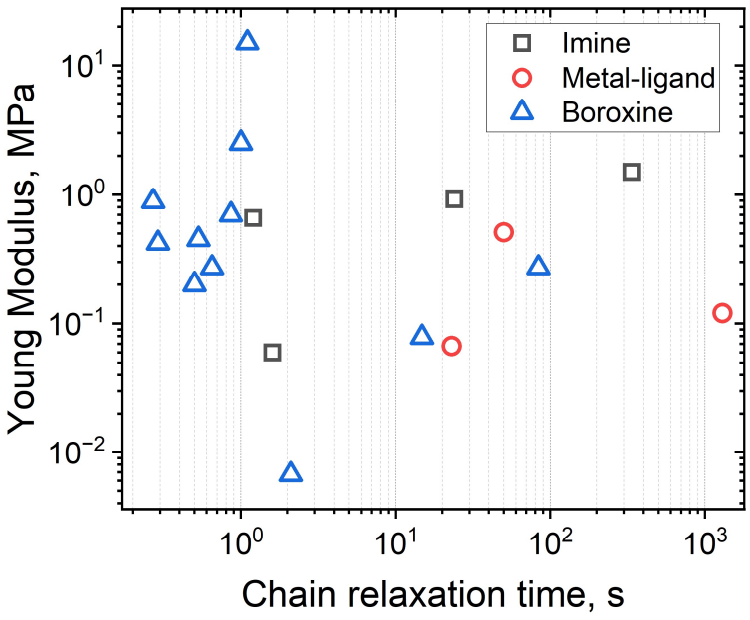

Figure 4. Relation of Young modulus to chain relaxation time for different PDMS based self-healing polymers.

1.3. Self-healing composites

1.3.1. Polymer-filler interaction

Polymer chains adsorb on particles, forming an interfacial layer with thickness t[27]. The interactions can be from weak Van der Waals forces to dynamic and covalent grafting. The properties of this layer are different from bulk polymer. The chain mobility is hindered and as a consequence relaxation time of the chain and segments ($\tau \sim e^{-\frac{1}{d}}$, d – distance from the particle), glass transition temperature T_g [28], as well as Young modulus[29], are larger. This change explains the reinforcement effect of the introduction of the nanoparticles in the polymer matrix.

The larger the interfacial volume, the stronger the reinforcement effect. It depends on the size and shape of the filler (aspect ratio of the particles) – geometrical factor, as well as the thickness – polymer nature factor. The largest interfacial volume per volume fraction of filler is reached for spherical particles with an aspect ratio equal to 1 (Figure 5a). The thickness of the interfacial layer depends on the interaction length (force) β between filler and polymer chain and temperature as

$$t(T) \approx \beta \left(\frac{T_g}{T - T_g} \right)$$

For the same polymer (or β value) the t depends on gyration radius[30], and as a consequence on molecular weight[31] and approximately equal to the gyration radius. Therefore, crosslinked rubber-like polymers will affect the interfacial thickness the most. The interfacial thickness can be estimated by various techniques such as scanning and transmission electron microscope (SEM/TEM)[32] (direct imaging of fracture) , atomic force microscopy (AFM)[29] (stiffness maps and direct imaging, Figure 5b), low field proton nuclear magnetic resonance (NMR) spectroscopy[27], mechanical spectroscopy[33]. For elastomers and rubber-like polymers, which is by properties are closer to dynamically crosslinked materials, the t value is about 10 nm[34]. For linear polymer, it is approximately equal to the gyration radius.

Before rheological percolation, the larger interfacial thickness leads to better dispersibility of filler due to a gain of enthalpy of polymer chains adsorption on the particles and entropy of non-agglomerated filler. The entropy decrease of adsorbed polymer chains is negligible[35]. However, after percolation, the enthalpy of particle-particle attraction takes place, which leads to particle aggregation.

The particle modifications of the surface or specific filler are used to enhance the interaction with the polymer and as a consequence ability of composite healing. It can be ionic[36], hydrogen and covalent bonds[37, 38], coordination bonds[39]. In such a system, the filler particles act as pseudo-crosslinking points. However, the filler network in such system is not percolated. Moreover, there is a lack of information about the dynamics of filler-polymer interaction. The hindering of polymer chains and segments will inevitably lead to a raise in the activation energy of dynamic bonds. It is also crucial to understand whether healing occurs at the interphase, how it changes with strain rate, its fatigue, and its behavior under non-linear conditions. Addressing this knowledge gap is essential to resolving a major issue in most self-healing composites: the recovery of a functional filler network.

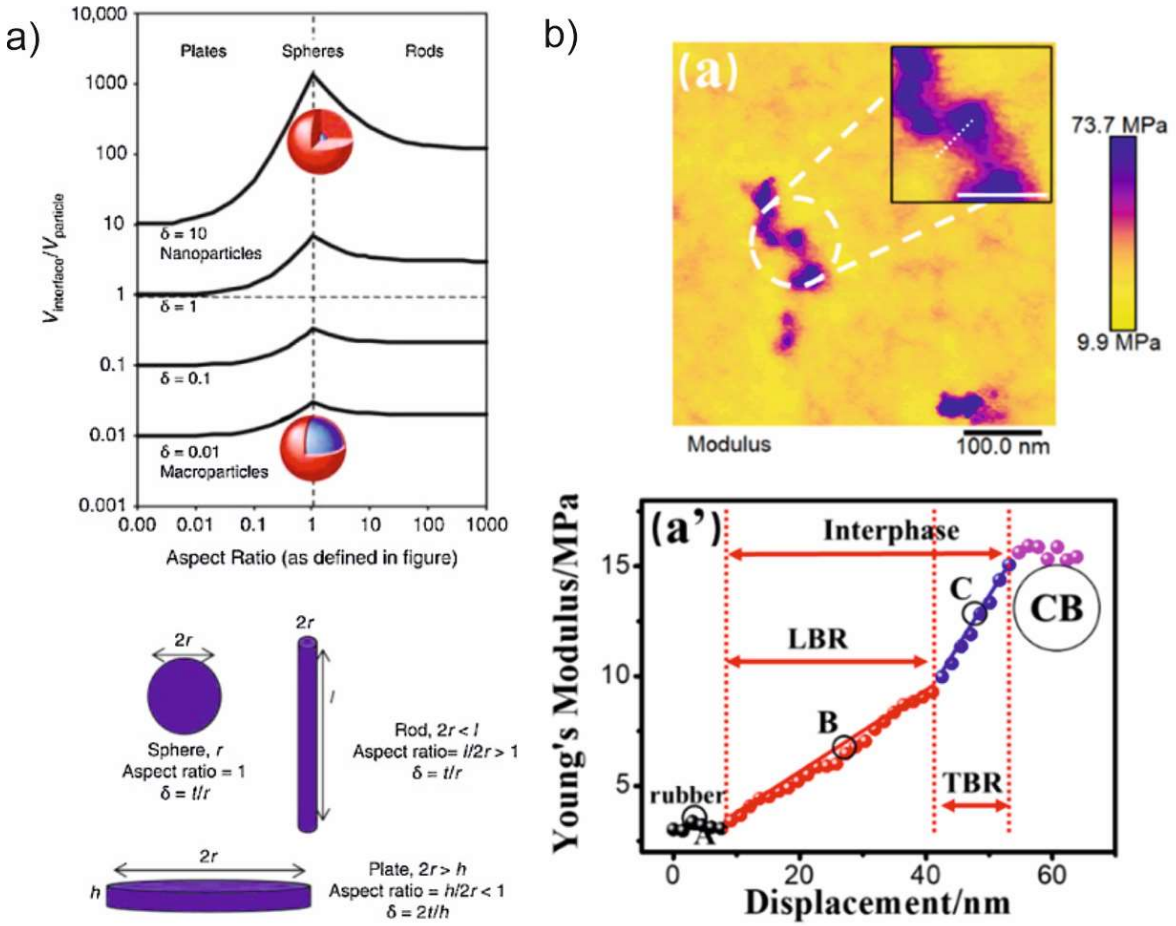

Figure 5. (a) Dependence of interfacial volume to filler volume fraction on aspect ratio of particles[40]. Copyrights 2015, Elsevier; (b)Young's modulus image and the corresponding Young's modulus-displacement curve from rubber matrix to loosely bound rubber (LBR), tightly bound rubber (TBR), and carbon black (CB) across interphase for large specific area carbon black in solution polymerised styrene butadiene rubber (CB-LSSA/SSBR)[29]. Copyrights 2022, Elsevier.

1.3.2. Percolation theory

The introducing of particles in a polymer matrix changes the properties of the polymer. The drastic change takes place and the point, where the particles achieve long-range connectivity, so-called percolation (Figure 6a). For conductive particles, like various carbon particles, two percolations can be considered: rheological and electrical.

Rheological percolation is achieved when the particles reach the long-range connectivity by overlapping interfacial volumes. It is believed that the agglomeration network of particles or intersections of their interfacial volumes at this point is formed which changes mechanical properties

dramatically. Change of material storage modulus G′ with an increase in particle volume fraction φ is used to determine percolation threshold value by following the power law relation

$$G' \sim (\varphi - \varphi_{cG'})^{n_{G'}}$$

where $\varphi_{cG'}$ is percolation threshold value, $n_{cG'}$ is critical exponent[41]. The rheological percolation also can be expressed by viscosity, loss modulus, or relaxation modulus which follows the same power law relation.

Electrical percolation is observed when particles form a network with direct contact or close enough for tunneling current contact between particles. At this point, for conductive particles, the dramatic raise of conductivity occurs which follows the same power law equation

$$\sigma \sim (\varphi - \varphi_{c\sigma})^{n_{c\sigma}}$$

Where $\varphi_{c\sigma}$ is electrical percolation value, $n_{c\sigma}$ – critical exponent.

The rheological percolation can be reached sooner than electrical[42] or later[43]. It depends on interfacial thickness. When it is higher than the tunneling current between particles – then the rheological percolation value is smaller, and vice versa.

For self-healing conductive composites, the percolation rheological occurs at lower concentrations of filler than electrical since due to dynamic crosslinking the effective molecular weight of such polymer, and consequently gyration radius, is large[44].

Percolation value also depends on the aspect ratio of particles and the anisotropy of their distribution. From a geometrical point of view, randomly distributed prolate ellipsoids (rod-like) reach geometrical percolation p_c at lower concentrations than oblate ellipsoids (plate-like) at the same ellipse axis ratio[45]: $p_c = \begin{cases} 0.6\left(\frac{b}{a}\right) \text{ (prolate)} \\ 1.27\left(\frac{a}{b}\right) \text{ (oblate)} \end{cases}$ (Figure 6b). Therefore, particles with low aspect ratio like graphene reach the percolation at higher concentration of the filler compared to high aspect ratio nanotubes. For instance, in chitosan composites the electrical percolation of MWCNT and GN was reached at 10 wt.% and 25 wt.%, respectively[46]; in PLA composites these values are 1.5wt.% and 5 wt.%[47]. According to theory and simulations, anisotropy of particles spatial distribution leads to an increase in percolation values[48-50]. However, experimental research demonstrates the opposite, for instance,

by electric field aligned MWCNT in epoxy matrix[51] or aligned by magnetic particles in magnetic field MWCNT filler in PDMS[52].

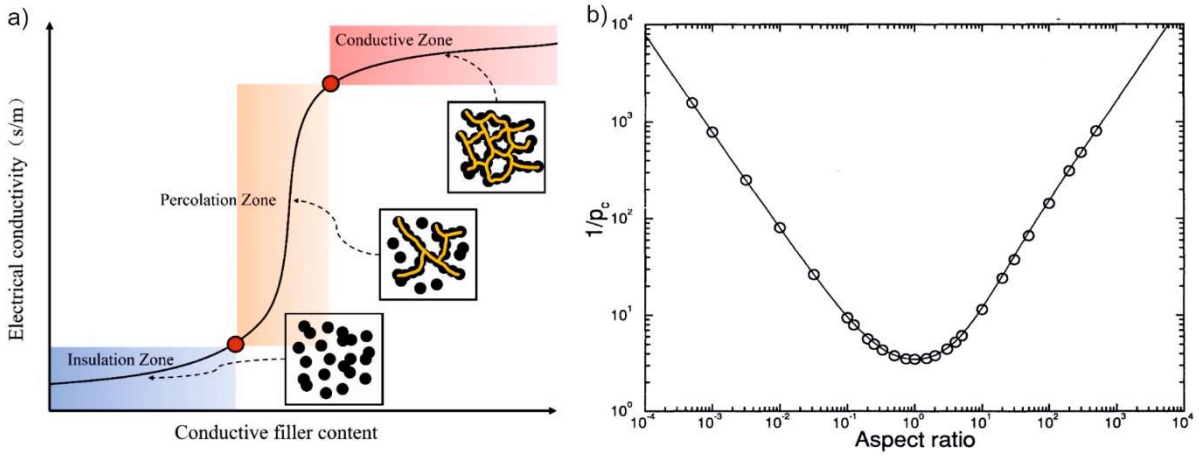

Figure 6. (a) Typical S-shape curve for electrical percolation of filler in composites[53]. Copyrights 2024, MDPI; (b) reciprocal geometrical percolation value as a function of aspect ratio of filler[45]. Copyrights 1995, American Physical Society.

1.3.3. Behaviour at different strain amplitude

Amplitude sweep behaviour of viscoelastic composites in general can be divided in three regions: viscoelastic (LVE), non-linear viscoelastic region, and flow (or failure of internal filler structure or the whole material) region (Figure 7). In LVE region no breaking of agglomeration structure is observed and only oscillation near the equilibria state takes place. In the second region, the breakage of filler agglomeration network occurs, which can be observed in the drop of G′ and pronounced maximum of G′′. The maximum is observed due to energy dissipation when the particles-particles van der Waals bonds are broken down. This effect is called Payne effect[54]. In the third region, depending on the time scale and type of polymer, the homogenization of bridging polymer chains or their failure occurs, along with the complete failure of the filler agglomeration network. This is recognized either by the formation of a new plateau in both storage and loss moduli or by a drop in both moduli and shear stress values.

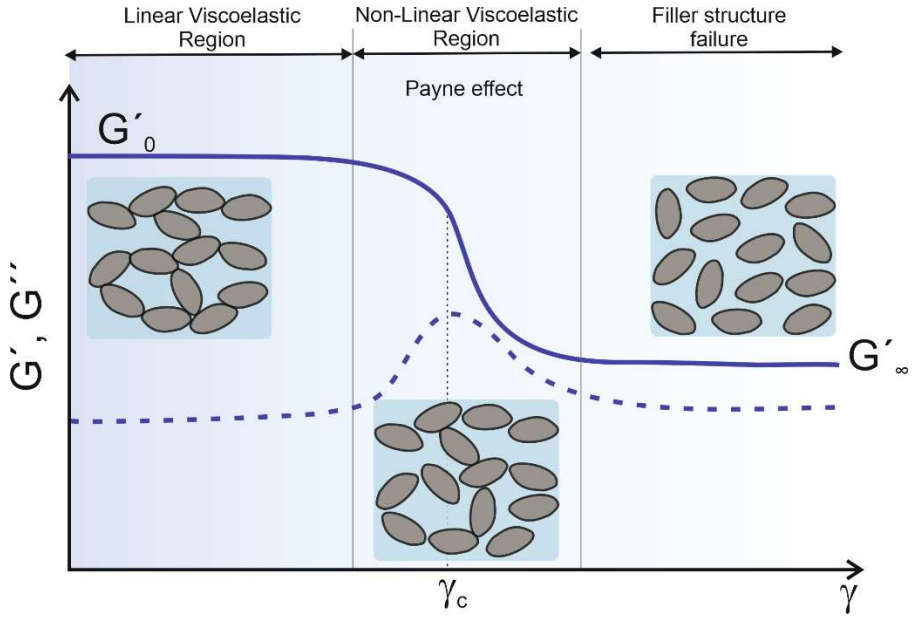

Figure 7. The typical curve for the amplitude sweep experiment of filled rubbers with the Payne effect observed.

The behavior at different strain amplitude can be characterized by the Krauss model

$$G'(\gamma) = G'_{\infty} + \frac{G'(\gamma) - G'_{\infty}}{1 + \left(\frac{\gamma}{\gamma_c}\right)^{2m}}$$

where $G'(\gamma) - G'_{\infty}$ is the difference of storage moduli at zero and infinite strain respectively, γ_c – critical strain or the amplitude at which $G'(\gamma) - G'_{\infty}$ has decreased to half of its zero-strain value and the strain of G´´ maximum, m is universal value (0.5…0.6)[55]. The higher the concentration of filler, the lower the critical strain[56].

At large strain, when filler contacts are broken, it is important to investigate the thixotropy of these composites, or in other words, the recovery rate of their initial mechanical and electrical properties. For thixotropy investigation, the general principle is to measure initial properties non-destructively at low strain (stress), then break the macro/micro structure at large strains and remeasure properties at low strain again to detect materials recovery. It can be done in the form of a thixotropy loop test via continuous step-strain or step shear rate measurements (the last one is mostly used for low viscous samples like paints)[57, 58]. Simultaneous measurements of electrical characteristics may allow to estimate the thixotropy of a material´s functionality.

1.3.4. Mechanical spectroscopy

Mechanical spectroscopy involves studying the dynamics of relaxation processes of material in its near equilibrium state. The strain and stress should be small enough to avoid perturbing the material's equilibrium structure, operating within the LVE region. The relaxation processes can be studied by various rheological techniques such as frequency sweep (FS), creep and relaxation (relaxation modulus $G(t)$) tests, expanding their measurement range using time-temperature superposition (TTS). In the end, the measured values are reduced to one – continuous relaxation spectra $H(\lambda)$. For the generalized Maxwell model, the conversion of relaxation modulus and G′,G′′ into continuous relaxation spectra can be implemented according to these equations

$$G(t) = G_e + \sum_{i=1}^{N} g_i e^{-t/\lambda_i}$$

$$\mathrm{G}'(\omega) - G_e = \sum_{i=1}^{N} g_i \frac{(\omega\lambda_i)^2}{1 + (\omega\lambda_i)^2}$$

$$\mathrm{G}''(\omega) = \sum_{i=1}^{N} g_i \frac{\omega\lambda_i}{1 + (\omega\lambda_i)^2}$$

$$H(\lambda) = \sum_{i=1}^{N} g_i \delta(\lambda/\lambda_i - 1)$$

where coefficients g_i, G_e, and relaxation times λ_i are material parameters, δ(y) is the Dirac delta function[59].

Also, the data can be plotted with an extended frequency range of FS experiment recalculating relaxation modulus to G′ and G′′

$$G'(\omega) = \omega \int_0^{\infty} G(t) \sin(\omega t)\, dt$$

$$G''(\omega) = \omega \int_0^{\infty} G(t) \cos(\omega t)\, dt$$

In viscoelastic polymer composite, the three main relaxation processes may take place: relaxation of bulk polymers (relaxation of chains, segments, macromolecular structure etc.), relaxation of polymer

in proximity of particles surface, and particles -particles aggregates and agglomerates related relaxation. The relaxation behavior of bulk dynamically crosslinked polymers is described by the Sticky-Rouse model proposed by Rubenstein[60]. The main difference from the Rouse dynamics is that the relaxation time of polymer chains flow is shifted to a larger time scale with the addition of another relaxation process related to the relaxation of stickers[61]. For instance, for ionomers based on polyethylene oxide -Na^+ the Rouse relaxation point for pure polymer is around 10^{-8}s and changes to 10^{-3}s with 100% of ionic content with additional sticky rouse relaxation of ionic associates at 10^{-2}s[62] (Figure 8a). Or sticky Rouse relaxation due to hydrogen bonds of 2-ureido-4[1H]-pyrimidone (UPy) groups in a copolymer with 2-methoxyethyl acrylate (MEA)[63] (Figure 8b).

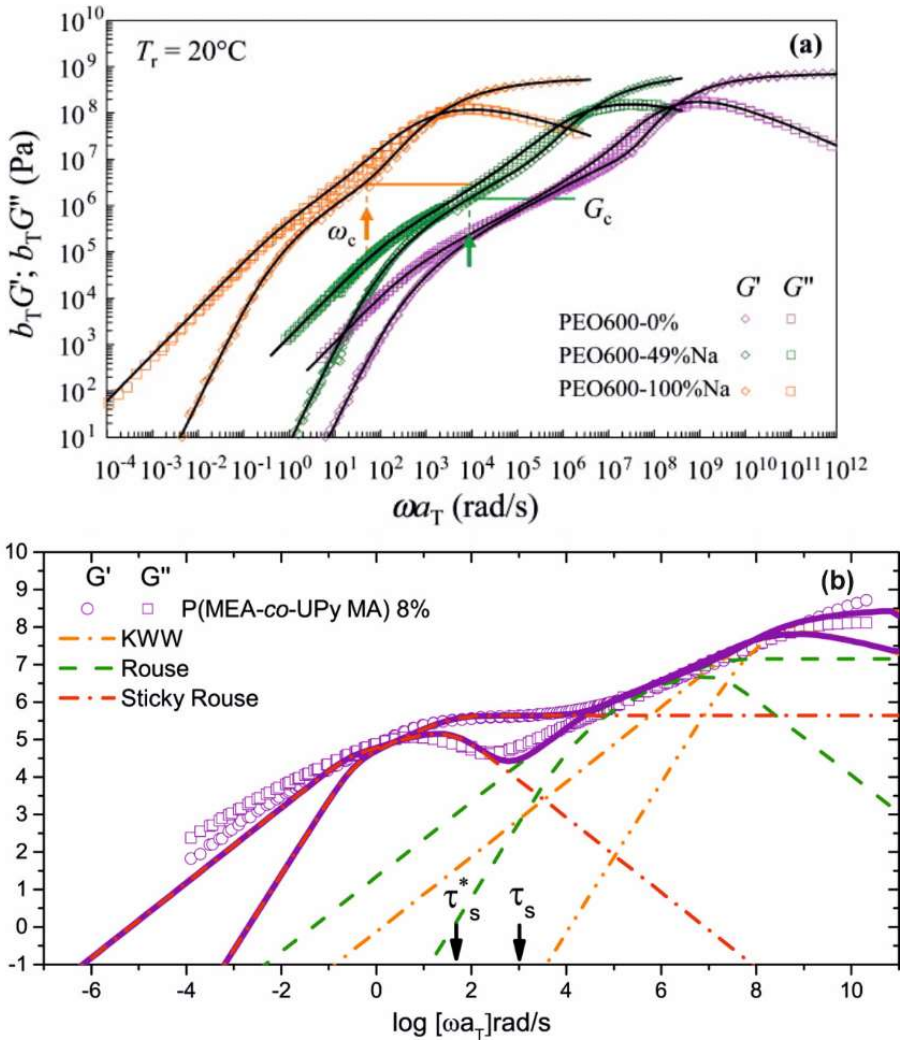

Figure 8. a) Master curves of storage and loss moduli, G′(ω) (diamonds) and G′′(ω) (squares), obtained as functions of frequency ω for PEO600-fNa samples having different ionic fractions f as indicated[62]. Copyrights 2013, The Society of Rheology; b) Linear viscoelastic master curves of

PMEA and P(MEA-*co*-UPyMA) systems shifted to T_{ref} = 60 °C and the model prediction (solid lines) considering a monodisperse molecular weight[63]. Copyrights 2016, American Chemical Society.

The shift of relaxation time in particle proximity may be seen on relaxation spectra. For instance silica particles with grafted polylactide polymer chains[33]. The interface relaxation of entanglements of long polymer chains at around 300s was observed as well as other relaxation processes such as adsorption of grafted chains on the particle surface and backbone relaxation. The relaxation spectra is a great instrument for the visualisation of these processes.

The relaxation of the filler is studied much less. It is often considered, that if the filler network is percolated it forms a stable network that does not relax within a reasonable time scale. However, a lot of dynamically crosslinked polymers possess low viscosity (10^3 – 10^5 Pa·s), and introducing a nanofiller (a particle with any of nano-scale dimension), as an example spherical particle 50 nm diameter, the translational diffusion $<x^2>=6D_t t$ on a distance of size of the particles will be on time scale 50-5000 s. It means, on a reasonable time scale the network may not be stable and can change with time. For instance, the dynamic experiment has confirmed the impact of silica NPs diffusion through the entangled PMMA melt ($\eta \approx 10^5$ Pa·s) in the relaxation of the composite[64].

To summarize, relaxation processes of bulk dynamically crosslinked self-healing polymers is well studied and described by the Sticky-rouse model. However, the dynamics of filler and filler interface still have scarce data and are mostly not considered, however, it directly influences the properties at a large time scale.

1.4. Wearable strain-sensors

Recent advances in skin-mountable and wearable electronic devices have attracted significant attention due to their seamless integration with the human body and their capacity for long-term monitoring[65]. These flexible sensors, designed for monitoring the physical, chemical, biological, and environmental parameters of the human body, offer high efficiency with minimal discomfort. One important example of wearable technology is the flexible strain sensor, which converts external mechanical stimuli into electrical signals. Flexible strain sensors find versatile applications, including the monitoring of vital signs such as pulse and breathing rates, electromuscular activity, gait analysis, and sleep tracking[66]. These sensors offer valuable insights for enhancing performance, injury prevention, and assisting in rehabilitation[67]. Moreover, flexible strain sensors can be integrated into

more intricate systems such as human-machine interfaces and soft robotics[68]. Such sensors involve several thousands of strain repetitions per day, which can lead to localized material failure and performance degradation. Therefore, the use of conductive self-healing composites could be a solution to this problem and fabricate a device with an infinite lifetime.

Strain sensitivity can be implemented through different mechanisms: optical (light intensity difference Bragg gratings[69, 70], color change[71]), potentiometric (variation of potential difference in ionically conductive composites[72]), piezoelectrical[73], capacitive[74], resistance (piezoresistance[75], microcrack propagation[76], tunnelling[77]). The latter type is more popular, easy to implement, and shows better performance compared to other types, and the functional part is a polymer-conductive filler composite whose characteristics will be discussed in the next chapter (Figure 9a).

1.4.1. Electromechanical characteristics

The wearable stress sensor from the mechanical point of view has three most important parameters: Gauge factor G, Working factor W, and Young modulus E (or stiffness). The Gauge factor is the sensitivity parameter of the sensor, which is the proportionality coefficient between the main signal of strain sensor – fractional amplitude of resistance $\frac{\Delta R}{R_0}$, and strain ε:

$$\frac{\Delta R}{R_0} = G\varepsilon$$

The Working factor is defined as a linear range of fractional resistance change with applied strain. It also relates to critical strain in Krauss model γ_c, or yield strain, meaning that the resistance change will be linear as long as the agglomeration structure is not broken. The larger the concentration of the filler, the higher the value of W, however, the sensitivity G drops down due to a decrease in a relative number of broken contacts. It can be expressed through the following relationship[78]

$$G = 2 + n_\sigma \left(\frac{1}{W}\right)$$

In order to get both large W and G values, the equation tells us to increase the percolation exponent. For randomized systems the n_σ<1 whereas for oriented structures this value is higher[79]. Therefore, to build a sensitive sensor with large sensitivity, the filler orientation is preferable.

The sensor also should possess the Young modulus lower than skin (<1 MPa) to avoid dampening of electromechanical signal. The stiffer the material, the lower the deformation of the sensor at the same

stress, and some of our body signals provide very low stress values (for instance artery pressure is around 5 kPa). Moreover, the current strain sensors are implied to be wearable on skin or as various textiles. Therefore, for best materials integration sensor's and skin moduli should be comparable.

In summary, the following challenge regions in order to implement good wearable strain sensor were proposed: $W > 1$ (to cover most healthcare monitoring signals), $G > 7$ (to overcome values of commercial metal foil strain gauges) (Figure 9b), and $E < 300$ kPa (compatibility with skin and better signal transfer). There a plenty of viscoelastic self-healing polymers that are soft enough ($E < 100$ kPa). Therefore, the proper design of the percolated conductive network in such a polymer matrix has a perspective to meet the aforementioned requirements.

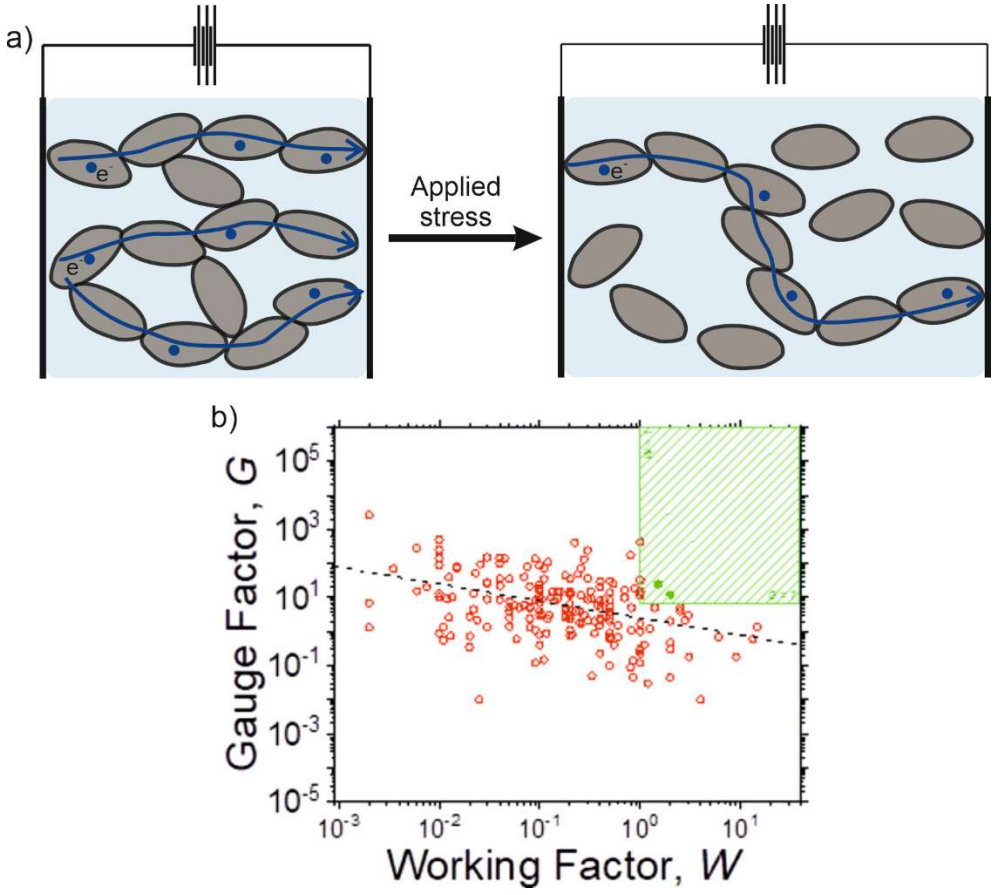

Figure 9. a) Scheme of piezoresistivity effect: the broken particle contacts increase the path for charge transfer leading to an increase in resistance; b) Gauge factor (G) as a function of working factor (W). The target region is designated by the values of $G > 7$ and $W > 1$. The dashed line represents an apparent intrinsic decay in the gauge factor of nano-based strain sensors with the working factor described by $G \propto 1/\sqrt{W}$[78]. Copyrights 2019, American Chemical Society

The strain sensor undergoes multiple cycles of deformation and it should have mechanical as well as electromechanical fatigue resistance. The characteristics should be stable no matter of number of deformation cycle. Therefore, it must be conditioned.

The conditioning is supposed to be performed within the working factor range of deformation. The electromechanical signal during deformation undergoes fatigue, following Basquin law

$$\frac{\Delta R}{R_0} = \alpha C^{-B}$$

Where C – number of cycle, α – reflects initial parameters of sensor ($\alpha = \frac{G_0 \sigma_0}{E_0}$, where G_0 is initial Gauge factor, σ_0 – initial stress at applied strain amplitude, E_0 – initial Young modulus), B – Basquin exponent. The typical fatigue measurements are demonstrated on Figure 10. The B value allows to estimate for elastomer-like materials of how fast a sensor reaches the endurance limit C_E (steady state in signal)

$$\ln (C_E) = \frac{\ln (0.5)}{-B}$$

Thus, the higher B value – the lower the number of cycles necessary to reach an endurance limit[80].

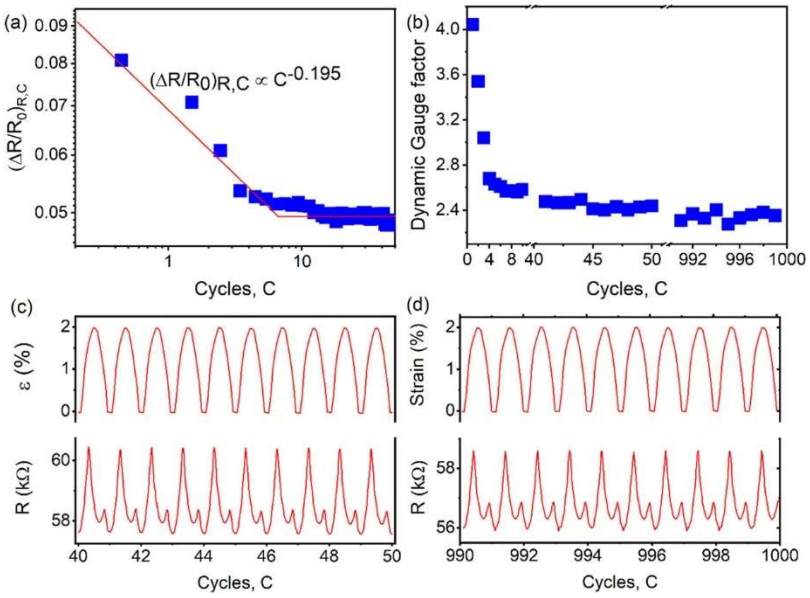

Figure 10. Resistance signal fatigue under dynamic cyclic loading. (a) Fractional resistance range versus cycle number for 50 cycles. (b) Dynamic gauge factor as a function of cycle number. (c) Plots

of signal stability immediately after exceeding the endurance limit (40–50), and (d) the last 10 cycles[81]. Copyrights 2022, American Chemical Society

1.4.2. Fiber-based strain-sensors

The wearability of materials implies not only comparable values of their Youngs modulus and modulus of skin (< 1 MPa), but also the ability to undergo considerable (up to 100%) deformations, as well as porous structure, which provides breathability, permeability, comfortability, and lightweight. From that point of view, fiber-based materials are great candidates, one of whose functions is to provide J-like stress-strain behavior and to limit large strains that can lead to failure of the soft component.

Fiber-based strain sensors were previously fabricated either by incorporating conductive filler (i) inside of the fiber matrix[82, 83], (ii) on top of it[84-86], or (iii) fully encapsulating carbon-fiber structure in other elastomer-like mold[87]. In the first and third cases, embedding of conductive filler inside the polymer matrix requires high colloidal stability of the particle dispersion. As a result, the fabrication of micron-size fibers is challenging due to coagulation and precipitation of a filler. Moreover, the mobility of the conductive filler is low, which may restrict recovery ability in case of network failure, and the chances of fatigue failure increase due to the weakening of the particle-polymer interface at multiple cycling deformation. The use of filler on top of the matrix (the second approach) does not provide high enough adhesion of the conductive particles to the fibrous material, which may lead to loss of conductive material. Thus, the main drawback of fibrous flexible soft sensors is their fatigue failure and signal fatigue.

The fatigue is observed due to softening followed by relaxation of polymers in the proximity of particles surface[9, 80]. To overcome this issue, several approaches can be used. First, one can avoid using filler replacing it with a conductive polymer like PEDOT:PSS, but then one significantly lower sensitivity of device[88]. Second, one can condition the fiber sensor by deforming it within a linear region to reach the endurance limit of the signal with not significant drop in Gauge factor. The endurance limit, as was discussed, depends on Basquin constant *B*. For instance, polyether block amide fibers functionalized by carbon black (CB) reach an endurance limit after 375 cycles at B=0.117[81], and 35 cycles at B=0.195 functionalized by MWCNT/CB filler[89] which is in agreement with theory. Unconditioned strain sensors will undergo reduction of the signal with every cycle of measurements and calibration of such devices will be challenging[90] (Figure 11).

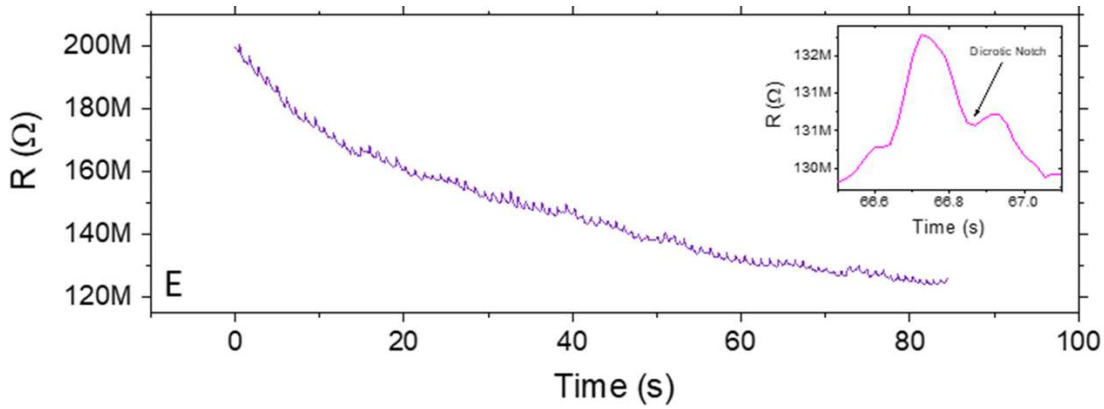

Figure 11. Heart monitoring testing of unconditioned strain sensor as a function of time (inset) showing characteristic waveform and dicrotic notch[90]. Copyrights 2021, American Chemical Society.

1.5. Conclusion

To summarize, self-healing materials for electronics have great potential to address the e-waste problem. Due to dynamic bonds, small damaged areas for pure polymers can regenerate autonomously. However, while the healing dynamics of pure polymers are relatively well-studied, the changes and mechanisms of healing behavior when introducing functionalized fillers into the healing matrix are scarcely investigated. There is limited data on the dynamics of fillers in self-healing matrices and on particle interfaces, which is crucial for predicting their stability and designing the mechanical properties of materials, as well as their ability to regenerate. Moreover, this knowledge may enable the design of self-healing composites that can withstand fatigue, a common issue for filled polymers.

2. Aim

The aim of the thesis was to investigate thoroughly the applicability limits of conductive self-healing composites based on viscoelastic liquid and carbon filler for soft wearable electronics.

The self-healing wearable soft electronics based on conductive self-healing composites are very promising solution for E-waste problem. However, the current gap in knowledge lies in the limited investigation of the changes and mechanisms of healing behaviour when functionalized fillers are introduced into self-healing polymer matrices, particularly regarding the dynamics of fillers and particle interfaces, which are crucial for predicting stability, designing mechanical properties, and enhancing the regenerative capabilities of these materials.

Thus, the aim of this project can be divided into three objectives:

Objective (1) is to investigate the influence of relaxation time of various self-healing PDMS based polymer matrix in their composites with various concentrations of carbon black filler. This implies the study of strain dynamics, both non-destructive and destructive, electromechanical properties, as well as their ability and mechanism to recover initial properties (healing). It shall provide an understanding of the relaxation processes of polymer chains, particles, and their agglomerates, and the processes at the particle-polymer interface. Additionally, it aims to offer insights into the choice of the initial self-healing polymer matrix to achieve the desired electromechanical performance of the composite.

Objective (2) is to investigate the influence of carbon filler aspect ratio in self-healing polyborosiloxane (PBS) matrix exploring the same fundamental materials characteristics. It aims to offer insights into the choice of the conductive filler to achieve the desired electromechanical performance of the composite.

Objective (3) is to fabricate a wearable self-healing strain sensor with PBS-graphene/carbon nanotubes composite functional layer reinforced by electrospun thermoplastic polyurethane fibers, and project aforementioned fundamental aspects on real application of self-healing carbon composites. It aims to address the inherent limitations of porous, flexible, fibrous, and self-healing strain sensors: their fatigue, healing ability, and long-term stability.

3. Synopsis

The results summarized in the dissertation are published in three first-author research publications. The publication list and my contribution to each can be found in section 5 and section 6, respectively.

The aforementioned aim and objectives point out the problem in comprehending mechanisms of autonomous properties and structure recovery in conductive particles-filled self-healing polymers. The conditions for autonomous healing and applicability limits of self-healing conductors are often left behind the scenes. In literature, there is a lack of information about the particle-self-healing polymer interaction, dynamic behavior of such composites as well as their large strain amplitude behavior. Therefore, in this aspect, we focus on a better understanding of these fundamental aspects which are crucial to understanding for fabrication of a self-healing conductor. For that, a well-known polyborosiloxane was used as polymer matrix with, hydrogen, dynamic covalent B-O, and dative B:O bonds which provide self-healing properties. To provide conductivity, various carbon fillers were used. As a first step, we investigated the influence of relaxation time of PDMS-based self-healing polymers with the same concentration of conductive filler. Second, the influence of the carbon filler aspect ratio was explored. Conclusions and trends in the first two publications were applied in the characterization of real self-healing composite-based devices for strain sensing.

3.1. Self-Healing and Electrical Properties of Viscoelastic Polymer-Carbon Blends

Self-healing polymer-carbon composites are seen as promising materials for future electronic devices, which must be able to restore not only their structural integrity but also electrical performance after cracking and wear. Despite multiple reports about self-healing conductive elements, there is a lack of a broad fundamental understanding of the correlation between the viscoelasticity of such composites, their electrical properties, and the self-healing of their mechanical as well as electrical properties.
In this work a thorough study of electromechanical and rheological properties of blends of carbon black particles and PDMS with different relaxation times was performed. Adding carbon filler to the polymers renders its properties, and behavior of composites depends strongly on the viscoelastic properties of polymers. The polyborosiloxane allows the dough-like behaviour of the blends. The material possesses elastomer-like behavior on a small time scale. It flows on a large time scale when large stress is applied and can withstand large deformation without brittle failure. On the other hand, the viscoelastic self-healing polymer negatively affects the stability of carbon-carbon contacts, which ensures high conductivity. As a result, the electrical properties of blends of viscoelastic polymers and carbon are worse than that of carbon and viscous polymer. Moreover, the viscoelastic polymer

degrades the conductive carbon networks with time, decreasing its conductivity. The ability of polymer-carbon composites to flow, which is utilized for self-healing, is an indication of an absence of 3D network formed by particles. It results in worse conductivity compared to the blends with low molecular weight polymer, which do not flow due to the formation of strong carbon network, have brittle failure but is able to immediately restore mechanical properties and conductivity after removing stress.

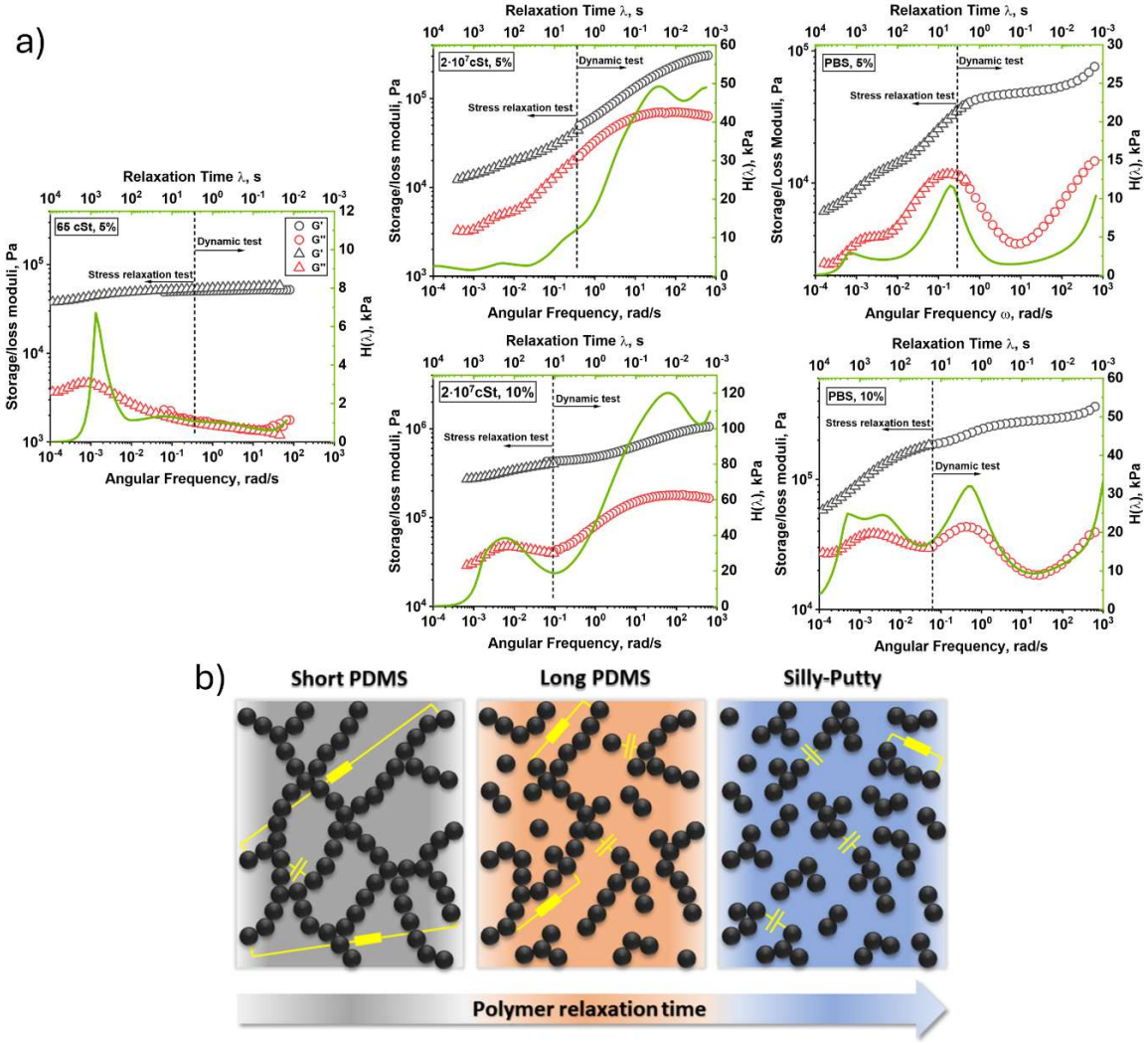

Figure 12. a) Viscoelastic behavior of PDMS-carbon blends at small deformation. Storage and loss moduli were obtained from both relaxation and dynamic experiments to demonstrate viscoelastic behavior ranging from around 10^{-4} to 10^{3} rad/s. The relaxation spectra calculated from merged experiments reveal the polymer and carbon black particle network's relaxation processes. b) The scheme of agglomeration network of CB in polymer matrix with very low relaxation time (PDMS 65 cSt), PDMS $2 \cdot 10^{7}$ cSt with relaxation time ~ 0.1s, and PBS with relaxation time ~1s. Pseudo capacitor and resistor elements of network are marked in yellow signs.

3.2. Superelastic, soft, stress-healable, recyclable conductive materials

In this work, we reported for the first time a multiwalled carbon nanotubes – Silly Putty composite material with a unique combination of self-healing ability, high electrical conductivity, softness (E=1 MPa) and, that is highly novel, extremely low loss coefficient (tan $\delta \approx 0.04$). This combination may be rarely observed, and such extreme values were not found in the literature.

Moreover, we accompany that with an in-depth analysis of the mechanical properties, flow characteristics, electrical properties, and self-healing properties, as well as the causal relationship between them of mixtures of viscoelastic polymer, and conductive carbon fillers with different aspect ratios (plate-like graphene, pseudospherical carbon black, and rode-like multiwalled carbon nanotubes). All fillers provide the dough-like behaviour of the blends. The material possesses elastomer-like behavior on a small time scale. At a large time scale it flows when large stress is applied and can withstand large deformation without brittle failure. On the other hand, the different ability to form agglomeration network of different fillers affects the stability of carbon-carbon contacts, which is responsible for conductivity, as well as healing ability. As a result at the same volume fraction the strong and immobile nanotube network gives the material high conductivity, but for this we sacrifice the ability to flow, or to self-heal, and ductility when large stress is applied on a small time scale. For weak, but mobile graphene networks the tendency is the opposite. Thus, it is a double-edged sword working with viscoelastic blends: either we sacrifice mechanical and healing properties or electrical.

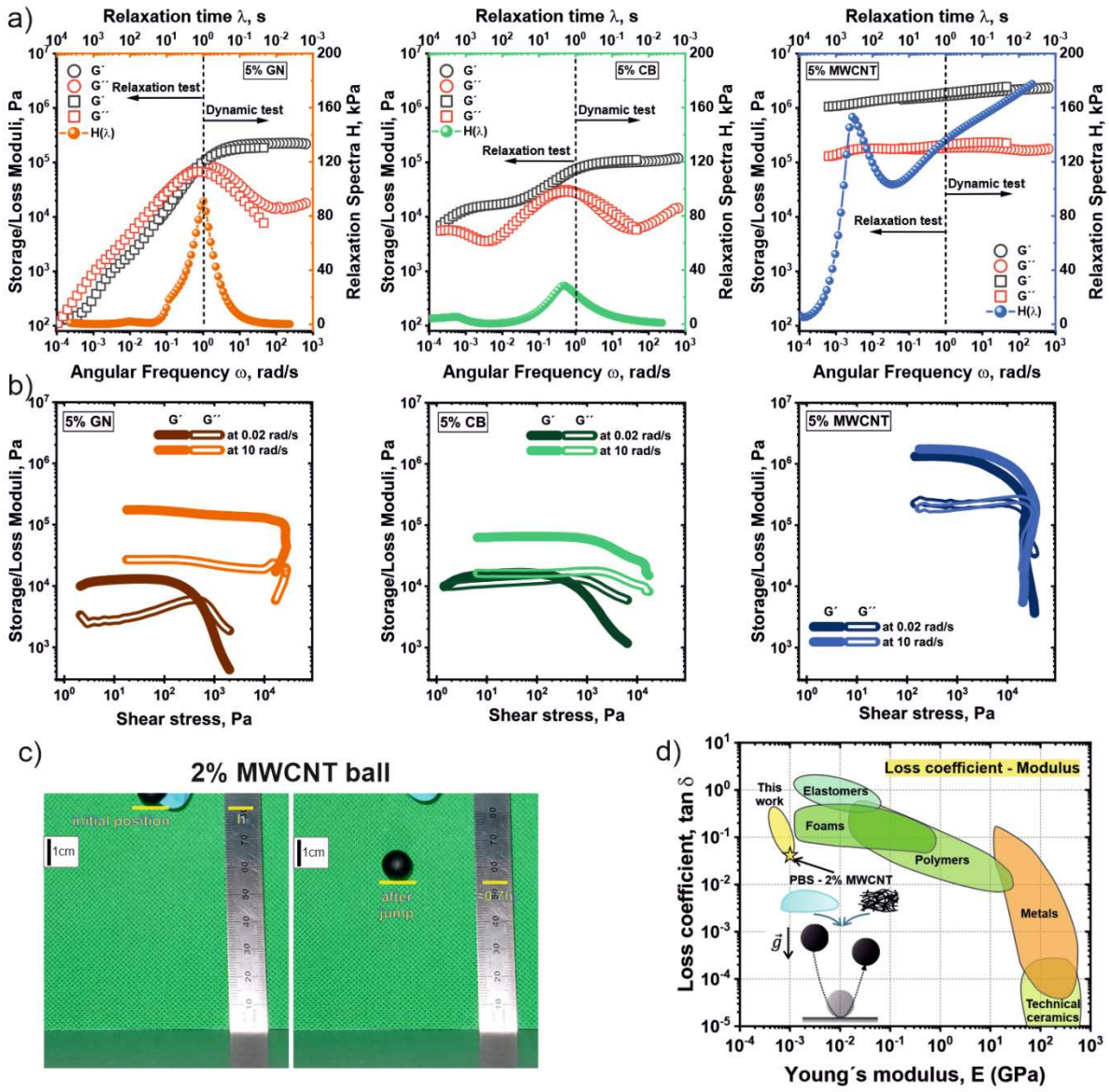

Figure 13 . Viscoelastic behavior of PBS – carbon blends PBS − 5 % GN, PBS − 5 % CB, PBS − 5 % MWCNT at small deformation: a) storage and loss moduli, obtained from both relaxation and dynamic experiments, demonstrate viscoelastic behavior ranging from around 10^{-2} to 10^{4} s. The relaxation spectra calculated from merged experiments reveal the polymer and carbon particles network relaxation processes; b) amplitude sweep of PBS blends with different carbon fillers at a frequency lower (0.02 rad/s) and higher (10 rad/s) than the relaxation frequency of pure PBS. The graph is plotted as G', G" vs shear stress; c) d) bouncing of super-elastic 2 % MWCNT ball; d) Obtained results placed on Ashby plot (Loss coefficient vs Young Modulus).

3.3. Fiber-Reinforced Super Self-Healing Flexible Strain Sensor

In this work, we report for the first time electrospun fiber reinforced carbon – Silly Putty composite material with unique combination of self-healing ability, high strain sensitivity, softness and, that is highly novel, deformation reversibility of viscoplastic Silly-putty carbon composites, along with their property recovery after large deformations. The values of the Gauge and Working factors are rate-dependent and influenced by particle mobility within the PBS matrix; higher polymer mobility increases the working factor and decreases the gauge factor due to reestablished conductive contacts during viscous flow, while limited particle rearrangement time in the elastic regime results in a higher gauge factor and lower working factor, with the critical strain indicating filler network breakage.

We quantitatively investigated sensor performance fatigue, often overlooked, and found that electromechanical properties fatigue follows Basquin's law. Fatigue occurs due to the softening of the polymer's interfacial layer near particles and is rate-dependent. Over long time scales, the interfacial layer resembles the material at rest, while at short time scales, it is glassy and the bulk polymer is rubbery. Thus, conditioning in the elastic regime requires more energy, resulting in a lower Basquin exponent.

The sensor recovers its initial characteristics (size and performance) after significant deformation (100% strain) due to the reversible deformation of the TPU mat, which restores size and shape, and the self-healing abilities of the PBS-based viscoelastic layers, which restore performance. Moreover, we demonstrated that large deformation of sensor results in an improvement of its sensitivity that is

explained by break of contact between conductive particles – partial failure of conductive network

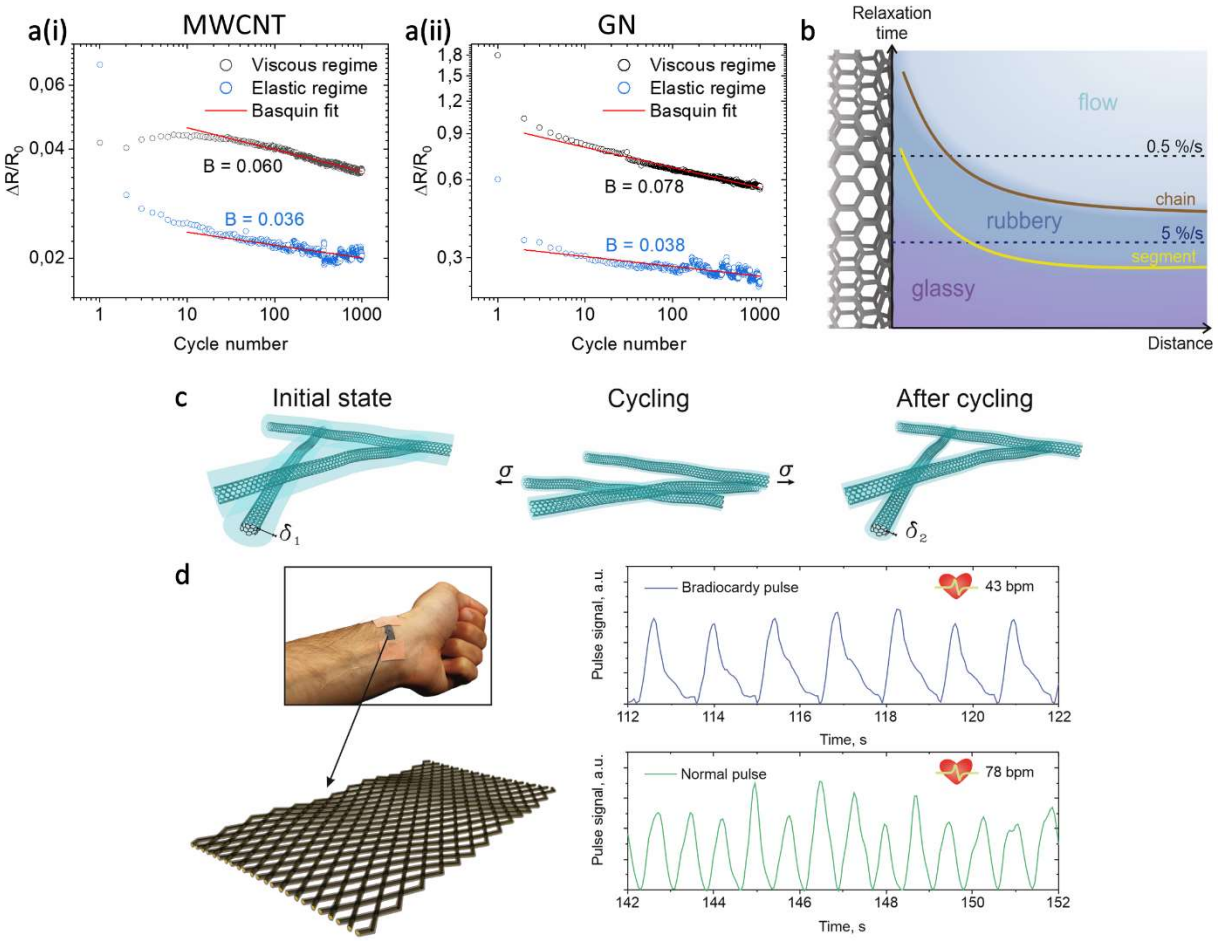

Figure 14. The S-N like curve for electrical response for a(i) MWCNT and a(ii) GN based sensor; b) scheme of interfacial layer behavior as a function of distance from particle surface: c) illustration of interfacial layer decrease during mechanical cycling: $\delta_1 > \delta_2$; d) visualization of a core-shell strain sensor on a wrist to measure a pulse and normalized signal of measurements of pulse by GN based strain sensor of a normal heart and one with bradycardia on person´s wrist.

3.4. Conclusion and outlook

Conclusion

These studies have shown that self-healing in materials is not autonomous but occurs only under forces greater than the yield point of the material. The healing abilities of materials depend on the relaxation time of the polymer matrix and, consequently, the flowability (creep) of the material. A lower relaxation time of the polymer results in a stronger filler agglomeration network and, as a result, higher yield stress. However, the composite possesses high conductivity. Conversely, a matrix with a

large polymer relaxation time results in a weaker filler network and lower yield stress (higher flowability), but lower conductivity.

A similar trend is observed when varying the aspect ratio of the carbon filler. High aspect ratio particles (rod-like) result in a stronger filler network, higher conductivity, and lower flowability. The opposite is true for low aspect ratio fillers. Moreover, we demonstrated that higher self-healing ability compromises the long-term stability of the composite due to the relaxation of filler and significantly shifted relaxation time of polymer at particle-polymer interface, forming a "percolated network" of polymer with significantly higher relaxation time.

For strain sensing applications, a stronger filler network of carbon nanotubes (large aspect ratio particles) demonstrated lower healing ability compared to graphene nanoplates (low aspect ratio particles). However, the lower healing abilities and reduced filler mobility of the nanotubes led to an increase in sensor sensitivity after extreme deformations. The particles network gets broken and is unable to recover, making percolation less effective and, consequently, more sensitive.

Thus, the key finding of this work is that in self-healing composites, there is always a trade-off between conductivity and healing ability. Depending on the application of the material, one will have to choose what to sacrifice in order to obtain a device with the desired properties.

Outlook

But it is worth asking the question, is self-healing even possible in functionalized materials? The straightforward approach of blending functionalized inorganic materials with self-healing polymers may lead to ***healing, but not to "self-healing"***. In nature, which we believe is most effective, what heals and what is cured are usually separate. Modern material design offers no such possibilities, or they are limited by the amount of self-healing.

Nevertheless, there's still a lot of room for research in this area. Future experiments should investigate the influence of dynamic bonds under various regimes and activation energies on the dynamics of both the polymer and the filler. This fundamental knowledge would help in understanding how to balance the stiffness and toughness of polymer composites with the relaxation time of polymer chains. Optimal materials should be identified for the fabrication of real components in electrical devices, particularly conductors and semiconductors. By controlling the rheological properties of composites, it is possible to investigate the possibility of solvent-free fabrication of custom-designed devices using FDM or DLP 3D printing technologies. Additionally, such functionalized composites should be

studied for the mobility of charge carriers and their transfer within self-healing polymer interfaces, along with the potential for constructing electrical components such as diodes and transistors.

4. References

1. Goyal, S.; Sharma, S.; Kharayat, P. S.; Gupta, S., E-Waste: Promoting the Need for Green Electronics. In *2023 International Conference on Power Energy, Environment & Intelligent Control (PEEIC)*, 2023; pp 326-329.
2. Kang, J.; Tok, J. B. H.; Bao, Z., Self-healing soft electronics. *Nature Electronics* **2019,** *2* (4), 144-150.
3. Ruiz, A. Latest Global E-Waste Statistics And What They Tell Us. https://theroundup.org/global-e-waste-statistics/.
4. Eming, S. A.; Martin, P.; Tomic-Canic, M., Wound repair and regeneration: Mechanisms, signaling, and translation. *Science Translational Medicine* **2014,** *6* (265), 265sr6-265sr6.
5. Speck, O.; Schlechtendahl, M.; Borm, F.; Kampowski, T.; Speck, T., Humidity-dependent wound sealing in succulent leaves of Delosperma cooperi – An adaptation to seasonal drought stress. *Beilstein Journal of Nanotechnology* **2018,** *9*, 175-186.
6. Qi, M.; Yang, R.; Wang, Z.; Liu, Y.; Zhang, Q.; He, B.; Li, K.; Yang, Q.; Wei, L.; Pan, C.; Chen, M., Bioinspired Self-healing Soft Electronics. *Advanced Functional Materials* **2023,** *33* (17).
7. Rao, Y. L.; Chortos, A.; Pfattner, R.; Lissel, F.; Chiu, Y. C.; Feig, V.; Xu, J.; Kurosawa, T.; Gu, X.; Wang, C.; He, M.; Chung, J. W.; Bao, Z., Stretchable Self-Healing Polymeric Dielectrics Cross-Linked Through Metal-Ligand Coordination. *J Am Chem Soc* **2016,** *138* (18), 6020-7.
8. Chen, Y.; Kushner, A. M.; Williams, G. A.; Guan, Z., Multiphase design of autonomic self-healing thermoplastic elastomers. *Nature Chemistry* **2012,** *4* (6), 467-472.
9. Rong, M.; Chen, D.; Hu, H.; Chen, F.; Zhang, Y.; Xie, C.; Chen, Z.; Yu, Y.; Xie, Y.; Yao, H.; Huang, Q.; Zheng, Z., Stretchable and Self-Healable Fiber-Shaped Conductors Suitable for Harsh Environments. *Small* **2023,** *19* (50), e2304353.
10. Chen, Y.; Pu, X.; Liu, M.; Kuang, S.; Zhang, P.; Hua, Q.; Cong, Z.; Guo, W.; Hu, W.; Wang, Z. L., Shape-Adaptive, Self-Healable Triboelectric Nanogenerator with Enhanced Performances by Soft Solid-Solid Contact Electrification. *ACS Nano* **2019,** *13* (8), 8936-8945.
11. Oh, J. Y.; Rondeau-Gagné, S.; Chiu, Y.-C.; Chortos, A.; Lissel, F.; Wang, G.-J. N.; Schroeder, B. C.; Kurosawa, T.; Lopez, J.; Katsumata, T.; Xu, J.; Zhu, C.; Gu, X.; Bae, W.-G.; Kim, Y.; Jin, L.; Chung, J. W.; Tok, J. B. H.; Bao, Z., Intrinsically stretchable and healable semiconducting polymer for organic transistors. *Nature* **2016,** *539* (7629), 411-415.
12. Vo, N. T. P.; Nam, T. U.; Jeong, M. W.; Kim, J. S.; Jung, K. H.; Lee, Y.; Ma, G.; Gu, X.; Tok, J. B.; Lee, T. I.; Bao, Z.; Oh, J. Y., Autonomous self-healing supramolecular polymer transistors for skin electronics. *Nat Commun* **2024,** *15* (1), 3433.
13. Samanta, S.; Kim, S.; Saito, T.; Sokolov, A. P., Polymers with Dynamic Bonds: Adaptive Functional Materials for a Sustainable Future. *J Phys Chem B* **2021,** *125* (33), 9389-9401.
14. Wu, M.; Han, L.; Yan, B.; Zeng, H., Self-healing hydrogels based on reversible noncovalent and dynamic covalent interactions: A short review. *Supramolecular Materials* **2023,** *2*, 100045.
15. Michael Rubinstein, R. H. C., *Polymer Physics*. Oxford University Press: Oxford, 2003.
16. Volkov, A., Polydimethylsiloxane (PDMS). In *Encyclopedia of Membranes*, Drioli, E.; Giorno, L., Eds. Springer Berlin Heidelberg: Berlin, Heidelberg, 2015; pp 1-2.
17. Qiu, L.; Zhou, Y.; Zhao, Z.; Wang, Q.; Chu, L.; Wen, S., Constructing Self-Healing Polydimethylsiloxane through Molecular Structure Design and Metal Ion Bonding. *Polymers (Basel)* **2024,** *16* (10).
18. Wang, P.; Wang, Z.; Cao, W.; Zhu, J., Facile Preparation of a Transparent, Self-Healing, and Recyclable Polysiloxane Elastomer Based on a Dynamic Imine and Boroxine Bond. *Polymers (Basel)* **2024,** *16* (9).

19. O'Driscoll, D. P.; Vega-Mayoral, V.; Harley, I.; Boland, C. S.; Coleman, J. N., Optimising composite viscosity leads to high sensitivity electromechancial sensors. *2D Materials* **2018,** *5* (3).
20. Zhang, B.; Zhang, P.; Zhang, H.; Yan, C.; Zheng, Z.; Wu, B.; Yu, Y., A Transparent, Highly Stretchable, Autonomous Self-Healing Poly(dimethyl siloxane) Elastomer. *Macromol Rapid Commun* **2017,** *38* (15).
21. Choi, C.; Self, J. L.; Okayama, Y.; Levi, A. E.; Gerst, M.; Speros, J. C.; Hawker, C. J.; Read de Alaniz, J.; Bates, C. M., Light-Mediated Synthesis and Reprocessing of Dynamic Bottlebrush Elastomers under Ambient Conditions. *J Am Chem Soc* **2021,** *143* (26), 9866-9871.
22. Wang, D. P.; Lai, J. C.; Lai, H. Y.; Mo, S. R.; Zeng, K. Y.; Li, C. H.; Zuo, J. L., Distinct Mechanical and Self-Healing Properties in Two Polydimethylsiloxane Coordination Polymers with Fine-Tuned Bond Strength. *Inorg Chem* **2018,** *57* (6), 3232-3242.
23. Ghosh, D.; Khastgir, D., Degradation and Stability of Polymeric High-Voltage Insulators and Prediction of Their Service Life through Environmental and Accelerated Aging Processes. *ACS Omega* **2018,** *3* (9), 11317-11330.
24. He, X.; Wu, J.; Xuan, S.; Sun, S.; Gong, X., Stretchable and Recyclable Liquid Metal Droplets Embedded Elastomer Composite with High Mechanically Sensitive Conductivity. *ACS Appl Mater Interfaces* **2022,** *14* (7), 9597-9607.
25. Wu, T.; Chen, B., Synthesis of Multiwalled Carbon Nanotube-Reinforced Polyborosiloxane Nanocomposites with Mechanically Adaptive and Self-Healing Capabilities for Flexible Conductors. *ACS Appl Mater Interfaces* **2016,** *8* (36), 24071-8.
26. Zhang, K.; Sun, J.; Song, J.; Gao, C.; Wang, Z.; Song, C.; Wu, Y.; Liu, Y., Self-Healing Ti(3)C(2) MXene/PDMS Supramolecular Elastomers Based on Small Biomolecules Modification for Wearable Sensors. *ACS Appl Mater Interfaces* **2020,** *12* (40), 45306-45314.
27. Papon, A.; Montes, H.; Lequeux, F.; Oberdisse, J.; Saalwächter, K.; Guy, L., Solid particles in an elastomer matrix: impact of colloid dispersion and polymer mobility modification on the mechanical properties. *Soft Matter* **2012,** *8* (15).
28. Merabia, S.; Sotta, P.; Long, D. R., A Microscopic Model for the Reinforcement and the Nonlinear Behavior of Filled Elastomers and Thermoplastic Elastomers (Payne and Mullins Effects). *Macromolecules* **2008,** *41* (21), 8252-8266.
29. Tian, C.; Cui, J.; Ning, N.; Zhang, L.; Tian, M., Quantitative characterization of interfacial properties of carbon black/elastomer nanocomposites and mechanism exploration on their interfacial interaction. *Composites Science and Technology* **2022,** *222*, 109367.
30. Winey, K. I.; Vaia, R. A., Polymer Nanocomposites. *MRS Bulletin* **2011,** *32* (4), 314-322.
31. Vega, J. F.; da Silva, Y.; Vicente-Alique, E.; Núñez-Ramírez, R.; Trujillo, M.; Arnal, M. L.; Müller, A. J.; Dubois, P.; Martínez-Salazar, J., Influence of Chain Branching and Molecular Weight on Melt Rheology and Crystallization of Polyethylene/Carbon Nanotube Nanocomposites. *Macromolecules* **2014,** *47* (16), 5668-5681.
32. Ding, W.; Eitan, A.; Fisher, F. T.; Chen, X.; Dikin, D. A.; Andrews, R.; Brinson, L. C.; Schadler, L. S.; Ruoff, R. S., Direct Observation of Polymer Sheathing in Carbon Nanotube−Polycarbonate Composites. *Nano Letters* **2003,** *3* (11), 1593-1597.
33. Wu, F.; Zhang, S.; Chen, Z.; Zhang, B.; Yang, W.; Liu, Z.; Yang, M., Interfacial relaxation mechanisms in polymer nanocomposites through the rheological study on polymer/grafted nanoparticles. *Polymer* **2016,** *90*, 264-275.
34. Qu, M.; Deng, F.; Kalkhoran, S. M.; Gouldstone, A.; Robisson, A.; Van Vliet, K. J., Nanoscale visualization and multiscale mechanical implications of bound rubber interphases in rubber–carbon black nanocomposites. *Soft Matter* **2011,** *7* (3), 1066-1077.
35. Schadler, L. S.; Kumar, S. K.; Benicewicz, B. C.; Lewis, S. L.; Harton, S. E., Designed Interfaces in Polymer Nanocomposites: A Fundamental Viewpoint. *MRS Bulletin* **2007,** *32* (4), 335-340.

36. Oberhausen, B.; Kickelbick, G., Induction heating induced self-healing of nanocomposites based on surface-functionalized cationic iron oxide particles and polyelectrolytes. *Nanoscale Adv* **2021,** *3* (19), 5589-5604.
37. Zhu, C.; Fu, Y.; Liu, C.; Liu, Y.; Hu, L.; Liu, J.; Bello, I.; Li, H.; Liu, N.; Guo, S.; Huang, H.; Lifshitz, Y.; Lee, S. T.; Kang, Z., Carbon Dots as Fillers Inducing Healing/Self-Healing and Anticorrosion Properties in Polymers. *Adv Mater* **2017,** *29* (32).
38. Wang, C.; Liu, N.; Allen, R.; Tok, J. B.; Wu, Y.; Zhang, F.; Chen, Y.; Bao, Z., A rapid and efficient self-healing thermo-reversible elastomer crosslinked with graphene oxide. *Adv Mater* **2013,** *25* (40), 5785-90.
39. Li, C. H.; Zuo, J. L., Self-Healing Polymers Based on Coordination Bonds. *Adv Mater* **2020,** *32* (27), e1903762.
40. Sarkar, B.; Alexandridis, P., Block copolymer–nanoparticle composites: Structure, functional properties, and processing. *Progress in Polymer Science* **2015,** *40*, 33-62.
41. Du, F.; Scogna, R. C.; Zhou, W.; Brand, S.; Fischer, J. E.; Winey, K. I., Nanotube Networks in Polymer Nanocomposites: Rheology and Electrical Conductivity. *Macromolecules* **2004,** *37* (24), 9048-9055.
42. Hu, G.; Zhao, C.; Zhang, S.; Yang, M.; Wang, Z., Low percolation thresholds of electrical conductivity and rheology in poly(ethylene terephthalate) through the networks of multi-walled carbon nanotubes. *Polymer* **2006,** *47* (1), 480-488.
43. Penu, C.; Hu, G. H.; Fernandez, A.; Marchal, P.; Choplin, L., Rheological and electrical percolation thresholds of carbon nanotube/polymer nanocomposites. *Polymer Engineering & Science* **2012,** *52* (10), 2173-2181.
44. Boland, C. S.; Khan, U.; Ryan, G.; Barwich, S.; Charifou, R.; Harvey, A.; Backes, C.; Li, Z.; Ferreira, M. S.; Möbius, M. E.; Young, R. J.; Coleman, J. N., Sensitive electromechanical sensors using viscoelastic graphene-polymer nanocomposites. *Science* **2016,** *354* (6317), 1257-1260.
45. Garboczi, E. J.; Snyder, K. A.; Douglas, J. F.; Thorpe, M. F., Geometrical percolation threshold of overlapping ellipsoids. *Phys Rev E Stat Phys Plasmas Fluids Relat Interdiscip Topics* **1995,** *52* (1), 819-828.
46. Mergen, Ö. B.; Arda, E.; Evingür, G. A., Electrical, optical and mechanical properties of chitosan biocomposites. *Journal of Composite Materials* **2019,** *54* (11), 1497-1510.
47. Ivanova, R.; Kotsilkova, R., Rheological study of poly (lactic) acid nanocomposites with carbon nanotubes and graphene additives as a tool for materials characterization for 3D printing application. *Applied Rheology* **2018,** *28* (5), 201854014.
48. Klatt, M. A.; Schröder-Turk, G. E.; Mecke, K., Anisotropy in finite continuum percolation: threshold estimation by Minkowski functionals. *Journal of Statistical Mechanics: Theory and Experiment* **2017,** *2017* (2).
49. Tarasevich, Y. Y.; Eserkepov, A. V., Percolation of sticks: Effect of stick alignment and length dispersity. *Physical Review E* **2018,** *98* (6).
50. Balberg, I.; Binenbaum, N., Computer study of the percolation threshold in a two-dimensional anisotropic system of conducting sticks. *Physical Review B* **1983,** *28* (7), 3799-3812.
51. Yakovenko, O.; Matzui, L.; Vovchenko, L.; Zhuravkov, A., Development of carbon nanotube-polymer composites with oriented distribution of MWCNTs induced by electric field. *physica status solidi (a)* **2014,** *211* (12), 2718-2722.
52. Dong, S.; Wu, X.; Wang, E.; Wang, X., Reduced percolation threshold of multi-walled carbon nanotubes/polymer composites by filling aligned ferromagnetic particles. *Journal of Intelligent Material Systems and Structures* **2019,** *31* (2), 187-197.
53. Zhang, Z.; Hu, L.; Wang, R.; Zhang, S.; Fu, L.; Li, M.; Xiao, Q., Advances in Monte Carlo Method for Simulating the Electrical Percolation Behavior of Conductive Polymer Composites with a Carbon-Based Filling. *Polymers (Basel)* **2024,** *16* (4).

54. Payne, A.; Whittaker, R., Low strain dynamic properties of filled rubbers. *Rubber chemistry and technology* **1971,** *44* (2), 440-478.
55. Heinrich, G.; Klüppel, M., Recent Advances in the Theory of Filler Networking in Elastomers. In *Filled Elastomers Drug Delivery Systems*, Springer Berlin Heidelberg: Berlin, Heidelberg, 2002; pp 1-44.
56. Yurekli, K.; Krishnamoorti, R.; Tse, M. F.; McElrath, K. O.; Tsou, A. H.; Wang, H. C., Structure and dynamics of carbon black-filled elastomers. *Journal of Polymer Science Part B: Polymer Physics* **2001,** *39* (2), 256-275.
57. Haring, M.; Diaz, D. D., Supramolecular metallogels with bulk self-healing properties prepared by in situ metal complexation. *Chem Commun (Camb)* **2016,** *52* (89), 13068-13081.
58. Hou, K. X.; Zhao, S. P.; Wang, D. P.; Zhao, P. C.; Li, C. H.; Zuo, J. L., A Puncture-Resistant and Self-Healing Conductive Gel for Multifunctional Electronic Skin. *Advanced Functional Materials* **2021,** *31* (49).
59. Mours, M.; Winter, H. H., Chapter 5 - Mechanical Spectroscopy of Polymers. In *Experimental Methods in Polymer Science*, Tanaka, T., Ed. Academic Press: Boston, 2000; pp 495-546.
60. Leibler, L.; Rubinstein, M.; Colby, R. H., Dynamics of reversible networks. *Macromolecules* **1991,** *24* (16), 4701-4707.
61. Golkaram, M.; Loos, K., A Critical Approach to Polymer Dynamics in Supramolecular Polymers. *Macromolecules* **2019,** *52* (24), 9427-9444.
62. Chen, Q.; Tudryn, G. J.; Colby, R. H., Ionomer dynamics and the sticky Rouse model. *Journal of Rheology* **2013,** *57* (5), 1441-1462.
63. Shabbir, A.; Javakhishvili, I.; Cerveny, S.; Hvilsted, S.; Skov, A. L.; Hassager, O.; Alvarez, N. J., Linear Viscoelastic and Dielectric Relaxation Response of Unentangled UPy-Based Supramolecular Networks. *Macromolecules* **2016,** *49* (10), 3899-3910.
64. You, W.; Yu, W., Slow Linear Viscoelastic Relaxation of Polymer Nanocomposites: Contribution from Confined Diffusion of Nanoparticles. *Macromolecules* **2019,** *52* (23), 9094-9104.
65. Sreenilayam, S. P.; Ahad, I. U.; Nicolosi, V.; Acinas Garzon, V.; Brabazon, D., Advanced materials of printed wearables for physiological parameter monitoring. *Materials Today* **2020,** *32*, 147-177.
66. Gao, Z.; Xiao, X.; Carlo, A. D.; Yin, J.; Wang, Y.; Huang, L.; Tang, J.; Chen, J., Advances in Wearable Strain Sensors Based on Electrospun Fibers. *Advanced Functional Materials* **2023,** *33* (18).
67. Wang, W.; Yang, S.; Ding, K.; Jiao, L.; Yan, J.; Zhao, W.; Ma, Y.; Wang, T.; Cheng, B.; Ni, Y., Biomaterials- and biostructures Inspired high-performance flexible stretchable strain sensors: A review. *Chemical Engineering Journal* **2021,** *425*.
68. Koivikko, A.; Lampinen, V.; Pihlajamäki, M.; Yiannacou, K.; Sharma, V.; Sariola, V., Integrated stretchable pneumatic strain gauges for electronics-free soft robots. *Communications Engineering* **2022,** *1* (1).
69. Li, T.; Su, Y.; Chen, F.; Zheng, H.; Meng, W.; Liu, Z.; Ai, Q.; Liu, Q.; Tan, Y.; Zhou, Z., Bioinspired Stretchable Fiber-Based Sensor toward Intelligent Human-Machine Interactions. *ACS Appl Mater Interfaces* **2022,** *14* (19), 22666-22677.
70. Guo, J.; Zhao, K.; Zhou, B.; Ning, W.; Jiang, K.; Yang, C.; Kong, L.; Dai, Q., Wearable and Skin-Mountable Fiber-Optic Strain Sensors Interrogated by a Free-Running, Dual-Comb Fiber Laser. *Advanced Optical Materials* **2019,** *7* (12).
71. Zhao, R.; He, Y.; He, Y.; Li, Z.; Chen, M.; Zhou, N.; Tao, G.; Hou, C., Dual-Mode Fiber Strain Sensor Based on Mechanochromic Photonic Crystal and Transparent Conductive Elastomer for Human Motion Detection. *ACS Appl Mater Interfaces* **2023,** *15* (12), 16063-16071.

72. Zhang, X.; Zhou, R.; Yang, F.; Zhang, J.; Wu, X., Bioinspired Potentiometric and Passive Strain Sensing Based on Mechanical Regulation of Ionically Conductive Percolating Networks. *Advanced Materials Technologies* **2024**.
73. Sun, R.; Carreira, S. C.; Chen, Y.; Xiang, C.; Xu, L.; Zhang, B.; Chen, M.; Farrow, I.; Scarpa, F.; Rossiter, J., Stretchable Piezoelectric Sensing Systems for Self-Powered and Wireless Health Monitoring. *Advanced Materials Technologies* **2019,** *4* (5).
74. Kim, S. R.; Kim, J. H.; Park, J. W., Wearable and Transparent Capacitive Strain Sensor with High Sensitivity Based on Patterned Ag Nanowire Networks. *ACS Appl Mater Interfaces* **2017,** *9* (31), 26407-26416.
75. Li, S.; Liu, G.; Li, R.; Li, Q.; Zhao, Y.; Huang, M.; Zhang, M.; Yin, S.; Zhou, Y.; Tang, H.; Wang, L.; Fang, G.; Su, Y., Contact-Resistance-Free Stretchable Strain Sensors with High Repeatability and Linearity. *ACS Nano* **2022,** *16* (1), 541-553.
76. Choi, S.; Lee, S.; Lee, B.; Yoon, J.; Lee, C. Y.; Kim, T.; Hong, Y., Crack-inducing Strain Sensor Array using Inkjet-Printed Silver Thin Film for Underplate and Off-centered Force Sensing Applications. *ACS Appl Mater Interfaces* **2023,** *15* (3), 4487-4494.
77. Liu, J.; Weng, L.; Zhang, X.; Wu, Z., Ultrasonic-Assisted Freeze-Drying for Polyimide/Carboxylated MWCNTs Aerogel Sensor with Excellent Aging Sensing Performance. *Advanced Materials Technologies* **2023,** *8* (23).
78. Boland, C. S., Stumbling through the Research Wilderness, Standard Methods To Shine Light on Electrically Conductive Nanocomposites for Future Healthcare Monitoring. *ACS Nano* **2019,** *13* (12), 13627-13636.
79. Ma, L.; Yang, W.; Wang, Y.; Chen, H.; Xing, Y.; Wang, J., Multi-dimensional strain sensor based on carbon nanotube film with aligned conductive networks. *Composites Science and Technology* **2018,** *165*, 190-197.
80. Boland, C. S., Quantifying the Contributing Factors toward Signal Fatigue in Nanocomposite Strain Sensors. *ACS Applied Polymer Materials* **2020,** *2* (8), 3474-3480.
81. Innocent, M. T.; Zhang, Z.; Boland, C. S.; Cao, R.; Hu, Z.; Geng, Y.; Zhai, G.; Liu, F.; Dai, H.; Chen, Z.; Zhang, Z.; Xiang, H.; Zhu, M., Electromechanical Properties and Resistance Signal Fatigue of Piezoresistive Fiber-Based Strain Gauges. *ACS Applied Polymer Materials* **2022,** *4* (11), 8335-8343.
82. Zhu, G. J.; Ren, P. G.; Guo, H.; Jin, Y. L.; Yan, D. X.; Li, Z. M., Highly Sensitive and Stretchable Polyurethane Fiber Strain Sensors with Embedded Silver Nanowires. *ACS Appl Mater Interfaces* **2019,** *11* (26), 23649-23658.
83. Ding, Y.; Yang, J.; Tolle, C. R.; Zhu, Z., A highly stretchable strain sensor based on electrospun carbon nanofibers for human motion monitoring. *RSC Advances* **2016,** *6* (82), 79114-79120.
84. Wang, Y.; Hao, J.; Huang, Z.; Zheng, G.; Dai, K.; Liu, C.; Shen, C., Flexible electrically resistive-type strain sensors based on reduced graphene oxide-decorated electrospun polymer fibrous mats for human motion monitoring. *Carbon* **2018,** *126*, 360-371.
85. Zhang, P.; Chen, Y.; Li, Y.; Zhang, Y.; Zhang, J.; Huang, L., A Flexible Strain Sensor Based on the Porous Structure of a Carbon Black/Carbon Nanotube Conducting Network for Human Motion Detection. *Sensors (Basel)* **2020,** *20* (4).
86. Wang, X.; Liu, X.; Schubert, D. W., Highly Sensitive Ultrathin Flexible Thermoplastic Polyurethane/Carbon Black Fibrous Film Strain Sensor with Adjustable Scaffold Networks. *Nanomicro Lett* **2021,** *13* (1), 64.
87. Zhan, P.; Zhai, W.; Wang, N.; Wei, X.; Zheng, G.; Dai, K.; Liu, C.; Shen, C., Electrically conductive carbon black/electrospun polyamide 6/poly(vinyl alcohol) composite based strain sensor with ultrahigh sensitivity and favorable repeatability. *Materials Letters* **2019,** *236*, 60-63.

88. Zhang, Z.; Chen, G.; Xue, Y.; Duan, Q.; Liang, X.; Lin, T.; Wu, Z.; Tan, Y.; Zhao, Q.; Zheng, W.; Wang, L.; Wang, F.; Luo, X.; Xu, J.; Liu, J.; Lu, B., Fatigue-Resistant Conducting Polymer Hydrogels as Strain Sensor for Underwater Robotics. *Advanced Functional Materials* **2023,** *33* (42).
89. Innocent, M. T.; Zhang, Z.; Cao, R.; Dai, H.; Zhang, Y.; Geng, Y.; Zhang, Z.; Jia, G.; Zhai, M.; Hu, Z.; Boland, C. S.; Xiang, H.; Zhu, M., Piezoresistive Fibers with Large Working Factors for Strain Sensing Applications. *ACS Appl Mater Interfaces* **2023,** *15* (1), 2277-2288.
90. Boland, C. S.; O'Driscoll, D. P.; Kelly, A. G.; Boland, J. B.; Coleman, J. N., Highly Sensitive Composite Foam Bodily Sensors Based on the g-Putty Ink Soaking Procedure. *ACS Appl Mater Interfaces* **2021,** *13* (50), 60489-60497.

5. Publication list

Included in dissertation

1. **Milkin P**.; Danzer M.; Ionov L. Self-Healing and Electrical Properties of Viscoelastic Polymer-Carbon Blends. *Macromolecular Rapid Communications* 2022, 43 (19). https://doi.org/10.1002/marc.202200307
2. **Milkin P.;** Zhanbassynova A.; Ionov L., Superelastic, soft, stress-healable, recyclable conductive materials. *Composite Structures* 2024, 327. https://doi.org/10.1016/j.compstruct.2023.117709
3. **Milkin P.,** Pavale S., Soreno Z., Ionov L. Fiber-Reinforced Super Self-Healing Flexible strain sensor. S*ubmitted in ACS Applied Materials & Interfaces,* 2024

Not included in dissertation

1. Vertegel P., **Milkin P.**, Murashko A., Parker M., Peranidze K., Yemashova N., Minko S., Reukov V. Cell Detachment: A Review of Techniques, Challenges, and Opportunities for Advancing Biomedical Research and Applications (2024), *submitted in ACS Applied Bio Materials.* https://doi.org/10.1021/acsami.4c10751
2. Sprenger L., Lu H., Trippmacher S., Mansfeld U., **Milkin P.**, Ionov L., Papastavrou G., Boccaccini A., Salehi-Müller S. Composite alginate dialdehyde-gelatin (ADA-GEL) hydrogel containing short ribbon-shaped fillers for skeletal muscle tissue biofabrication, *ACS Applied Materials & Interfaces 2024,*
3. Constante G., Apsite I., Auerbach P., Aland S., Schönfeld D., Pretsch T., **Milkin P**., Ionov L. Smart mechanically tunable surfaces with shape memory behavior and wetting-programmable topography, *ACS applied materials and interfaces,* 2022, 14, 17, 20208-20219. https://doi.org/10.1021/acsami.2c01078
4. Xu R., Bermudez G., Pylypovskyi O., Volkov O., Mata E., Zabila Y., Illing R., Makushko P., **Milkin P.,** Ionov L., Fassbender J., Makarov D. Self-healable printed magnetic field sensors using alternating magnetic fields. *Nature Communications*, 2022, 13, 1, 6587. https://doi.org/10.1038/s41467-022-34235-3
5. Orlov N., Kiseleva A., **Milkin P.,** Evdokimov P., Putlayev V., Günster J., Biesuz M., Sglavo V.M., Tyablikov A. Sintering of mixed Ca–K–Na phosphates: Spark plasma sintering vs flash-sintering. *Open Ceramics*, 2021, 5, 100072. https://doi.org/10.1016/j.oceram.2021.100072

6. Individual contribution to publications and manuscripts

1. **Milkin P**.; Danzer M.; Ionov L. Self-Healing and Electrical Properties of Viscoelastic Polymer-Carbon Blends (2022). *Macromolecular Rapid Communications* 2022, 43 (19). https://doi.org/10.1002/marc.202200307

The concept of research was developed by Leonid Ionov and myself. Material and sample preparation, rheology, EIS, SEM as well as the analysis of obtained data were carried out by myself. Prof. Danzer has provided analysis of distribution of relaxation times for EIS results. The Manuscript (text and images) were created by myself and modified by Prof. Ionov. Prof. Ionov supervised the project and contributed to the completion of the manuscript.

2. **Milkin P.;** Zhanbassynova A.; Ionov L., Superelastic, soft, stress-healable, recyclable conductive materials (2024). *Composite Structures* 2024, 327. https://doi.org/10.1016/j.compstruct.2023.117709

The concept of research was developed by Leonid Ionov and myself. Material and sample preparation and rheology were performed by Ainur Zhanbassynova and myself. Tensile test, EIS, SEM as well as the analysis of obtained data were carried out by myself. The Manuscript (text and images) were created by myself and modified by Prof. Ionov. Prof. Ionov supervised the project and contributed to the completion of the manuscript.

3. **Milkin P.,** Pavale S., Soreno Z., Ionov L. Fiber-Reinforced Super Self-Healing Flexible strain sensor (2024) (*submitted in ACS Applied Materials & Interfaces*)…

The concept of research was developed by Leonid Ionov and myself. Electrospinning was performed by Shubham Pavale and Zhander Soreno. Material and sample preparation, electromechanical characterization as well as the analysis of obtained data were performed by Shubham Pavale and myself. SEM and TGA were carried out by myself. The Manuscript (text and images) were created by myself and modified by Prof. Ionov. Prof. Ionov supervised the project and contributed to the completion of the manuscript.

Publications

Part 1. Self-Healing and Electrical Properties of Viscoelastic Polymer-Carbon Blends

Milkin P.; Danzer M.; Ionov L.

Published in Macromolecular Rapid Communications, 43 (19)

2022

RESEARCH ARTICLE

Macromolecular Rapid Communications
www.mrc-journal.de

Self-Healing and Electrical Properties of Viscoelastic Polymer–Carbon Blends

*Pavel Milkin, Michael Danzer, and Leonid Ionov**

Self-healing polymer–carbon composites are seen as promising materials for future electronic devices, which must be able to restore not only their structural integrity but also electrical performance after cracking and wear. Despite multiple reports about self-healing conductive elements, there is a lack of a broad fundamental understanding of correlation between viscoelasticity of such composites, their electrical properties, and self-healing of their mechanical as well as electrical properties. Here, it is reported thorough investigation of electromechanical properties of blends of carbon black (CB) as conductive filler and viscoelastic polymers (polydimethylsiloxanes (PDMS) and polyborosiloxane (PBS)) with different relaxation times as matrices. It is shown that behavior of composites depends strongly on the viscoelastic properties of polymers. Low molecular polymer composite possesses high conductivity due to strong filler network formation, quick electrical, and mechanical properties restoration, but for this the ability is sacrificed to flow and ductility at large deformation (material is brittle). In contrary, high relaxation time polymer composite behaves elastically on small time and flows at large time scale due to weak filler network and can heal. However, the electrical properties are worse than that of carbon and viscous polymer and degrade with time.

1. Introduction

Nowadays, electronic devices are ineradicably integrated into our everyday life. They underwent evolution from calculators occupying an entire room to nanoscale transistors that now ensure the operation of any circuit board. One important field is wearable, flexible electronics, which can be integrated, for example, in apparel. One essential problem of flexible electronics is its robustness—materials must be able to withstand multiple cycles of bending or stretching.[1] All solid materials inevitably undergo failure after many loading/unloading cycles. As results, devices endure failure due to mechanical or electrical stress and cannot be easily repaired that contributes to the E-waste problem.[2] Furthermore, such electronics contain nondegradable polymers (polyethers, polyimide, etc.) and metals, which require proper recycling to avoid environmental pollution.[3,4] On the other hand, nature shows that living organisms can fight for survival against injuries, by repairing damaged tissues through self-healing. This ability of living organisms inspired scientists to develop materials, which are able to heal cracks after failure.

Due to this, self-healing polymers have recently attracted attention to solve the problem of degradation and failure of soft electronic devices as well as to eliminate their fragility, existing fatigue strength, and weakness of contacts with metal conductors within the time.[5–7] The self-healing may include mechanisms of autogenous healing,[8] vascular,[9] and capsule-based[10] materials, shape memory effect,[11] and reformation of different chemical bonds.[2,12,13] The last one provides unlimited self-healing capability and seems as most promising. Self-healing in such polymers goes through reactions of metal–ligand coordination,[14] H-bonding,[15] $\pi-\pi$ stacking,[16] dynamic covalent bonding,[17] etc. These mechanisms require relatively high mobility of chain segments to implement the self-healing purpose. Therefore, these not-electrically-conductive polymers, which are used in their viscoelastic state above glass transition temperature, are combined with functional fillers with electrical properties.[18,19] In such blends, the matrix and filler impart viscoelastic material properties as a combination of both, which are important to consider in various applications. In most cases, research was focused on restoration of integrity of broken objects and their mechanical properties. Restoration of other functionalities such as electrical conductivity of materials is also an important topic.[20,21]

Functionality of self-healing materials is often achieved by blending self-healing polymers and functional filler. Therefore, the understanding the matrix-filler interaction of such systems

P. Milkin, L. Ionov
Faculty of Engineering Sciences
University of Bayreuth
Ludwig Thoma Str. 36A, Bayreuth 95447, Germany
E-mail: leonid.ionov@uni-bayreuth.de
M. Danzer
Chair of Electrical Energy Systems
University of Bayreuth
Universistätsstr. 30, Bayreuth 95447, Germany
L. Ionov
Bavarian Polymer Institute
University of Bayreuth
Bayreuth 95447, Germany

The ORCID identification number(s) for the author(s) of this article can be found under https://doi.org/10.1002/marc.202200307

DOI: 10.1002/marc.202200307

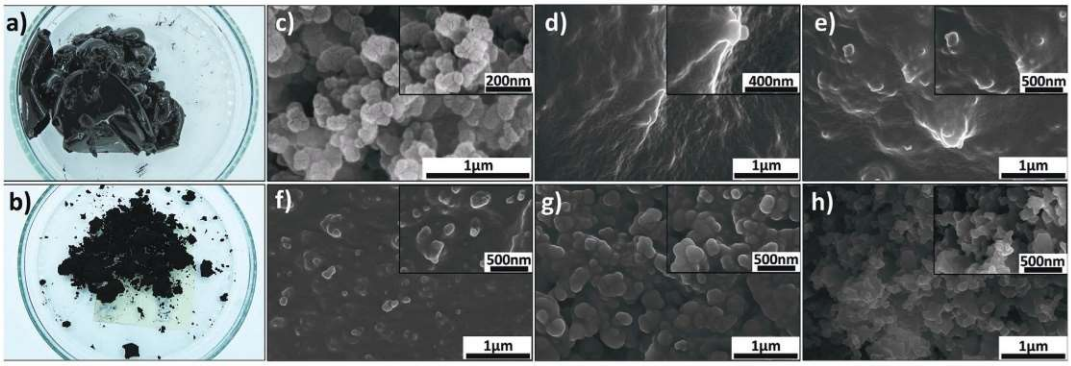

Figure 1. Morphology of polymer–carbon blends: a) image of PDMS 105 cSt, 5 vol% of CB. b) image of PDMS 10^5 cSt 20 vol% of CB. c) SEM images of prictine CB. SEM images of PDMS 10^5 cSt – CB composites with d) 5 vol%, e) 10 vol%, f) 15 vol%, g) 20 vol%, h) 30 vol%.

is the key to meaningful tailoring material properties. However, many papers on this topic present scarce data obtained by one or another rheological method that does not allow building a complete picture of viscoelastic properties of a viscoelastic self-healing matrix and a functional filler. As an example of a viscoelastic matrix, the Silly–Putty, PBS based material, may be considered. Several authors used composites based on PBS—and several carbon fillers (graphene, multiwalled carbon nanotubes) as a pressure sensor,[18] strain rate sensor,[22] triboelectric nanogenerator,[23] gas sensor,[24] and do demonstrate their functionality. Nevertheless, authors leave a significant block behind the scenes of the choice of polymer, its interaction with filler while providing scanty rheological investigation and demonstrating material properties out of its linear range of electrical and mechanical responses without a bit of justification of applicability and reliability of such conditions for actual devices.[25] Including the electrical characteristics are often measured at one particular voltage, assuming that Ohm´s law is fulfilled in the whole voltage range. However, the volt-ampere characteristic of such materials may be nonlinear.[24,26]

In this study, we performed a thorough investigation of the influence of different PDMS/PBS polymer matrices on the electromechanical properties of carbon-based composites. In comparison to other studies, we seek to elucidate the applicability limits of such materials through detailed rheological, mechanical, and electrical investigation instead of considering any specific application field. Carbon black was chosen as a model conductive carbon filler with various concentrations. The filler-polymer interaction in such composites, the viscoelastic properties, relaxation processes, and electrical conductivity mechanisms of material are discussed.

2. Experimental Results

2.1. Pure Materials

To understand the influence of polymer on the rheological and self-healing behavior of carbon–polymer composites, we prepared blends of carbon black as conductive filler and polydimethylsiloxanes (PDMS) as a matrix with up to 30 vol% of nanoparticles. The carbon black particles are ≈48 nm in size, according to Brunauer-Emmett-Teller analysis results, assuming spherical particles shape. As matrix material, three polydimethylsiloxane-based polymers of different molecular weights (Figure S5, Supporting Information) with various relaxation times were chosen. The first one is linear PDMS 65 cSt, which is a linear polymer with a molecular mass (M_w = 6.5 kg mol^{-1}) lower than the critical molecular mass (M_c = 24.5 kg mol^{-1}[27]) when entanglements start to play an important role. The relaxation time is low and cannot be measured, the polymer behaves as Newtonian liquid. The second one is PDMS 2×10^7 cSt, a viscoelastic polymer (M_w = 388 kg mol^{-1}) with ≈32 entanglements per chain. Its average relaxation time $\lambda \approx 0.1$ s (Figure S5, Supporting Information), although the relaxation time peak is quite broad due to high polydispersity. Due to high polydispersity, the elastic plateau cannot be achieved but is expected to be in the range between 0.1 and 1 MPa, meaning that the polymer behaves as a melt. The third polymer—polyborosiloxane (PBS)—is a product of polycondensation of boric acid and hydroxy-terminated PDMS, creating crosslinked network due to Si–O–B bonds and supramolecular structure through hydrogen and dative Si–O:B bonds.[28] The effective degree of polymerization is about 3650 monomer units per chain which is much higher than ≈90 units per chain for the initial PDMS oligomer (Figure S1b, Supporting Information). The PBS has two relaxations times. First one is at around 1 s, which is relaxation time of polymer chain. The other relaxation process is the fast relaxation of supramolecular structure with $\lambda \leq$ 10–3 s.[28] The $G´$ at the plateau is ≈4 kPa that is lower than that of polymer melts (≈0.5 MPa), meaning that the polymer behaves as an entangled solution, where a solvent is initial low molecular weight PDMS. The $G´$ of PDMS melt at the elastic plateau is ≈0.5 MPa meaning that $G´$(solution)/$G´$(melt) = 0.01 that gives the concentration of very long chains in solvent formed by short chains 10%.[29] The rise in the ratio of boric acid to hydroxyl-terminated PDMS results in increased relaxation time and $G´$ at the elastic plateau (Figure S4, Supporting Information).

Visual appearance of blends. We observed that carbon volume fraction strongly affects the appearance and mechanical properties of blends (**Figure 1**). Blends with a low fraction of carbon

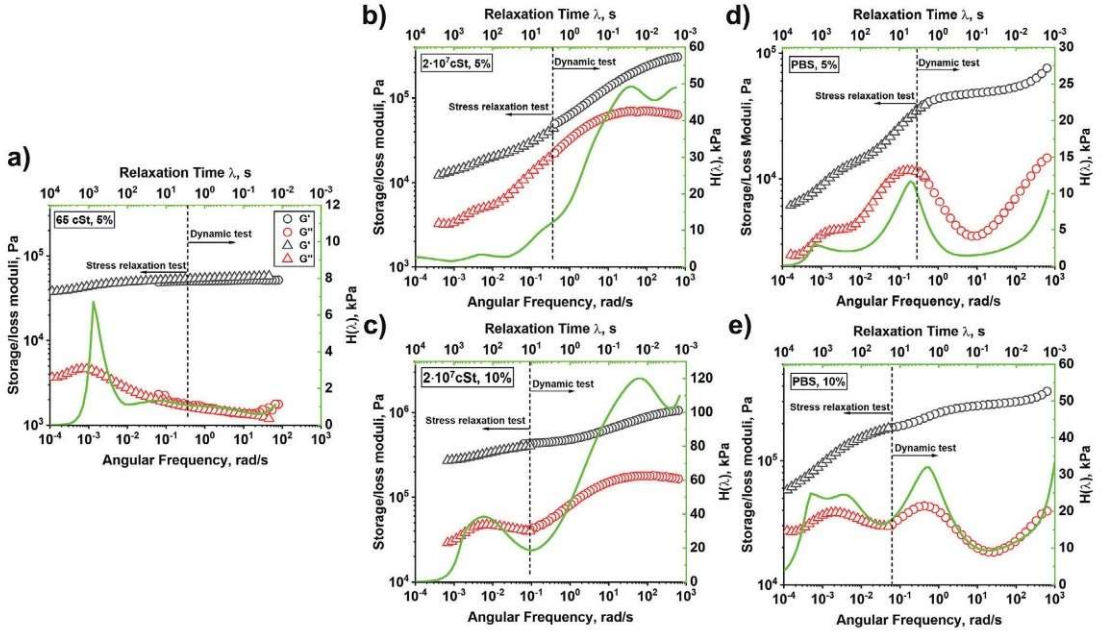

Figure 2. Viscoelastic behavior of PDMS-carbon blends at small deformation: a) PDMS 65 cSt 5% CB; PDMS 2×10^7 cSt b) 5% CB and c) 10% CB; PBS d) 5% CB and e) 10% CB. Storage and loss moduli were obtained from both relaxation and dynamic experiments demonstrate viscoelastic behavior ranging from around 10^{-4} to 10^3 rad s^{-1}. The relaxation spectra were calculated from merged experiments reveal the polymer and carbon black particle network's relaxation processes.

nanoparticles (5–10%) behave as dough. Nanoparticles are meanwhile barely observable on the surface of the polymer. An increase in the fraction of nanoparticles makes them visible on the surface. At CB content larger than 10 vol%, the composites become brittle and start behaving as a wet sand rather than as dough-like material. Thus, composites with 5 and 10 vol% of CB were chosen for further experiments

2.2. Viscoelastic Behavior of Blends at Small Deformations

Next, we studied the viscoelastic behavior of blends at small deformation, which does not introduce structural changes in materials (linear viscoelastic regime, $\epsilon = 0.05\%$). Frequency sweep experiment performed in the range 10^{-2}–10^2 Hz shows that for blends of PDMS 65 cSt with 5% and 10%, both storage and loss moduli increase with the rise of carbon content (Figures S2, S3, and S5, Supporting Information). The blends behave as elastic materials over the whole studied frequency range ($G' > G''$) and moduli are nearly independent of frequency. It means that the materials are stable and do not flow on studied time scale at small deformation, i.e., small stress. Viscoelastic properties of blends of carbon with PDMS 2×10^7 cSt and PBS are more complex. We observed the relaxation process on a time scale close to the relaxation time of corresponding polymers. This effect becomes less pronounced with the growth in carbon content. The transition to terminal flow regime was not observed within studied frequency range, and G' is always larger than G'' as well, confirming the stability of material at small deformation. Thus, it is notable that the addition of carbon nanoparticles to polymers renders its elastic properties—even blends of PDMS 65 cSt, which is Newtonian liquid, start to behave as pure elastic materials. The observed rheological behavior of blends of PDMS 2×10^7 cSt and PBS with carbon show that it is a combination of viscoelastic properties provided by particles, similar to ones exhibited by PDMS 65 cSt blends, viscoelastic properties of long polymer chains and their interaction.

A relatively narrow probed time-scale range does not allow understanding of the whole picture of the viscoelastic behavior of the blends. Therefore, we combined frequency sweep and stress relaxation experiment to cover a broad time scale range in the range 10^{-2}–10^4 s (**Figure 2**; and Figure S7, Supporting Information). The obtained results have been used for reconstruction of the dependence of G' and G'' on the frequency and relaxation spectra according to Equations (3)–(6). It is important that all blends do not demonstrate transition to terminal flow regime even on the largest time scale and G' is always larger than G''. Relaxation time spectra of blends with the shortest PDMS (65 cSt) show a single weak peak at large time and nearly no relaxation of stress. The spectra of blends with long PDMS (2×10^7 cSt) chains and PBS contain two peaks: one at a short time scale (10^{-2}–10^1 s) and one at a large time scale (10^2–10^3 s). The position of the first peak nearly does not change with the increase in particle content (Figure 2). This peak can be

Table 1. Amplitude sweep data for shear strain and stress at G'' and sol–gel transition/breakage points for polymers blends with various CB content.

Polymer matrix	vol% of CB	Elongation at max G'' [%]	Stress at max G'' [kPa]	Elongation at $G'' = G'$ [%]	Stress at $G'' = G'$ [kPa]
65 cSt	5	1.5	0.6	5.1	0.7
	10	0.9	5.8	9.4	7.7
2×10^7 cSt	0	—	—	52	16
	5	—	—	21	13
	10	1.3	6	49	48
PBS	0	—	—	206	5
	5	1.8	0.2	130	13
	10	0.8	1.6	82	32

Properties of PDMS 2×10^7 cSt are also affected by the presence of the carbon. As discussed above, PDMS 2×10^7 cSt blends have elastic behavior at small deformation: $G' > G''$. Rise of amplitude to 0.1% results in deviations from the linear regime. No maximum of G'' was observed at a low concentration of carbon that is most probably due to the domination of mechanic properties of PDMS: PDMS 2×10^7 has a much higher elastic modulus than particle network does. Similar to PDMS 65 cSt blend, maximum for 10% of carbon in blend with PDMS 2×10^7 cSt was observed at $\epsilon = 1.3\%$. However, the further increase in amplitude does not result in G'' dominating G' and only at $\epsilon = 21\%$ and 49% for 5 and 10 vol% of carbon, respectively, at which pure polymer fails, G'' becomes larger than G'. The failure has a different character depending on the fraction of particles: 5% blend fail with drop of stress upon increase of strain, which is usual behavior of pure polymer; 10% blend shows plastic behavior that is similar to that of blends of low molecular weight PDMS (65 cSt) and stress is independent of deformation above flow point. This observation can be explained by the assumption that polymer determines failure at low particle content, and particles determine failure at their high content.

Blends of PBS with carbon particles behave as elastomer-particle blends described by Payne[30]—G' is constant at small deformation, an increase of amplitude results in its gradual decrease, accompanied by a pronounced peak of G'', and then it again becomes constant. Similar to the previous two cases, an increase of amplitude to ≈0.1% results in deviations from the linear regime. Then G'' goes over a maximum with a decrease in storage modulus, but the material still maintains its elastic properties. The drop of G' at large amplitude increases with the growth of particle content, although it does not reach the value of G' of pure polymer observed at large amplitude. The materials undergo failure at higher amplitude $\epsilon \geq 130\%$ and $\epsilon \geq 82\%$ for 5 and 10 vol% of carbon, respectively. which is quite close to the strain value for pure polymer, but still lower—stress drops with the increase of strain. One can say that particles determine viscoelastic properties at low amplitude and polymer determine at high amplitude. The polymer also determines the failure. Thus, an increase of relaxation time of polymer matrix results in a decrease in the influence of particles on failure.

Apparently, the relation between the relaxation time of matrix and time scale of deformation determines properties of viscoelastic blends not only at small but also at large deformations: either they are plastic or elastic. We tested this hypothesis by making an amplitude test at various frequencies: 0.02 and 10 rad s^{-1} (**Figure 4**), at which PBS undergoes terminal flow and is elastic, respectively. The same experiments were conducted with PDMS 65cSt blends as reference material (Figure 4a; and Figure S15, Supporting Information). We observed nearly no effect of deformation rate of the behavior of PDMS 65 cSt blends—all of them are elastic before yield point and plastic after yield point independently of deformation rate.

Contrary to the behavior PDMS 65 cSt blends, the behavior of PBS is strongly affected by deformation rate. The blend is elastic at small deformation amplitude at low frequency when carbon network exists, and polymer matrix undergoes flow (0.02 rad s^{-1}), and it flows at large deformation amplitude at low frequency. Contrary to PDMS 65 cSt blend, which shows plastic behavior of particle dispersion—stress is independent of amplitude above yield point (modulus drops at constant stress), PBS blends show flow behavior of polymer solution—loss modulus dominates, and it comes to the plateau with the increase in the amplitude. The same transition from particle flow behavior to polymer flow is observed in 5% of CB blends upon the increase of molecular weight of PDMS (Figures S9 and S10, Supporting Information). At high frequency, the PBS blend behaves as rubber with a filler—an increase in amplitude results in a break of particle agglomerates and elastic modulus decrease. The deformation, at which deviation from linear viscoelastic behavior and maximum of G'' were observed at ≈0.1% and ≈1.8%, respectively, for 5 vol% of CB and ≈0.1% and ≈0.8% for 10 vol% of CB, and are independent of deformation rate. Thus, one can say that both polymer and particles determine nearly pure elastic behavior at high frequency at low amplitude, mostly polymer determines nearly pure elastic behavior at high frequency at high amplitude, particles determine nearly pure elastic behavior at low frequency at low amplitude and mostly polymer determines viscous flow behavior at low frequency at high amplitude (Table S3 and Figure S16, Supporting Information). Important, storage moduli of PBS 5% and 10% blends at low frequency (when polymer flows) and at low amplitude are lower than storage of PDMS 65 cSt blends with the same fraction of carbon, indicating the lower density of particle network in the case of PBS blend for the same CB volume fraction.

Increase in the fraction of carbon in blend with PBS results in the change of the character of the dependence of moduli on amplitude (Figure 4, PBS 10% CB). First, G' and G'' become less dependent on frequency at low amplitude that is qualitatively

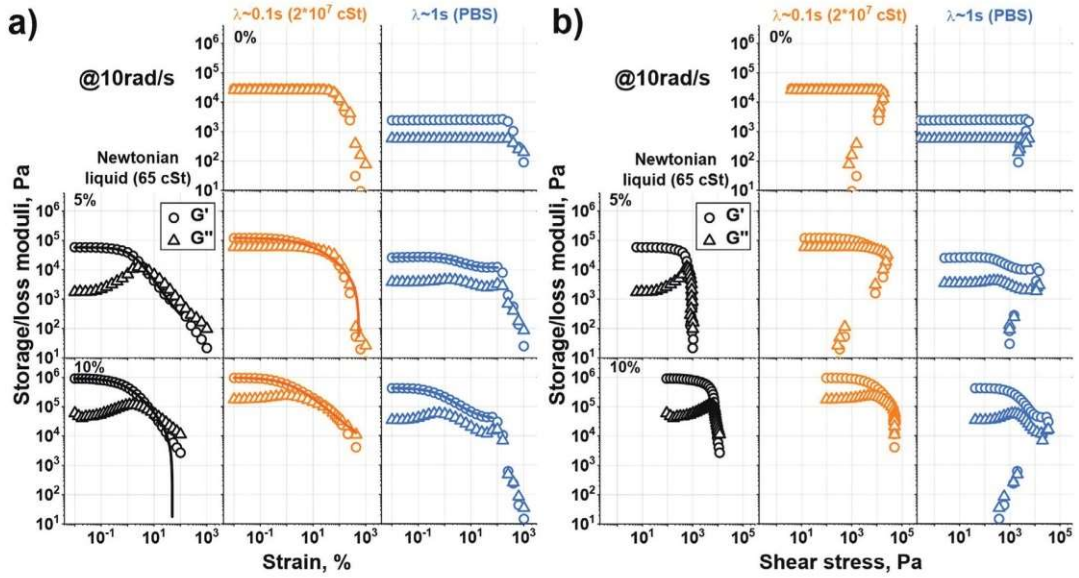

Figure 3. Amplitude sweep (at frequency 10 rad s^{-1}) results of the pure polymers and their composites with 5 and 10 vol% of CB with G' and G'' dependency on both a) shear strain and b) shear stress applied to a material.

attributed to the relaxation of polymer chains. The intensity of peak on large time increases with the increase of carbon content meaning that is associated with the movement of the particles. We calculated the time needed for the individual particles to move to the distance of their own size (average the square root of the mean square of displacement is ≈50 nm), which is expected to correlate with relaxation time, to be in range $\approx 10^3$ s (Figure S6, Supporting Information). This time scale correlates with time scale of the relaxation peak of the particles in high viscous PDMS 2×10^7 cSt and PBS matrixes. However, relaxation in low viscous PDMS 65 cSt is observed on a much larger time scale than that corresponding to movement of the individual particles. The process occurring on this time scale in this polymer can be attributed either to the relaxation of small individual aggregates of particles or/and elements of carbon particles network. The weakness of this peak indicates that number of relaxing elements (individual aggregates of particles or elements of carbon particles network) is small. Thus, the addition of particles results in considerable change of viscoelastic behavior of polymers at small deformation—particles introduce elastic behavior on time scale at least up to 10^4 s (2 h), meaning that polymer–particle blends are not able to spread if applied force is small. There is, however, a difference between the behavior of blends with low molecular weight PDMS, high molecular weight PDMS and PBS—the higher is the relaxation time of the polymer matrix, the more pronounced is the drop of moduli on the larger time scale and the lower is the value of stress at large time scale: 40 kPa for 65 cSt, 10 kPa for 2×10^7 cSt, and 6 kPa for PBS at 5 vol% of CB. This means that the quality of the particle network degrades with an increasing relaxation time of the polymer matrix.

2.3. Viscoelastic Properties at Large Deformations

It is essential to investigate behavior of the composites at different amplitudes of deformations to understand limits of their applicability. We applied amplitude sweep at 10 rad s^{-1} corresponding to time $t = 0.1$ s, which is larger than relaxation time of PDMS 65cSt, nearly corresponds to the relaxation time of PDMS 2×10^7 cSt and less than the relaxation time of PBS. The results are plotted as the dependence of G' and G'' versus amplitude and versus stress (**Figure 3**; and Figures S9–S12, Supporting Information). Pure PDMS 65cSt is Newtonian liquid, and its viscosity is independent of strain amplitude. Both G' and G'' of PDMS 2×10^7 cSt are nearly independent of amplitude and applied stress at small and moderate deformations. Both moduli decay—material fails at large deformations ≈52% and stress 16 kPa. G' and G'' of PBS are constant over the amplitude range up to 206% and stress ≈5 kPa (Figure S8, Supporting Information).

The addition of particles changes rheological behavior. PMDS 65 cSt blends, as it was also discussed above, has elastic behavior at small deformation ($G' > G''$). Increase in amplitude to ≈0.1% results in deviations from the linear regime, then G'' goes over a maximum followed by domination of G'' over G', where gel–sol transition occurs (quantitative data are presented in the **Table 1**). The stress, at which deviations from the linear regime and domination of G'' over G' increases with the fraction of particles. Thus, blends of Newtonian liquid and particle behave here as plastic materials—moduli drop at tiny deformations due to cohesion failure (Figure S14, Supporting Information). The stress becomes independent of deformation, meaning that contacts between particles do not break irreversibly but restore.

Table 1. Amplitude sweep data for shear strain and stress at G'' and sol–gel transition/breakage points for polymers blends with various CB content.

Polymer matrix	vol% of CB	Elongation at max G'' [%]	Stress at max G'' [kPa]	Elongation at $G'' = G'$ [%]	Stress at $G'' = G'$ [kPa]
65 cSt	5	1.5	0.6	5.1	0.7
	10	0.9	5.8	9.4	7.7
2×10^7 cSt	0	—	—	52	16
	5	—	—	21	13
	10	1.3	6	49	48
PBS	0	—	—	206	5
	5	1.8	0.2	130	13
	10	0.8	1.6	82	32

Properties of PDMS 2×10^7 cSt are also affected by the presence of the carbon. As discussed above, PDMS 2×10^7 cSt blends have elastic behavior at small deformation: $G' > G''$. Rise of amplitude to 0.1% results in deviations from the linear regime. No maximum of G'' was observed at a low concentration of carbon that is most probably due to the domination of mechanic properties of PDMS: PDMS 2×10^7 has a much higher elastic modulus than particle network does. Similar to PDMS 65 cSt blend, maximum for 10% of carbon in blend with PDMS 2×10^7 cSt was observed at $\epsilon = 1.3\%$. However, the further increase in amplitude does not result in G'' dominating G' and only at $\epsilon = 21\%$ and 49% for 5 and 10 vol% of carbon, respectively, at which pure polymer fails, G'' becomes larger than G'. The failure has a different character depending on the fraction of particles: 5% blend fail with drop of stress upon increase of strain, which is usual behavior of pure polymer; 10% blend shows plastic behavior that is similar to that of blends of low molecular weight PDMS (65 cSt) and stress is independent of deformation above flow point. This observation can be explained by the assumption that polymer determines failure at low particle content, and particles determine failure at their high content.

Blends of PBS with carbon particles behave as elastomer-particle blends described by Payne[30]—G' is constant at small deformation, an increase of amplitude results in its gradual decrease, accompanied by a pronounced peak of G'', and then it again becomes constant. Similar to the previous two cases, an increase of amplitude to ≈0.1% results in deviations from the linear regime. Then G'' goes over a maximum with a decrease in storage modulus, but the material still maintains its elastic properties. The drop of G' at large amplitude increases with the growth of particle content, although it does not reach the value of G' of pure polymer observed at large amplitude. The materials undergo failure at higher amplitude $\epsilon \geq 130\%$ and $\epsilon \geq 82\%$ for 5 and 10 vol% of carbon, respectively. which is quite close to the strain value for pure polymer, but still lower—stress drops with the increase of strain. One can say that particles determine viscoelastic properties at low amplitude and polymer determine at high amplitude. The polymer also determines the failure. Thus, an increase of relaxation time of polymer matrix results in a decrease in the influence of particles on failure.

Apparently, the relation between the relaxation time of matrix and time scale of deformation determines properties of viscoelastic blends not only at small but also at large deformations: either they are plastic or elastic. We tested this hypothesis by making an amplitude test at various frequencies: 0.02 and 10 rad s^{-1} (**Figure 4**), at which PBS undergoes terminal flow and is elastic, respectively. The same experiments were conducted with PDMS 65cSt blends as reference material (Figure 4a; and Figure S15, Supporting Information). We observed nearly no effect of deformation rate of the behavior of PDMS 65 cSt blends—all of them are elastic before yield point and plastic after yield point independently of deformation rate.

Contrary to the behavior PDMS 65 cSt blends, the behavior of PBS is strongly affected by deformation rate. The blend is elastic at small deformation amplitude at low frequency when carbon network exists, and polymer matrix undergoes flow (0.02 rad s^{-1}), and it flows at large deformation amplitude at low frequency. Contrary to PDMS 65 cSt blend, which shows plastic behavior of particle dispersion—stress is independent of amplitude above yield point (modulus drops at constant stress), PBS blends show flow behavior of polymer solution—loss modulus dominates, and it comes to the plateau with the increase in the amplitude. The same transition from particle flow behavior to polymer flow is observed in 5% of CB blends upon the increase of molecular weight of PDMS (Figures S9 and S10, Supporting Information). At high frequency, the PBS blend behaves as rubber with a filler—an increase in amplitude results in a break of particle agglomerates and elastic modulus decrease. The deformation, at which deviation from linear viscoelastic behavior and maximum of G'' were observed at ≈0.1% and ≈1.8%, respectively, for 5 vol% of CB and ≈0.1% and ≈0.8% for 10 vol% of CB, and are independent of deformation rate. Thus, one can say that both polymer and particles determine nearly pure elastic behavior at high frequency at low amplitude, mostly polymer determines nearly pure elastic behavior at high frequency at high amplitude, particles determine nearly pure elastic behavior at low frequency at low amplitude and mostly polymer determines viscous flow behavior at low frequency at high amplitude (Table S3 and Figure S16, Supporting Information). Important, storage moduli of PBS 5% and 10% blends at low frequency (when polymer flows) and at low amplitude are lower than storage of PDMS 65 cSt blends with the same fraction of carbon, indicating the lower density of particle network in the case of PBS blend for the same CB volume fraction.

Increase in the fraction of carbon in blend with PBS results in the change of the character of the dependence of moduli on amplitude (Figure 4, PBS 10% CB). First, G' and G'' become less dependent on frequency at low amplitude that is qualitatively

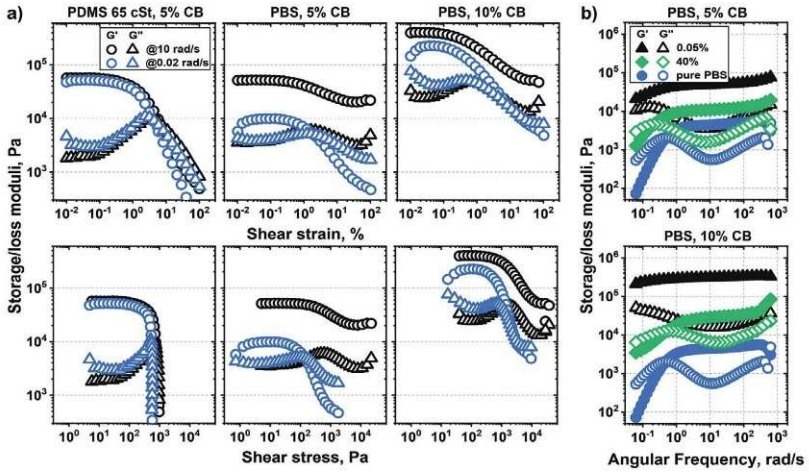

Figure 4. Viscoelastic behavior of polymer–carbon blends at large amplitude: a) amplitude sweep results, performed at various frequencies, of composites of PDMS 65 cSt as Newtonian liquid and PBS with relaxation time $\lambda \approx 1$ s with 5 and 10 vol% of CB where G' and G'' dependency is on both shear strain and shear stress applied to a material. b) The frequency sweep test of PBS with 5 and 10 vol% of CB at 0.05% and 40% of shear strain corresponding to first and second linear region of the materials, respectively.

similar to behavior of PDMS 65 cSt blend. Second, G' and G'' drop sharper and at higher stress that is similar to behavior of carbon-PDMS 65 cSt blend. These two effects originate from increasing particle contribution to mechanical properties. On the other hand, G'' dominates over G' at high-stress, and come to a plateau corresponding to behavior of polymer that is qualitatively similar to sample with 5% carbon—10% PBS blend flows as particle-filled polymer dispersion at large amplitude and stress.

In order to obtain the whole picture of viscoelastic behavior of blends at different amplitudes and frequencies, we made frequency sweep experiment at low strain ($\epsilon = 0.05\%$, particle network exists) and large strain ($\epsilon = 40\%$, particle network of carbon is broken) (Figure 4b). Decrease of angular frequency results in relaxation of polymer chains and decrease of moduli, which becomes pronounced at large amplitude of deformation. Both PBS 5% and 10% blends show the drop of G' in the rubbery plateau region upon increase of amplitude, and the drop increases with carbon fraction. However, value of G' of composites in rubbery plateau region at large amplitude of deformation is still higher than that of pristine PBS. The essential difference between small- and large-amplitude frequency sweep is observed at the time scale above the relaxation time of polymer. Both PBS 5% and 10% composites are elastic ($G' > G''$) at low amplitude of deformation and flow at large amplitude at low frequency with cross-section point at a frequency slightly lower than that of pristine PBS (Figure 2) that is due to lower mobility of partially adsorbed on particles polymer chains. Thus, the material rheological properties with lower carbon content at large shear strain are determined mostly by polymer matrix since gel network is broken and carbon particles play reinforcing function due to direct interaction with polymer chains only. On the other hand, it is challenging to disregard the CB network entirely with higher filler content, which explains the brittleness of materials.

2.4. Creep Experiment

We performed creep experiment by applying stress below the value at which particle–particle contact breaks and above with 5% of CB blends and different matrices (Figure S17, Supporting Information). It was found that applying low stress results in negligible creep—viscosity is in the range of 0.1–10 GPa s. Notably, blend with PBS creeps better (viscosity is lower) than ones with PDMS 65 cSt that is an indication on defects in the network or worse contact between particles. Applying large stress results in cohesion failure (Figure S14, Supporting Information) in the case of PDMS 65 cSt—the rheometer plate starts to rotate very quickly. The viscosity of PDMS 2×10^7 cSt and PBS blends drop down to ≈210 and 79 kPa s, respectively. At this force, the carbon network is broken; meanwhile, the polymer matrix maintains material integrity and provides its flow. Thus, the creep experiment indicates defects in the particles network in PBS blends.

2.5. Steady State Rheology

The rotational experiment was performed to understand spreading (flow) properties of blends (**Figure 5**). Pure PDMS 65 cSt behaves as a Newtonian liquid, and its viscosity is rate-independent. The viscosity of PDMS 2×10^7 cSt and PBS is also independent of rate when the rate is below reciprocal relaxation time ($1/\lambda$) because materials are in a terminal flow regime. The viscosity of PBS slightly increases upon approach to the rate corresponding to relaxation time. It then rapidly drops in the way that stress decreases with further increase of rate—materials undergo failure. Apparently, materials flow at low rates, at some point undergoes transition to elastic states, in which it breaks upon stretching. Similar behavior is observed in the case of PDMS 2×10^7 cSt—viscosity is independent of rotation rate polymer fails at time scale close to relaxation time.

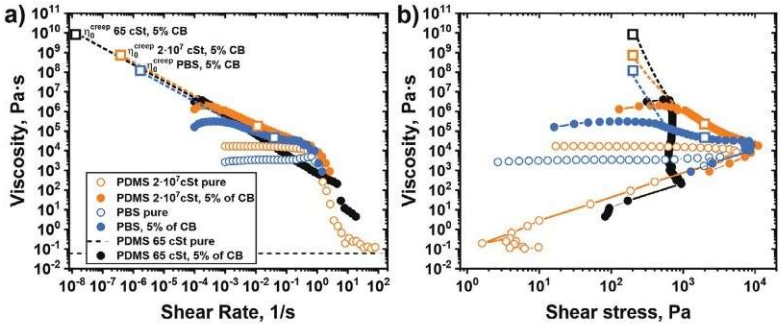

Figure 5. Rotational test results of the pure polymers and their composites with 5 vol% of CB with viscosity dependency on both a) shear rate and b) shear stress applied to a material. Empty squares are results of creep experiment. Dashed lines show expected evolution of viscosity with rate and stress when steady state flow at low shear rates will be achieved.

The addition of filler particles increases the viscosity of materials. It becomes strongly dependent on the rate of rotation – the blends demonstrate a pronounced decrease in viscosity with increase of rate—shear thinning behavior. The character of the decrease depends on viscoelastic behavior of polymer matrix. In the case of PDMS 65 cSt, viscosity drops rapidly upon the increase in shear rate as soon as applied stress is > 600 Pa, and an increase in rotation rate does not increase stress. Such behavior can be attributed to cohesion failure. Further increase of rotation rate (above 50 s^{-1}) results in rapid drop of stress—material comes out from the space between rotating plates. Blends of PDMS 2×10^7 cSt and PBS demonstrate classical shear thinning behavior—viscosity drops at certain value of stress (≈300–400 Pa) that is due to failure of contacts between particles. Viscosity remains constant for PBS blend with further increase in rotation rate and applied stress because the polymer is terminal flow regime and contribution of particles to viscosity is low because contacts between them are broken. Similar to pure polymer, an increase in rotation rate to the value corresponding to the relaxation time of polymer results in its transition to elastic state, and polymer fails—both stress and viscosity drop rapidly. It is also worth noting that the highest Newtonian viscosity of the blends obtained by steady state measurement is not reliable since for each point the measurement time should be at least $1/\dot{\gamma}$ s (the materials does not achieve a plateau at low shear rate). Therefore, the viscosity values are more credible from much longer creep experiment (square points on the plot). Thus, steady-state rheology revealed three distinct flow regimes of polymer–particle blends with viscoelastic polymer matrix: i) high viscosity regime at low stress when particle–particle contacts exist; ii) shear thinning and transition to polymer flow, and iii) polymer failure.

2.6. Electrical Characterization

According to the literature, all investigated polymer–particle blends lie behind the percolation threshold, which is around 0.25 vol% for linear low viscous PDMSs[31] and 1.25 vol% for PBS-like Silly Putty.[32] Therefore, we investigated the character of electric resistivity (real/imaginary) of polymer–carbon blends to understand the nature of structures formed by particles. We first analyzed the current–voltage behavior of materials (scanning rate is 100 V s^{-1}). There are two distinct regimes: low conductivity at low (−1 ÷ 1 V) voltage and higher conductivity at high (V > 2 V, V < −2 V) voltage (**Figure 6**a,b; and Figure S18, Supporting Information). The voltage range of low conductivity regime apparently decreases with increase of carbon content. To understand effects of relaxation properties of polymer and amount of particles on electrical properties of composite, we tested the electrical conductivity properties of the materials by electrochemical impedance spectroscopy (EIS) at different offset voltages and amplitudes of oscillations that covers low- and high-conductivity regimes.

It was found that frequency range, at which impedance is mostly real, decreases with the increase of relaxation time (and molecular weight) of polymer in low conductivity regime (small voltage amplitude (10 mV and 0 V offset) (Figures S19–S21 and 23a,b, Supporting Information). Bode plots also show that increase of relaxation time results in appearance of two relaxation transitions that can also be seen in the Nyquist plots (Figure 6c)—carbon blends of PDMS 2×10^7 cSt and PBS show two semicircles, while the Nyquist plot for the 65 cSt 5% composite has one semicircle. We fitted the Nyquist plot according to the equivalent scheme of the impedance spectra shown in Figure 6c, which consists of resistor R_0 in series with two RC-elements of resistor R_i and capacitor C_i, connected in parallel. As fitting algorithm, the Levenberg–Marquardt method was used. The fitting parameters are summarized in **Table 2**, where R_0 can be attributed to the resistivity of measuring system contacts and bulk conductivity of CB network between direct contacts of the particles, and R_1, C_1, R_2, C_2 to materials parameters. We speculate that the resistivity R_1 and R_2 can be attributed to tunneling (hopping) conductivity across small gaps (<10 nm) between CB particles aggregates, which is typically observed in CB—polymer composites.[33,34] Particles that are close to each other but do not form contacts form a pseudocapacitor on interface. The EIS results may also be described by a finite number of RC elements, spread over a wider range of time constants, since the distance between the aggregates is nonuniform. It can then be presented as a distribution of relaxation times function[35–37] (Figures S19b and S22, Supporting Information). However, for our evaluation, we have only taken two such elements for an average estimate of this conductivity contribution

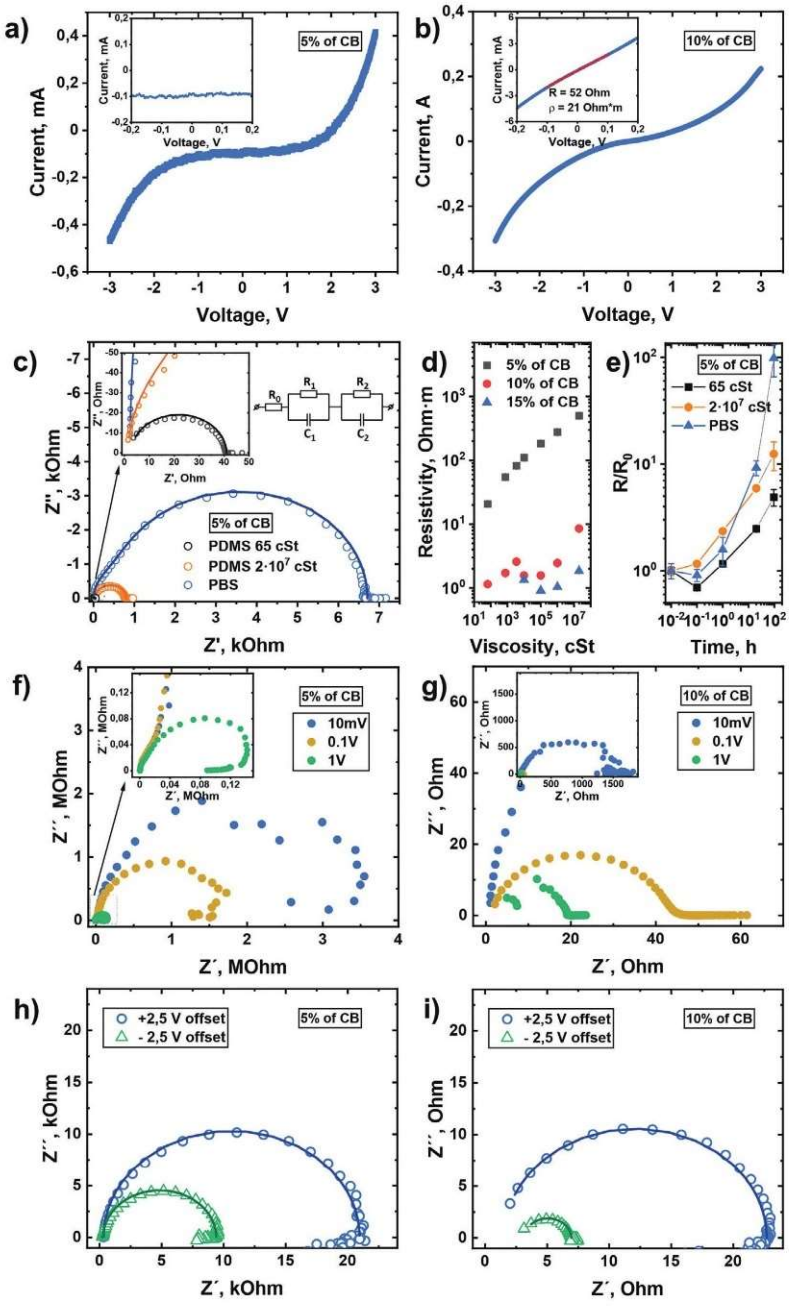

Figure 6. a) Volt-ampere characteristic of PBS–CB blends in voltage range -3 V < V < $+3$ V measured at 100 mV s^{-1} scanning rate. c) Nyquist plot of EIS of a polymer-CB composites at 0 V offset with 10 mV amplitude fitted according to equivalent electrical circuit by Levenberg–Marquardt method of optimization. d) Resistivity dependence of composites of different molecular weight linear PDMS with various CB content. e) Resistivity change of CB-polymer composites with 5% of CB with time at rest. f,g) Nyquist plot of EIS of a PBS–CB composites at 0 V offset with 2.5 V amplitude. h,i) Nyquist plot of EIS of a PBS–CB composites at 2.5 V offset with 10 mV amplitude fitted by Levenberg–Marquardt method with the same equivalent circuit.

Table 2. Fitting parameters of EIS data for polymers composites with 5 vol% of CB at offset V = 0 V, amplitude 10 mV (Figure 6c) and for PBS composites with 5 and 10 vol% of CB at offset V = ±2.5 V, amplitude 10 mV data (Figure 6h,i).

	Offset [V]	R_0 [Ohm]	R_1 [Ohm]	C_1 [nF]	R_2 [Ohm]	C_2 [nF]
65 cSt, 5%	0	2.7	—	—	38	19
2×10^7 cSt, 5%	0	1.5	766	41	38	43
PBS 5%	0	2.3	6151	28	557	29
PBS 5%	2.5	202	20 640	17	117	2.6
	−2.5	196	9112	19	92	6
PBS 10%	2.5	1.5	19	41	2.3	331
	−2.5	3.2	2.4	162	1.4	286

Character of evolution of conductivity of polymer–carbon blends with relaxation time of polymers depends on fraction of carbon (Figure 6d). For linear PDMSs blends, we observed that the resistivity at low frequency ($R_0+R_1+R_2$) increases with the increase in viscosity (molecular weight, relaxation time) at low carbon content (5%) (Figure S23, Supporting Information) and is nearly independent on viscosity at higher carbon content >10%. The highest resistivity is observed for PBS composites. This observation is in accordance with rheological data, which indicate that quality of particle network becomes worse with the increase of molecular weight and relaxation time of polymer.

Important, resistivity of polymer–carbon blends changes with time, and the character depends on relaxation time of polymer matrix (Figure 6e). While the resistivity of PDMS 65 cSt—carbon blends increases fourfold (nearly a half an order of magnitude) on time scale of 100 h, resistivity of PBS-carbon blend increases by 100 times—two orders of magnitude. These changes in resistivity indicate on worsening of quality of carbon network with time.

Increase in the amplitude of voltage oscillation results in the decrease of the impedance as it could also be expected from character of *V–I* dependence—a transition from low conductivity regime to high conductivity regime shall be observed (Figure 6f,g; and Figure S24, Supporting Information). The character of decrease of impedance depends on fraction of carbon. An increase in amplitude from 10 to 100 mV results in considerable decrease of electrical impedance at 10%, while impedance at 5% decreases relatively weak. Further increase of amplitude to 1 V results in significant decrease of impedance at 5% of carbon, while impedance at 10% decreases relatively weakly. This means that the voltage range, at which low conductivity regime is observed becomes narrower with increasing carbon content.

Next, we measured electrical impedance in high conductivity regime by applying low amplitude oscillations (10 mV) at positive and negative at offset voltages ($V_0 \pm 2.5$ V) (Figure 6h–i; and Figure S25, Supporting Information). The Nyquist plot of EIS results shows only one semicircle, which we attribute to the tunneling conductivity of materials. The tunneling current ceases to dominate at these voltage values,[38] and electrical breakdowns between separated CB particles and aggregates occur. Therefore, for the application of the composite, where high conductivity is required, a voltage higher than ≈2 V should be used to prevent the impact of nonlinear tunneling current.

Thus, conductivity measurements allow making conclusions about structure of polymer–particle blends. The low conductivity at 0 V offset with low voltage amplitude is due to absence of direct contacts between the particles—they are most probably separated by polymer chains. Hopping conductivity at small voltage barely occurs and material possess high resistivity. The particles are, however, close to each other, and by applying higher voltages, "electrical breakdown" is observed that increases conductivity. The higher the fraction of particles and the lower the molecular weight and relaxation time of insulating polymer are, the more direct contacts between the particles and the closer are the particles, which do not have direct contact with each other. As a consequence, stronger filler network forms and material possesses higher conductivity.

2.7. Self-Healing Behavior

Finally, we studied the self-healing behavior—recovery of electrical and mechanical properties of the blends after mechanical shear deformation at different amplitudes. The time-sweep measurements of impedance (at 50 Hz at offset voltage 0 V,) and storage/loss moduli (at shear stress 0.01% and frequency 1 rad s^{-1}) were carried out simultaneously after a sequence of several one-step shear strains followed by materials restoration (**Figure 7**; and Figures S26–S28, Supporting Information). We selected several amplitudes, which correspond to different structural transitions in materials. The 1% of shear strain related to pseudolinear viscoelastic region (before ϵ_c), 10% corresponds to nonlinear region, where agglomerates network undergoes breakage, and 1000% corresponds to material failure. At ϵ = 1%, the storage modulus of PDMS 65 cSt with 5% of CB changes negligibly. The loss modulus rapidly increases and then decreases back to the initial value within experiment time. The energy dissipates due to the friction between particles, however, the agglomerates network is not broken yet. Resistivity qualitatively follows behavior of G''—it increases upon deformation and then decreases to initial value. Applying of large deformations (10% and 1000%) results is a drop of storage modulus due to the destruction of the carbon grid in the polymer matrix. As soon as the deformation is removed, G' immediately restores. The restoration of G'' and resistivity at large deformations (10% and 1000%) is similar to that after 1% deformation.

Blends of carbon with PDMS 2×10^7cSt and PBS behaves differently than PDMS 65 cSt—carbon blend. At small deformation (1% and 10%), the storage modulus drops and then restores, while loss modulus remains nearly unchanged—elastic behavior of polymer dominates at the conditions of rheological experiment and contribution of particles is not visible. Increase of amplitude to 1000% (failure of polymer) results in drop of both storage and loss moduli, and they increase upon recovery. Important, the recovery of moduli after deformation of PDMS 2×10^7 cSt and PBS—carbon blends is much slower than of PDMS 65 cSt—carbon blend (Figure S28, Supporting Information). That is due to high viscosity of polymer, which slows down restoration of carbon network—evidence of thixotropic behavior. In the case of these two polymers, resistivity was not able to reach its initial value before. Moreover, deviation of value of resistivity after recovery from that before mechanical stimula-

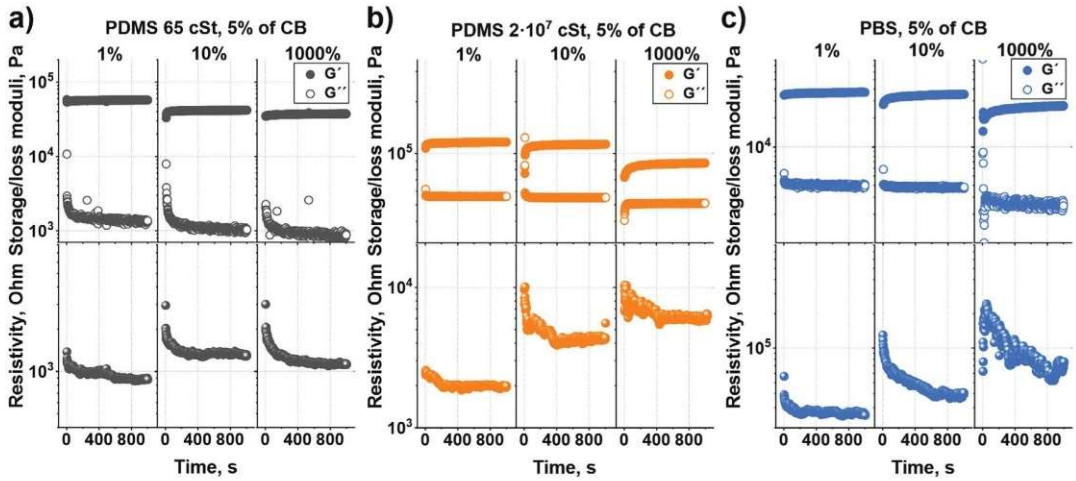

Figure 7. Time-sweep measurements of resistivity and storage/loss moduli of 5% CB-polymer composites with a) PDMS 65 cSt, b) PDMS 2×10^7 cSt, and c) PBS as polymer matrix after one-step shear strain varying from 0.05% and 1000% followed by moduli measurements at small strain (0.01%) and frequency (1 Hz).

tion is larger in the case of PDMS 2×10^7 cSt blend that is due to its higher viscosity comparing to that of PBS. Thus, the recovery of the mechanical and conductive properties of blends of viscoelastic polymers with CB worsens with increasing polymer viscosity, rather than with increasing polymer relaxation time.

3. Discussion

We performed a thorough characterization of rheological, mechanical, and electrical properties of self-healing PBS-carbon blends and reference carbon blends with low and high molecular weight PDMS. There are several indications that the quality of particle network in PBS-carbon blends is worse than that in blends of carbon with low molecular weight PDMS. There are individual particles, large individual agglomerates, and dangling agglomerates in PBS-carbon blends that is evidenced by i) polymer-like character failure PBS-carbon blend, ii) low modulus at frequency below relaxation time of polymer, iii) relaxation peak corresponding to individual particles; iv) more pronounced creep at stress below yield point, v) lower conductivity, and it decreases with time—network break down by itself, and vi) slow restoration of mechanical properties and conductivity after failure. The reason for formation of poor carbon network in PBS-carbon blends is apparently the adsorption of polymer chains on particles via weak Van der Waals interaction, forming a special interfacial insulating shell with thickness t, properties of which differ from bulk polymer. For linear polymers, the t can be accepted as half of the gyration radius, which is 0.25 and 1.94 nm for PDMS 65 cSt and 2×10^7 cSt, respectively. For elastomers, this value is about 10 nm. The larger the interfacial volume, the more substantial entropy impact, which leads to better dispersion of CB in polymer matrix overcoming enthalpy of CB particle–particle attraction. Consequently, the composites of Newtonian liquid PDMS 65 cSt with the lowest interfacial volume, where polymer–particles interaction is due to capillary forces only, form a strong agglomeration network. Apparently, the formation of polymer shell around particles occurs not immediately. It is a slow process as can be concluded from rate of increase of resistivity with time. The structure of low and high molecular weight polymer–carbon blends is schematically depicted in **Figure 8**.

4. Conclusions

We performed a thorough study of electromechanical and rheological properties of blends of carbon particles and PDMS with different relaxation times. Adding carbon filler to the polymers renders its new properties, and behavior of composites depends strongly on the viscoelastic properties of polymers. The polyborosiloxane allows the dough-like behavior of the blends. The material possesses elastomer-like behavior on a small time scale. It flows on a large time scale when large stress is applied and can withstand large deformation without brittle failure. On the other hand, the viscoelastic self-healing polymer negatively affects the stability of carbon–carbon contacts, which ensures high conductivity. As a result, the electrical properties of blends of viscoelastic polymers and carbon are worse than that of carbon and viscous polymer. Moreover, the viscoelastic polymer degrades the conductive carbon networks with time, decreasing its conductivity. Ability of polymer–carbon composites to flow, which is utilized for self-healing, is an indication of absence of 3D network formed by particles. It results in worse conductivity compared to the blends with low molecular weight polymer, which do not flow due to formation of carbon network, have brittle failure but is able to immediately restore mechanical properties and conductivity after removing stress.

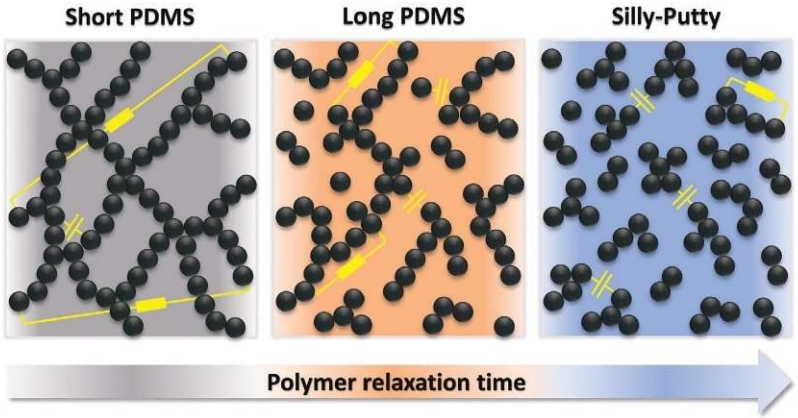

Figure 8. The scheme of agglomeration network of CB in polymer matrix with very low relaxation time (PDMS 65 cSt), PDMS 2×10^7 cSt with relaxation time ≈0.1 s, and PBS with relaxation time ≈1 s. Pseudocapacitor and resistor elements of network are marked in yellow signs.

5. Experimental Section

Materials: The hydroxyl-terminated PDMS with kinematic viscosity 65 cSt, 750 cSt, and 3500 cSt and methyl-terminated PDMS with kinematic viscosity 10^4 cSt, 10^5 cSt, 10^6 cSt, and 2×10^7 cSt were purchased from Sigma-Aldrich and Gelest company, respectively. The highest Newtonian viscosity was calculated using the value of specific gravity for each precursor. The number average molecular mass, M_n, and weight average molecular weight, M_w, and polydispersity index, PDI (PDI = M_w/M_n), were determined by GPC (Agilent 1260 Infinity) (Figure S1b, Supporting Information). The measurements were carried out at 30 °C. The eluent for GPC measurements was tetrahydrofuran (THF) of high-prformance liquid chromatography grade, and the standards used for calibration were monodisperse poly(methyl methacrylate). All obtained parameters are listed in Table S1 (Supporting Information). The plot η versus M_w for PDMS with kinematic viscosity from 3500 to 2×10^7 cSt correlates with the typical power low $\eta \approx M_w^{4.8}$ (Figure S1a, Supporting Information). The carbon black with by BET determined surface area 62 $m^2\ g^{-1}$ was purchased from Nanografi Company. Toluene (≥99.5%) and boric acid (≥99.5%) from Sigma-Aldrich, and Diclormethan (DCM) (99.8%) from ACROS Organics were purchased and used as it is.

PBS Synthesis: To prepare PBS, the ratios between the hydroxyl-terminated PDMS 65 cSt and H_3BO_3 100:0.85 (relaxation time is ≈1 s), 100:1.0 (relaxation time is ≈10 s), and 100:1.5 (relaxation time is ≈100 s) by mass were used. First, the PDMS was dissolved in toluene. Then, boric acid was added to the solution, and the mixture was dispersed for a couple of minutes in an ultrasonic bath. The mixture was heated to 120 °C and left for 24 h with further stirring. After this time, the mixture became transparent. Excess solvent was removed with a vacuum evaporator, and the rest of the solvent was removed by storing the sample in a vacuum oven at 60 °C for 24 h.

Preparation of Polymer-CB Composites: CB/PDMS and PBS/CB composites with various volume fractions of carbon material were synthesized, assuming that CB and polymers density are 2 and 1 g cm^{-3}, respectively. For composites with PDMS viscosity up to 10^5 cSt CB was added to PDMS solution in dichloromethane (DCM), which initially was taken in excess to permit easy mixing and dispersion of compounds. All compounds were preliminary dispersed in ultrasound bath and mixed with IKA RW 20 disperser for 30 min at 1200 rpm. Excess of DCM was evaporated in an ultrasonic bath and then in a vacuum desiccator for 30 min at 10 mbar and 20 °C. For composites with PDMSs with viscosity higher than 10^6 cSt and PBS, toluene as a solvent was used due to their low solubility in DCM. First, the polymer was dissolved in toluene at 60 °C in 1 h. Then, CB was added to polymer solution in toluene, and all compounds were first dispersed in ultrasound bath and then mixed with the same disperser for 30 min at 1200 rpm. Excess of toluene was evaporated in a vacuum desiccator. The rest of the solvent was removed by storing samples in a vacuum oven at $T = 60$ °C for 24 h.

Characterization: The microstructure of composites was investigated by field emission scanning electron microscopy (FESEM) (Thermo Scientific, Germany). Rheological measurements were carried out with 25 mm parallel plate geometry on MCR 702 (Anton Paar, Graz, Austria) coupled with dielectric measuring cell. All samples were roughly flattened before lowering the rheometer to a gap size of ≈1 mm. Then samples were allowed to relax and reach measurement temperature for 15 min. EIS measurements were performed at 25 °C in frequency range from 0.1 Hz to 1 MHz on Gamry 1010E potentiostat.

The relaxation time λ is defined as the peak time of continuous relaxation spectra $H(\lambda)$, which is for infinite time-scale generalized Maxwell model can be expressed as

$$G'(\omega) - G_e = \int_{-\infty}^{\infty} H(\lambda) \frac{\omega^2\lambda^2}{1+\omega^2\lambda^2} d(ln\lambda) \quad (1)$$

$$G''(\omega) = \int_{-\infty}^{\infty} H(\lambda) \frac{\omega\lambda}{1+\omega^2\lambda^2} d(ln\lambda) \quad (2)$$

The time-scale extension was achieved by relaxation experiment, where relaxation modulus was recalculated into relaxation spectra $H(\lambda)$ and storage/loss moduli according to generalized Maxwell model as well[39]

$$G(t) = G_e + \sum_{i=1}^{N} g_i e^{-t/\lambda_i} \quad (3)$$

$$H(\lambda) = \sum_{i=1}^{N} g_i \delta(\lambda/\lambda_i - 1) \quad (4)$$

$$G'(\omega) = \omega \int_0^{\infty} G(t) \sin(\omega t)\, dt \quad (5)$$

$$G''(\omega) = \omega \int_0^{\infty} G(t) \cos(\omega t)\, dt \quad (6)$$

where coefficients g_i, G_e, and relaxation times λ_i are material parameters, $\delta(y)$ is the Dirac delta function.

Supporting Information

Supporting Information is available from the Wiley Online Library or from the author.

Acknowledgements

This work was supported by the DFG (Grant No IO 68/20-1, IO 68/21-1). Also, the authors would further like to thank Professor Scheibel for allowing the authors to use SEM equipment to conduct this research.

Open access funding enabled and organized by Projekt DEAL.

Conflict of Interest

The authors declare no conflict of interest.

Data Availability Statement

The data that support the findings of this study are available in the Supporting Information of this article.

Keywords

carbon black, carbon-based materials, polyborosiloxane, polydimethylsiloxane, self-healing, self-healing electrodes, silly-putty

Received: March 30, 2022
Revised: April 22, 2022
Published online: May 15, 2022

[1] P. Tan, H. Wang, F. Xiao, X. Lu, W. Shang, X. Deng, H. Song, Z. Xu, J. Cao, T. Gan, B. Wang, X. Zhou, *Nat. Commun.* **2022**, *13*, 358.
[2] J. Kang, J. B. H. Tok, Z. Bao, *Nat. Electron.* **2019**, *2*, 144.
[3] E. Bozo, H. Ervasti, N. Halonen, S. H. H. Shokouh, J. Tolvanen, O. Pitkanen, T. Jarvinen, P. S. Palvolgyi, A. Szamosvolgyi, A. Sapi, Z. Konya, M. Zaccone, L. Montalbano, L. De Brauwer, R. Nair, V. Martinez-Nogues, L. San Vicente Laurent, T. Dietrich, L. Fernandez de Castro, K. Kordas, *ACS Appl. Mater. Interfaces* **2021**, *13*, 49301.
[4] A. C. Marques, J.-M. Cabrera Marrero, C. de Fraga Malfatti, *SpringerPlus* **2013**, *2*, 521.
[5] M. Kaltenbrunner, T. Sekitani, J. Reeder, T. Yokota, K. Kuribara, T. Tokuhara, M. Drack, R. Schwodiauer, I. Graz, S. Bauer-Gogonea, S. Bauer, T. Someya, *Nature* **2013**, *499*, 458.
[6] Y. Zhang, C. K. Jeong, J. Wang, H. Sun, F. Li, G. Zhang, L.-Q. Chen, S. Zhang, W. Chen, Q. Wang, *Nano Energy* **2018**, *50*, 35.
[7] K. Narumi, F. Qin, S. Liu, H.-Y. Cheng, J. Gu, Y. Kawahara, M. Islam, L. Yao in Proceedings of the 32nd Annual ACM Symposium on User Interface Software and Technology, 2019293, https://dl.acm.org/doi/pdf/10.1145/3332165.3347901.
[8] N. De Belie, E. Gruyaert, A. Al-Tabbaa, P. Antonaci, C. Baera, D. Bajare, A. Darquennes, R. Davies, L. Ferrara, T. Jefferson, C. Litina, B. Miljevic, A. Otlewska, J. Ranogajec, M. Roig-Flores, K. Paine, P. Lukowski, P. Serna, J.-M. Tulliani, S. Vucetic, J. Wang, H. M. Jonkers, *Adv. Mater. Interfaces* **2018**, *5*, 1800074.
[9] S. M. Bleay, C. B. Loader, V. J. Hawyes, L. Humberstone, P. T. Curtis, *Composites, Part A* **2001**, *32*, 1767.
[10] S. R. White, N. R. Sottos, P. H. Geubelle, J. S. Moore, M. R. Kessler, S. R. Sriram, E. N. Brown, S. Viswanathan, *Nature* **2001**, *409*, 794.
[11] X. Luo, P. T. Mather, *ACS Macro Lett.* **2013**, *2*, 152.
[12] J. C. Cremaldi, B. Bhushan, *Beilstein J. Nanotechnol.* **2018**, *9*, 907.
[13] Y. Yang, M. W. Urban, *Chem. Soc. Rev.* **2013**, *42*, 7446.
[14] Y. L. Rao, A. Chortos, R. Pfattner, F. Lissel, Y. C. Chiu, V. Feig, J. Xu, T. Kurosawa, X. Gu, C. Wang, M. He, J. W. Chung, Z. Bao, *J. Am. Chem. Soc.* **2016**, *138*, 6020.
[15] F. Herbst, S. Seiffert, W. H. Binder, *Polym. Chem.* **2012**, *3*, 3084.
[16] S. Burattini, B. W. Greenland, D. H. Merino, W. Weng, J. Seppala, H. M. Colquhoun, W. Hayes, M. E. Mackay, I. W. Hamley, S. J. Rowan, *J. Am. Chem. Soc.* **2010**, *132*, 12051.
[17] A. Kurkin, V. Lipik, K. B. L. Tan, G. L. Seah, X. Zhang, A. I. Y. Tok, *Macromol. Mater. Eng.* **2021**, *306*, 2100360.
[18] E. D'Elia, S. Barg, N. Ni, V. G. Rocha, E. Saiz, *Adv. Mater.* **2015**, *27*, 4788.
[19] Z. Chang, Y. He, H. Deng, X. Li, S. Wu, Y. Qiao, P. Wang, H. Zhou, *Adv. Funct. Mater.* **2018**, *28*, 1804777.
[20] Y. J. Tan, J. Wu, H. Li, B. C. K. Tee, *ACS Appl. Mater. Interfaces* **2018**, *10*, 15331.
[21] H. Wang, B. Zhu, W. Jiang, Y. Yang, W. R. Leow, H. Wang, X. Chen, *Adv. Mater.* **2014**, *26*, 3638.
[22] P. Qu, C. Lv, Y. Qi, L. Bai, J. Zheng, *ACS Appl. Mater. Interfaces* **2021**, *13*, 9043.
[23] Y. Chen, X. Pu, M. Liu, S. Kuang, P. Zhang, Q. Hua, Z. Cong, W. Guo, W. Hu, Z. L. Wang, *ACS Nano* **2019**, *13*, 8936.
[24] T. Wu, E. Gray, B. Chen, *J. Mater. Chem. C* **2018**, *6*, 6200.
[25] C. S. Boland, *ACS Nano* **2019**, *13*, 13627.
[26] L. Van Beek, B. Van Pul, *J. Appl. Polym. Sci.* **1962**, *6*, 651.
[27] L. J. Fetters, D. J. Lohse, S. T. Milner, W. W. Graessley, *Macromolecules* **1999**, *32*, 6847.
[28] M. Tang, W. Wang, D. Xu, Z. Wang, *Ind. Eng. Chem. Res.* **2016**, *55*, 12582.
[29] R. H. C. Michael Rubinstein, *Polymer Physics*, Oxford University Press, Oxford **2003**.
[30] A. R. Payne, R. E. Whittaker, *Rubber Chem. Technol.* **1971**, *44*, 440.
[31] M. Kontopoulou, M. Kaufman, A. Docoslis, *Rheol. Acta* **2008**, *48*, 409.
[32] C. S. Boland, U. Khan, G. Ryan, S. Barwich, R. Charifou, A. Harvey, C. Backes, Z. Li, M. S. Ferreira, M. E. Möbius, R. J. Young, J. N. Coleman, *Science* **2016**, *354*, 1257.
[33] P. Sheng, E. K. Sichel, J. I. Gittleman, *Phys. Rev. Lett.* **1978**, *40*, 1197.
[34] A. Narayanan, F. Mugele, M. H. Duits, *Langmuir* **2017**, *33*, 1629.
[35] M. Hahn, D. Rosenbach, A. Krimalowski, T. Nazarenus, R. Moos, M. Thelakkat, M. A. Danzer, *Electrochim. Acta* **2020**, *344*, 136060.
[36] M. A. Danzer, *Batteries* **2019**, *5*, 53.
[37] M. Hahn, S. Schindler, L.-C. Triebs, M. A. Danzer, *Batteries* **2019**, *5*, 43.
[38] Z. Samir, Y. El Merabet, M. P. F. Graça, S. S. Teixeira, M. E. Achour, L. C. Costa, *Polym. Compos.* **2018**, *39*, 1297.
[39] M. Mours, H. H. Winter, in *Experimental Methods in Polymer Science* (Ed: T. Tanaka), Academic Press, Boston, MA **2000**, p. 495.

Macromolecular Rapid Communications

Supporting Information

for *Macromol. Rapid Commun.*, DOI 10.1002/marc.202200307

Self-Healing and Electrical Properties of Viscoelastic Polymer–Carbon Blends

*Pavel Milkin, Michael Danzer and Leonid Ionov**

Supporting Information

Self-Healing and Electrical Properties of Viscoelastic Polymer-Carbon Blends

*Pavel Milkin, Michael Danzer, and Leonid Ionov**

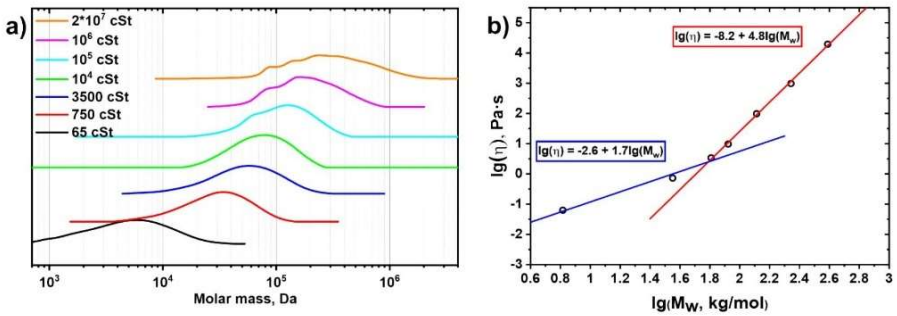

Figure S1. a) Linear approximation of lg(η) vs lg M_w. The viscosity $\eta \sim M_w^{1.7}$ below and $\eta \sim M_w^{4.8}$ behind the critical molecular mass of entanglements formation. b) Gel permeative chromatography results for pure PDMSs (swap left and right images)

Table S1. The parameters of PDMS precursors

Kinematic viscosity, cSt	***Viscosity, Pa·s***	***Mn, kg/mol***	***Mw, kg/mol***	***PDI***
65	0.06	3.5	6.5	1.9
750	0.73	23	36	1.5
3500	3.4	39	64	1.6
10^4	9.7	62	84	1.4
10^5	97.7	91	130	1.4

1

10^6	978	150	220	1.5
$2 \cdot 10^7$	19580	208	388	1.9

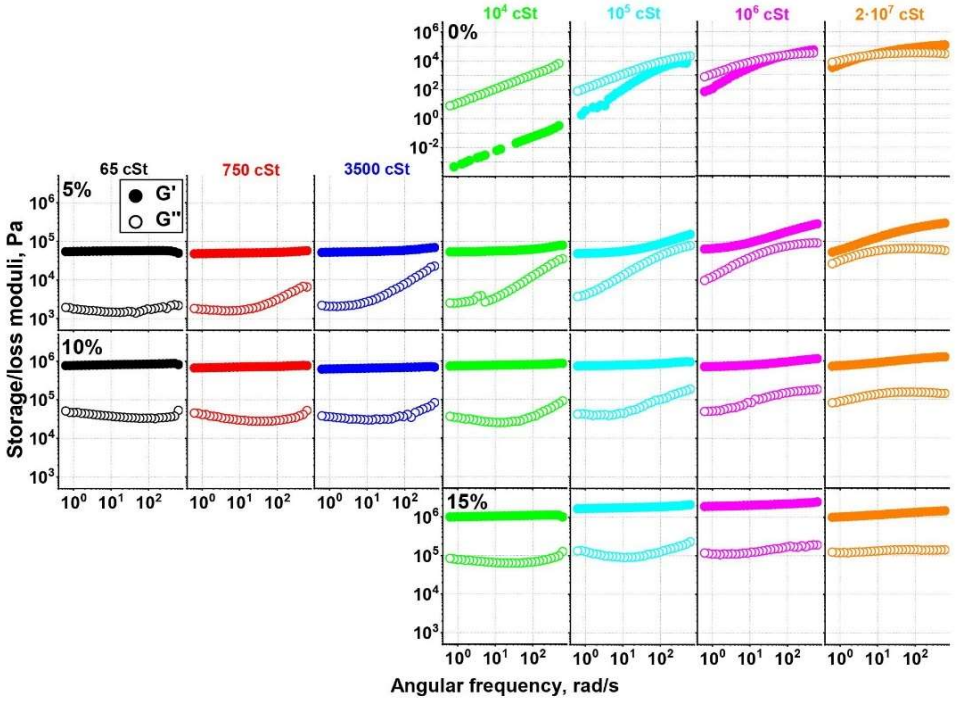

Figure S2. Frequency sweep data for different linear PDMSs with various CB content: 5, 10, and 15 vol.%.

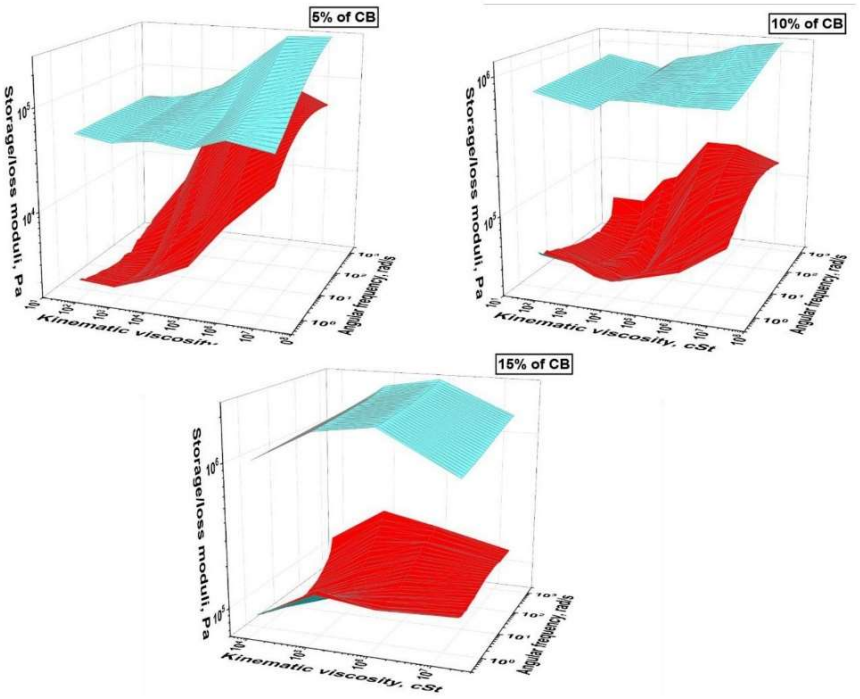

Figure S3. Frequency sweep of linear PDMS with various CB content plotted as G′/G′′(Pa) vs η (cSt) vs ω (rad/s). Cyan and red colours are attributed to storage and loss modulus, respectively.

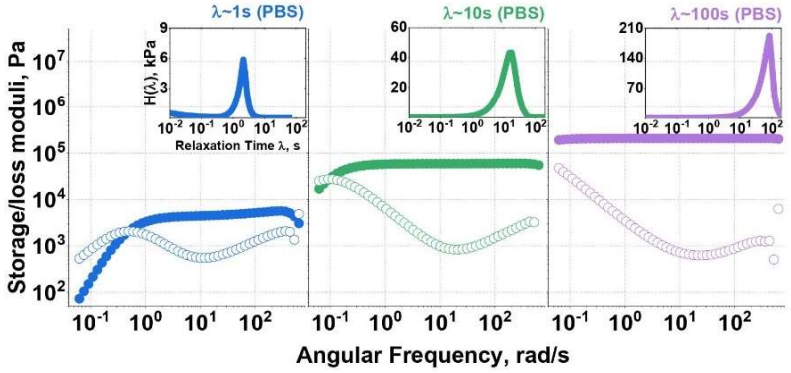

Figure S4. PBS with different content of boric acid. The higher boric acid content leads to increase in relaxation time of the polymer.

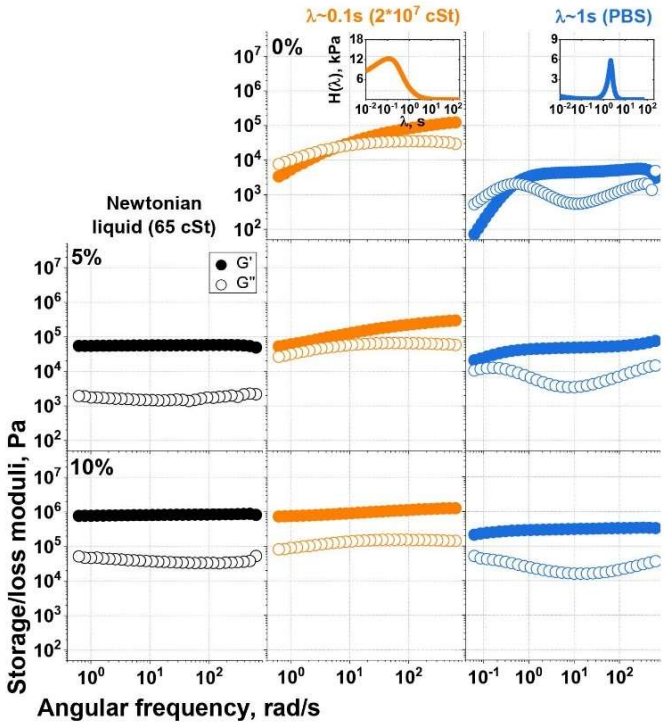

Figure S5. Dynamic test of the pure polymers and their composites with 5 and 10 vol.% of CB where black plots are PDMS 65 cSt as Newtonian liquid, orange plots are PDMS $2 \cdot 10^7$ cSt with relaxation time $\lambda \approx 0.1$s, and blue plots are PBS with relaxation time $\lambda \approx 1$s.

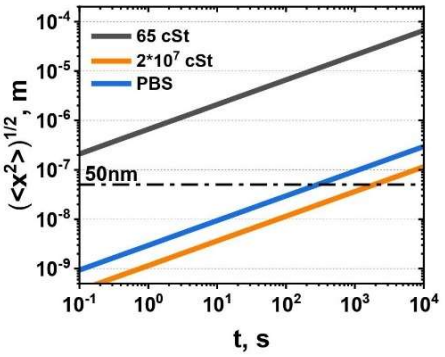

Figure S6. The translation diffusion of spherical carbon black particles. The displacement is given by $\langle x^2 \rangle = 6D_t t$, where D_t is translation diffusion coefficient given by $D_t = kT/(6\pi\eta r)$, where η is zero strain viscosity, r – radius of particles, T – temperature.

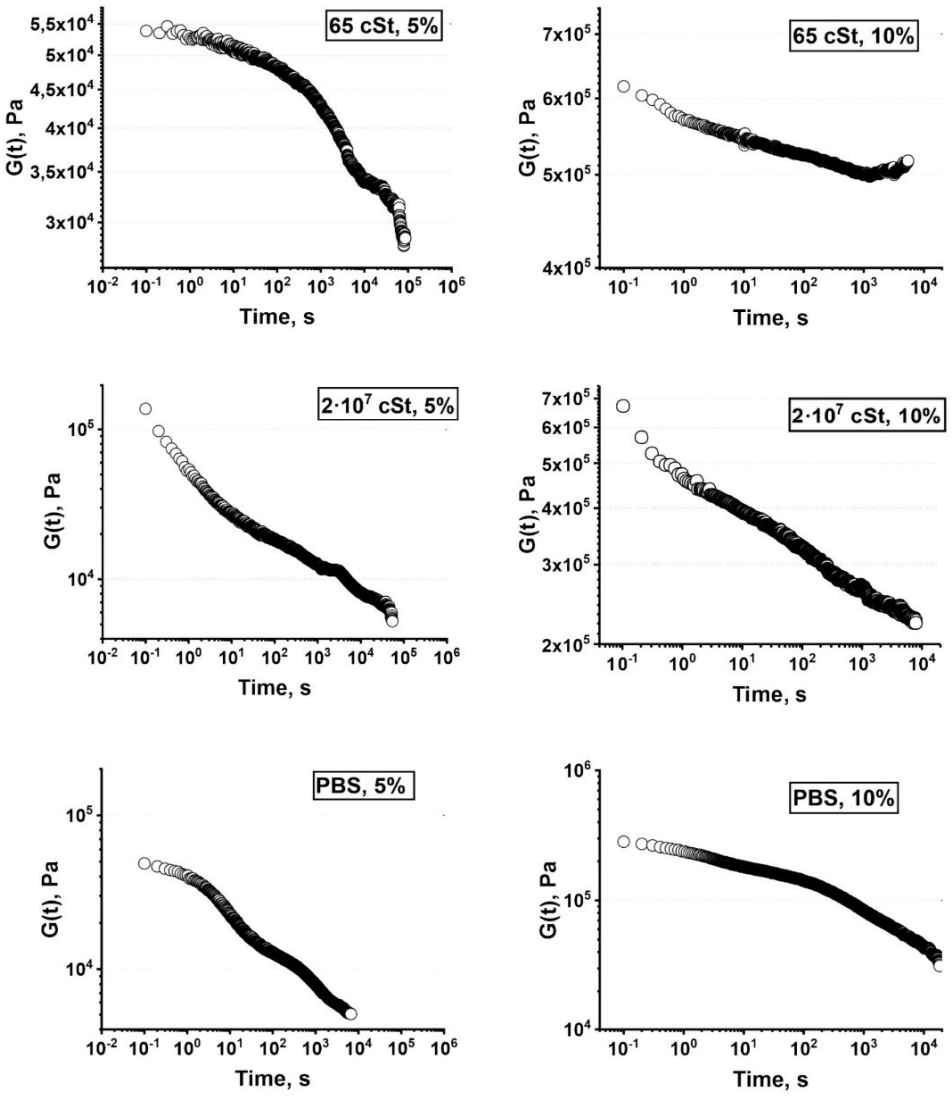

Figure S7. Relaxation modulus data for several PBS-PDMSs composites measured at constant strain γ=0.05%

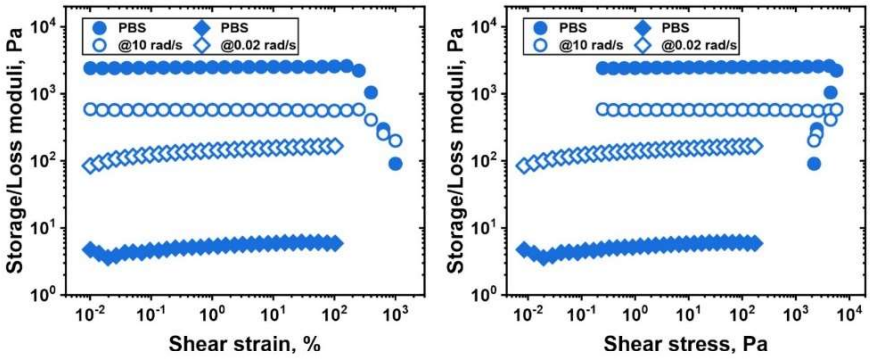

Figure S8. Amplitude sweep of pure PBS with relaxation time λ~1s at different frequency

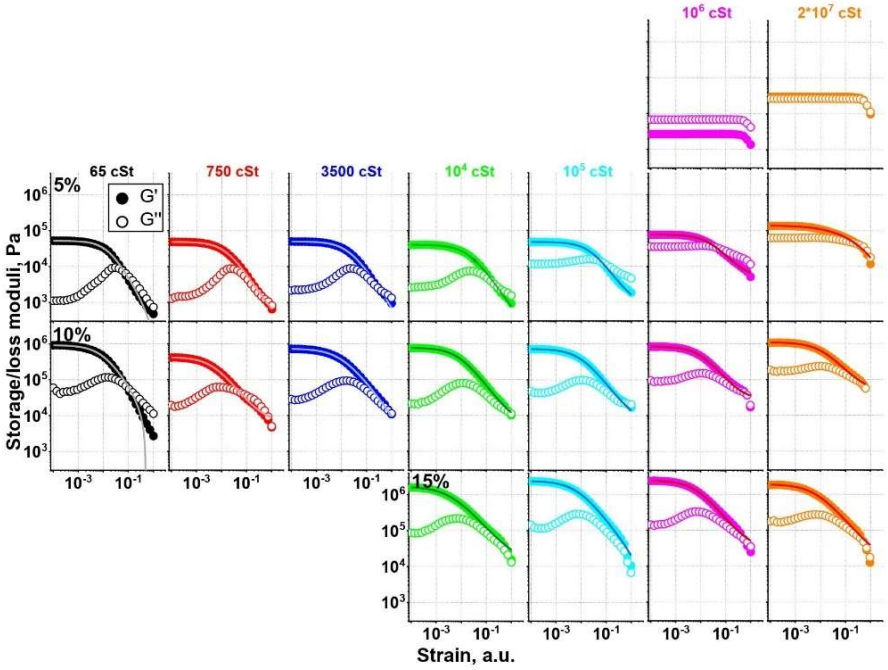

Figure S9. Amplitude sweep data plotted as Moduli vs Strain for different linear PDMSs with various CB content. The G´ vs Strain is fitted with the Krauss model according to the equation:

$$G'(\gamma_c) = G'_\infty + \frac{G'(\gamma_0) - G'_\infty}{1 + \left(\frac{\gamma_0}{\gamma_c}\right)^{2m}}$$

where $G'(\gamma_0) - G'_\infty$ is the difference of storage moduli at zero and infinite strain respectively, γ_c is the amplitude at which $G'(\gamma_0) - G'_\infty$ has decreased to half of its zero-strain value; m is a universal value ($m \approx 0.5 \ldots 0.6$) which is independent of the specific type of filler. The value γ_c can also be expressed as $\gamma_c = \left(\frac{k_r}{k_b}\right)^{\frac{1}{2m}}$, where k_r and k_b are rate constants of network reformation and breaking, respectively

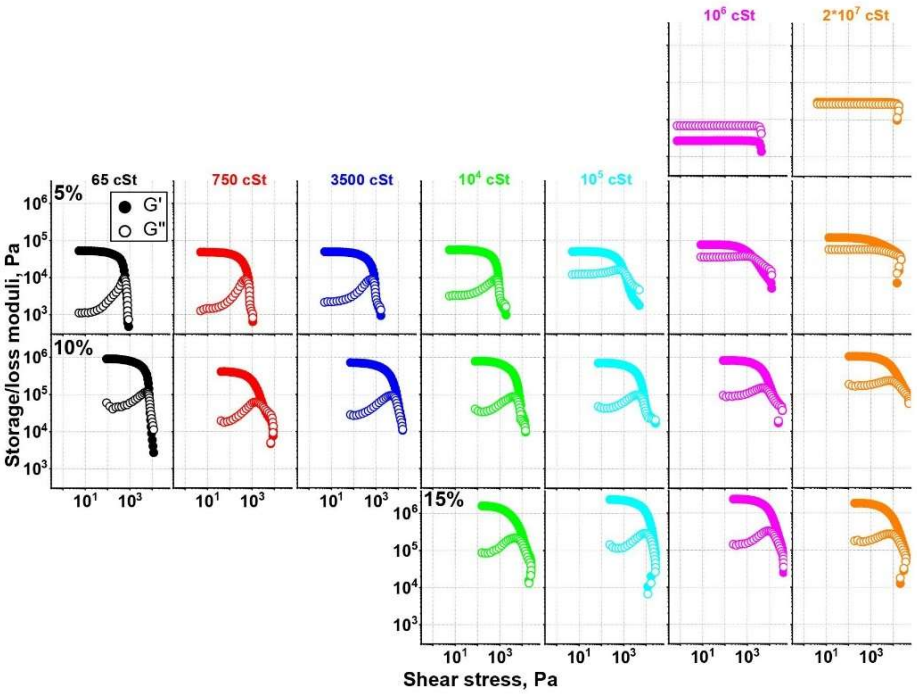

Figure S10. Amplitude sweep data plotted as Moduli vs Shear stress for different linear PDMSs with various CB content.

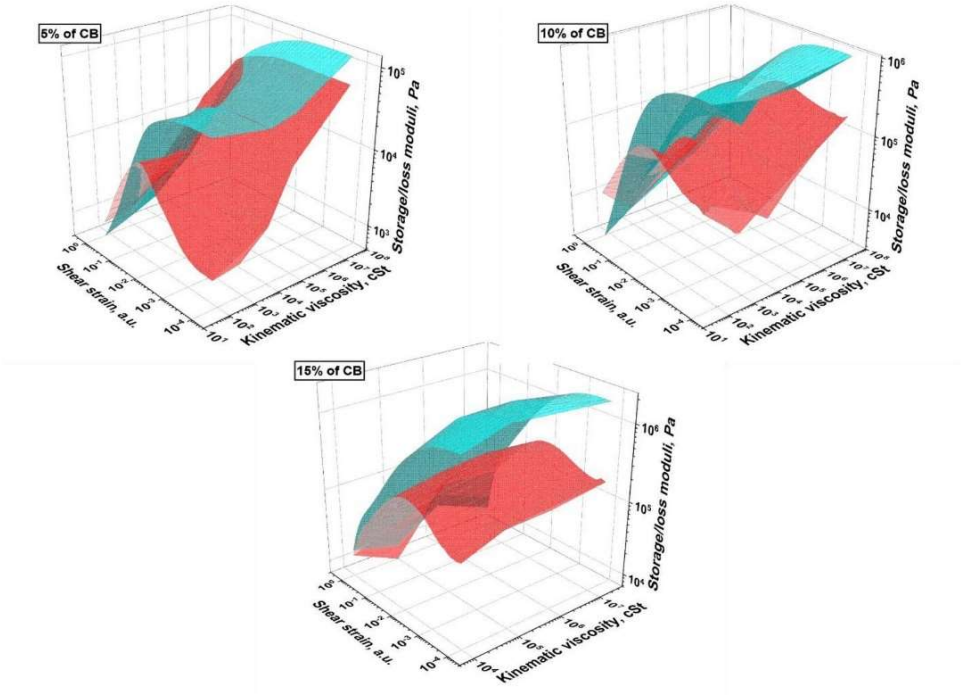

Figure S11. Amplitude sweep of linear PDMS with various CB content plotted as G′/G′′(Pa) vs η (cSt) vs γ_{shear} (a.u.). Cyan and red colours are attributed to storage and loss modulus, respectively.

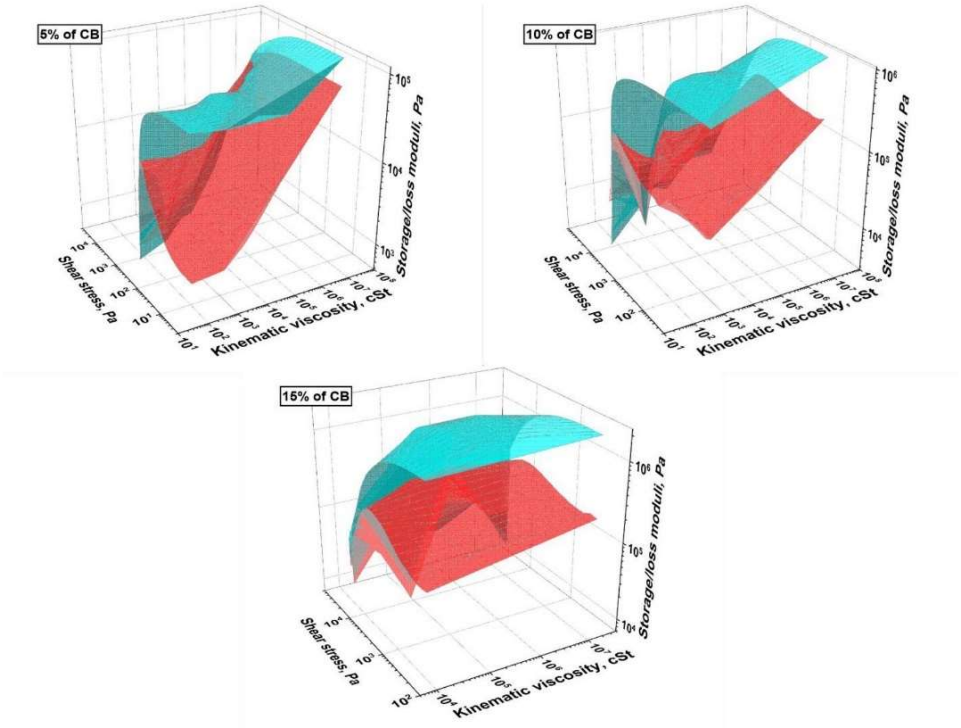

Figure S12. Amplitude sweep of linear PDMS with various CB content plotted as G′/G′′(Pa) vs η (cSt) vs τ_{shear} (Pa). Cyan and red colours are attributed to storage and loss modulus, respectively.

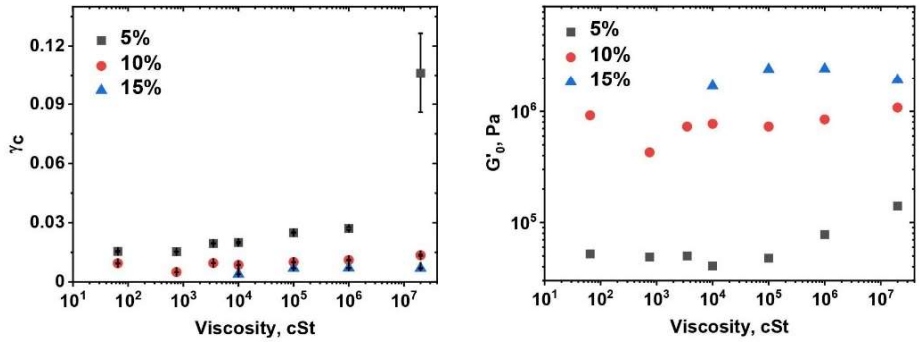

Figure S13. Krauss model fitting parameters for different linear PDMSs with various CB content.

Table S2. Krauss model fitting parameters for different linear PDMSs with various CB content

PDMS	Vol. fr. of CB	$G'_{inf.}$ kPa	G'_0. kPa	G'_0-$G'_{inf,}$ kPa	γ_c	m	k_r/k_b
65	5	-0.3	52	52	0.015	0.60	0.007
	10	17	921	938	0.009	0.50	0.009
750	5	0.1	49	49	0.015	0.54	0.011
	10	6	428	421	0.005	0.49	0.006
3500	5	-0.1	50	50	0.02	0.52	0.016
	10	-2	729	732	0.001	0.44	0.016
10^4	5	0.02	41	41	0.02	0.51	0.019
	10	5	772	767	0.009	0.49	0.009
	15	12	1695	1683	0.004	0.41	0.010
10^5	5	0.8	48	47	0.025	0.54	0.019
	10	5	728	723	0.01	0.48	0.012
	15	-7	2430	2437	0.007	0.45	0.011
10^6	5	5	78	73	0.027	0.50	0.028
	10	27	846	819	0.011	0.50	0.011
	15	29	2450	2421	0.007	0.50	0.009
$2*10^7$	5	15	141	156	0.11	0.30	0.27
	10	45	1082	1037	0.013	0.46	0.019
	15	12	1929	1917	0.007	0.43	0.014
PBS	5	20	52	32	0.018	0.60	0.008
	10	45	413	368	0.008	0.50	0.008

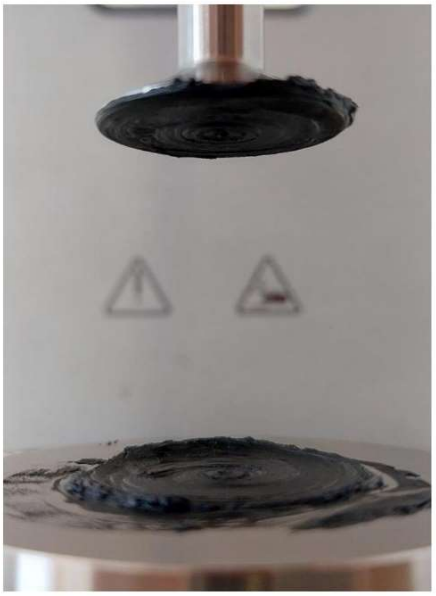

Figure S14. Tack test of PDMS 65 cSt – 5% of CB blend. The test demonstrates cohesion type of failure of the blend at high shear deformations

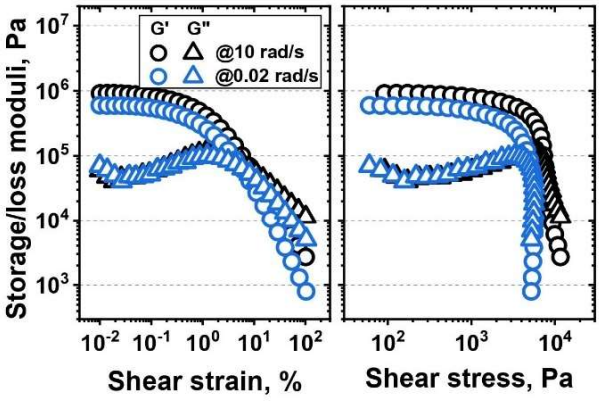

Figure S15. Amplitude sweep test for PDMS 65 cSt composite with 10% of CB at various frequencies

Table S3. Mechanical properties of PBS – CB blends at different amplitude/frequency in a nutshell

Frequency

13

		low	high
Amplitude	**low**	Elastic (particles)	Elastic (polymer + particles)
	high	Viscous (polymer)	Elastic (polymer)

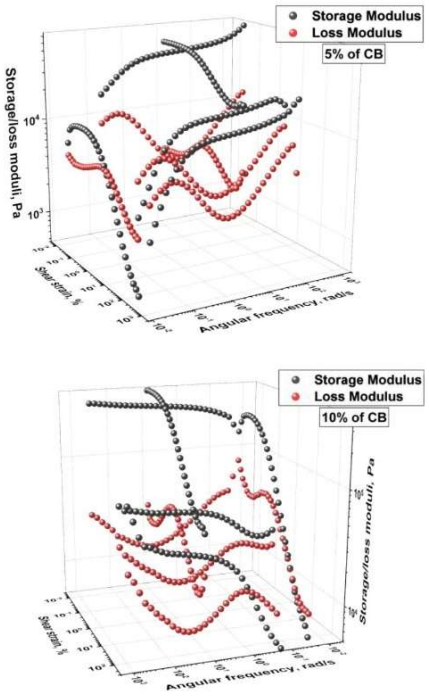

Figure S16. Several sections of 3D plot Storage/loss moduli vs Shear strain vs Angular frequency, received from Amplitude sweep and Frequency sweep experiments at different conditions

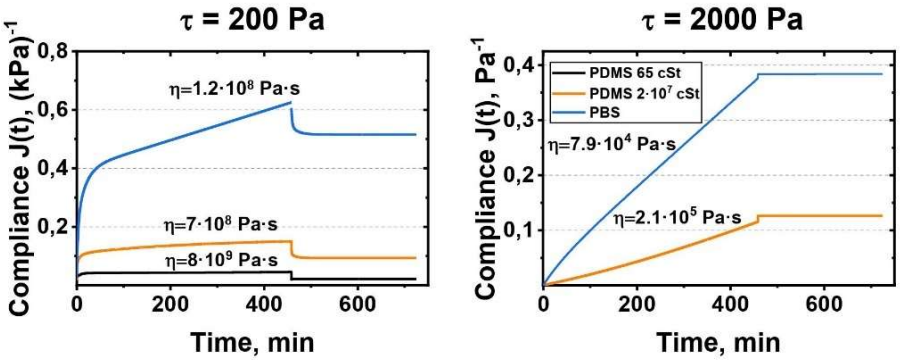

Figure S17. Creep compliance of the polymers composites with 5 vol.% of CB at 200 Pa and 2000 Pa shear

Table S4. The materials parameters and retardation times λ_i at load phase of creep test. The retardation times are extracted from compliance curve fitting

$$J(t) = J_0 + \sum_{i=1}^{3} J_{m_i}\left(1 - e^{-\frac{t-t_0}{\lambda_i}}\right)$$

	τ_0, Pa	η_0, MPa*s	J_0, μPa^{-1}	λ_1, s	λ_2, s	λ_3, s	$\dot{\gamma}$, ms^{-1}
65 cSt, 5% of CB	**200**	7613	27.3	315	112.7	53.5	0.003
	2000	*Cohesion rapture*					
2·10^7 cSt, 5% of CB	**200**	676	13.3	882	60.8	5.6	0.019
	2000	0.16	21.1	27371	273.7	11.3	0.95
PBS, 5% of CB	**200**	120	24.0	1057	170.2	15.6	0.17
	2000	0.08	79.4	2995	143.7	4.7	2.55

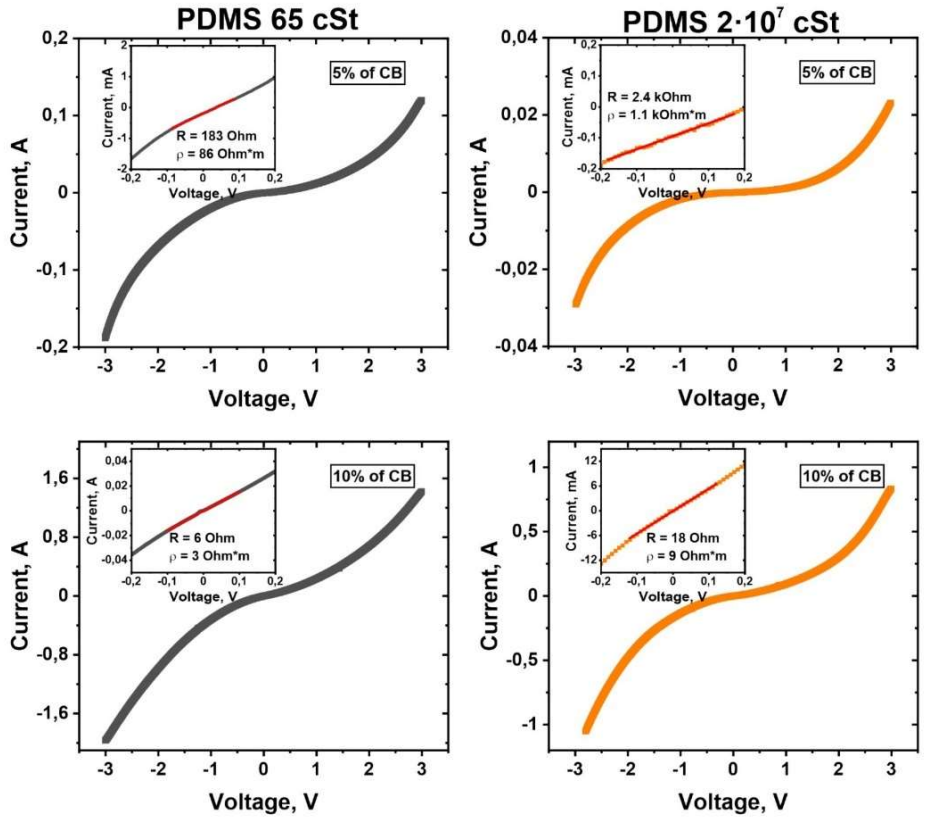

Figure S18. Volt-ampere characteristic of linear PDMS 65 and $2 \cdot 10^7$ cSt with 5 and 10 vol.% of CB at 100 mV/s scanning rate

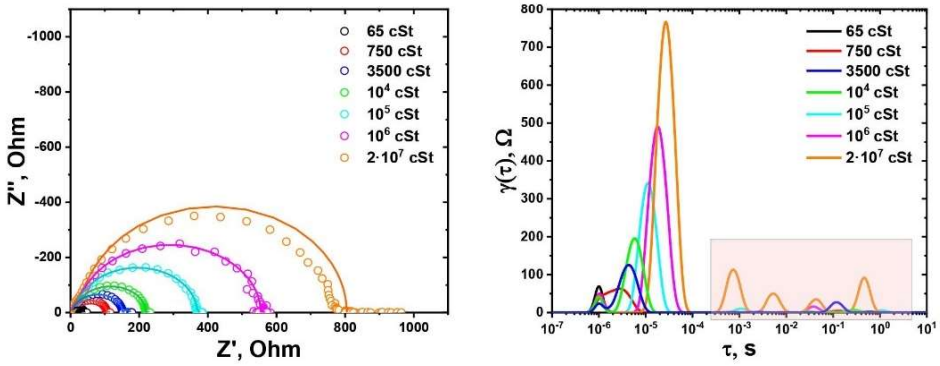

Figure S19. a) Nyquist plot of EIS for linear PDMSs with various chain lengths with 5 vol.% of CB. b) DRT (distribution of relaxation times) functions for these composites. The following DRT model was used:

$$Z_{DRT} = R_{\infty} + \int_{-\infty}^{\infty} \frac{\gamma(\ln \tau)}{1 + i2\pi f\tau} d \ln \tau$$

where R_{∞} is the Ohmic resistance, and $\gamma(\ln \tau)$, the DRT, is a suitable function that describes the time relaxation characteristics of the electrochemical system studied [40]

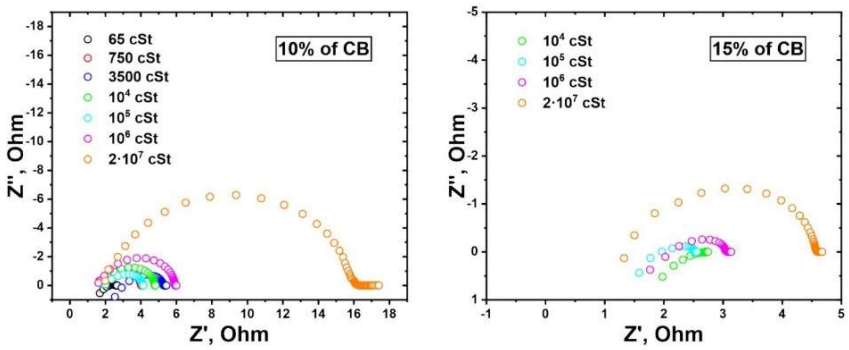

Figure S20. Nyquist plot of EIS for linear PDMSs with various chain lengths with 10 and 15 vol.% of CB

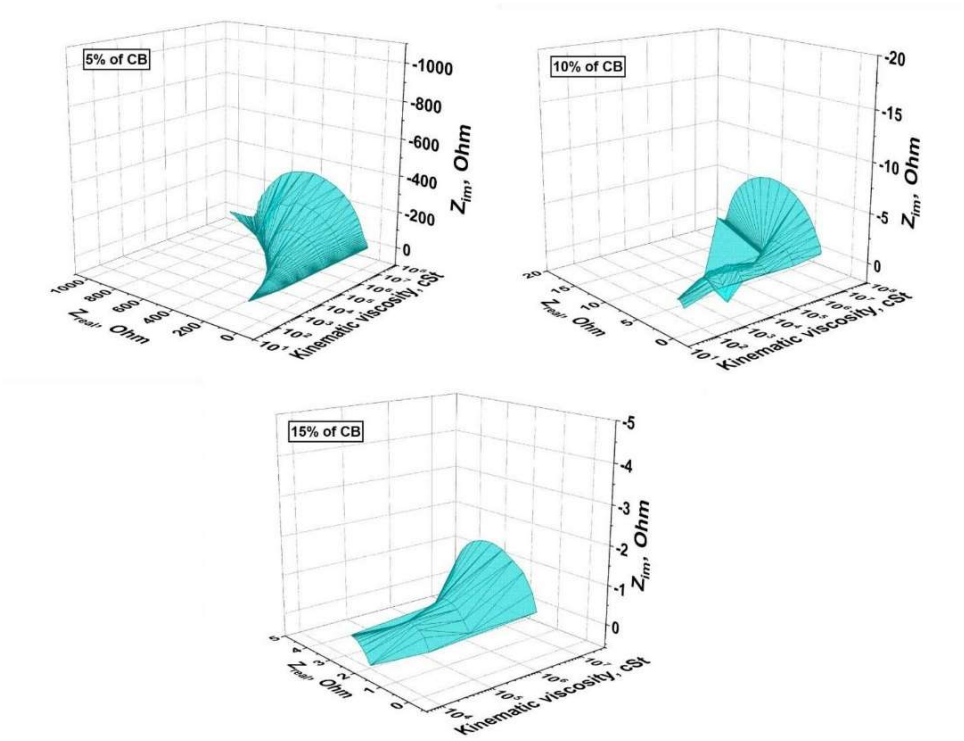

Figure S21. 3D visualisation of Nyquist plot for linear PDMS with different carbon content as a function of PDMS viscosity

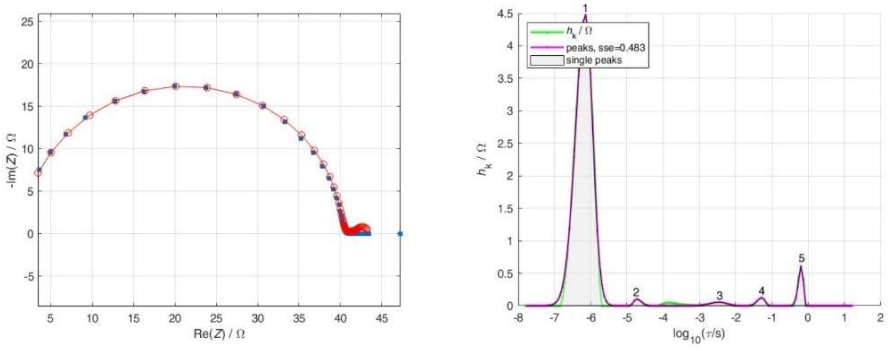

18

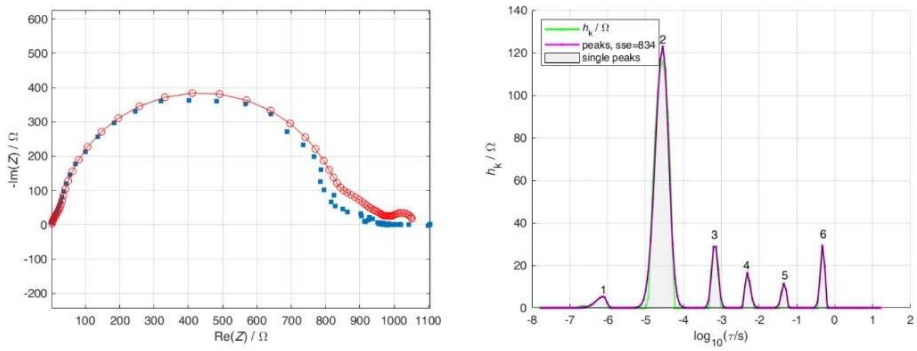

Figure S22. The EIS Nyquist plot modelling and DRT analysis of 5 vol.% CB composites with polymer matrix a) 65 cSt, b) $2 \cdot 10^7$ cSt

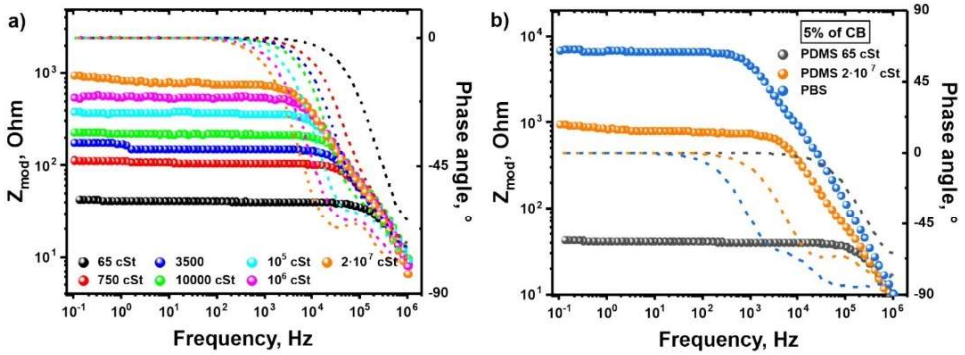

Figure S23. a) Bode plot of EIS at 0V offset with 10mV amplitude of various linear PDMS with different molecular weight with 5% of CB; b) Bode plot of blends of polymer with different relaxation time and 5% of CB

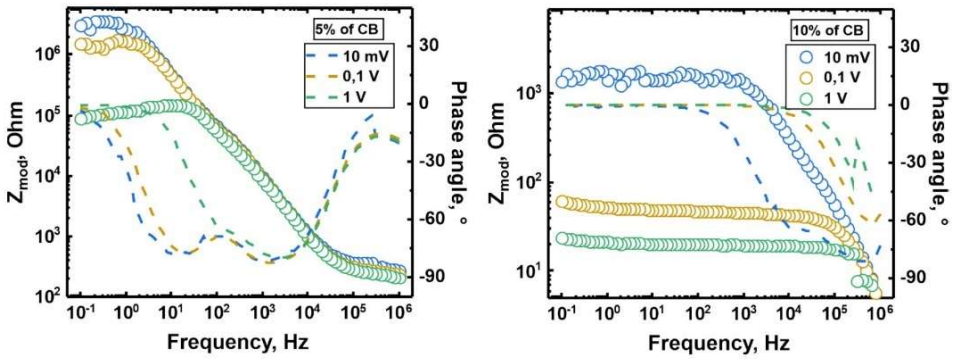

Figure S24. Bode plot of EIS of a PBS-CB composites at 0V offset with various amplitude

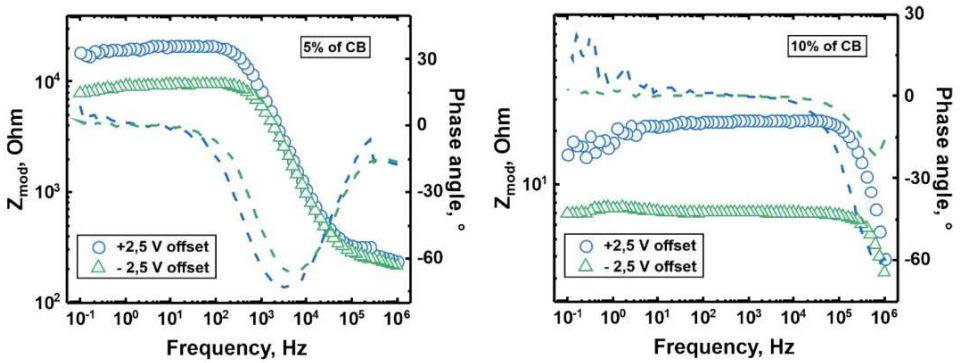

Figure S25. Bode plot of EIS of a PBS-CB composites at 2.5V offset with 10mV amplitude

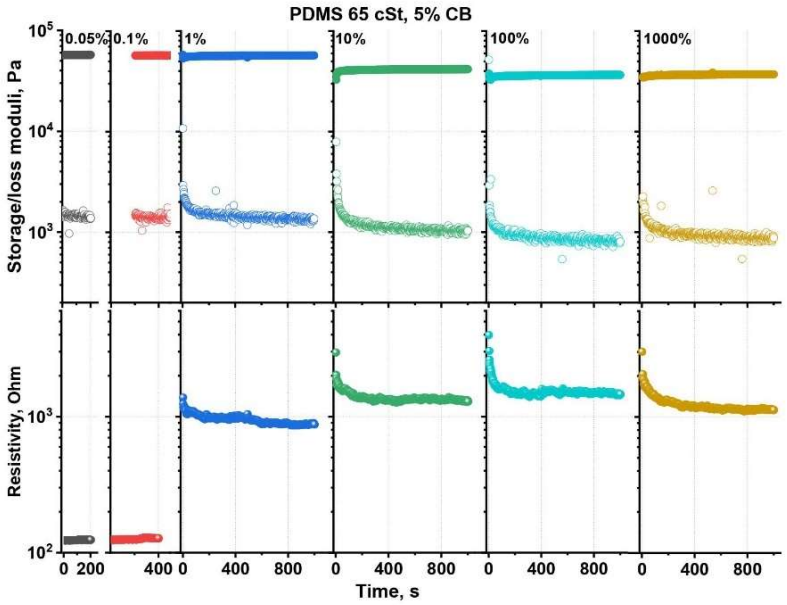
PDMS 65 cSt, 5% CB
0.05%
0.1%
1%
10%
100%
1000%
Storage/loss moduli, Pa
Resistivity, Ohm
Time, s

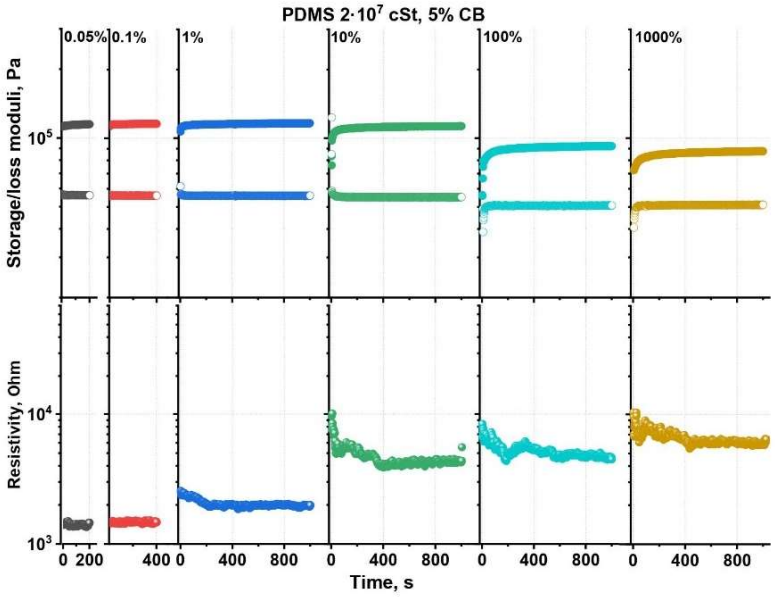
PDMS 2·10^7 cSt, 5% CB
0.05%
0.1%
1%
10%
100%
1000%
Storage/loss moduli, Pa
Resistivity, Ohm
Time, s

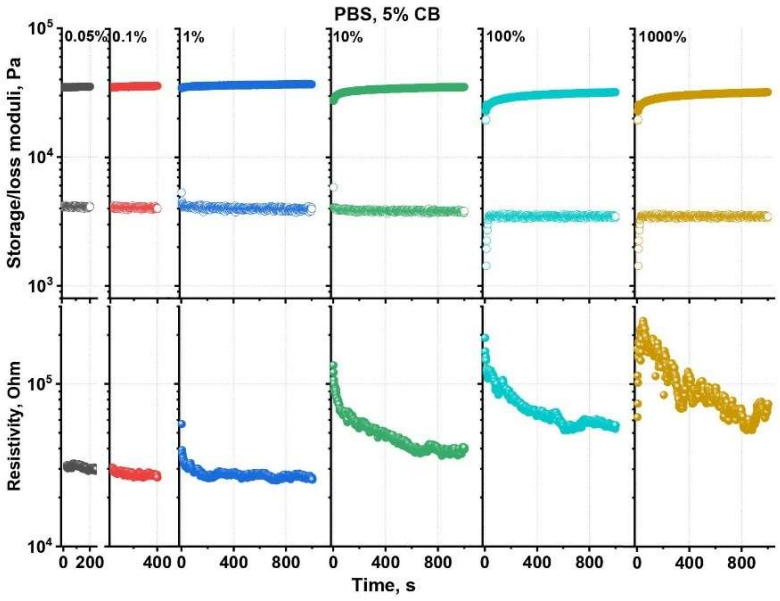

Figure S26. Recovery of electromechanical characteristics of PDMS/PBS – CB blends after sequence of several shear deformations

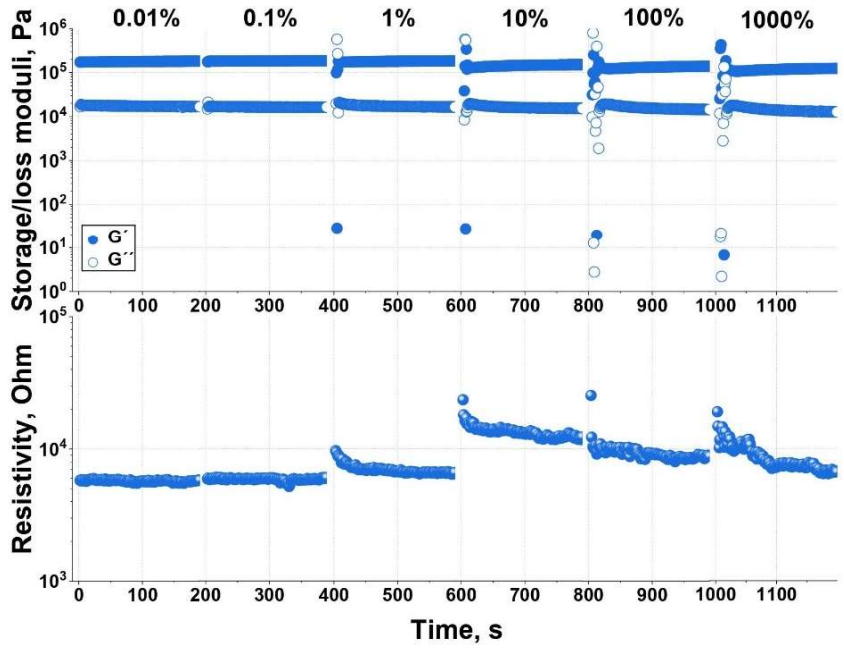

Figure S27. Recovery of electromechanical characteristics of PBS blend with 10% of CB after sequence of several shear deformation

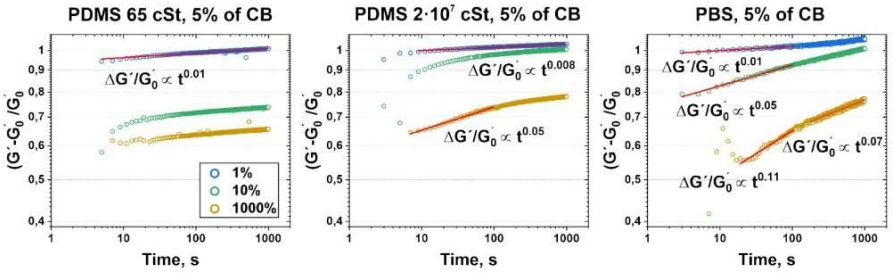

Figure S28. Restoration of storage moduli after various one step shear deformation of polymer-CB blends with 5 vol.% of CB as *(G´- G₀´)/G₀´=f(t)*.

References

1. Wan, T.H., et al., *Influence of the Discretization Methods on the Distribution of Relaxation Times Deconvolution: Implementing Radial Basis Functions with DRTtools.* Electrochimica Acta, 2015. **184**: p. 483-499.

Part 2. Superelastic, soft, stress-healable, recyclable conductive materials

Milkin P.; Zhanbassynova A.; Ionov L.

Publiched in Composite Structures, 327

2024

Composite Structures 327 (2024) 117709

Contents lists available at ScienceDirect

Composite Structures

journal homepage: www.elsevier.com/locate/compstruct

Superelastic, soft, stress-healable, recyclable conductive materials

Pavel Milkin [a], Ainur Zhanbassynova [a], Leonid Ionov [a,b,*]

[a] Faculty of Engineering Sciences, University of Bayreuth, Ludwig Thoma Str. 36A, 95447 Bayreuth, Germany
[b] Bavarian Polymer Institute, University of Bayreuth, 95447 Bayreuth, Germany

ARTICLE INFO

Keywords:
Self-healing
Viscoelasticity
Silly-putty
Conductive composite
Low loss coefficient

ABSTRACT

We report the design of materials with a unique combination of self-healing ability, electrical conductivity (8–150 Ohm·m), softness (G = 1 MPa), extremely low loss coefficient (tan δ ≈ 0.04) even at large deformations and linearity of resistivity dependence on strain in a broad range. The conductive material can bounce with very low energy dissipation at fast deformation, and it flows and self-heals at a large time scale and when sufficient stress is applied. The key to such properties is a combination of very stable interpenetrated networks formed by multiwalled carbon-nanotubes (MWCNT) filler and by viscoelastic polyborosiloxane (PBS) polymer matrix rendering relaxation processes and self-healing ability. We demonstrated the promise of the developed materials for the design of strain sensors with a very large linear regime and rubber-substitute as a protective coating or a sealing agent material.

1. Introduction

Self-healing materials i.e. materials, which are able to recover their structural integrity and/or functionality, are highly desirable for a variety of applications including coating industry, civil engineering [1], electronics [2], etc. There are many approaches for the design of self-healing materials using encapsulated reactive fluid substances, interchain diffusion, covalent bond reforming, shape-memory, van der Waals interaction, etc [3]. In most of the reported examples, the self-healing of mechanical integrity (repair of scratches, re-joining of cut pieces) was targeted. The self-healing of functionality is more exotic and more challenging because it assumes reconstruction of the micro/nano-structure of materials as it was before the failure. The most widely explored self-healing functionality is conductivity. There are examples of materials with self-healing electrical conductivity based on viscoelastic polymer filled with conductive particles [4] and self-healing ionic conductivity based on viscoelastic polyelectrolyte gels [5]. These and other self-healing conductive materials were explored to be used in different elements of soft electronics [6] such as gas sensors [7], strain sensors [8], photovoltaic devices [9], batteries [10], etc.

The main approach for the fabrication of self-healing electrical conductors is based on embedding a conductive filler into/on a self-healing polymer matrix. The most popular conductive fillers are carbon materials such as carbon black, graphene, carbon nanotube etc. due to their low cost, low weight, and relatively high conductivity. The autonomous healing mechanisms are defined by the nature of the polymer and its interaction with a filler and itself through metal–ligand coordination [11], H-bonding [12], π-π stacking [13], dynamic covalent bonding[14], etc i.e. bonds with relatively low dissociation activation energy. Important requirements for the realization of these mechanisms are relatively high mobility of filler inside of polymer matrix, as well as the high mobility of polymer chains to allow self-healing. As consequence, the polymer should be at a temperature higher than its glass transition temperature. It implies the viscoelastic behavior of such blends, which is the combination of viscoelastic properties of both filler and polymer. Therefore, the demonstration of restoration of structural integrity alone is not enough to prove the healing abilities of material, but it is also crucial to consider relaxation processes, rheological, and electromechanical properties under different conditions for the definition of device limits since it directly affects its functionality. As result of viscoelastic nature of self-healing polymers, the self-healing materials dissipate mechanical energy and do not demonstrate highly elastic deformation [15].

We previously investigated the effect of polymer viscoelasticity on healing, mechanical and conductive properties of PDMS/polyborosiloxane (PBS) – carbon black (CB) blends with different filler

Abbreviations: PBS, polyborosiloxane; PDMS, polydimethylsiloxane; CB, carbon black; MWCNT, multiwalled carbon nanotubes; GN, Graphene nanoplates THF, tetrahydrofuran; LVE, linear viscoelastic region; FESEM, field emission scanning electron microscopy; EIS, electroimpedance spectroscopy; AC, alternating current.

* Corresponding author.
E-mail address: leonid.ionov@uni-bayreuth.de (L. Ionov).

https://doi.org/10.1016/j.compstruct.2023.117709
Received 22 May 2023; Received in revised form 30 August 2023; Accepted 6 November 2023
Available online 7 November 2023

concentrations [16]. We demonstrated the influence of the relaxation time of the viscoelastic polymer matrix on the rheological properties of the composites. A polymer matrix with a small relaxation time allows the formation of a stronger filler network, and quick restoration of electrical and mechanical properties, good conductivity, but for that, we sacrifice the ability to flow and ductility of material at large deformation. In contrast, the composites with a large relaxation time of polymer matrix behave elastically on a small time scale due to a weak network: they flow at a large time scale and can heal. However, electrical properties are worse compared to that formed by low molecular weight analogs and degrade with time. Thus, it is a double edge sword working with viscoelastic blends: either we sacrifice mechanical and healing properties, or electrical. Although these materials are able to demonstrate the reversibility of deformation on a time scale smaller than the relaxation time of polymer chains, they still dissipate a considerable fraction of energy, in particular, at large deformations and values of applied stress.

Here we make a step forward in the design of self-healing conductive materials and report the design of superelastic self-healing conductive materials with a unique combination of properties such as (i) relatively high conductivity, (ii) self-healing of both mechanical integrity and (iii) conductivity at large time scales as well as (iv) highly elastic behavior (energy loss is < 4 %) at short time scales in a very broad range of applied deformation. In other words, it is self-healing conductive material that is able to bounce when it is dropped on a solid surface independently if it falls from a low or large height - the material does not get smashed. In order to approach this goal, we studied the effect of the nature of conductive carbon particles on the mechanical, electrical, and self-healing properties of polyborosiloxane (PBS)-carbon composites. Carbon fillers were chosen with different aspect ratios (δ) (rode-like multiwalled carbon nanotubes (MWCNT) with $\delta > 1$, spherical Carbon Black (CB) with $\delta \approx 1$, and Graphene Nanoplates (GN) with $\delta < 1$) in a viscoelastic PBS matrix. Due to the viscoelasticity of composites, we investigated the relaxation processes of polymer and filler in their blends, internal microstructure, and a variety of mechanical and electrical responses on large and small time scales. In addition, we examined the self-healing kinetics of electro-mechanical characteristics of composites through simultaneous rheological and electrical impedance measurements *in situ*. The study allows understanding of the internal processes occurring in carbon viscoelastic blends, defining their limits, and better choosing a material for specific applications.

2. Experimental section/methods

Materials. The hydroxyl-terminated PDMS with kinematic viscosity 65 cSt was purchased from Sigma-Aldrich. The carbon black with BET determined surface area 62 m^2/g was purchased from Nanografi Company. Multiwalled carbon nanotubes (MWCNT) (NC7000^{TM}, Nanocyl SA, Belgium) and graphene nanoplates (GN) (Sigma-Aldrich) were used. Toluene (Sigma Aldrich, ≥99.5 %), tetrahydrofuran (Roth, ≥99.5 %), and boric acid (Sigma Aldrich, ≥99.5 %) were purchased and used as it is.

PBS synthesis. PBS was synthesized by the following Tang et al. essay [17]. To prepare PBS (relaxation time is ca 0.5 s and plateau shear modulus is ca $2{\cdot}10^4$ Pa), the mass ratio between the hydroxyl-terminated PDMS 65 cSt and H_3BO_3 100:0.88 was chosen. First, the PDMS was dissolved in toluene. Then, boric acid was added to the solution, and the mixture was dispersed for a couple of minutes in an ultrasonic bath. The mixture was heated to 120 °C with Dean-Stark trap, and left for 48 h with further stirring. After this time, the mixture became transparent. Excess solvent was removed with a vacuum evaporator, and the rest of the solvent was removed by storing the sample in a vacuum oven at 60 °C for 24 h.

Preparation of polymer-carbon composites. PBS/carbon composites with various volume fractions of carbon material were synthesized, assuming that GN, CB, MWCNT, and polymers densities are 2.2 g/cm^3, 2 g/cm^3, 2 g/cm^3, and 1 g/cm^3, respectively. First, the polymer was dissolved in toluene at 60 °C in 1 h. Then, carbon filler was added to polymer solution in toluene. The mixture was dispersed in an ultrasound bath and then mixed with IKA RW 20 disperser for 30 min at 1200 rpm. Excess toluene was evaporated in a vacuum desiccator. The rest of the solvent was removed by storing samples in a vacuum oven at T = 60 °C for 24 h.

Characterization. The microstructure of composites and pristine filler particles was investigated by field emission scanning electron microscopy (FESEM) (Thermo Scientific, Germany). Rheological measurements were carried out with 25 mm parallel plate geometry on MCR 702 (Anton Paar, Graz, Austria) coupled with a dielectric measuring cell. All samples were roughly flattened before lowering the rheometer to a gap size of approximately 1 mm. Then samples were allowed to relax and reach measurement temperature for 15 min. Electrochemical Impedance Spectroscopy (EIS) measurements were performed at 25 °C in the frequency range from 0.1 Hz to 1 MHz on Gamry 1010E potentiostat. The resistivity of the sample during the tensile test was performed on the same potentiostat, the electrical contacts were wired with copper tape on rheometer clamps.

The relaxation time λ is defined as the peak time of continuous relaxation spectra H(λ), which is for infinite time-scale generalized Maxwell model can be expressed as

$$G'(\omega) - G_e = \int_{-\infty}^{\infty} H(\lambda) \frac{\omega^2\lambda^2}{1+\omega^2\lambda^2} d(ln\lambda) \quad (1)$$

$$G''(\omega) = \int_{-\infty}^{\infty} H(\lambda) \frac{\omega\lambda}{1+\omega^2\lambda^2} d(ln\lambda) \quad (2)$$

where ω is frequency, G_e is a material parameter (residual moduli after complete material relaxation).

The time-scale extension was achieved by relaxation experiment, where relaxation modulus was recalculated into relaxation spectra H(λ) and storage/loss moduli according to the generalized Maxwell model as well:

$$G(t) = G_e + \sum_{i=1}^{N} g_i e^{-t/\lambda_i} \quad (3)$$

$$H(\lambda) = \sum_{i=1}^{N} g_i \delta(\lambda/\lambda_i - 1) \quad (4)$$

$$G'(\omega) = \omega \int_0^{\infty} G(t)\sin(\omega t)dt \quad (5)$$

$$G''(\omega) = \omega \int_0^{\infty} G(t)\cos(\omega t)dt \quad (6)$$

where coefficients g_i, G_e, and relaxation times λ_i are material parameters, δ(y) is the Dirac delta function.

3. Results and discussion

3.1. Pure materials and composites fabrication

To investigate the influence of different types of filler on mechanical, rheological, and electrical characteristics of viscoelastic polymer–carbon composites, we chose carbon compounds with various aspect ratios δ (Fig. 1**a**): rod-like MWCNT with $\delta > 1$, spherical Carbon Black with $\delta \approx 1$, and plate-like Graphene Nanoplates with $\delta < 1$. The aspect ratio δ is presented as the ratio of the thickness of the interface to the smallest dimension of the particle. As polymer matrix material, viscoelastic polyborosiloxane was used. The PBS is a product of polycondensation of hydroxyl-terminated PDMS and boric acid, creating crosslinked network due to Si – O – B bonds and supramolecular

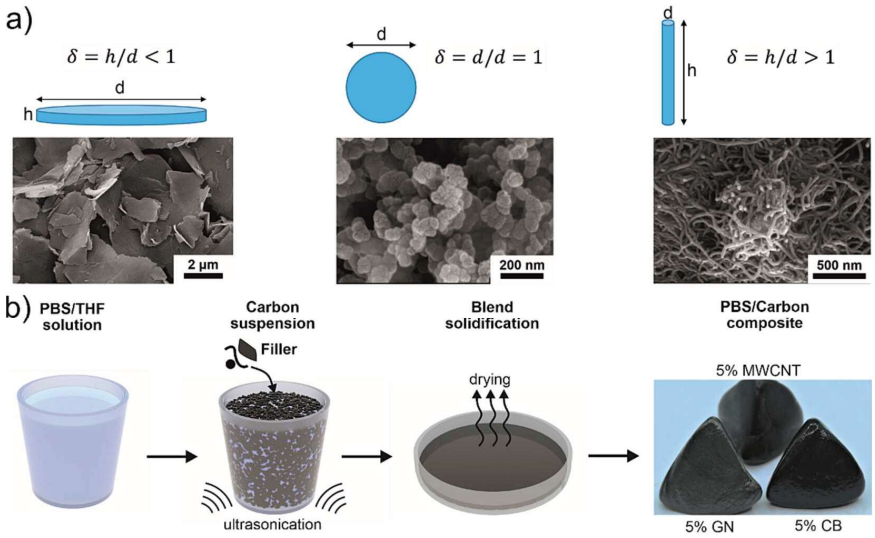

Fig. 1. Preparation of carbon-polymer composites: a) SEM pictures of pristine carbon particles with various aspect ratios δ; b) schematic illustration of the composites fabrication process.

structure through hydrogen and dative Si – O:B bonds. For product characterization and verification mechanical characteristics (relaxation time and plateau storage modulus) were used. The PBS has two relaxation times. First, we observe around 0.3–0.6 s (**Figure S1**), which relates to a slowly relaxed network structure. The other relaxation process is the fast relaxation of supramolecular structure with $\lambda \leq 10^{-3}$s

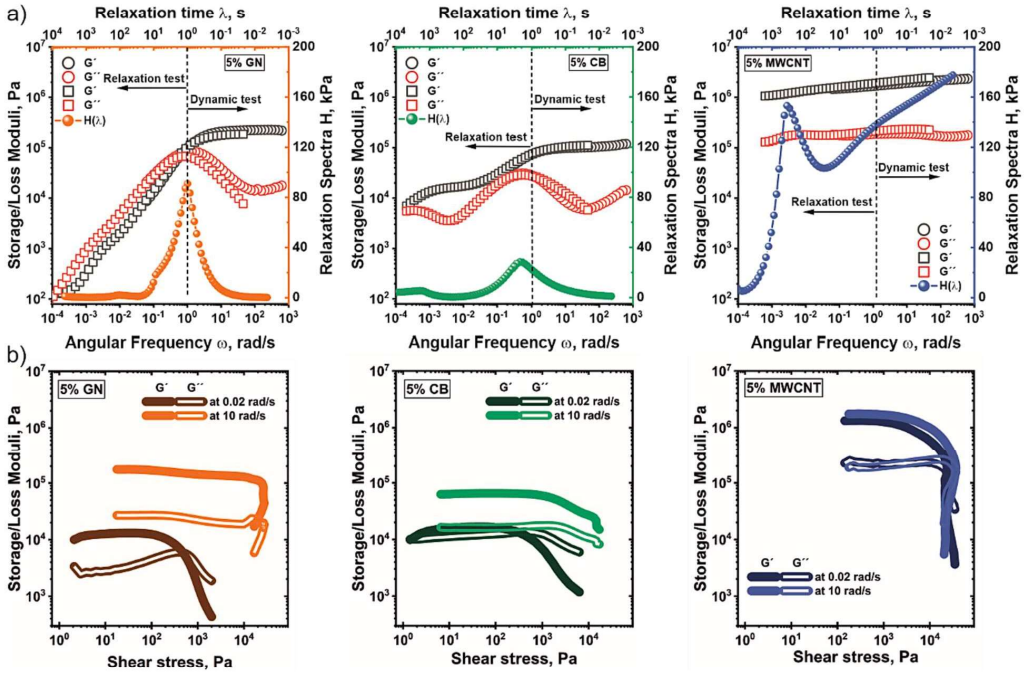

Fig. 2. Viscoelastic behavior of PBS – carbon blends PBS – 5 % GN, PBS – 5 % CB, PBS – 5 % MWCNT at small deformation: a) storage and loss moduli, obtained from both relaxation and dynamic experiments, demonstrate viscoelastic behavior ranging from around 10^{-2} to 10^{4} s. The relaxation spectra calculated from merged experiments reveal the polymer and carbon particles network relaxation processes; b) amplitude sweep of PBS blends with different carbon fillers at a frequency lower (0.02 rad/s) and higher (10 rad/s) than the relaxation frequency of pure PBS. The graph is plotted as G', G'' vs shear stress.

[17]. The G' at the plateau is ca 10 kPa meaning that the polymer behaves as an entangled solution, where a solvent is initially low molecular weight PDMS. The G' of PDMS melt at the elastic plateau is ca 0.5 MPa meaning that G'(solution)/G'(melt) = 0.01 which gives the concentration of very long chains in solvent formed by short chains 20 % [18].

The scheme of blends fabrication process is illustrated in Fig. 1**b** and can be divided into three stages: (i) preparation of polymer solution, (ii) preparation of carbon suspension, and (iii) solidification of a blend. The obtained composites with 5 and 10 % of filler behave as dough, manually demonstrating their viscoelasticity.

3.2. Relaxation properties

We have studied the viscoelastic behavior of the blends in a linear range of deformation, when the structures formed by particles and polymer remain undestroyed, using frequency sweep and stress relaxation (at $\varepsilon = 0.05$ %) experiments that allowed covering relaxation process on the time scale $10^{-2} - 10^{4}$ s **(**Fig. 2**a, S2)**. The obtained results of the relaxation test were recalculated in dependence of G' and G'' on frequency and relaxation time spectra $H(\lambda)$ according to **Equations (1–6).** All blends do not demonstrate a transition to a terminal flow regime even on the largest time scale (G' is larger than G''), showing the stability of the material, although the stress relaxation becomes more pronounced (more pronounced decrease of G' and G'' with decreasing frequency) in the sequence MWCNT – CB – GN. We also observed two distinct relaxation peaks: the first one is at ca. 1 rad/s that is close to the relaxation time of pure polymer **(Figure S1)**, and the second one is at ca. $10^{-1} - 10^{-3}$ rad/s that is related to filler network relaxation processes. As we showed in our previous work, for CB – PBS blends the relaxation of individual small aggregates or parts of the agglomeration network of CB occurs at time scale $\approx 10^{3}$ s. At a similar time, a relaxation peak is observed for MWCNT. For GN blend two peaks are observed at much lower times around 10 s and 100 s. The relaxation occurs much faster, which can be beneficial for the restoration of initial properties after deformation – self-healing. This fast relaxation was also discussed by Boland et al. [8] and explained by the high mobility of the graphene particles in PBS matrix, and their relaxation due to rotational and translational diffusion. The ratio between intensities of these relaxation processes decreases in the sequence GN – CB – MWCNT. These observations indicate that the quality of the particle network (its strength) is the highest for MWCNT and lowest for GN. The value of storage modulus at the rubbery plateau region (before the relaxation of polymer chains occur), however, does not follow this sequence: it is highest for MWCNT, intermediate for GN, and lowest for CB blends. The reason for this effect could be the low relative surface area of CB particles that results in fewer contacts area with the polymer and between particles. Furthermore, adsorbed on particle surfaces polymer chains not only form a shell but also may end up in form of occluded polymer or trapped polymer between agglomerates, which weakens the filler network. In addition, at a large time scale for 5 % blends the storage modulus does not reach a plateau value, which implies the presence of other relaxation processes. Thus, the introduction of different fillers to polymer renders its viscoelastic properties. All filler types introduce the elastic behavior on a large time scale range. The viscoelastic properties of composites become a combination of effects produced by the supramolecular structure of polymer chains, filler network, and their interaction. However, at the same volume fraction of filler, the impact of the polymer matrix becomes less pronounced with an increase in the aspect ratio of particles, which can be evidence of a strong filler network.

3.3. Viscoelastic properties at large deformation

The investigation of the blends at different amplitudes is essential for the estimation of applicability limits. We performed an amplitude sweep at a frequency 10 rad/s corresponding to the time 0.1 s, which is lower than the relaxation time of pure polymer (the polymer is elastic), and at 0.02 rad/s corresponding to the time 50 s, which is higher than the relaxation time of PBS (the polymer is viscous) **(**Fig. 2**b, S3)**. The pure PBS behaves independently on the applied amplitude of stress and strain at small and moderate deformation at both time scales. The moduli decay at shear strain $\varepsilon = 63$ % and stress 7 kPa due to material failure **(Figure S1 e-f.).**

The addition of particles alters blend rheology, with effects dependent on the time scale. As previously discussed [16], the following observations were made: (i) High frequency, low amplitude: Both polymer and particles contribute to elastic behavior. (ii) High frequency, high amplitude: Predominantly elastic behavior is driven by the polymer. (iii) Low frequency, low amplitude: Particles dictate elastic behavior. (iv) Low frequency, high amplitude: Polymer governs viscous flow.

Comparable trends were identified in the GN and CB blend investigations carried out in this study. Nonetheless, the GN network exhibits higher mobility (signified by the transition to G'' > G' regime at lower frequencies occurring at the lowest amplitude and stress levels). Simultaneously, it demonstrates enhanced toughness, endowing the material with increased stability and the capacity to flow effectively even when the filler content is high **(Figure S4, S5).** Conversely, the behavior of MWCNT blends diverges significantly from this scenario. On both small and large time scale material shows elasticity at small strain; increasing deformation shifts to plasticity, with deviation of stress of LVE regime rising with particle content (Table S1). Thus, 5 % and 10 % MWCNT content maintain elastic behavior until yield point, then shift to plastic behavior irrespective of deformation rate, with minimal polymer influence.

3.4. Conductivity

The volt-ampere characteristic (Fig. 3**a, S6**) of studied samples is non-linear and reveals two regimes of conductivity: low conductivity at low voltage (ca. $|U| < 1$ V) and high conductivity at high voltage ($|U| > 2$ V). The reason for this non-linear dependence is the granular nature of the material. Such carbon composites in general possess two types of conductivity: bulk and tunneling. Bulk conductivity is due to direct contact between particles and due to the conductivity of particles by themselves, while tunneling conductivity is due to the hopping of electrons across small gaps between particles (<10 nm). Hoping of electrons between the particles may be hindered by interfacial charge (electric double layer) that results in low conductivity at low voltage, higher voltage gives electrons sufficient energy to overcome a barrier between particles. With the increase in particle content, the resistivity in both regimes decreases due to stronger filler network formation and as consequence higher number of direct contacts.

The difference between conductivity in the two regimes decreases with the increase in the aspect ratio of the particles (from GN to MWCNT). This evidences the different abilities of these particles to form a filler network at the same volume fraction. As we observed from rheology that the entangled MWCNT network is stronger, which results in a higher impact of bulk conductivity. On the other hand, the weaker GN network creates a lot of gaps between particles, acting as pseudo capacitors, which reduces the material's ability to conduct electrical current. The carbon black blends show intermediate behavior. Thus, with the increase in particle network quality, which can be achieved either using high aspect ratio filler or large filler content, higher conductivity can be achieved, and partial alignment of I-U curve non-linearity.

To understand and confirm the aforementioned effects of particles aspect ratio and their concentration on the electrical properties of studied blends, we performed electrical impedance spectroscopy (EIS) study at low 10 mV voltage amplitude at different offset voltages, corresponding to low (0 V) and high (3 V, 4 V) conductivity regimes. The Bode plot **(Figure S7)** reveals the increase in the frequency range, at which the impedance is dominantly real, with the increase in carbon content. The same tendency is observed with an increase in particle

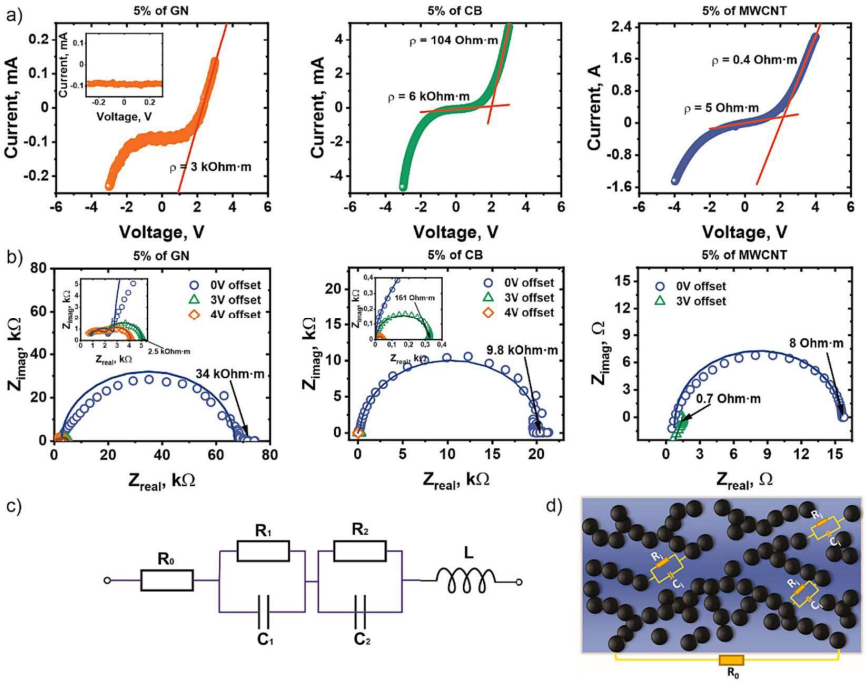

Fig. 3. Conductivity properties of composites: a) the volt-ampere characteristic of PBS - carbon blends: GN, CB, and MWCNT blends with 5 % of filler. The scanning rate is 10 mV/s; b) the Nyquist plot of EIS results made at different offset voltages (at low and high conductivity regimes) for PBS - GN, CB, and MWCNT blends with 5 % of filler: c) equivalent circuit used for fitting EIS results and d) schematic illustration of correspondence between circuit parts and sample microstructure.

aspect ratio for composites with low carbon content (when the strong network is not formed yet). Moreover, the inductance behavior is observed for MWCNT composites and 10 % CB blend at high frequency (positive value of phase angle). The inductance in MWCNT and 10 % CB blends can be explained by the wavy nature of MWCNT and the agglomeration network of conductive filler. The Nyquist plots (Fig. 3**b, S8**) show a semicircle shape in both regimes, except for the high conductivity regime of MWCNT blends. The impedance spectra were fitted with the equivalent electrical circuit (Fig. 3**c**), containing resistor R_0 in series with inductance element L and two RC elements of resistor $R_{1,2}$ and capacitor $C_{1,2}$ connected in parallel (**Table S2**). The R_0 can be attributed to the resistivity of measuring system contacts and the bulk conductivity of the material, which depends on the amount of direct contact between the particles (Fig. 3**d**). RC elements we attribute to the hopping (tunneling) conductivity across small gaps (<10 nm) between particles and their aggregates that are not in contact. For all blends the character of changes is similar. With the increase in voltage, the imaginary part of impedance becomes less pronounced. The higher voltage, the more electron hopping between particles occurs and the samples demonstrate less pseudo-capacitor behavior. With the increase in carbon content, a similar tendency is observed. The more particles are embedded in the polymer matrix, the more conductive material is and the less impact of the hopping mechanism of conductivity.

Thus, the volt-ampere characteristics and EIS study allow us to make conclusions about the microstructure of the blends. The low aspect ratio particles (GN) network is weaker and possesses fewer direct contacts between particles, which results in lower conductivity, higher non-linearity of I-V curve, and pseudo-capacitor behavior of the filler network. An increase in the conductivity of such blends can be achieved by an increase in voltage, amplifying the electron hopping between particles. Opposite, rod-like MWCNT network demonstrates higher quality with more direct particle–particle contact, which provide higher conductivity, and is closer to a linear dependence of I-V, though such a strong network may provide an inductance at high-frequency AC. An increase in voltage does not provide drastic raise in the conductivity of the material.

3.5. Healing behavior

The restoration of conductivity after applying shear stress, which breaks contacts between the particles but does not disintegrate the polymeric matrix, demonstrated the difference in sensitivity to shear deformation and properties restoration rate between blends. One step 10 % shear strain was applied to the blends with simultaneous measurement of storage/loss moduli at relatively small frequency and strain, and resistivity within the time (Fig. 4**a**). The applied deformation value (ε = 10 %) corresponds to the region of the non-linear behavior of materials, where the particle network is broken, but the flow or materials failure point is not achieved. The sensitivity of materials, such as strain sensors, is usually defined by Gauge factor, G_ε which is the factor of proportionality in linear dependency $\Delta R/R_0$ vs ε, where ε is the extensional strain in a.u. In our experiments, we applied shear stress in non-linear region. Therefore, this "shear" Gauge factor G_γ shows the resistivity change due to changes in internal material structure without consideration of geometrical size changes. The values of G_γ value decrease in the sequence GN ($G_\gamma = 117$), CB ($G_\gamma = 61$), and MWCNT ($G_\gamma = 3.7$) i.e. with the increase of the aspect ratio of particle and with an increase of the quality of the network formed by particle. The theory says that the higher Gauge factor is achieved when the filler volume fraction is closer to the percolation threshold value [19]. The percolation value for prolate ellipsoids is lower than for oblate [20]. Moreover, the isotropic dispersion of 2D materials demonstrates a higher electrical

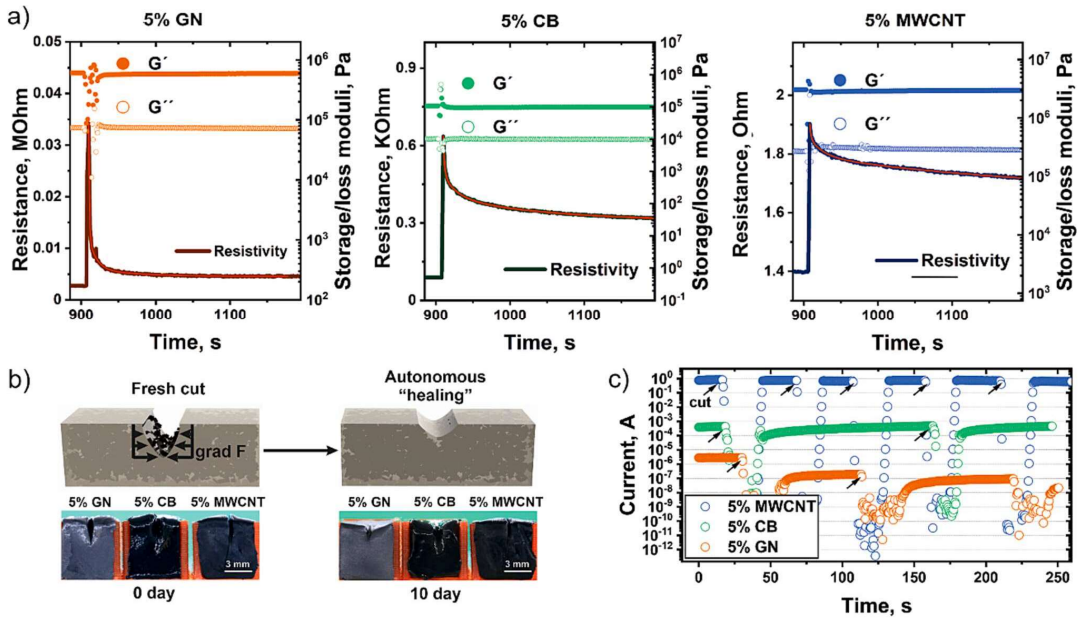

Fig. 4. Self-healing behavior of polymer-carbon composites: a) Time-sweep measurement of resistivity and storage/loss moduli of PBS – carbon filler blends with 5% GN, 5% CB, and 5% MWCNT; b) scheme of autonomous self-healing condition of a cut and visual experiment of healing of a cut of different carbon/PBS blends; c) integrity healing experiment of 5% carbon filler composites after cut, bringing them together applying minimal sufficient force.

response compared to 1D materials [21]. Therefore, the results we obtained correlate well with theoretical models and other experimental results.

The relaxation processes affect the rate, at which the resistivity is restored after applied stress. For a demonstration of this effect, we fitted the data with tree exponential decay functions to define the characteristic relaxation times and their contribution to the relaxation process (**Table S3**). The GN blend demonstrates the first relaxation time around 1–2 s, which is close to the time of polymer relaxation with negligible shift due to hindering of mobility of polymer chains, which adsorbed on the particles surface. The other relaxation processes occur at 11 s and 62 s, which can be attributed to the relaxation of particles and elements of the particles network and correlates with the results of the rheological relaxation test (Fig. 2**a**). The most relaxation (contribution is 84 %) of the resistivity according to the impact of pre-exponential coefficients occurs due to fast polymer relaxation. The impact of the third exponent term (62 s) is insignificant. The polymer relaxation is observed for CB particles at 1.8 s and its contribution becomes smaller (81 %). The impact of the second (19 s) and third (143 s) terms are equal and their impact, compared to polymer relaxation, is relatively higher than that for GN blend. Therefore, the relaxation occurs longer and after 300 s of the experiment, there are still high unrelaxed parts of the material remaining. Similar behavior was observed in the case of MWCNT blend. The t_1 value as well corresponds to polymer relaxation and is equal to 1.7 s, its contribution is 24 %. However, the highest relaxation impact (52 %) demonstrates processes at a large time scale (344 s). Residual unrelaxed resistivity (R_0) is large as well compared to initial resistivity before deformation. Thus, the blend with a weaker filler network (GN blend), possesses higher relaxation of electrical characteristics after applied strain. The GN particles are more mobile and form fewer particle–particle contacts which result in higher sensitivity to strain. The resistivity relaxation of weaker GN networks occurs fast due to higher particle mobility and the large impact of polymer relaxation. Consequently, such material possesses superb self-healing properties. The relaxation is slower and the contribution of relaxation processes at a large time scale is higher for the particles with a higher aspect ratio and stronger filler network that also results in relatively high residual unrelaxed resistivity. Therefore, such material has weaker self-healing abilities. Thus, there is an opposite trend of the behavior of self-healing and functionality (conductivity) on the quality of the network formed by particles. The better the quality of the particle network, the higher the conductivity but the self-healing ability gets worse.

The ability of self-healing of different composite without applied stress and only due to gravity and self-diffusion was confirmed by a visual test of healing a cut without applying any external forces (Fig. 4 **b, c**). As we mentioned before, the stronger the filler network, the less ability to heal should be. The experiment confirms that: after 10 days the GN blend visually healed the cut more efficiently, whereas CB and MWCNT blends barely underwent any changes. Thus, the better ability to creep at low stress and low shear stress at LVE point of GN composite gave good prediction about superb self-healing properties.

Even though the GN blends demonstrated promising mechanical characteristics, the cut-healing test showed that healing cannot be fully completed without applying any external forces. As it is shown in Fig. 4**b**, the shear force gradient of the polymer column pressure itself acts on the cut. The deeper point of the cut, the larger the force. The cut will heal till the stress, created by this force, is larger than the flow stress of the material. It implies, that at some point the healing process nearly stops. Of course, we should not avoid an impact of self-diffusion of material at the low point of the crack, but with healing, the curvature will decrease, and the impact becomes negligible. Thus, the full autonomous healing of such blends could hardly be achieved. Unfortunately, making the network even weaker, which means less filler content and potentially higher healing ability, we may overcome the rheological and electrical percolation threshold, and the material will lose its structural stability and conductivity, which is unlikely for almost every application in the electronics field. If the network is too strong, as we showed, there is almost no self-healing ability. Therefore, the researcher should always

consider that they may be sacrificing this or that property of the material, working with viscoelastic blends.

While MWCNT-polymer blend heals under influence of gravity (around 20 Pa for 2 mm deep scratch) very slowly that is due to the low mobility of network formed MWCNT, they can heal when sufficiently large stress (above the threshold value of the transition to plastic deformation) is applied. In order to demonstrate this, we cut a piece of 5 % MWCNT-PBS and applied sufficient force to bind two pieces back together (Fig. 4**c, S9**). The conductivity of the material is restored as well as structural integrity. We also expect that self-healing of microcracks may be fast because surface tension forces are considerable on micro and nano-scales. Thus, the healing of such an object is possible, by applying stress higher than the yield stress of the material.

The 5 % CB material also restored its initial current, albeit over a slightly longer duration. However, for the 5 % GN material, a complete restoration of its initial conductivity was not achieved. This observation can be attributed to the mobility of fillers and polymer chains. In the case of MWCNTs, the cut surface exposed to air remains relatively unchanged, whereas GN particles on the cut section are rapidly covered by polymer, facilitating surface healing. Consequently, restoring electrical

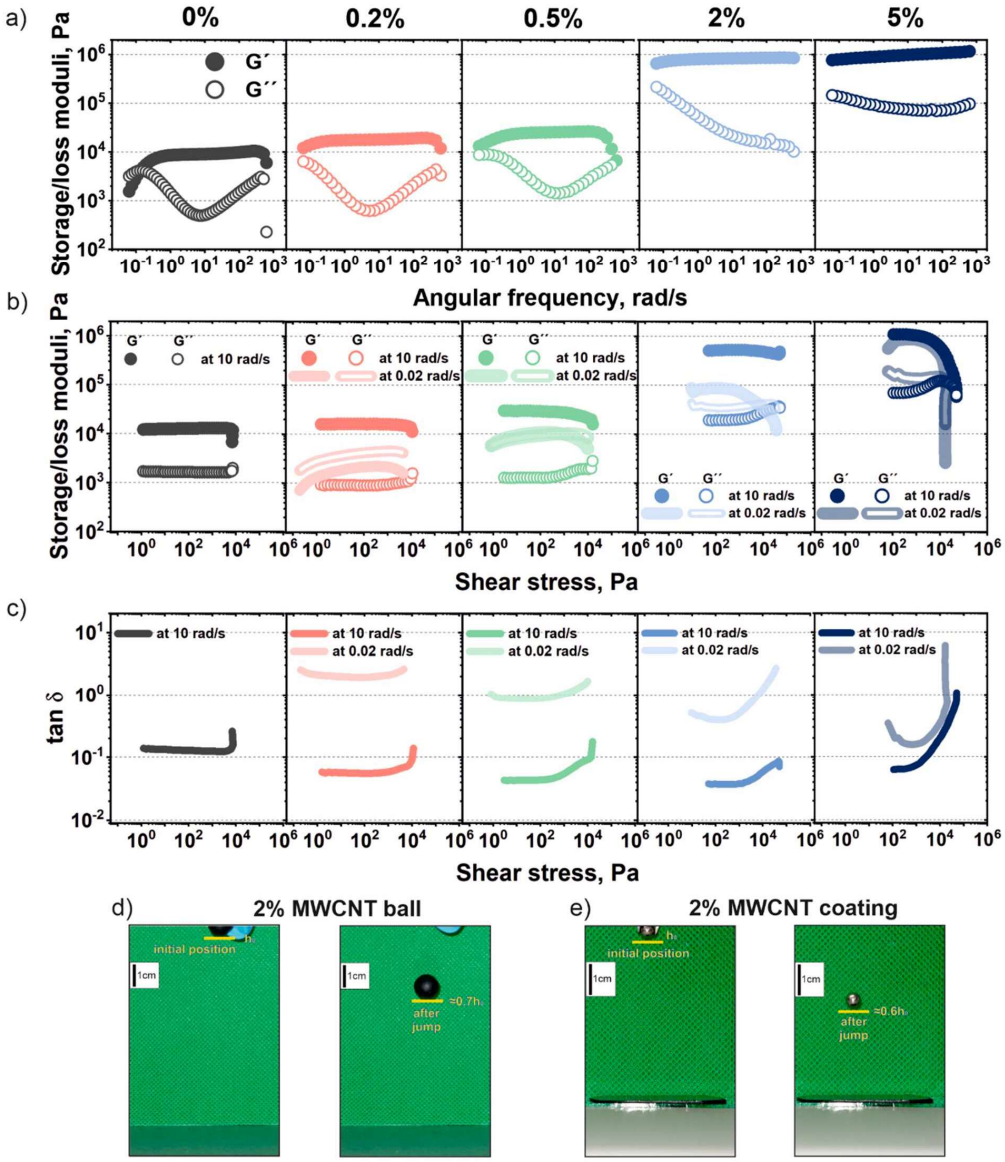

Fig. 5. Rheological study of MWCNT composites with different filler content: a) frequency sweep at 0.05 % shear strain; amplitude sweep at 10 rad/s and 0.02 rad/s plotted as b) G', G'' vs. stress, and c) loss factor vs. stress; d) bouncing of super-elastic 2 % MWCNT ball and e) metallic ball bouncing on super-elastic MWCNT coating.

characteristics to their initial values without applying significant stress (beyond the flow point) is not feasible.

3.6. Superelastic behavior

Our experiments showed that 5 % MWCNT blend possesses a strong filler network, and as result, high conductivity leads to weaker strain sensitivity and self-healing abilities without applied stress, while healing under influence of large stress is possible. We further studied the effect of filler on the mechanical properties of these composites to find out if the material with high aspect ratio filler may have the same or even better electrical and self-healing properties with lower carbon content (closer to percolation point) at similar mechanical characteristics.

First, the behavior at low strain was studied by frequency sweep experiment (Fig. 5**a).** The carbon nanotubes introduce the elastic behavior over the whole studied frequency range (0.0628 – 628 rad/s) due to percolated network formation. The rheological percolation is below 0.2 % MWCNT content. We found that the higher the MWCNT content, the higher the plateau value of storage modulus and the less pronounced become the relaxation of PBS chains. The relaxation spectra reveal the shift of PBS relaxation peak to higher times due to hindering polymer chains mobility (**Figure S10 a-b**). Therefore, the increase in MWCNT concentration leads to a higher impact of the filler network on the mechanical properties of blends. Meanwhile, the MWCNT-PBS 2 % blend shows the most pronounced difference between storage and loss modulus – its dissipation of energy is very weak. Notably, the loss factor measured for MWCNT-PBS 2 % blend decays with the increase of the frequency that is not observed for samples with higher and lower MWCNT content, and the loss factor is lower than that measured for pure PBS at 10 rad/s.

The behavior of blends at large strain range was studied by amplitude sweep test at 10 rad/s (the polymer is in the elastic state) and 0.02 rad/s (the polymer is in the viscous state) to define the mechanical limits of blends applicability (Fig. 5**b, c**). The raise in carbon content leads to the reduction in the linear viscoelastic region (**Figure S12**), which is evidenced by higher energy loss due to the sliding of particles with respect to each other (breakage of network) during shear deformation. Another interesting observation is that the loss factor decreases upon the increase in carbon content, reaches a minimum at 2 % of MWNTs, and increases upon further increase of carbon, which is evidence of energy dissipation due to particle–particle friction. The minimum reached the value of the loss factor is 0.04 which is a very low value and rarely observed for such soft materials (G = 1 MPa) (**Figure S14**). To put this into context, the closest comparable result in the literature, from Wang et al.'s paper, reported a tan $\delta \approx 0.6$ and E = 0.9 MPa[22], which is one order of magnitude lower. It is very important to note that the 2 % sample is also highly strong and tough at 10 rad/s– we didn't observe the decay of both moduli indicating failure until maximal torque of the DMA machine was achieved. Moreover, the dissipation of energy remains low when the maximal force limit of our device was achieved ($\varepsilon = 10$ % and $\tau = 10^5$ Pa). We measured the strength and maximal elongation of the material using a tensile experiment (Fig. 7**c**). It was found that the material breaks at strain 45 % at ca 1.4 MPa tensile stress which corresponds to ca. 1 MPa shear stress that is even higher than that measured for blends with 5 % MWNTs. Furtheromore, at large time scale and applying sufficient force (beyond flow point) material can be recycled without significant changes of its properties (**Figure S13**).Thus, MWCNT-PBS 2 % blend is the strongest, toughest, and most elastic among all blends.

The observed properties of the MWCNT-PBS 2 % blend allow us to assume that the material shall bounce upon contact with another elastic material or elastic object shall bounce out of the surface of the composite. We tested the elastic properties of the 2 % sample by dropping the ball of this blend and pure PBS (as reference) on a solid elastic substrate (Fig. 5**d, S15**). The ball-bouncing experiment reveals significant energy savings of carbon composite and pristine PBS. In this experiment, balls of both materials were dropped down from relatively low high ($h \approx 8$ cm $\sim v \approx 1.3$ m/s). The carbon composite bounced back to approximately 70 % of initial height, while PBS ball didn't bounce at all. The elastic response is also observed when the composite material was as a coating. The metallic ball was able to bounce on the composite-coated surface which evidenced high energy saving.

Improving elastic behavior by a strong filler network and its interaction with polymer is quite common for stiff polymers in glassy or semicrystalline states [22–24], which are not able to self-heal. Our material, on the contrary, is very soft and is able to restore its integrity and functionality after being cut at room temperature, applying some minimal force, to overcome the yield point. That also means that the material is recyclable and can be shaped in any necessary shape repeatedly. There is a correlation between the elastic modulus of materials and energy dissipation (**Figure S14**) – the harder the material, the lower the energy dissipation. The typical loss coefficient of elastomers (the softest pure (not swollen) polymers) is $\tan\delta \approx 1$ – rubbers are quite efficient energy dissipators that allow their use for mechanical damping. Our material is as soft as the softest rubber but is way more elastic (dissipates more than ten times less energy) than rubbers. Moreover, it is highly conductive and also is able to heal under mechanical stress. Thus, we possess a highly elastic, conductive material with self-healing ability, which potentially may replace conventional rubber materials as protective coatings, sealing agents, etc. [22].

Energy dissipation of polymers can be reduced in the following way – by increasing the range of time scale between two relaxation processes relaxation of the whole polymer chain (flow) and relaxation of chain segment, which is associated with glass transition. The fraction of freely dangling chain ends, which do not contribute to elastic deformation, shall be minimized. The relaxation time of the whole polymer chain can be increased by increasing in molecular weight, and the relaxation time of the chain segment can be reduced by taking more flexible polymer chains (polymers with the lowest T_g). The most ideal polymer must be crosslinked PDMS ($T_g = -127$ °C) This polymer, however, is chemically crosslinked, and broken bonds cannot heal. PBS with a relaxation time of 100 s (**Figure S16**) also shows very low energy dissipation ($\tan\delta \geq 0.01$). This polymer bounces very well. However, it is not able to heal efficiently due to large relaxation time. Moreover, it is not conducive. Thus, our material (MWCNT 2 % - PBS ($\lambda = 1$ s)) demonstrated a unique combination of properties, which not achievable for other materials: conductivity, self-healing of shape and conductivity as well as extremely high elasticity for polymer-based material with low Youngs modulus.

Pure-used PBS shows quite a low loss factor at a certain frequency range (this loss factor is still higher than that of MWCNT-PBS 2 % blend). It allows us to assume that the "superelastic" behavior of MWCNT-PBS 2 % blend originates from a network formed by MWCNT. We made a reference experiment and investigated the viscoelastic behavior of blends of MWCNT with low molecular weight PDMS (65cSt) (**Figure S17**), where the MWCNT shall also be able to form a network. The MWCNT- PDMS (65cSt) blends do not show such an elastic behavior and behave rather like wet sand – breaks at low stress and strain. This observation means that none of the pure components (PBS and MWCNT) possess the "superelastic" behavior at it originates from their interactions and formation of a certain structure. The materials (PBS and MWCNT) apparently form interpenetrating networks, which are both elastic on a time scale below the relaxation time of the polymer.

In order to explain why superplastic behavior is observed within a certain concentration range, we proposed the following simple qualitative model (Fig. 6), where the ΔG_{comp} is a combination Gibbs energies of pure PBS (ΔG_{PBS}), highly concentrated and entangled MWCNT dispersion in Newtonian liquid ΔG_{MWCNT} (no interaction of filler with matrix, **Figure S17**), and their mixing Gibbs energy ΔG_{mix}, which takes into account adsorption of polymer chains on nanotubes and dispersibility of filler.

The quality of the carbon network within a polymer matrix hinges on the interaction between polymer chains and fillers. Polymer chains

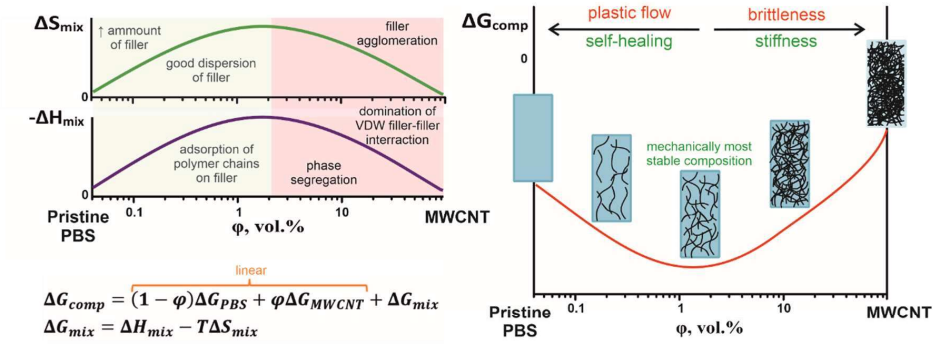

Fig. 6. Schematic thermodynamic model of two component system of PBS and MWCNT filler in Newtonian liquid.

adhere to particle surfaces through weak Van der Waals interactions, forming a distinctive insulating shell at the interface with a thickness denoted as 't.' This interfacial shell possesses properties distinct from those of the bulk polymer. In the case of elastomers, this shell thickness typically measures around 10 nm. As the interfacial volume increases, it exerts a more significant entropy effect, enhancing the dispersion of the filler within the polymer matrix. This effect counteracts the enthalpic attraction between carbon particles.

Consequently, a point is reached where the combined influences of enthalpy and entropy result in the mixture's Gibbs energy reaching a minimum. When we view nanotube networks as akin to long polymer chains, we effectively have a system comprising two polymers, amenable to a model similar to the Flory-Huggins theory. As a result, the mixing energy assumes a pseudo-parabolic shape, with a minimum in Gibbs energy. At this point, we attain a composition that is highly elastic with the lowest loss coefficient, making it resistant to perturbations from equilibrium.

3.7. Piezoresistivity

Finally, we demonstrated a possible application of a super-elastic conductive healable blend for the design of electrical sensors, which are sensitive to stress and stress rate (Fig. 7). The measurements of stress and resistivity were performed at different strain rates: 0.1 % /s (polymer flows), 1 %/s (around polymer relaxation time), and 10 %/s (polymer is elastic). The material demonstrated nearly independence of Young's modulus in 0.001 – 0.1 s^{-1} strain rate range (E = 1.3 – 1.5 MPa). The ultimate strength, on the other hand, increases with an increase in strain rate as well as the character of failure changes from viscous to brittle. This means that both MWCNT and PBS are responsible for elastic behavior.

Although tensile modulus is independent of the deformation rate that was also shown in shear experiments, the character of the evolution of resistivity with strain depends strongly on the deformation rate. Resistivity almost does not change with strain at a low deformation rate and increases with the increase of deformation rate. At 0.1 %/s the resistance nearly does not change during stretching, followed by drastic raise in resistivity due to material breakage. The deformation rate, is probably, slow enough that allows particles to reorient without losing contact, keeping the resistivity nearly constant - polymer flows and the MWCNT network remains intact. At a high deformation rate, the resistivity changes linearly up to 30 %. This strain range with the linear change of resistivity is much broader compared to that demonstrated before [8,25], which makes this material suitable for sensing large strains [19]. Interestingly, the material demonstrates nearly no change in resistivity in the shear deformation experiment.

4. Conclusion

In summary, we designed the material with a unique combination of properties, such as softness, elasticity, conductivity, self-healing ability, piezoresistivity, and recyclability. Such properties are due to the reinforcement of entangled and interpenetrated network of carbon nanotubes (MWCNT), which renders relaxation properties of viscoelastic self-healing polyborosiloxane (PBS) matrix. The material demonstrated promise as a strain-sensor material due to large linear regime of resistivity change, and as a replacement for conventional rubbers in coatings and sealing agent application. Moreover, the effect of the

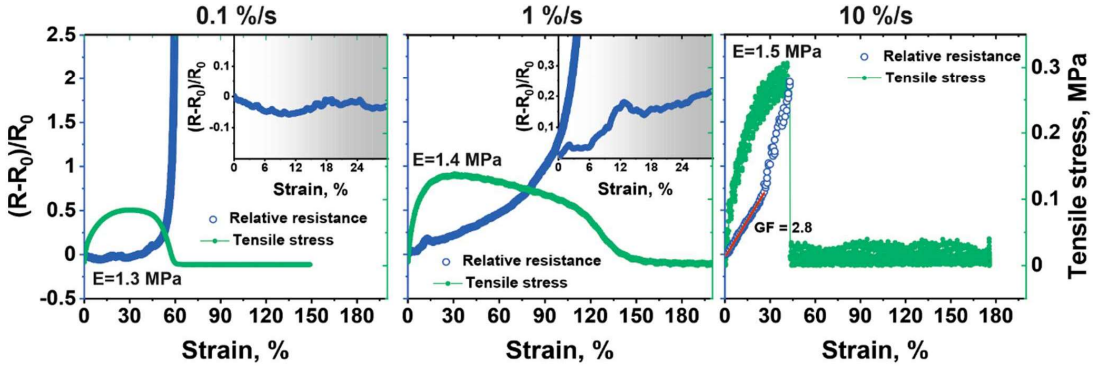

Fig. 7. Electromechanical characteristics of 2% MWCNT blend during extension with various strain rates: 0.1, 1, and 10 %/s.

nature of different conductive carbon particles with various aspect ratios was studied in order to understand the viscoelasticity phenomena of such materials. The eight key parameters were found to influence the material properties: (i) polymer relaxation; (ii) plateau region at large time scale; iii) relaxation of individual particles; iv) character of failure of material at large strain; v) creep ability; vi) conductivity; vii) linearity of I-V curve; viii) restoration of functional characteristics after a filler network failure. Understanding the nature and adjusting of these parameters allows one to better choose a material for specific applications.

Funding sources

This work was supported by DFG (Grant No IO 68/20-1, IO 68/21-1).

CRediT authorship contribution statement

Pavel Milkin: Investigation, Conceptualization, Writing – original draft, Visualization, Formal analysis. **Ainur Zhanbassynova:** Investigation, Visualization. **Leonid Ionov:** Conceptualization, Writing – review & editing, Supervision, Project administration, Formal analysis.

Declaration of Competing Interest

The authors declare that they have no known competing financial interests or personal relationships that could have appeared to influence the work reported in this paper.

Data availability

Data will be made available on request.

Acknowledgment

We would further like to thank Professor Scheibel for allowing us to use SEM equipment to conduct this research.

Appendix A. Supplementary material

Supplementary data to this article can be found online at https://doi.org/10.1016/j.compstruct.2023.117709.

References

[1] Li W, Dong B, Yang Z, Xu J, Chen Q, Li H, et al. Recent advances in intrinsic self-healing cementitious materials. Adv Mater 2018;30(17):e1705679.
[2] Kang J, Tok JBH, Bao Z. Self-healing soft electronics. Nat Electron 2019;2(4):144–50.
[3] Wang S, Urban MW. Self-healing polymers. Nat Rev Mater 2020;5(8):562–83.
[4] Wu T, Chen B. Synthesis of multiwalled carbon nanotube-reinforced polyborosiloxane nanocomposites with mechanically adaptive and self-healing capabilities for flexible conductors. ACS Appl Mater Interfaces 2016;8(36):24071–8.
[5] Wang Z, Lai YC, Chiang YT, Scheiger JM, Li S, Dong Z, et al. Tough, self-healing, and conductive elastomer horizontal line ionic PEGgel. ACS Appl Mater Interfaces 2022.
[6] Huynh TP, Sonar P, Haick H. Advanced materials for use in soft self-healing devices. Adv Mater 2017;29(19).
[7] Wu T, Gray E, Chen B. A self-healing, adaptive and conductive polymer composite ink for 3D printing of gas sensors. J Mater Chem C 2018;6(23):6200–7.
[8] Boland CS, Khan U, Ryan G, Barwich S, Charifou R, Harvey A, et al. Sensitive electromechanical sensors using viscoelastic graphene-polymer nanocomposites. Science 2016;354(6317):1257–60.
[9] Banerjee S, Tripathy R, Cozzens D, Nagy T, Keki S, Zsuga M, et al. Photoinduced smart, self-healing polymer sealant for photovoltaics. ACS Appl Mater Interfaces 2015;7(3):2064–72.
[10] Sun Y, Lopez J, Lee HW, Liu N, Zheng G, Wu CL, et al. A Stretchable graphitic carbon/Si anode enabled by conformal coating of a self-healing elastic polymer. Adv Mater 2016;28(12):2455–61.
[11] Rao YL, Chortos A, Pfattner R, Lissel F, Chiu YC, Feig V, et al. Stretchable self-healing polymeric dielectrics cross-linked through metal-ligand coordination. J Am Chem Soc 2016;138(18):6020–7.
[12] Nam J, Kim E, KK R, Kim Y, Kim TH. A conductive self healing polymeric binder using hydrogen bonding for Si anodes in lithium ion batteries. Sci Rep 2020;10(1):14966.
[13] Burattini S, Greenland BW, Merino DH, Weng W, Seppala J, Colquhoun HM, et al. A healable supramolecular polymer blend based on aromatic π– π stacking and hydrogen-bonding interactions. J Am Chem Soc 2010;132(34):12051–8.
[14] Chen X, Sun P, Tian H, Li X, Wang C, Duan J, et al. Self-healing and stretchable conductor based on embedded liquid metal patterns within imprintable dynamic covalent elastomer. J Mater Chem C 2022;10(3):1039–47.
[15] Guo H, Han Y, Zhao W, Yang J, Zhang L. Universally autonomous self-healing elastomer with high stretchability. Nat Commun 2020;11(1):2037.
[16] Milkin P, Danzer M, Ionov L. Self-healing and electrical properties of viscoelastic polymer-carbon blends. Macromol Rapid Commun 2022;43(19):e2200307.
[17] Tang M, Wang W, Xu D, Wang Z. Synthesis of structure-controlled polyborosiloxanes and investigation on their viscoelastic response to molecular mass of polydimethylsiloxane triggered by both chemical and physical interactions. Ind Eng Chem Res 2016;55(49):12582–9.
[18] Michael Rubinstein RHC. Polymer Physics. Oxford: Oxford University Press; 2003.
[19] Boland CS. Stumbling through the research wilderness, standard methods to shine light on electrically conductive nanocomposites for future healthcare monitoring. ACS Nano 2019;13(12):13627–36.
[20] Garboczi EJ, Snyder KA, Douglas JF, Thorpe MF. Geometrical percolation threshold of overlapping ellipsoids. Phys Rev E Stat Phys Plasmas Fluids Relat Interdiscip Topics 1995;52(1):819–28.
[21] Boland CS. Approaching the limit of electromechanical performance in mixed-phase nanocomposites. ACS Applied Nano Materials 2020;3(11):11240–6.
[22] Wang C, Liu N, Allen R, Tok JBH, Wu Y, Zhang F, et al. A rapid and efficient self-healing thermo-reversible elastomer crosslinked with graphene oxide. Adv Mater 2013;25(40):5785–90.
[23] Pötschke P, Abdel-Goad M, Alig I, Dudkin S, Lellinger D. Rheological and dielectrical characterization of melt mixed polycarbonate-multiwalled carbon nanotube composites. Polymer 2004;45(26):8863–70.
[24] Jyoti J, Dhakate SR, Singh BP. Phase transition and anomalous rheological properties of graphene oxide-carbon nanotube acrylonitrile butadiene styrene hybrid composites. Compos B Eng 2018;154:337–50.
[25] D'Elia E, Barg S, Ni N, Rocha VG, Saiz E. Self-healing graphene-based composites with sensing capabilities. Adv Mater 2015;27(32):4788–94.

Superelastic, soft, stress-healable, recyclable conductive materials

Pavel Milkin[1], Ainur Zhanbasynova[1], Leonid Ionov[1,2]*

[1]Faculty of Engineering Sciences, University of Bayreuth, Ludwig Thoma Str. 36A, 95447 Bayreuth, Germany

[2]Bavarian Polymer Institute, University of Bayreuth, 95447 Bayreuth, Germany

* E-mail: leonid.ionov@uni-bayreuth.de

Supplementary information

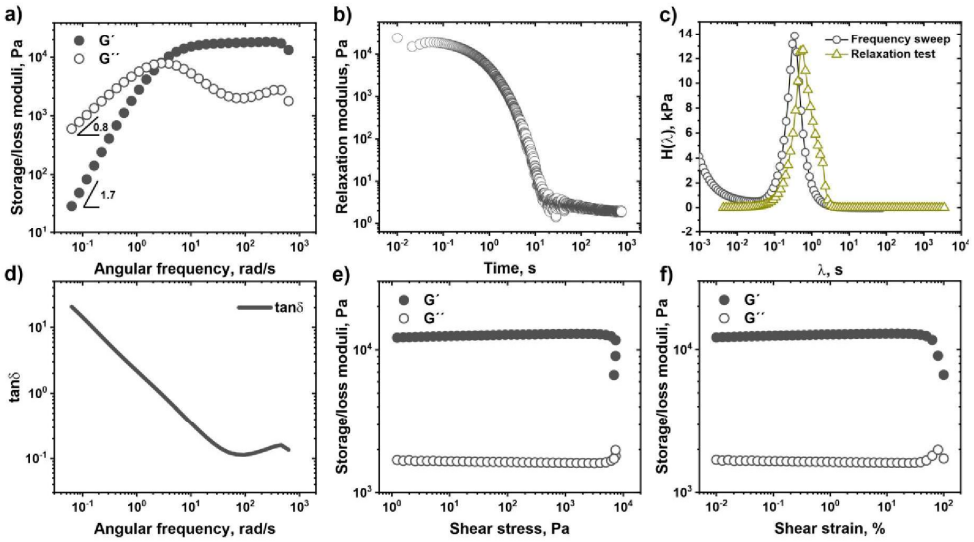

Figure S1. Initial PBS properties: a) frequency sweep measurement (ε =0,1%); b) relaxation experiment (ε = 0,1%); c) relaxation spectra calculated from frequency sweep and relaxation test results; d) loss factor as function of frequency; amplitude sweep measurements: e) moduli vs stress (ω = 10 rad/s) and f) moduli vs strain (ω = 10 rad/s).

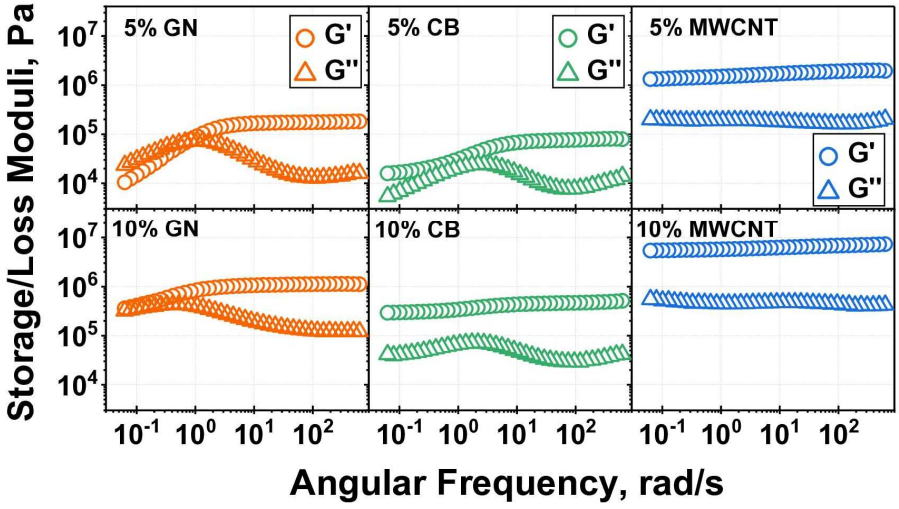

Figure S2. Frequency sweep experiment of blends of PBS with 1s relaxation time and various carbon fillers (ε =0.05%)

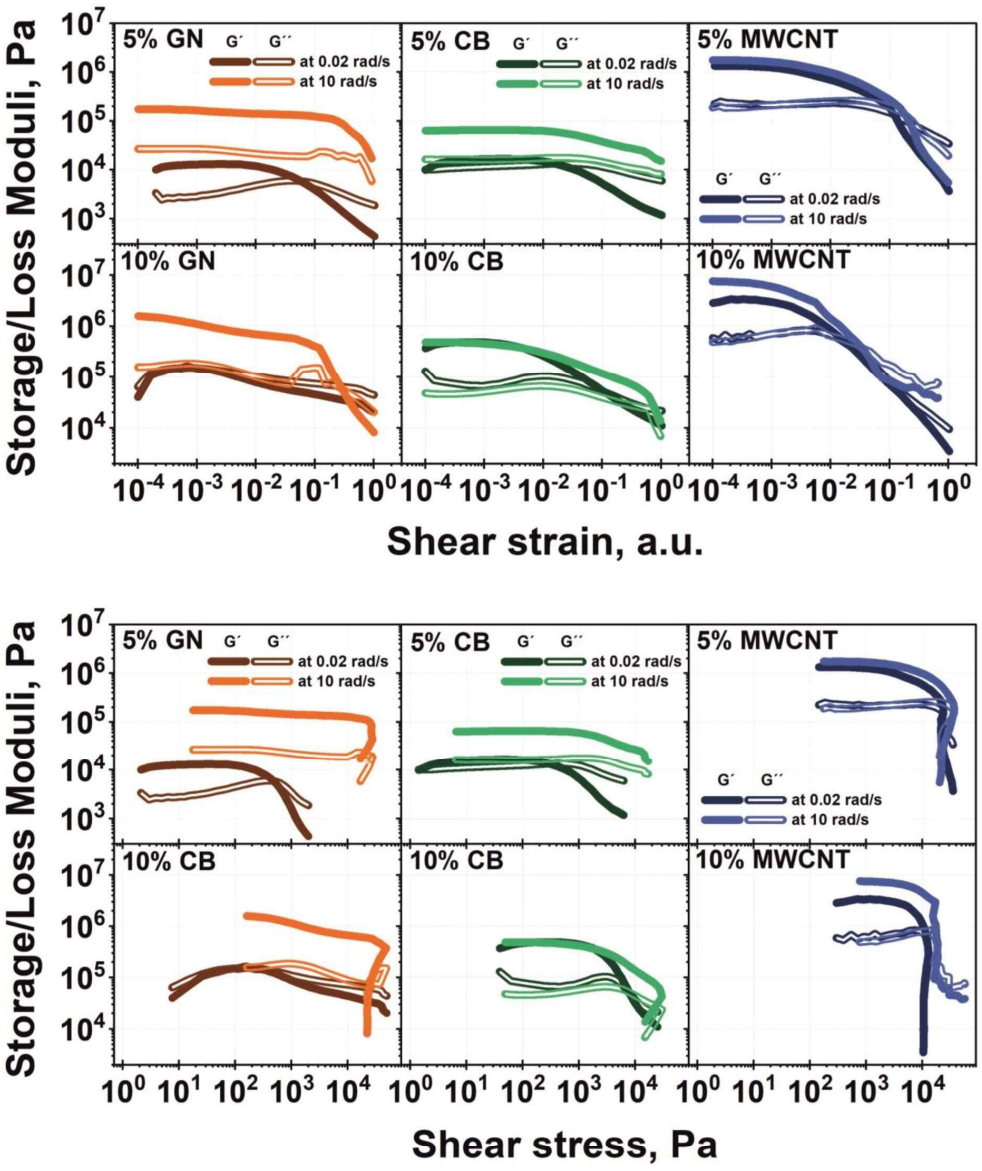

Figure S3. amplitude sweep of PBS blends with different carbon fillers at a frequency lower (0.02 rad/s) and higher (10 rad/s) than the relaxation frequency of pure PBS. The graph is plotted as G´, G´´ vs shear strain and G´, G´´ vs shear stress

Table S1. Amplitude sweep data (at 10 rad/s) for shear strain and stress at LVE region value, and sol-gel transition/breakage point for PBS – carbon blends

Carbon type	vol. % of filler	Elongation at end of LVE region, a.u.	Stress at end of LVE region, kPa	Elongation at G´´=G´, a.u.	Stress at G´´=G´, kPa
GN	5	0.0017	0.2	-	-
	10	0.00029	0.4	0.29	24
CB	5	0.023	1.4	-	-
	10	0.0017	0.8	-	-
MWCNT	5	0.003	2.1	0.19	35
	10	0.0005	3.6	0.028	18

Flow and creep behavior.

Creep behavior (**Figure S4**) was investigated at stress below stress of particles contact breaking to define creep viscosity. The test was performed at low constant stress 100 Pa, which is within linear region for all studied blends. The creep viscosity is a reference of particles network quality. Despite nearly equal volume fraction of particles, the range of defined viscosity is enormous and within 0.001 – 10 GPa·s. The lowest viscosity was observed for GN composite, around 5 MPa·s. Increase in particles aspect ratio leads to significant increase in creep viscosity. Thus, we additionally confirmed that the weaker the network, the lower viscosity composite possesses. Therefore, the composites with low aspect ratio particles has higher abilities to flow meaning that the quality of carbon particles network is the worst in this case.

To investigate flow properties of the blends, the rotational experiment was performed **(Figure S5)**. The pure PBS only slightly demonstrates shear thickening at small shear rates, followed by materials failure at shear rate and stress, corresponding to polymer relaxation time and failure stress of polymer, respectively, from previous experiments. Addition of filler increases viscosity of polymer and their behavior. All blends demonstrate classical shear thinning regime: the viscosity decreases after certain stress due to the breakage of particles contacts (20 kPa for GN, 1 kPa for CB, 6 kPa for MWCNT) followed by material failure at higher strain rates and shear stresses: the materials transit to elastic state and undergo brittle breakage. Compared to the other blends, at low strain rate the 5% GN demonstrated a shear thickening behavior as well as pristine

PBS. Moreover, the highest Newtonian viscosity of creep test is comparable with rotational experiment value. Thus, those are evidence of a weak particles network with lower impact in mechanical properties of the composite. Due to strong CB and MWCNT networks and complicated relaxation processes occurring in these materials, most probably the time of steady-state experiment was not enough to investigate properly the viscosity curve at low strain rates. Therefore, shear thinning in these composites occurs even at lower strain rates and the highest Newtonian viscosity, obtained from creep experiment, is more reliable.

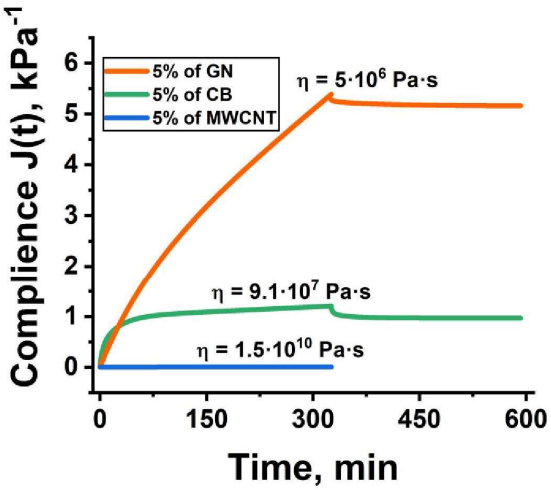

Figure S4. Creep compliance of PBS – carbon composites at shear stress 100 Pa.

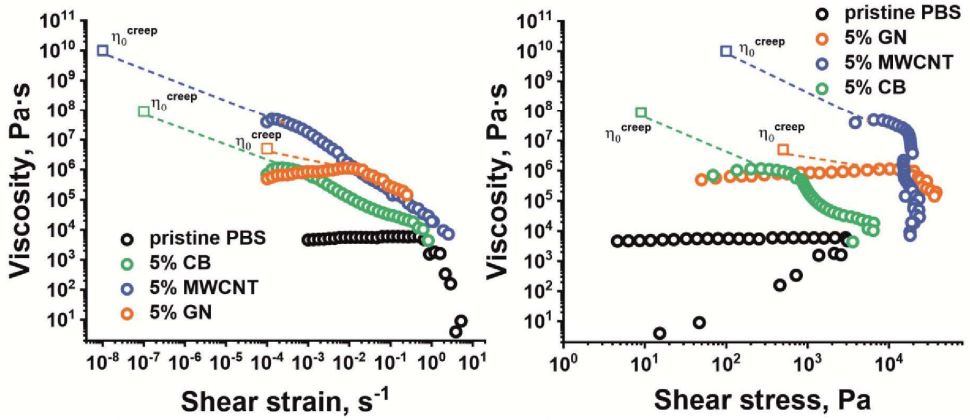

Figure S5. Viscosity measurements of PBS-carbon blends

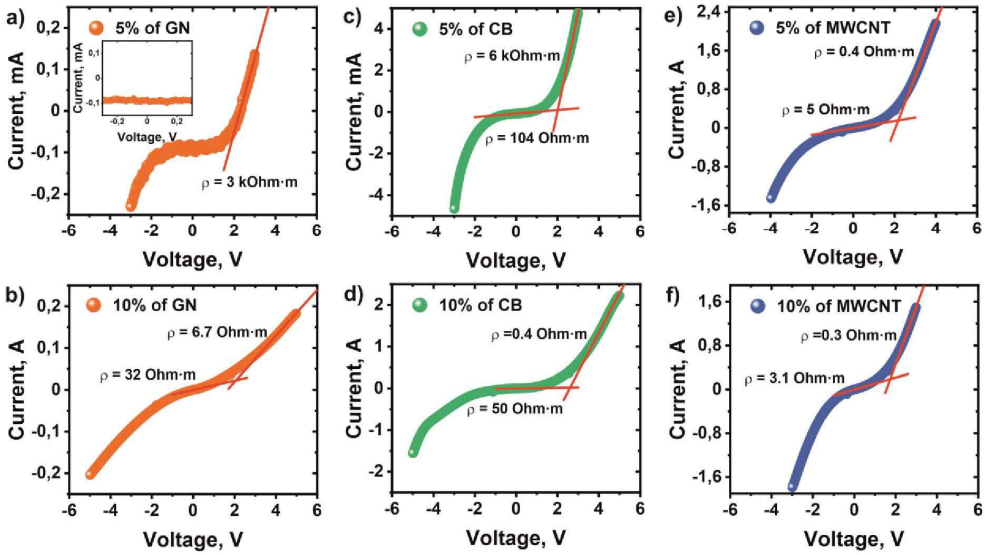

Figure S6. The volt-ampere characteristic of PBS - carbon blends: GN, CB and MWCNT blends with 5% and 10% of filler. The scanning rate is 10 mV/s;

Table S2. Fitting parameters of Nyquist plot of PBS-carbon blends

Filler	Vol. %	Offset Voltage	R_0, Ohm	R_1, Ohm	C_1, nF	L, nH	R_2, Ohm	C_2, Ohm
MWCNT	5	0	0,7	14,8	198	421		
		3	0,6	1,4	97	500		
	10	0	0,6	10,5	317	220		
		3	0,6	0,9	104	299		
CB	5	0	2,2	20070	52	266	280,2	50,7
		3	4	317	19			
		4	4	40	21			
	10	0	0,4	143	121	413	6	97
		3						
		4						
GN	5	0	763	64080	10		2000	0,4
		3	569	3007	4,6		1472	0,3
		4	422	2130	3,8		1572	0,3
	10	0	10	54	57		23	41
		3	10	15	29			
		4	11	9	35			

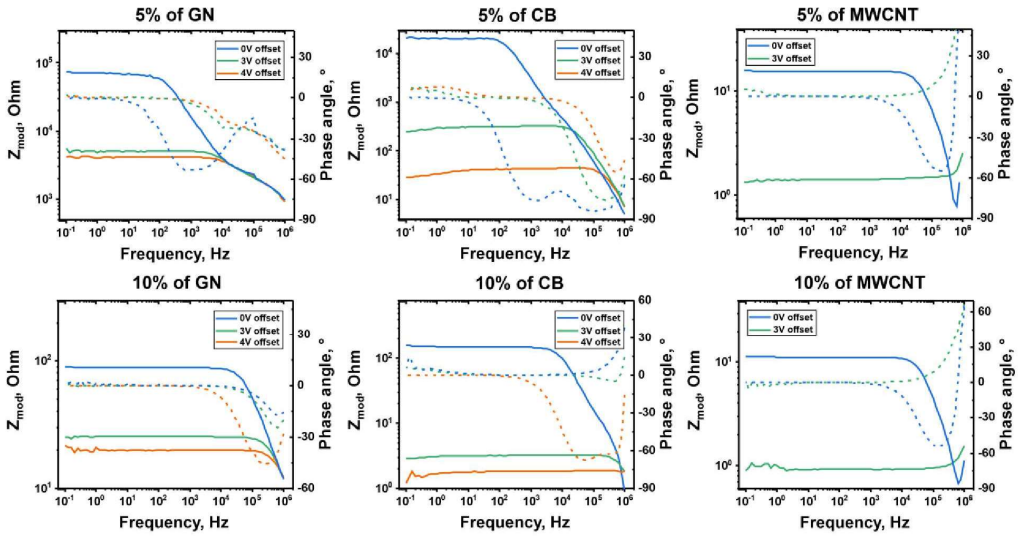

Figure S7. Bode plot of blends of PBS with carbon filler having various aspect ratio.

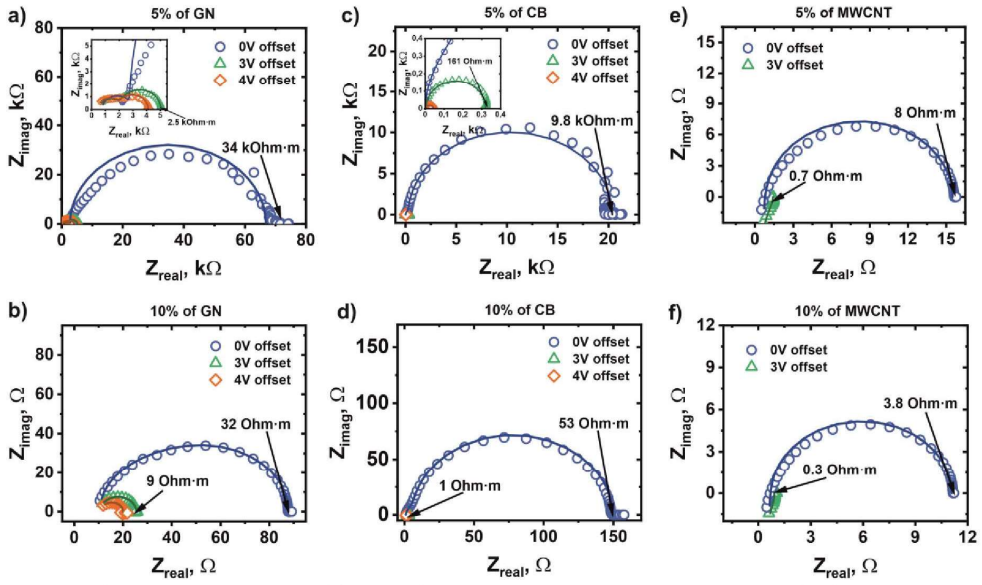

Figure S8. the Nyquist plot of EIS results made at different offset voltages (at low and high conductivity regimes) for PBS - GN, CB, and MWCNT blends with 5% and 10%of filler

Table S3. Fitting values of exponent decay of resistivity curve after applied one step 10% of shear strain: $R = R_0 + A_1 \cdot \exp(-(t-t_0)/t_1) + A_2 \cdot \exp(-(t-t_0)/t_2) + A_3 \cdot \exp(-(t-t_0)/t_3)$

	GN	CB	MWCNT
R_0, kOhm	4.5	0.3	0.0017
A_1, Ohm	41118 (≈84%)	834 (≈81%)	0.06 (≈24%)
t_1, s	1	1.8	1.7
A_2, Ohm	6298 (≈13%)	100 (≈10%)	0.06 (≈24%)
t_2,s	11	19	19
A_3, Ohm	1468(≈3%)	98 (≈9%)	0.13 (≈52%)
t_3, s	62	143	344
Coeff. of determination	0.995	0.999	0.996

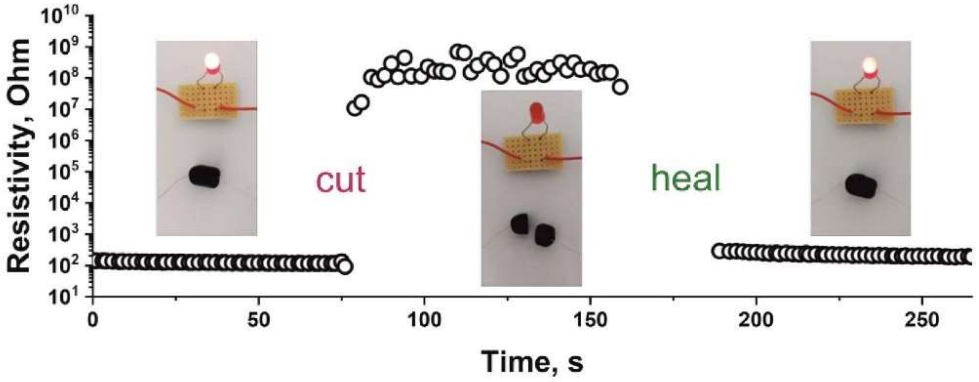

Figure S9. Healing demonstration of 2% MWCNT composite after cut followed by bringing two pieces together with minimal force applied.

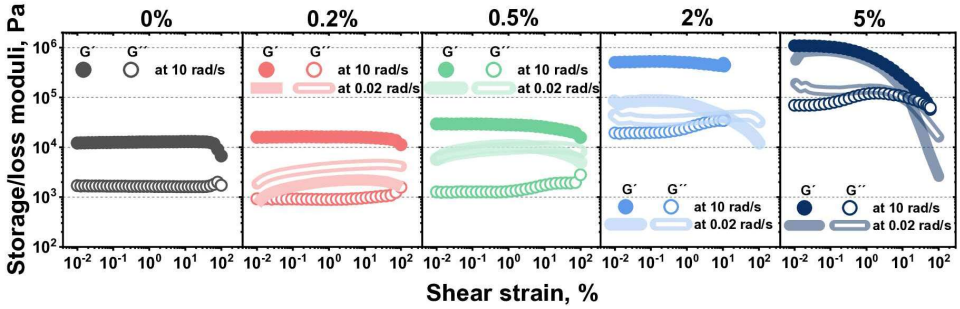

Figure S11. Amplitude sweep at 10 rad/s and 0.02 rad/s plotted as G´, G´´ vs. strain

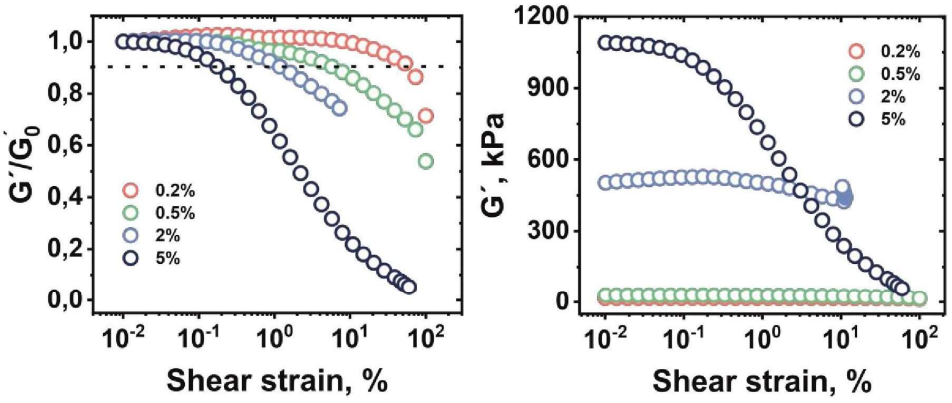

Figure S12. Definition of linear viscoelastic region for MWCNT – PBS composites. The linear region corresponds to the value of the shear strain at 10% drop of storage modulus.

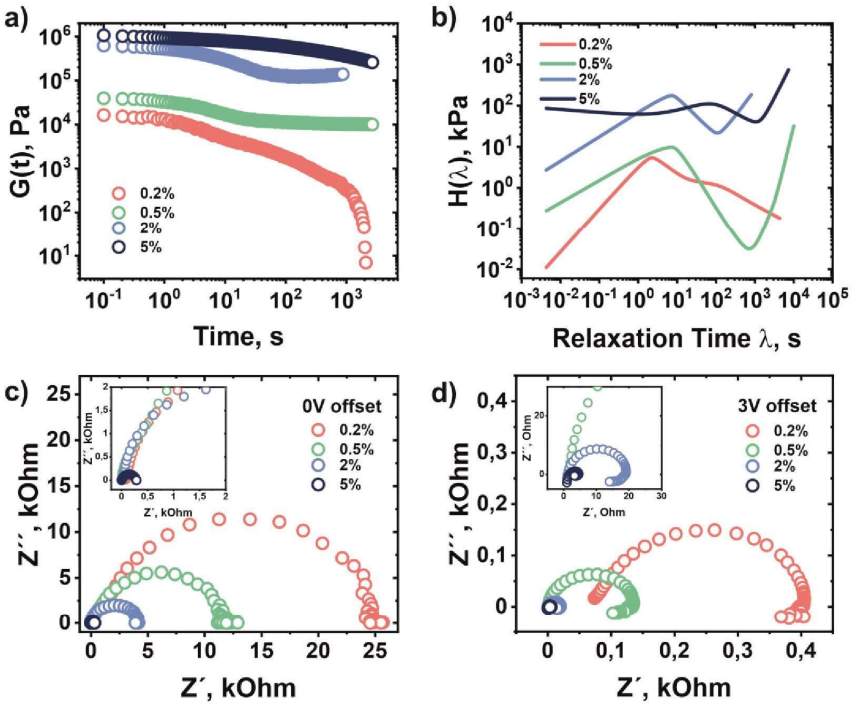

Figure. S10. a) the relaxation modulus G(t) measurement and recalculated from G(t) b) relaxation spectra for MWCNT/PBS blends with various MWCNT concentration; Nyquist plot of impedance measurements for the same blends at c) 0V offset voltage, and d) 3V offset voltage with 10mV amplitude

We studied relaxation process on larger time scale using stress relaxation experiment (Figure 9). The sample with lowest CNT content show complete stress relaxation on time scale of 10^3 s, while samples with higher CNT content do not exhibit complete stress relaxation. Moreover, relaxation modulus of the samples with 0.5 and 2% of CNT comes to a plateau on the studied time scale. The resistivity increases with decrease in filler content. The Nyquist plot shows the decrease of imaginary part of impedance with increase in filler content due to amplification of MWCNT network and decrease of average distance between particles. Despite low content of filler, even 0.2 MWCNT blend possesses higher conductivity compared to 5% GN blend, though conductivity of individual MWCNT and Graphene plate are nearly the same

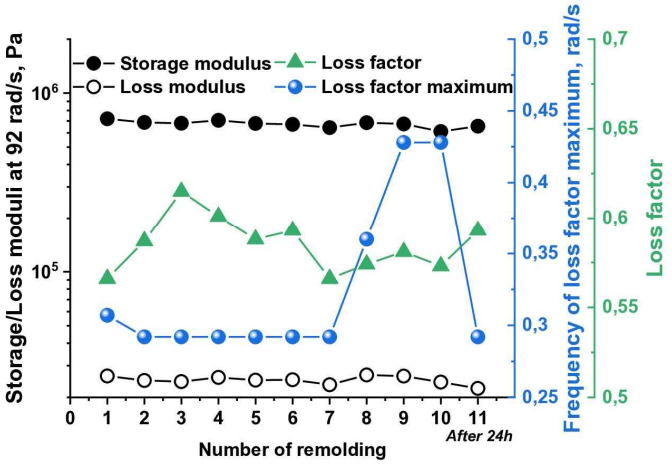

Figure S13. Changes of storage/loss moduli, loss factor maximum value and its position after several remolding (10 times) followed by 11th remolding after 24h of relaxation

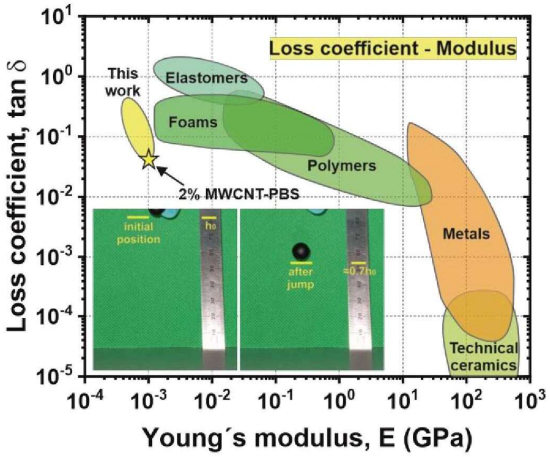

Figure S14. Ashby plot loss coefficient vs Young modulus. The 2% MWCNT region is cover by orange ellipsis.

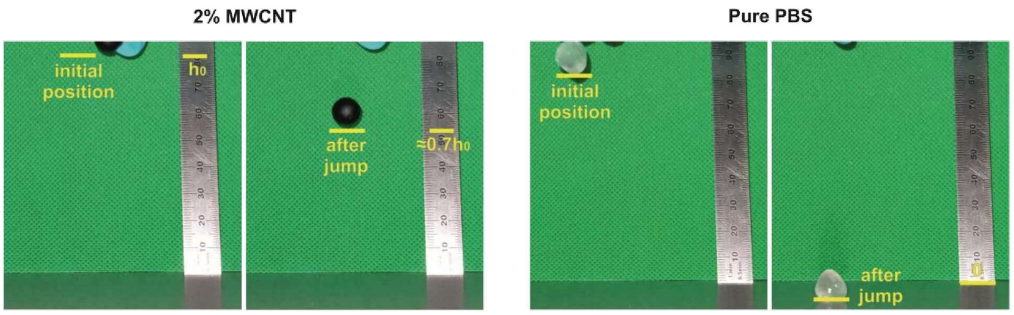

Figure S15. a) bouncing of super-elastic 2% MWCNT ball compared to pristine PBS polymer;

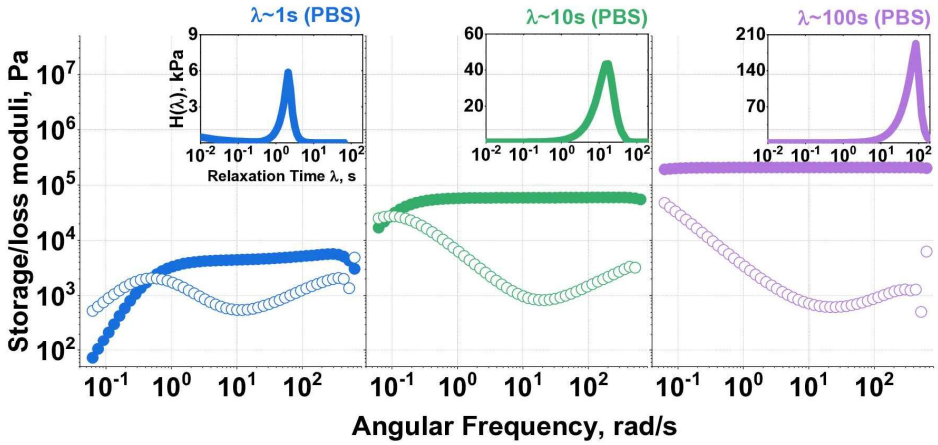

Figure S16. PBS with different content of boric acid. The higher boric acid content leads to increase in relaxation time of the polymer.

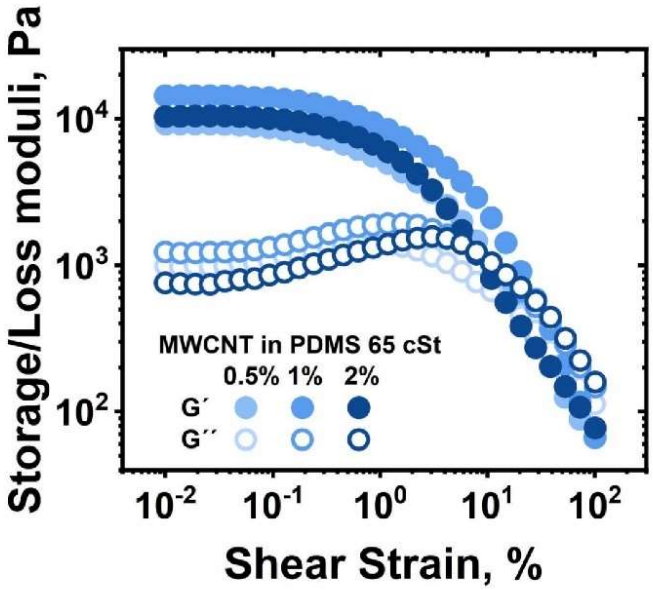

Figure S17. Amplitude sweep of MWCNT with various concentration in Newtonian liquid-like PDMS 65 cSt. Change of concentration does not lead to almost any difference in curves. Therefore it seems logical to assume that there is only interaction of particles with each other, forming a single huge agglomerate. The polymer-filler interaction is negligible.

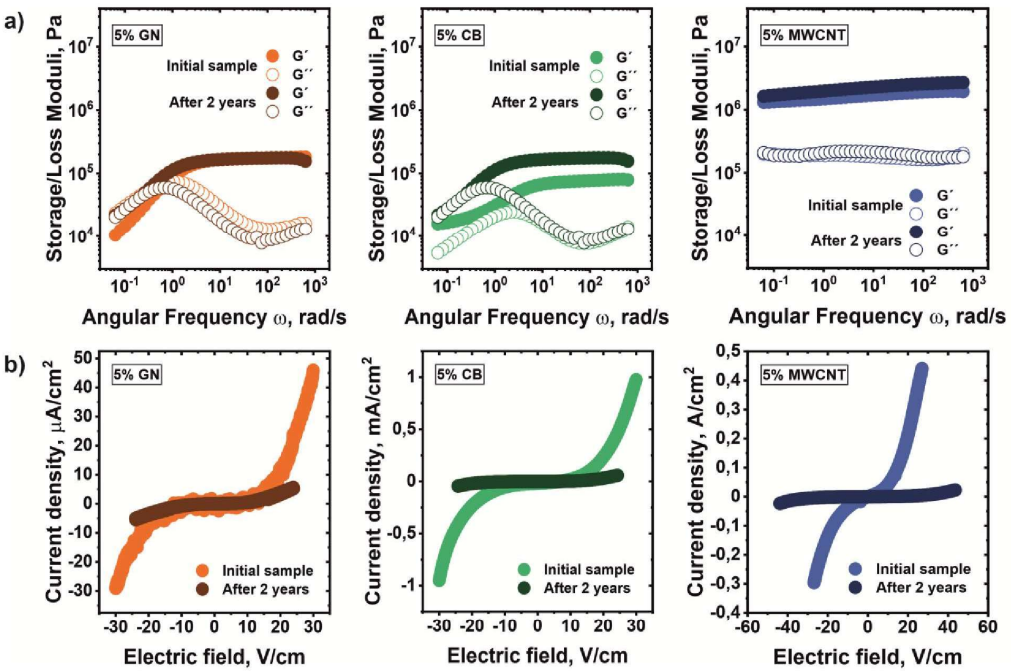

Figure S18. a) Frequency sweep experiment of PBS composites with carbon filler with various aspect ratio: initial sample and after 2 years of storage at room temperature; b) cyclic voltammetry of the composites of initial samples and after 2 years of storage

With time the properties of viscoelastic materials change. We observe that the presence of non-adsorbed filler polymer becomes more prominent in influencing the material's properties due to increased filler agglomeration. First and foremost, this phenomenon is reflected in the higher plateau values of storage moduli. This effect is notably more pronounced in the case of CB composites, while it is less conspicuous in the composites containing GN and MWCNT. The agglomeration of the filler material leads to the formation of a stiffer network, resulting in larger values of the storage modulus (G´), as opposed to a scenario where carbon is evenly distributed within the polymer matrix.

This hypothesis is further substantiated by the characteristic voltage-amperage (CVA) curves of the composites. Increased filler agglomeration creates greater distances between particles, resulting in higher resistivity and requiring a higher voltage for the hopping mechanism of conductivity to occur. Consequently, our findings indicate that viscoelastic conductive composites

do not exhibit long-term stability in their electrical and mechanical properties. The enthalpy of attraction between the carbon filler and the polymer surpasses the entropy-driven effects of polymer chain adsorption on the carbon filler. Over time, this leads to a deterioration in the dispersion of particles within the material.

Printability

3D printing. Printing of conductive self-healing composites was performed by 3D Discovery printer Regen Hu (Villaz-St-Pierre, Switzerland) on a glass slide. For better adhesion of filament the glass slide was covered by pure PBS using spin-coating of the polymer solution in tetrahydrofuran. The printing occurred at following conditions: 190°C, 800 μm nozzle diameter, 3.5 bar pressure, 5 mm/s feeding rate, 1 mm height, 4 kV voltage.

No matter all disadvantages of the viscoelastic composites, the ability to flow at certain conditions may imply printability, which opens doors to additive manufacturing devices based on these blends. The best flowability demonstrated the 5% GN sample due to the weakness of its filler network. At pressure higher then flow point, the material can be extruded without plastifying of it in any solvent. To demonstrated that we printed the 5% GN composite in pattern of Gauge element.

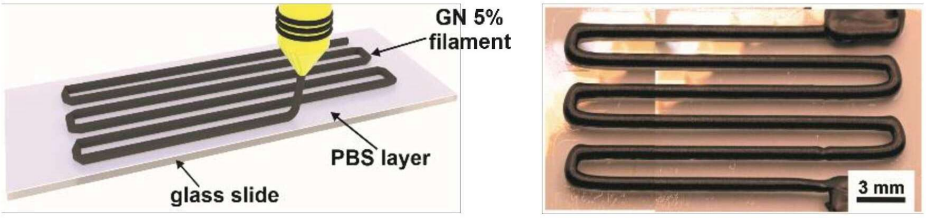

Figure S19. 3D printed Gauge element from 5% GN blend using solvent free FDM method

Part 3. Fiber-reinforced flexible self-healing strain sensor with failure-improving sensitivity recovery.

Milkin P., Pavale S., Soreño Z., Ionov L.

Submited in ACS Applied Materials & Interfaces

2024

Fiber-Reinforced Flexible Self-Healing Strain Sensor with Failure-Improving Sensitivity Recovery

Pavel Milkin[1], Shubham Pavale[1], Zhander Vohr Soreño[1], Leonid Ionov[1,2]

[1]Faculty of Engineering Sciences, University of Bayreuth, Ludwig Thoma Str. 36A, 95447 Bayreuth, Germany

[2]Bavarian Polymer Institute, University of Bayreuth, 95447 Bayreuth, Germany

* E-mail: leonid.ionov@uni-bayreuth.de

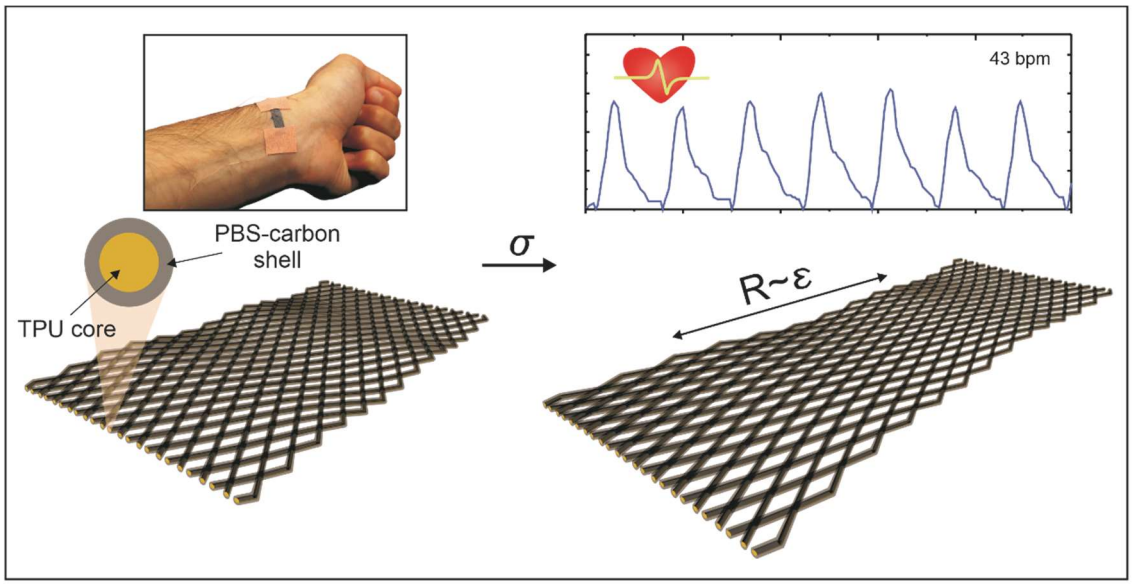

KEYWORDS: Silly-Putty, electrospinning, fatigue, strain-sensor, fibers, self-healing

ABSTRACT

In this work, we address the inherent limitations of porous, flexible, fibrous, and self-healing strain sensors. Specifically, we tackle issues such as the fatigue failure of carbon-fibrous materials and the long-term flow and low mechanical stability of self-healing materials. We achieve this by combining self-healing carbon blends with fibrous materials, creating a fiber-reinforced self-healing composite. The self-healing carbon blends provide strain sensitivity and the ability to recover after fatigue and

impact failure, while the fibers prevent the long-term flow of material and the scattering of pieces during impact and fatigue failure within the elastic deformation regime, enabling shape recovery.

We fabricated composite wearable strain sensors with a viscoelastic functional layer composed of two continuous phases: (i) a self-healing polymer-carbon blend and (ii) long electrospun fibers of commercial polyurethane. This setup also eliminates other drawbacks of bulk materials, such as non-linearity of volt-ampere characteristics, irreversibility of deformation, and a low working factor and allows improvement of working factor after failure and healing. The most important, we discovered that hindered self-healing enables improvement of sensor sensitivity after large strains and failure that is due to partial failure of network formed by conductive particles.

Introduction

Recent advances in skin-mountable and wearable electronic devices have attracted significant attention due to their seamless integration with the human body and capacity for long-term monitoring[1]. These flexible sensors, designed for monitoring the human body's physical, chemical, biological, and environmental parameters, offer high efficiency with minimal discomfort. One important example of wearable technology is the flexible strain sensor, which converts external mechanical stimuli into electrical signals. Flexible strain sensors find versatile applications, including monitoring vital signs such as pulse and breathing rates, electromuscular activity, gait analysis, and sleep tracking[2]. These sensors offer valuable insights for enhancing performance, injury prevention, and assisting in rehabilitation[3]. Moreover, flexible strain sensors can be integrated into more intricate systems such as human-machine interfaces and soft robotics[4].

The wearability of materials implies comparable values of their Young's modulus and modulus of skin (< 1 MPa), ability to undergo considerable (up to 100%) deformations, as well as porous structure, which provides breathability, permeability, comfortability, and lightweight. For that purpose, the electrospun elastomeric fiber materials are great candidates ($E = 10^5 – 10^6$ Pa), which have structural similarities with extracellular matrix (ECM)[5]. Particularly, thermoplastic polyurethane-based materials, which are superelastic, cheap, recyclable, and may be soft enough, are well suited for this purpose. Polyurethane-fiber-based and other fiber-based strain sensors were previously fabricated either by incorporating conductive filler (i) inside of the fiber matrix[6, 7], (ii) on top of it[8-10], or (iii) fully encapsulating carbon-fiber structure in other elastomer-like mold[11]. In the

first and third cases, embedding conductive filler inside the polymer matrix requires high colloidal stability of the particle dispersion. As a result, the fabrication of micron-sized fibers is challenging due to coagulation and precipitation of a filler. Moreover, the low mobility of the conductive filler may restrict recovery ability in case of network failure, and increase the chances of fatigue failure due to the weakening of the particle-polymer interface during multiple cycles of deformation. Applying the filler on top of the matrix (the second approach) does not provide sufficient adhesion of the conductive particles to the fibrous material, which may lead to loss of conductive material. Thus, the main drawback of fibrous flexible soft sensors is their fatigue failure.

To solve this problem of fatigue failure, the self-healing viscoelastic polymer matrix may be used. This implies the use of a polymer with relatively high chain mobility (low glass transition temperature) and presence of different nature of polymer chains interaction, including metal-ligand coordination, H-bonding, π-π stacking, and dynamic covalent bonding[12]. The chain relaxation time should range from 10 s – 1 day to ensure elastic behaviour during use and flow behaviour needed for self-healing at rest. One of such polymers is the widely used self-healing polyboroxiloxane (PBS), which has a dynamically crosslinked network due to Si – O – B bonds and supramolecular structure *via* hydrogen, and dative Si – O:B bonds[13]. Previously, PBS-carbon composites were investigated as strain sensors and demonstrated an extremely high Gauge factor (>500)[14], and were attempted to use as strain rate sensor[15], flexible conductor[16], and gas sensor[17]. O´Driscoll et al. demonstrated that the hysteresis and rate dependence of electromechanical properties in viscoplastic solids can be eliminated by segregating a filler layer on top of a viscoelastic polymer matrix in a thin composite layer of such composite[18]. Boland et al. fabricated a compressive sensor by functionalizing a commercial polymer foam through soaking it in PBS-graphene-based ink[19]. Their sensor underwent signal fatigue without reaching the endurance limit. Moreover, the polymer foams are not considered as wearable materials due to their gas impermeability. Earlier, we investigated the impact of viscoelasticity on PBS/carbon composites with different aspect ratios of carbon filler[20, 21]. The particles with a low aspect ratio (graphene plates) possess higher mobility and enhanced toughness, endowing the material with increased stability and the capacity to flow effectively even when the filler content is high. Conversely, the behavior of high aspect ratio filler (MWCNT blends) diverges significantly from this scenario. On both small- and large-time scales material shows elasticity at small strain; increasing deformation shifts to plasticity, with deviation of stress of linear viscoelastic regime rising with particle content. Generally, PBS-based materials have several drawbacks, constraining their application in sensor technology: small linear viscoelastic range (2% strain

followed by plastic deformation), low working factor (2% for GN-based materials), non-linear voltampere dependence, and most importantly, flow on large time scale resulting in disability to keep its shape and lack of wearable possibility.

In this work, we overcome the intrinsic limitations of porous and flexible fibrous- and self-healing strain sensors. In particular, the problems of fatigue failure of carbon-fibrous materials and flow of self-healing materials on a large time scale as well as their low mechanical stability are solved by combining self-healing carbon blends with fibrous material – it is fiber-reinforced self-healing composite. The role of self-healing carbon blends is to enable strain sensitivity and restoration after fatigue and impact failure, the fiber shall prevent the spreading of material on a large time scale due to flow and lump scatter of pieces during impact and fatigue failure in elastic deformation regime and allow shape recovery of material. In particular, we fabricated composite wearable strain sensors with a viscoelastic functional layer consisting of two continuous phases: (i) self-healing PBS-carbon blend and (ii) long electrospun fibers of commercial TPU. Using this setup also eliminated other drawbacks of its bulk *vis-a-vis*, such as the non-linearity of voltampere characteristics, irreversibility of deformation, and small working factor. Cycling tests at different strain amplitudes revealed creep and fatigue in the material, with deterioration in both electrical and mechanical properties, including their strain rate dependence. However, due to the soft self-healing functional layer, the material can restore its initial properties and does not compromise the mechanics of the initial TPU mat. Notably, the sensitivity of the sensors was substantially improved after large deformation. In addition, practical applications, such as heart rate measurements were implemented. Our results demonstrate the importance of self-healing material for piezoresistive layer, underscore the significance of exploring fatigue in piezoresistive signals, a frequently neglected aspect in research articles, and suggest the potential suitability of viscoelastic layers when paired with an appropriate elastomeric substrate.

Materials and methods

Materials. The hydroxyl-terminated polydimethylsiloxane (PDMS) with kinematic viscosity 65 cSt was purchased from Sigma-Aldrich. Multiwalled carbon nanotubes (MWCNT) (NC7000^{TM}, Nanocyl SA, Belgium) and graphene nanoplates (GN) (Sigma-Aldrich), Thermoplastic polyurethane (TPU) (Filaflex 70A, 'Ultra-Soft', Recreus Industries, S.L.) were used. Toluene (Sigma Aldrich, ≥99.5%), tetrahydrofuran (THF) (Roth, ≥99.5%), Chloroform (Sigma-Aldrich, ≥99.5%), Dimethylformamide (DMF) (Sigma-Aldrich, ≥99.5%), and boric acid (Sigma Aldrich, ≥99.5%) were purchased and used as it is.

TPU mats electrospinning. The electrospinning system was a custom-made set-up consisting of a high-voltage power supply, a box collector (grounded conductor) covered with paper tape (substrate), and a pneumatic-based multi-syringe digital pump for the dispersion of spinning solution through a syringe tipped with a stainless needle. The collector rotated at 350 rpm (0.92 m/s). A stainless-steel blunt end needle with an inner diameter of 0.8 mm (21 G) was used for the experiment, connected to the high-voltage power supply. The distance between the needle and the collector was fixed at 15 cm. The flow rate varied between 1-2 mL/h, while the applied voltage was 20 kV. The spinning dope was prepared by dissolving thermoplastic polyurethane (TPU) in the mixture of solvents; Chloroform, THF, and DMF in the mass ratio 1.6:0.5:1.0 respectively. The solution concentration was fixed at 10 wt% of polymer. Magnetic stirring was used overnight to ensure a homogenized solution. Once completely dissolved, the solution was transferred to a disposable polypropylene syringe (6 ml). The collector was covered in paper tape to facilitate easy collection and removal of the fiber mats. After electrospinning, the fiber mats were left undisturbed on the collector for 48 hours before removal. It led to the creeping of TPU fibers over time, thereby reducing the shrinkage and improving structural integrity, making them easy to handle.

PBS synthesis. PBS was synthesized by the following Tang et.al essay[22]. To prepare PBS (relaxation time is ca 10 s and plateau shear modulus is ca $2 \cdot 10^3$ Pa), the mass ratio of 100:0.88 between the hydroxyl-terminated PDMS 65 cSt and H_3BO_3 was chosen. First, the PDMS was dissolved in toluene. Then, boric acid was added to the solution, and the mixture was dispersed for a couple of minutes in an ultrasonic bath. The mixture was heated to 120 °C with Dean-Stark trap and left for 48 h with further stirring. After this time, the mixture became transparent. Excess solvent was removed with a vacuum evaporator, and the remaining solvent was removed by storing the sample in a vacuum oven at 60 °C for 24 hours.

Strain sensor fabrication. In our work the strain sensor is composed of two parts: a constructive layer of electrospun TPU mat and functional layer of PBS/carbon. The ratio of carbon/filler was chosen based on the percolation volume fraction found in literature for a carbon filler in PBS matrix. The higher sensitivity can be reached at a value close to the percolation value. 1 vol.% of MWCNT and 5 vol.% of GN filler in ratio to PBS was chosen and fixed. Based on that, various concentration of inks were prepared: 2%, 5%, 10%, and 15% for MWCNT/PBS ink and 2%, 5%, and 10% for GN/PBS ink. Initially, PBS was accurately weighed and dissolved in toluene using a magnetic stirrer to make the inks. Subsequently, the measured amount of carbon nanoparticles was dispersed in the solution. The resulting suspension was stirred at 1000 rpm for 5 minutes. Following this, further mixing of

suspension was carried out using an ultrasonicator to ensure the homogenous dispersion of carbon nanoparticles in the suspension. The sonicator was used in pulse mode (1 minute ON, 30 seconds OFF) for 2 minutes. Once the ink was prepared, the TPU fiber mats were cut into 3 cm x 2 cm pieces and immersed in ink suspension with continuous stirring at 700 rpm for functionalization. The TPU mats were then sonicated six times, each pulse lasting 2 minutes, to ensure that PBS and carbon nanoparticles penetrated the electrospun fiber mat. After approximately two hours, the coated mats were removed from the ink suspension and dried under a vacuum at room temperature for 48 hours to allow the toluene to evaporate. The mats were stored at room temperature until further processing.

Scanning electron microscopy. The fiber and sensor morphology, and mats thickness was characterized using field emission scanning electron microscope (FESEM) (Thermo Scientific, Germany). To provide conductivity, samples were sputtered with 2 nm Pt layer.

Electrical characterization. The electrical properties of the fabricated sensor were investigated by Gamry 1010E potentiostat. The sample was fixed between two clamps and connected to the potentiostat. The measurements were conducted in two-electrode mode. The volt-ampere characteristic was measured in voltage range $|V| \leq 3$.

Mechanical and electromechanical characterization. The mechanical tests in tensile test mode were performed on MCR 702 Multidrive (Anton Paar, Graz, Austria). Custom-made insulated adapters for clamps were made to fix the sample. The electrical contacts were made from copper tape followed by copper wire, connected to the potentiostat. Deformation rate was varying depending on experiment requirements. The applied voltage was equal to 3V.

Sensor live-performance. The electrical contacts were made from copper wire and fixed to a cut-fabricated sensor using conductive silver glue. The fabricated sensor was fixed and attached to a hand using an adhesive band. For measurements, the same potentiostat was used in two-electrode mode with a 3V applied voltage.

Results and discussions

Sensor fabrication

The fabricated strain sensor has a bicontinuous structure and was made in three main steps: (i) fabrication of e-spun TPU mats as constructive part; (ii) synthesis of PBS followed by filling it with

conductive carbon filler, the PBS-carbon blend shell acts as functional layer of the sensor; (iii) combining functional and constructive parts.

The constructive part - TPU exhibits superelastic properties that are evidenced by its ability to undergo considerable reversible deformation. In our study, this material was utilized in the form of randomly distributed fibers. We obtained an isotropic fiber mat using an e-spinning device, ensuring consistent thickness (approximately 100 μm for convenient handling) and a fiber diameter of approximately 1.1 μm **(Figure S1-2)**. Notably, the Young's modulus of this porous mat was equal to 0.9 MPa **(Figure S3)** (the Youngs modulus of bulk polymer is around 8 MPa), a value comparable to the modulus of human skin at large strain[23]. Additionally, the electrospun TPU mat offers deformation reversibility, lightness, porosity, and permeability, rendering it a suitable and skin-compatible material for wearables.

The PBS, which is healing component of functional part, was synthesized by polycondensation of hydroxy terminated PDMS and boric acid, forming dynamically crosslinked network *via* Si – O – B bonds and supramolecular structures, formed by dative Si – O:B and hydrogen bonds. To characterize the product, two main parameters were measured: relaxation time and plateau value of storage modulus **(Figure S4).** The polymer possesses two relaxation times. First relaxation time we observe at $\lambda = 7$ s, which is attributed to relaxation of polymer chain. The second relaxation time is the fast relaxation of supramolecular structure with $\lambda \approx 10^{-2}$ s [22]. The PBS behaves as a solution of entangled long polymer chains with plateau value of storage modulus G′ = 2 kPa (G′ of "solution"), whereas the G′ of PDMS melt at the plateau region is 0.5 MPa[20]. The ratio of G′(solution)/G′(melt) = 0.004 indicates the concentration of very long polymer chains around 9%[24].

The graphene nanoplates (GN) and multiwalled carbon nanotubes (MWCNT) are functional components of functional layer. Their role is to ensure electrical conductivity. Both GN and MWCNT were used without additional modification. The functional layer is a composite of the carbon material and a viscoelastic PBS polymer capable of self-healing.

The functional layer was applied by immersion of TPU mat in suspension of carbon filler and dissolved PBS in toluene followed by drying in a vacuum oven **(Figure 1a)**. The material forms a piezoresistive shell around TPU fibers, maintaining mats visual porosity and permeability. Due to vigorous ultrasonication, the ink covered fibers surface not only on top of the mat, but also penetrated inside, creating the piezoresistive network over the whole volume of the mat **(Figure S5-6)**.

Electromechanical characteristics in linear region

Most important characteristics of piezoresistive strain sensors are its sensitivity (or Gauge factor, G) and working factor *W*. Gauge factor is the slope of fractional change of resistance vs. strain

$$\frac{\Delta R}{R_0} = G\varepsilon$$

The working factor (W) represents the critical strain up to which the fractional resistance maintains a linear dependency. This value clarifies the distinction between strain sensing ranges and mechanical strain tolerance. An optimal sensor should exhibit high values of both G and W.

We first investigated effects of composition of blends on the values of Gauge and Working factors - we varied the concentration of carbon filler in PBS and condition of deposition of carbon-PBS blends. According to the theory, the highest Gauge factor can be achieved at volume fraction of filler close to percolation threshold [25]. The volume fraction of MWCNT and GN in PBS was chosen as 1% and 5%, respectively, which are close to percolation values of these composites. We found that the concentration of these PBS-carbon blends in toluene solution used for their deposition influences the electromechanical characteristics of the deposited blend non-monotonically **(Figure S7-8), Table 1).** A high ink concentration (≥10 wt.%) causes carbon particles to aggregate on the mat's surface, constraining to internal pores. At low ink concentration (2 and 5 wt.%), the filler was evenly distributed, maintaining the mat's visual porosity without causing significant differences in microstructure. Noticeably, the volt-ampere characteristic is linear for all materials **(Figure S9)** which is not the case for bulk materials[17, 21]. We attribute it to the higher efficient concentration of the filler in PBS than that of the original mixture (7.4 vol.% and 17.7% for MWCNT and GN based sensors, respectively) (**Figure S10**) – the concentration of particles on surface may be higher than that in the bulk due to inhomogeneous drying. As a result, electron transfer through direct contact between the filler dominates as a charge transfer mechanism over electron hopping and pseudocapacitor behavior. The Gauge factor (**Table 1**) for all mats were either consistently small (1.4 - 4.0, in case of MWCNT based sensor) or consistently large (61 - 154, in case of GN based materials) when the concentration of blends in solution varied in range 2%-15%. Therefore, the material with the largest working factor was chosen (5% ink concentration in both cases): GN based material with W = 2% and G = 47, and MWCNT based material with W = 15.3% and G = 2.3 **(Figure 1b(ii), c(ii))**.

The materials electromechanical behavior depends on the deformation rate **(Figure 1b(i)-c(i)).** PBS composites, as was shown in our previous study, possesses strain rate dependent behavior due to thier viscoelastic nature, as was shown in our previous study[21]. To observe such behavior in our fiber-reinforced material the electromechanical characterization of material was carried out at 0.5 %/s and 5%/s, corresponding to the viscous and elastic behavior of bulk PBS, respectively **(Table 2)**. The material in viscous regime demonstrates larger working factor compared to that in elastic regime in case of MWCNT based materials ($W_{0.5\%/s}$ = 15.3% vs $W_{5\%/s}$ = 9%). However, the Gauge factor is larger for faster deformation ($G_{5\%/s}$ = 3.7 vs $G_{0.5\%/s}$ = 2.3). In the case of GN based material the working factor is nearly the same W = 2% at both low and high deformation rate, however the Gauge factor has the same tendency as in the case of MWCNTs: $G_{5\%/s}$= 98 vs $G_{0.5\%/s}$=47 for elastic and viscous regime, respectively. The values of the Gauge and Working factors may be attributed to the mobility of the particles within the PBS matrix – the higher mobility of polymer, the larger working factor and smaller gauge factor. In order to explain this trend, we consider that the change of resistivity upon deformation is attributed to break of contacts between conductive particles. On a large time scale (viscous flow of PBS) the particles rearrange during continuous deformation and reestablished contacts, reducing the increment of resistance, whereas in elastic regime temporal window for such reorganization is diminished. The same principle explains the larger working factor in case of viscous regime: the working factor is limited at so called critical strain (Kraus model)[26], when the filler agglomeration network is broken. Filler network breaks at lower strain at higher deformation rates in lack of rearrangements time window.

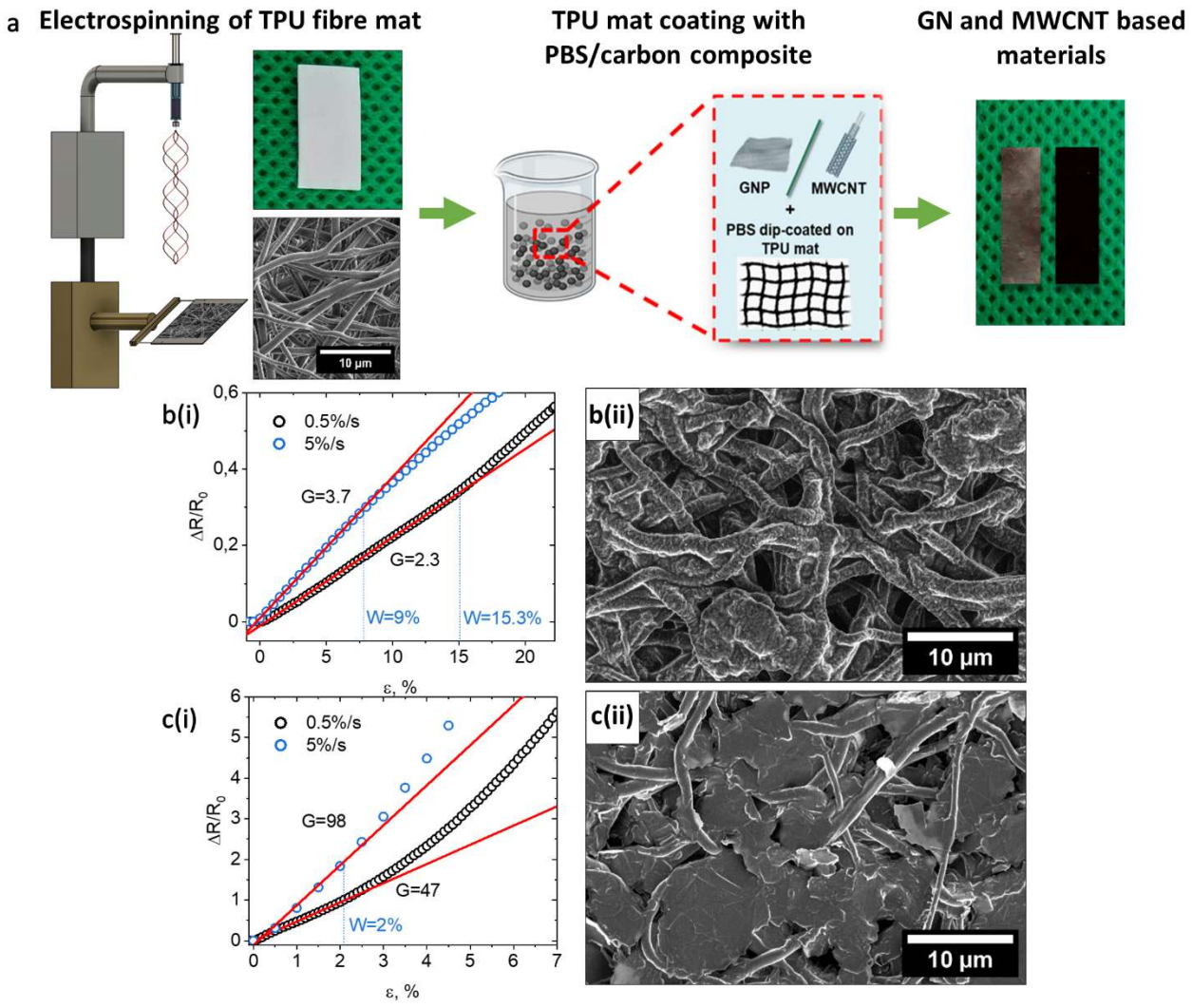

Figure 1. a) Scheme of fabrication process of electrospun TPU – carbon/PBS strain sensor fabrication; b) (i) fractional resistance response vs strain of MWCNT based strain sensor in elastic and viscous regime and (ii) top view of the fiber mat after fabrication; c) (i) fractional resistance response vs strain of GN based strain sensor in elastic and viscous regime and (ii) top view of the fiber mat after fabrication.

Table 1. Gauge and Working factors as a function of concentration of PBS/carbon (MWCNT and GN) blends in solution

Concentration of blend in solution	MWCNT/PBS		GN/PBS	
	Gauge Factor (G)	Working Factor (W, %)	Gauge Factor (G)	Working Factor (W, %)
2%	4.0	14.7	61	0.8
5%	2.3	15.3	47	2
10%	2.8	5.3	154	0.15
15%	1.4	3.0		

Table 2. Gauge and Working Factors of 5% PBS/carbon blends at different strain rates (at viscous and elastic regimes of the polymer)

Regime of PBS matrix	MWCNT/PBS		GN/PBS	
	Gauge Factor (G)	Working Factor (W, %)	Gauge Factor (G)	Working Factor (W, %)
Viscous (0.5%/s)	2.3	15.3	47	2.0
Elastic (5%/s)	3.7	9.0	98	2.0

Creep and Fatigue behavior

One of the important factors of wearable fiber-based strain sensors is long term stability at multiple deformations, also known as fatigue resistance. The health monitoring signals, such as heart rate and voice vibrations, happen several thousand times per day and making the stability of signal crucial. However, this factor often remains overlooked, even though conditioning of some sensors requires several thousand of cycles[7, 27].

Amplitude tensile sweep – like test of GN and MWCNT based sensors was performed at different strain amplitude with a constant strain rate of 0.1 %/s (viscous flow of bulk PBS), 50 cycles for each amplitude **(Figure 2a-b)**. After several cycles, apparent mechanical conditioning of both materials occurs – a cycle with increased amplitude follows the same curve as previous one. We observed the material creep that is expressed in (i) downwards parallel shifting of stress-strain curve - the residual strain (length of sample at zero stress) increases and (ii) decreases in stress while slope of stress-strain curve at linear increase of stress with strain remains unchanged. To explain these tendencies, we speculate that some structures in materials break during stretching and the material undergoes plastic deformation that is expressed in the increase of residual strain, however, new structures, identical to broken ones, form, that is expressed in unchanged stress-strain slope.

The electromechanical signal also underwent conditioning (Figure 2a(ii),2b(ii)). The Gauge factor at the 1st cycle is much larger than in the following cycles, attributed to the rearrangement of the filler network. The decrease in Gauge factor during cycling is more pronounced for GN -based sensors, as they exhibit higher percolation at higher concentrations than MWCNT-based sensors. The more stable and continuous the network formed by conductive particles, the lower the gauge factor, but the less pronounced its decay during cycling.

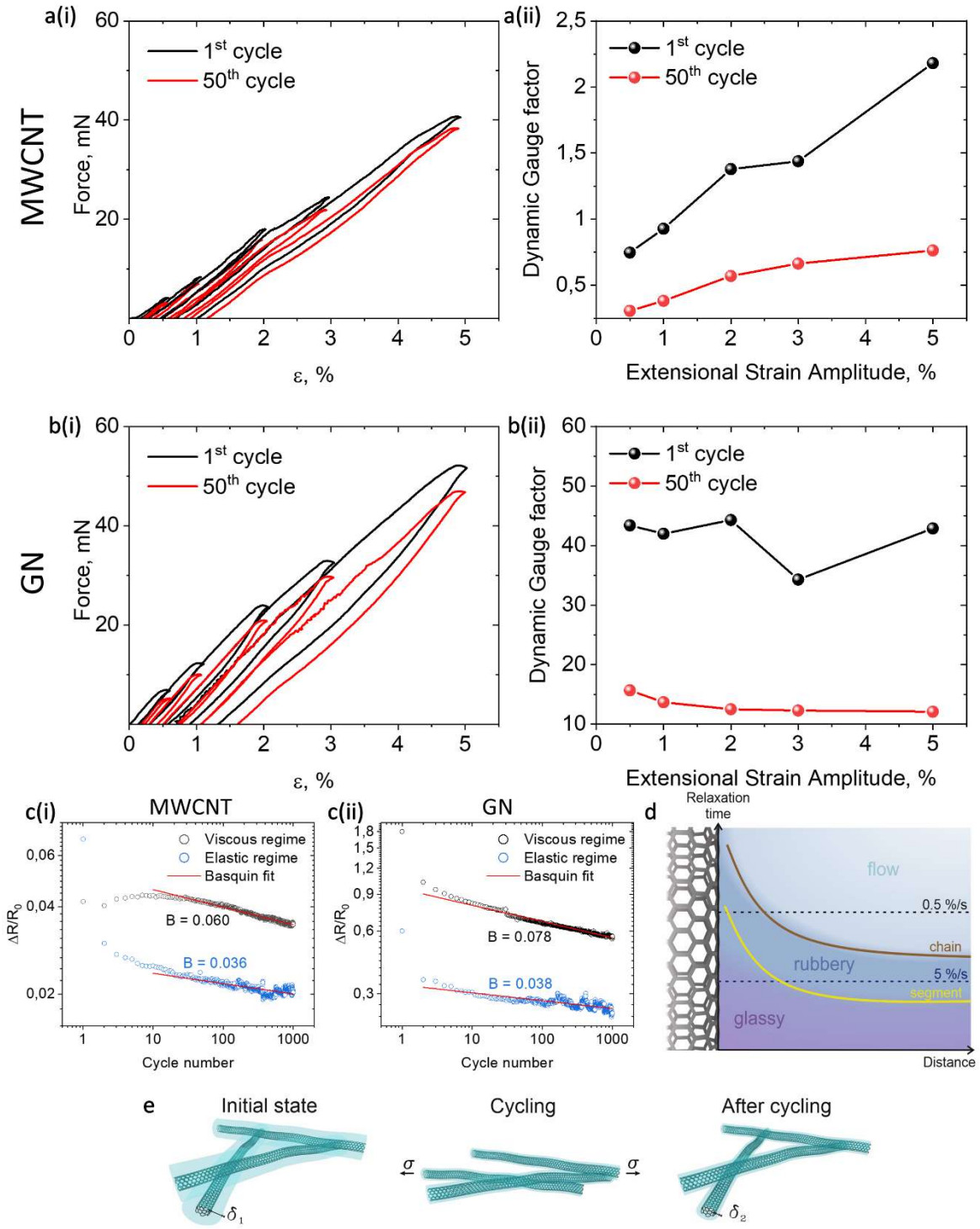

Figure 2. Amplitude sweep and dynamic gauge factor of strain sensor mats based on a) MWCNT and b) GN carbon filler. Fatigue test of MWCNT and GN based strain sensors. The S-N like curve for electrical response for c(i) MWCNT and c(ii) GN based sensor; d) scheme of interfacial layer behavior as a function of distance from particle surface: e) illustration of interfacial layer decrease during mechanical cycling: $\delta_1 > \delta_2$

The fatigue behavior **(Figure 2c, S11)** was quantified by using Basquin equation.

$$\left(\frac{\Delta R}{R_0}\right) \approx \alpha C^{-B},$$

where α – electromechanical response in the first cycle ($\alpha = \frac{G_0 \sigma_0}{E_0} = G\varepsilon_0 = \left(\frac{\Delta R}{R_0}\right)_{C=1}$, where G_0 - initial Gauge factor, σ_0 – initial stress at applied strain amplitude, E_0 – initial Young modulus), B – Basquin exponent which characterizes the rate of decay of the resistivity response during cycling, C – number of cycles[28, 29]. To estimate endurance limit C_E (number of cycles of steady state in signal, infinite life of sensor) the empirical equation can be used

$$\ln\left(C_E\right) = \frac{\ln(0.5)}{-B}$$

where 0.5 is the fatigue ratio for elastomers[28, 29].

Both GN and MWCNT strain sensors undergo at least two stages of fatigue when PBS is elastic and viscous: at low and large number of cycles. During first 3 cycles the material undergoes considerable diminishing of signal - the B value is equal to around 0.6 for GN composite and 1.0 for MWCNT composite (except MWCNT in viscous regime). The fatigue during following cycling follows the usual power law Basquin-equation - behavior with constant slope in double log coordinate. The B value in elastic regime is 0.04 and in range 0.06-0.08 in viscous regime for both materials – the decay is more pronounced in viscous regime.

The complex fatigue behaviour of a layered composite such as this can be understood as a stepwise contribution of each component. Initially, the sharp decrease of fractional resistance observed in the first stage can be attributed to the irreversible plastic creep (settling down) of the PBS–carbon composite layer. Subsequently, the second stage is primarily associated with fatigue of TPU mat. While TPU possesses elastomeric properties and exhibits reversible deformation, it does not fully recover due to the sliding of fibers and creep of non-covalent crosslinking, as the energy of activation of intermolecular bonds is not as high as that of covalent bonds. -The TPU creep's impact on the

electrical response is evidenced by the similarity of the Basquin exponent (B = 0.024) observed in cyclic experiments (**Figure S12**) compared to cycling of the sensor at high strain rates, where the fatigue of the PBS layer has a significantly lower impact. Additionally, we observe secondary shoulder peak in the resistance profile during cycle test, which can be explained by the Mullins effect (**Figure S11**). Due to fatigue experienced by both the shell layer and the TPU core, wrinkles can be observed on the structure after the experiment under both regimes (**Figure S14**). Nonetheless, given that only the initial large fraction of the signal is essential for monitoring purposes, the material can still be effectively utilized as a wearable strain sensor for detecting bodily signals.

The restricted mobility of polymer chains adjacent to the particles causes the difference between the values of Basquin coefficients obtained for viscous and elastic regimes of deformation. The polymer chains, which adhere to the particle's surface due to intermolecular interactions, form interfacial layer δ, whose properties differ from those of the bulk polymer. The mobility of polymer chains decreases in the vicinity of the particle surface – both the relaxation time of chains segments (glass transition temperature) and the relaxation time of polymer chains (flow time scale) increase (**Figure 2d**). While the PBS bulk remains in the flow regime, the interfacial layer exhibits a predominantly rubbery state with slight glassy part[21]. The typical δ thickness for elastomer-like polymers is in the range of 10 nm[30]. Applying mechanical energy, softening of δ layer occurs, leading to its decrease (**Figure 2e**) and material conditioning. At large time scale the structure of interfacial layer is same as for material at rest. At low time scale, the interfacial layer is glassy, and bulk polymer is in rubbery state. Thus, since activation energy of segments are larger than one of chains (for linear PDMS $\approx$ 46 kJ/mol[31] vs 15 kJ/mol[32]), the conditioning in elastic regime requires much more energy and it results in lower B value.

To recap, the materials undergo fatigue according to Basquin´s law, with significant contribution in electrical signal of TPU mat creep at large number of cycles. Subsequently, it results in second shoulder peak on resistance cycling profile and wrinkles on the mat. Moreover, the conditioning is faster in viscous regime due to higher mobility of chains and segments in interfacial layer which is confirmed experimentally in larger B values.

PBS impact and healing properties

The sensor is able to recover its initial characteristics (size and performance) after considerable deformation due to both the reversibility of deformation of TPU mat, which restores size and shape, and self-healing abilities of the PBS based viscoelastic layers, which restores performance. The

recovery of function occurs due to the movement of polymer chains in bulk, in proximity of particles surface, and due to the movement of particles in polymer matrix. In our previous work the GN-PBS composites demonstrated faster restoration of electrical properties (conductivity) compared to that MWCNT-PBS material did due to higher particles mobility and weaker particle network[21]. Here we demonstrate the healing properties of functional PBS-carbon layer and compare it to materials covered only with carbon filler of the same amount without PBS.

To assess the electromechanical characteristics and the effectiveness of self-healing materials, the following strain profile was utilized: I) low strain cycling (50 cycles) at ε = 5% - sensing regime; II) large deformation cycling (5 cycles) with high amplitude ε = 100% which causes failure of the piezoresistive layer; III) rest period for self-recovery: material left at ε = 0% for 15 minutes; (IV) low strain cycling (50 cycles) at ε = 5% - sensing after failure and self-healing **(Figure 3)**. The deformation rate was 5%/s – the PBS was in elastic state so that the failure of PBS can occur at large deformation. For comparing materials, two key parameters were considered. First one is the change in α ($\alpha = \frac{G_0\sigma_0}{E_0}$, initial properties of sensor) at Stages I (initial) and IV (healed), which reflects the change of piezoresistive properties before failure and after healing. The second one is the recovery of resistance within 15 Minutes after Stage II (failure), which indicates the material's ability to restore its resistive properties following the large deformation cycling.

When comparing the electromechanical properties, it is evident that sensors lacking healing materials (just carbon on TPU fiber mat) experience significant deterioration in performance compared to those with PBS. The polymer plays a dual role here. First, although it separates the particles and reduces conductivity, it allows them to flow better (low-stress viscosity is reduced). Second, in the flowing state, the polymer allows the particles to flow plastically and not undergo brittle fracture. During the healing process (stage III), GN based sensor with PBS demonstrate notable recovery, with a resistance restoration of 72% in 15 min. (**Figure 3c(ii), e**). In contrast, sensors without PBS exhibit a comparatively lower recovery of 53%. Hence, PBS plays a crucial role in facilitating faster recovery, as evidenced by lower characteristic exponential decay times, as depicted in **Figure S15 and Table S1**). The characteristics recovery times of sample with PBS is lower than the one for sample without PBS: for instance, t_1(PBS)= 5s vs t_1(No PBS) = 8.7s. Following the healing process, sensors with PBS exhibit a decrease in α value of 19% **(Figure 3c(i), d, Table S2)**. Conversely, sensors without PBS display a significantly higher decrease in α value, reaching 57%, indicating a less efficient recovery mechanism.

MWCNT based sensors behave slightly different after healing stage than GN-based one does. During the healing process (stage III), sensors with PBS demonstrate a notable recovery, achieving a resistance restoration of 47%. In contrast, sensors lacking PBS display a significantly lower resistance recovery of only 11%. The inclusion of the healing matrix also contributes to a faster recovery, as evidenced by lower characteristic exponential decay times. The characteristics times of sample with PBS is lower than the one for sample without PBS: for instance, t_1(PBS)= 5.9s vs t_1(No PBS) = 10s. Of particular interest is the observation that following the healing process, sensors based on PBS show a remarkable increase in the α value by 200% i.e. This suggests that the quality of recovered CNT network is not as good as that before failure because. This conclusion was drawn from the fact that α factor represents quality and stability of network – the less stable is network, the high the α factor. On contrary, α factor in the case of GN-based sensor decreases after failure because mobility of GN is higher that is expressed in lower viscosity of GN-PBS blends. In other words, the higher aspect ratio of particles, the lower Gauge and α factors due to formation of percolated network, but the more they increase after failure due to slow recovery of network. Conversely, sensors without PBS exhibit a decrease in the α value, dropping by 18%. To conclude, PBS enables better healing of sensor. The healing is more efficient in the case of PBS-MWCNT-based sensors in the way that the healed sensor is better than as prepared one due to unrecovered failed MWCNT network.

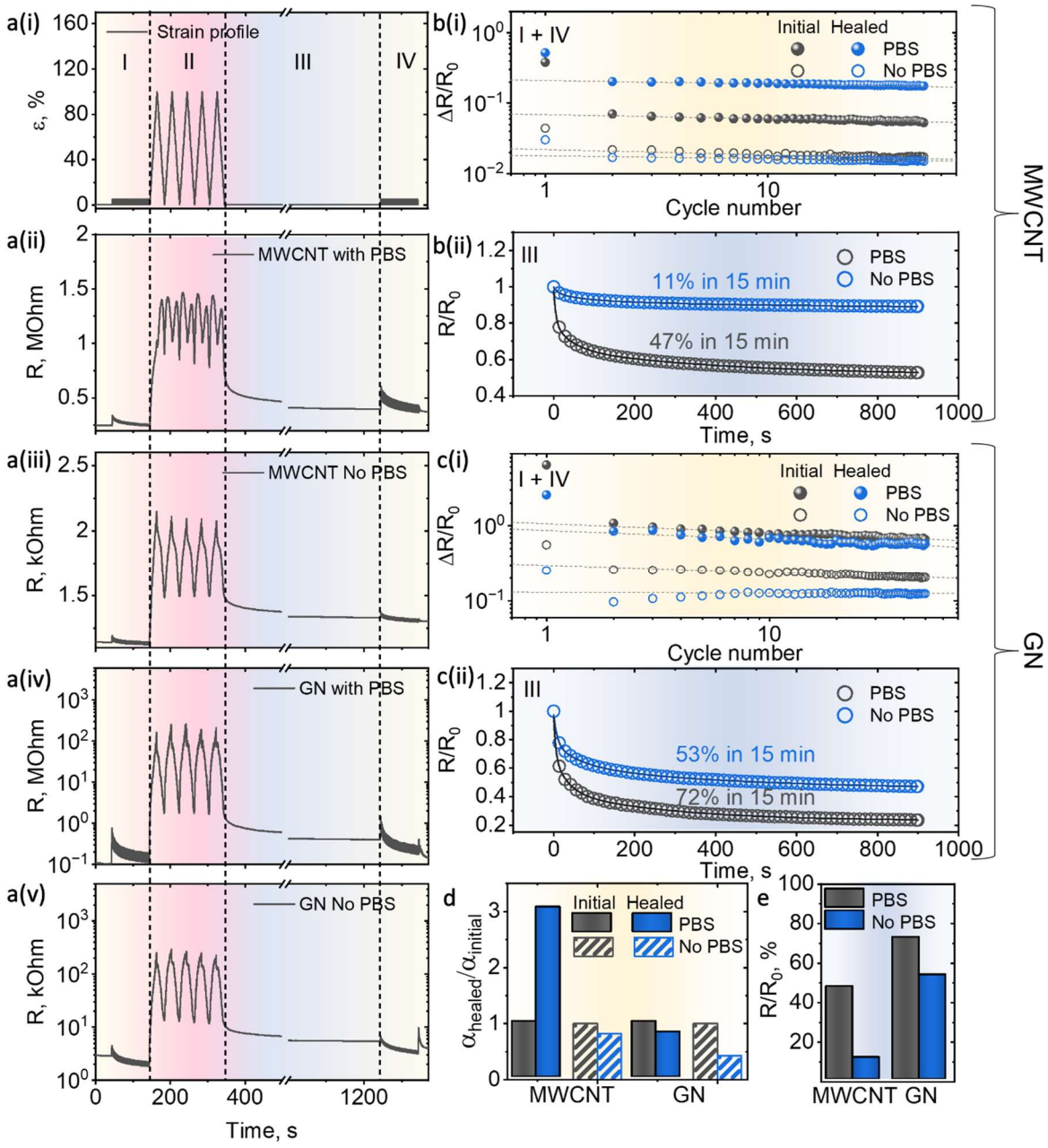

Figure 3. a) strain profile and resistance raw data of electromechanical properties recovery for MWCNT and GN based sensors with and without PBS: Stage I – oscillation in linear region with strain amplitude ε=5%; Stage II – Oscillation at large non-linear range ε=100%; Stage III – healing at ε=0 for 15 minutes; Stage IV – verification of electrochemical properties in linear range at ε=5%; Fractional resistance change at stages I and IV (i) and relative resistance recovery(ii) for sensors with and without PBS based on b) MWCNT and c) GN; d) change of electromechanical characteristics of sensors before and after the breaking-healing process at stages I and IV expressed as $\alpha_{healed}/\alpha_{initial}$ ratio, where $\alpha_{initial}$ and α_{healed} are values at I and IV stages, respectively; e) resistance recovery at stage III

In addition, we analyzed an impact of the viscoelastic PBS matrix as a comparison of the loss coefficient η and Young modulus of materials without PBS compared to those with it (**Figure 4, Table 3**). The self-healing matrix reduces friction between particles and dissipates energy almost as a pristine TPU mat. The values of loss coefficients are 0.23 vs 0.35 for MWCNT based materials and 0.46 vs 0.51 for GN based sensors. Moreover, due to its inherently low modulus (E ≈ 6 kPa) the incorporation of PBS matrix assists in aligning mechanical composite properties more closely with the original TPU mat (E=0.9 MPa), resulting in lower Young's modulus, which are, respectively with and without PBS, 0.9 MPa vs 4.8 MPa for MWCNT based and 2.8 MPa vs 6 MPa for GN based materials. Furthermore, PBS significantly influences the G and W values, which notably decrease in sensors lacking PBS (**Figure S16**): only G=0.14 and W=1.55% for MWCNT-based, and G=3.8 and W=0.55 for GN based sensors. These observations further validate the quasi-composite structure of PBS/GN on TPU fibers.

Thus, utilizing self-healing viscoelastic polymers as the matrix for carbon fillers unequivocally enhances the electromechanical properties. This enhancement is evidenced by larger G and W values, faster resistance recovery, and significantly less degradation of α even after experiencing substantial deformation. The larger mobility of particles facilitated by the PBS matrix enables partial self-healing capabilities. Moreover, the enhancement of properties may occur, as in case of MWCNT based sensor, due to alignment of particles along deformation axis. The incorporation of a PBS matrix serves to reduce friction between particles, improving their dispersibility. In addition, the PBS matrix does not compromise the original mechanical properties of the TPU mat while concurrently reducing the stiffness of the carbon agglomeration network.

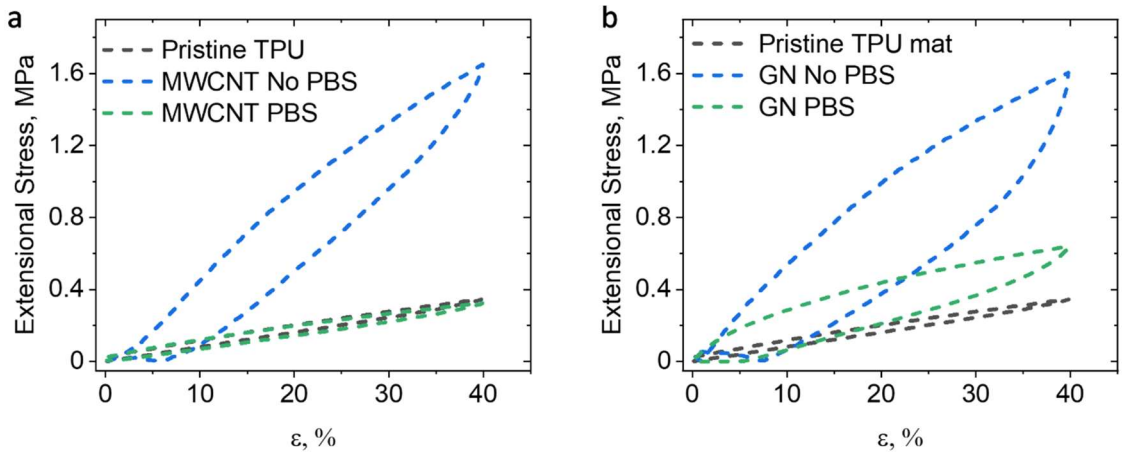

Figure 4. comparison of strain stress curves of sensors with PBS, without PBS and pristine TPU for a) GN and b) MWCNT based sensors, respectively

Table 3. Comparison of Young moduli and mechanical loss coefficient of pristine TPU mat and mats with carbon ink with and without PBS

	Pure TPU	**w/o PBS**	**with PBS**
Material with MWCNT			
E, KPa	943	4826	947
Mechanical loss coefficient (η)	0.16	0.35	0.23
Materials with GN			
E, KPa	943	6034	2794
Mechanical loss coefficient (η)	0.16	0.51	0.46

Pulse measurements

Finally, we demonstrate the application of our sensors for pulse measurements. The fabricated graphene-based sensor, which was chosen as material with highest sensitivity, can determine the small deformation signals of a person such as pulse on a human wrist **(Figure 5)**. For the demonstration of pulse measurement the sensor was attached to the wrist of two persons with a adhesive band, maintaining direct contact of sensor with skin, and connecting it to the potentiostate. Due to high flexibility of the sensor ($E \approx 0.9$ MPa), lightness and wearability, attachment of sensor to the skin was sound. Relatively large sensitivity after conditioning ($G \approx 11$) resulted in detection of the deformation of skin on the wrist and distinguish pulse of healthy person and a person with bradycardia. Skin deformation shows usually strain around 2% which is within working range of the sensor. When a bradycardic pulse was detected with well distinguished systolic and diastole waves, the signal of normal (with higher deformation rate) is only enough for heartbeat counting. The reason for this is the rate dependence of sensor and non-sufficient time for particles relaxation at low time scale.

The MWCNT-based sensor demonstrated the ability to count heartbeats, but the signal was significantly weaker and noisier, making it challenging to distinguish individual peaks. This can be

attributed to the significantly lower sensitivity of the MWCNT-based sensor, indicating that it is not suitable for detecting small deformation signals.

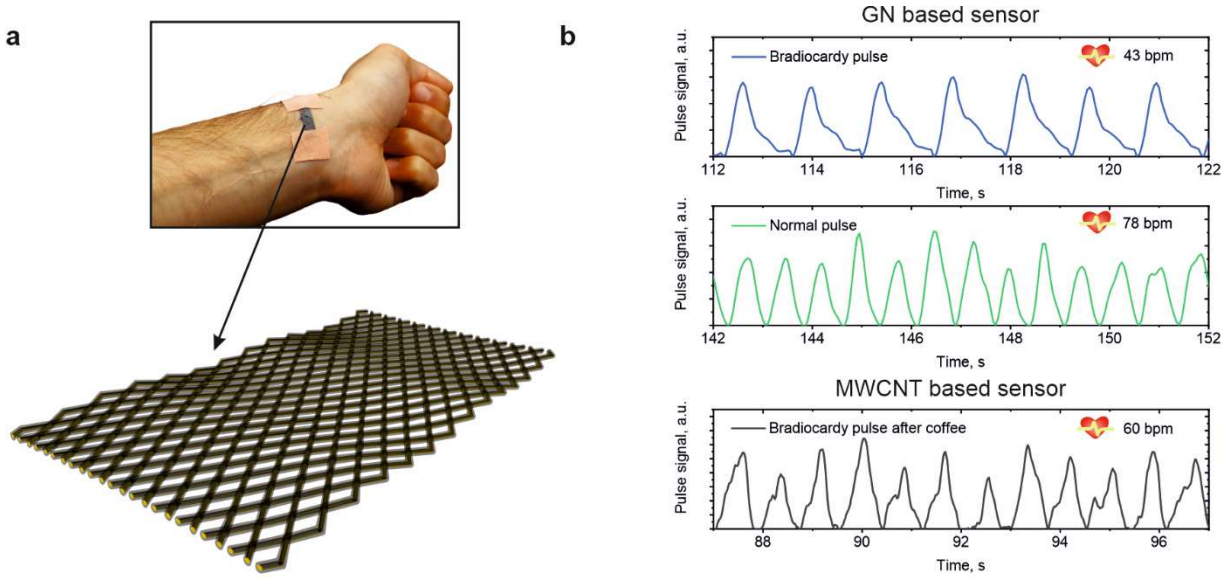

Figure 5. a) Visualization of a core-shell strain sensor on a wrist to measure a pulse; b) Normalized signal of measurements of pulse by GN based strain sensor of a normal heart and one with bradycardia on person´s wrist and MWCNT based sensor of person with bradycardia after coffee.

Conclusions

In this study, we have addressed the inherent limitations of porous, flexible, fibrous, and self-healing strain sensors. Specifically, we have considered issues such as the fatigue failure of carbon fiber materials and the prolonged flow and low mechanical stability of self-healing materials. Our solution involved integrating self-healing carbon blends with fiber porous materials to create a fiber-reinforced self-healing composite. Sensitivity and the ability to recover the performance characteristics are provided by self-healing carbon blends, while fibers prevent long term material flow and fragment dispersion during impact and fatigue failures in the elastic deformation regime, providing shape recovery.

We have successfully created composite wearable strain sensors in which the viscoelastic functional layer is composed of two continuous phases: (i) a self-healing polymer-carbon blend and (ii) long electrospun fibers made of commercial polyurethane. This design also addresses other issues associated with bulk materials, such as nonlinear volt-ampere characteristics, irreversible deformation, and low working factor. Notably, the healing process enhances the sensitivity of self-

healing materials based on multi-walled carbon nanotubes (MWCNTs), making the sensors more sensitive after fracture and subsequent healing.

AUTHOR INFORMATION

Corresponding Author

*Leonid Ionov. Faculty of Engineering Sciences, University of Bayreuth, Ludwig Thoma Str. 36A, 95447 Bayreuth, Germany. Bavarian Polymer Institute, University of Bayreuth, Bayreuth, Germany. E-mail: leonid.ionov@uni-bayreuth.de

Funding Sources

This work was supported by DFG (Grant No IO 68/20-1, IO 68/21-1).

ACKNOWLEDGMENT

We would further like to thank Professor Scheibel for allowing us to use SEM equipment to conduct this research.

References

1. Sreenilayam, S. P.; Ahad, I. U.; Nicolosi, V.; Acinas Garzon, V.; Brabazon, D., Advanced materials of printed wearables for physiological parameter monitoring. Materials Today 2020, 32, 147-177.

2. Gao, Z.; Xiao, X.; Carlo, A. D.; Yin, J.; Wang, Y.; Huang, L.; Tang, J.; Chen, J., Advances in Wearable Strain Sensors Based on Electrospun Fibers. Advanced Functional Materials 2023, 33 (18).

3. Wang, W.; Yang, S.; Ding, K.; Jiao, L.; Yan, J.; Zhao, W.; Ma, Y.; Wang, T.; Cheng, B.; Ni, Y., Biomaterials- and biostructures Inspired high-performance flexible stretchable strain sensors: A review. Chemical Engineering Journal 2021, 425.

4. Koivikko, A.; Lampinen, V.; Pihlajamäki, M.; Yiannacou, K.; Sharma, V.; Sariola, V., Integrated stretchable pneumatic strain gauges for electronics-free soft robots. Communications Engineering 2022, 1 (1).

5. Apsite, I.; Constante, G.; Dulle, M.; Vogt, L.; Caspari, A.; Boccaccini, A. R.; Synytska, A.; Salehi, S.; Ionov, L., 4D Biofabrication of fibrous artificial nerve graft for neuron regeneration. Biofabrication 2020, 12 (3), 035027.

6. Zhu, G. J.; Ren, P. G.; Guo, H.; Jin, Y. L.; Yan, D. X.; Li, Z. M., Highly Sensitive and Stretchable Polyurethane Fiber Strain Sensors with Embedded Silver Nanowires. ACS Appl Mater Interfaces 2019, 11 (26), 23649-23658.

7. Ding, Y.; Yang, J.; Tolle, C. R.; Zhu, Z., A highly stretchable strain sensor based on electrospun carbon nanofibers for human motion monitoring. RSC Advances 2016, 6 (82), 79114-79120.

8. Wang, Y.; Hao, J.; Huang, Z.; Zheng, G.; Dai, K.; Liu, C.; Shen, C., Flexible electrically resistive-type strain sensors based on reduced graphene oxide-decorated electrospun polymer fibrous mats for human motion monitoring. Carbon 2018, 126, 360-371.

9. Zhang, P.; Chen, Y.; Li, Y.; Zhang, Y.; Zhang, J.; Huang, L., A Flexible Strain Sensor Based on the Porous Structure of a Carbon Black/Carbon Nanotube Conducting Network for Human Motion Detection. Sensors (Basel) 2020, 20 (4).

10. Wang, X.; Liu, X.; Schubert, D. W., Highly Sensitive Ultrathin Flexible Thermoplastic Polyurethane/Carbon Black Fibrous Film Strain Sensor with Adjustable Scaffold Networks. Nanomicro Lett 2021, 13 (1), 64.

11. Zhan, P.; Zhai, W.; Wang, N.; Wei, X.; Zheng, G.; Dai, K.; Liu, C.; Shen, C., Electrically conductive carbon black/electrospun polyamide 6/poly(vinyl alcohol) composite based strain sensor with ultrahigh sensitivity and favorable repeatability. Materials Letters 2019, 236, 60-63.

12. Kang, J.; Tok, J. B. H.; Bao, Z., Self-healing soft electronics. Nature Electronics 2019, 2 (4), 144-150.

13. Liu, Z.; Picken, S. J.; Besseling, N. A. M., Polyborosiloxanes (PBSs), Synthetic Kinetics, and Characterization. Macromolecules 2014, 47 (14), 4531-4537.

14. Boland, C. S.; Khan, U.; Ryan, G.; Barwich, S.; Charifou, R.; Harvey, A.; Backes, C.; Li, Z.; Ferreira, M. S.; Möbius, M. E.; Young, R. J.; Coleman, J. N., Sensitive electromechanical sensors using viscoelastic graphene-polymer nanocomposites. Science 2016, 354 (6317), 1257-1260.

15. Wu, Q.; Xiong, H.; Peng, Y.; Yang, Y.; Kang, J.; Huang, G.; Ren, X.; Wu, J., Highly Stretchable and Self-Healing "Solid-Liquid" Elastomer with Strain-Rate Sensing Capability. ACS Appl Mater Interfaces 2019, 11 (21), 19534-19540.

16. Wu, T.; Chen, B., Synthesis of Multiwalled Carbon Nanotube-Reinforced Polyborosiloxane Nanocomposites with Mechanically Adaptive and Self-Healing Capabilities for Flexible Conductors. ACS Appl Mater Interfaces 2016, 8 (36), 24071-8.

17. Wu, T.; Gray, E.; Chen, B., A self-healing, adaptive and conductive polymer composite ink for 3D printing of gas sensors. Journal of Materials Chemistry C 2018, 6 (23), 6200-6207.

18. O'Driscoll, D. P.; McMahon, S.; Garcia, J.; Biccai, S.; Gabbett, C.; Kelly, A. G.; Barwich, S.; Moebius, M.; Boland, C. S.; Coleman, J. N., Printable G-Putty for Frequency- and Rate-Independent, High-Performance Strain Sensors. Small 2021, 17 (23), e2006542.

19. Boland, C. S.; O'Driscoll, D. P.; Kelly, A. G.; Boland, J. B.; Coleman, J. N., Highly Sensitive Composite Foam Bodily Sensors Based on the g-Putty Ink Soaking Procedure. ACS Appl Mater Interfaces 2021, 13 (50), 60489-60497.

20. Milkin, P.; Danzer, M.; Ionov, L., Self-Healing and Electrical Properties of Viscoelastic Polymer-Carbon Blends. Macromol Rapid Commun 2022, 43 (19), e2200307.

21. Milkin, P.; Zhanbassynova, A.; Ionov, L., Superelastic, soft, stress-healable, recyclable conductive materials. Composite Structures 2024, 327.

22. Tang, M.; Wang, W.; Xu, D.; Wang, Z., Synthesis of Structure-Controlled Polyborosiloxanes and Investigation on Their Viscoelastic Response to Molecular Mass of Polydimethylsiloxane Triggered by Both Chemical and Physical Interactions. Industrial & Engineering Chemistry Research 2016, 55 (49), 12582-12589.

23. A, K.; A, L., Mechanical Behaviour of Skin: A Review. Journal of Material Science & Engineering 2016, 5 (4).

24. Michael Rubinstein, R. H. C., Polymer Physics. Oxford University Press: Oxford, 2003.

25. Boland, C. S., Approaching the Limit of Electromechanical Performance in Mixed-Phase Nanocomposites. ACS Applied Nano Materials 2020, 3 (11), 11240-11246.

26. Heinrich, G.; Klüppel, M., Recent Advances in the Theory of Filler Networking in Elastomers. In Filled Elastomers Drug Delivery Systems, Springer Berlin Heidelberg: Berlin, Heidelberg, 2002; pp 1-44.

27. Zhou, Y.; Zhan, P.; Ren, M.; Zheng, G.; Dai, K.; Mi, L.; Liu, C.; Shen, C., Significant Stretchability Enhancement of a Crack-Based Strain Sensor Combined with High Sensitivity and Superior Durability for Motion Monitoring. ACS Applied Materials & Interfaces 2019, 11 (7), 7405-7414.

28. Boland, C. S., Quantifying the Contributing Factors toward Signal Fatigue in Nanocomposite Strain Sensors. ACS Applied Polymer Materials 2020, 2 (8), 3474-3480.

29. Fleck, N. A.; Kang, K. J.; Ashby, M. F., Overview no. 112: The cyclic properties of engineering materials. Acta Metallurgica et Materialia 1994, 42 (2), 365-381.

30. Qu, M.; Deng, F.; Kalkhoran, S. M.; Gouldstone, A.; Robisson, A.; Van Vliet, K. J., Nanoscale visualization and multiscale mechanical implications of bound rubber interphases in rubber–carbon black nanocomposites. Soft Matter 2011, 7 (3), 1066-1077.

31. Osicka, J.; Mrlik, M.; Ilcikova, M.; Munster, L.; Bazant, P.; Spitalsky, Z.; Mosnacek, J., Light-Induced Actuation of Poly(dimethylsiloxane) Filled with Graphene Oxide Grafted with Poly(2-(trimethylsilyloxy)ethyl Methacrylate). Polymers (Basel) 2018, 10 (10).

32. Roland, C. M.; Santangelo, P. G., Effect of temperature on the terminal relaxation of branched polydimethysiloxane. Journal of Non-Crystalline Solids 2002, 307-310, 835-841.

33. Ma, L.; Yang, W.; Wang, Y.; Chen, H.; Xing, Y.; Wang, J., Multi-dimensional strain sensor based on carbon nanotube film with aligned conductive networks. Composites Science and Technology 2018, 165, 190-197.

Fiber-Reinforced Flexible Self-Healing Strain Sensor with Failure-Improving Sensitivity Recovery

Supplementary information

Pavel Milkin[1], Shubham Pavale[1], Zhander Soreno[1], Leonid Ionov[1,2]

[1]Faculty of Engineering Sciences, University of Bayreuth, Ludwig Thoma Str. 36A, 95447 Bayreuth, Germany

[2]Bavarian Polymer Institute, University of Bayreuth, 95447 Bayreuth, Germany

* E-mail: leonid.ionov@uni-bayreuth.de

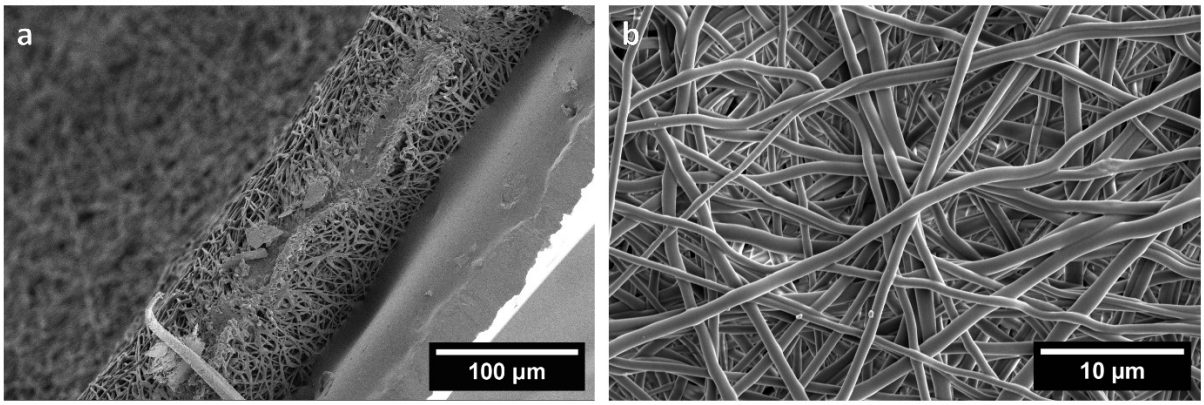

Figure S1. SEM pictures of pristine TPU mat: a) cross-section view; b) top view

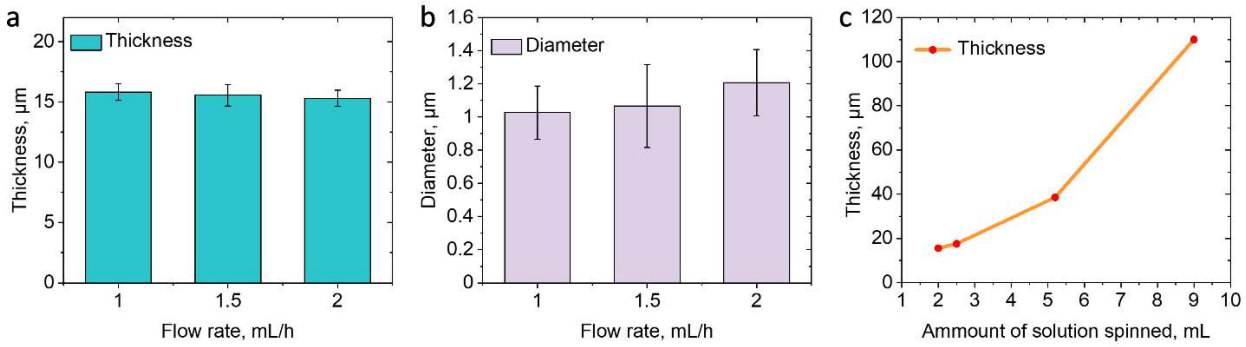

Figure S2. Electrospinning parameters for TPU mat: a) mat thickness vs flow rate; b) Fiber diameter vs flow rate; c) mat thickness vs amount of spined solution.

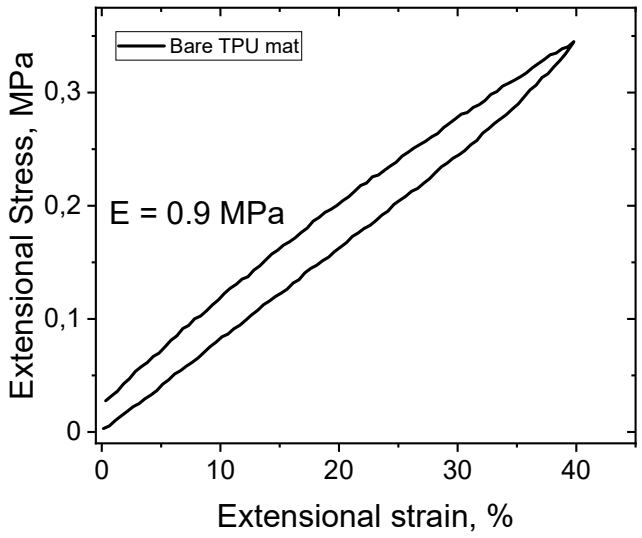

Figure S3 Stress-strain curve of pure electrospun TPU mat

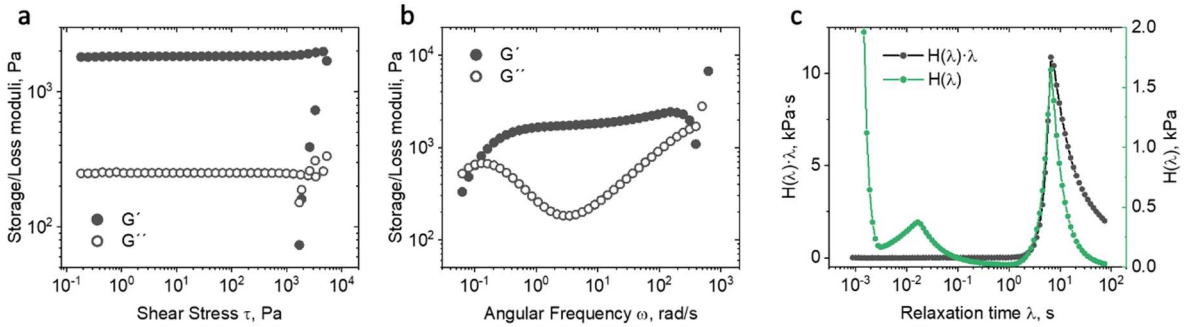

Figure S4. Rheological characteristics of pristine PBS: a) amplitude sweep test at 10 rad/s, moduli vs shear stress; b) Frequency sweep test at ε = 0.1%; c) weight relaxation and relaxation spectra

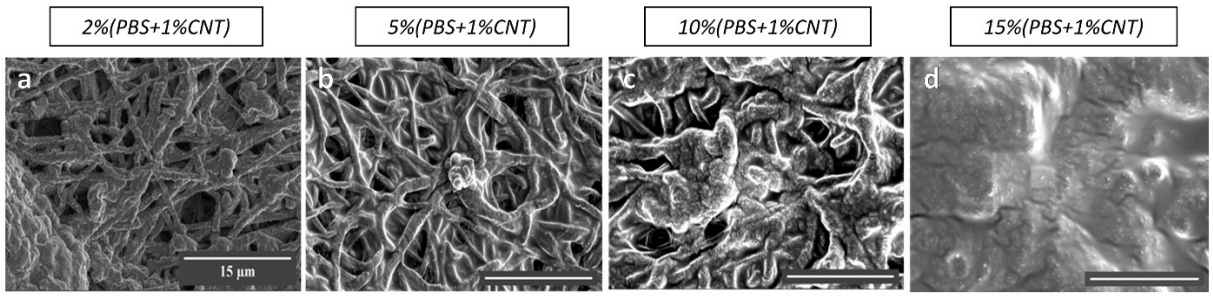

Figure S5. SEM picture of top view of fabricated sensor with PBS+1% MWCNT functional layer with different ink concentration: a) 2%; b) 5%; c) 10%; d) 15%.

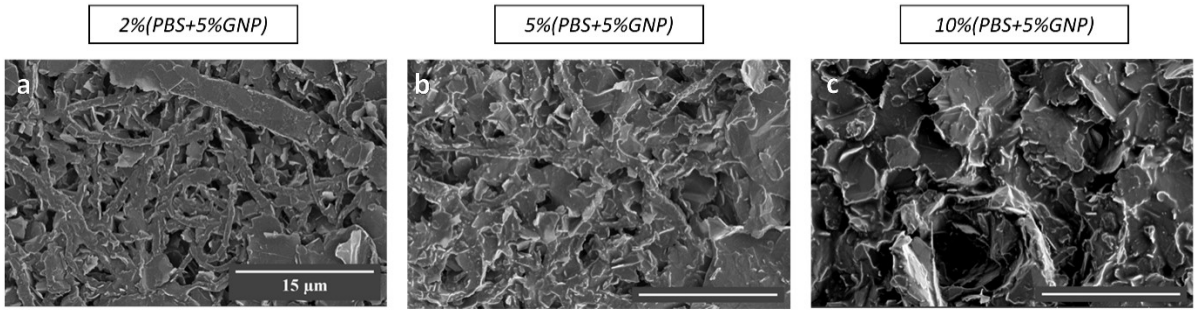

Figure S6. SEM picture of top view of fabricated sensor with PBS+1% GN functional layer with different ink concentration: a) 5%; b) 10%; c) 15%.

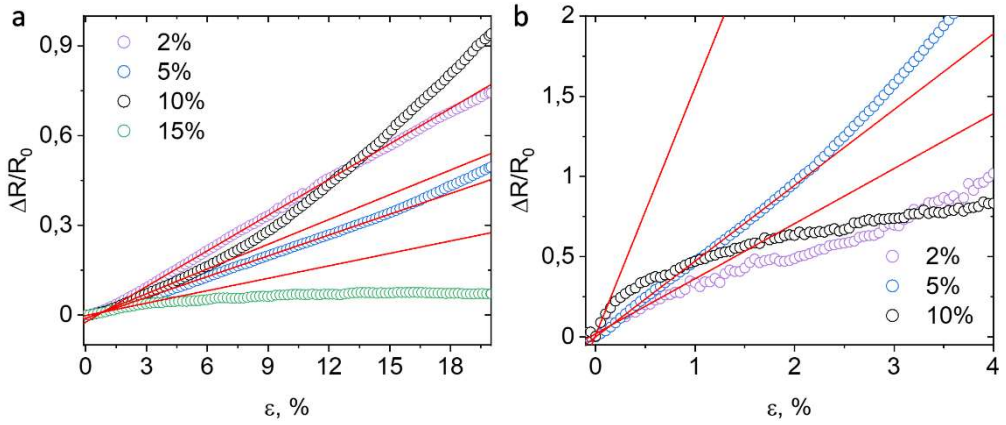

Figure S7. Fractional resistance vs strain plot with linear fit of linear region to determine working and Gauge factors: a) 5% GN and b) 1% MWCNT mats with various concentration of ink

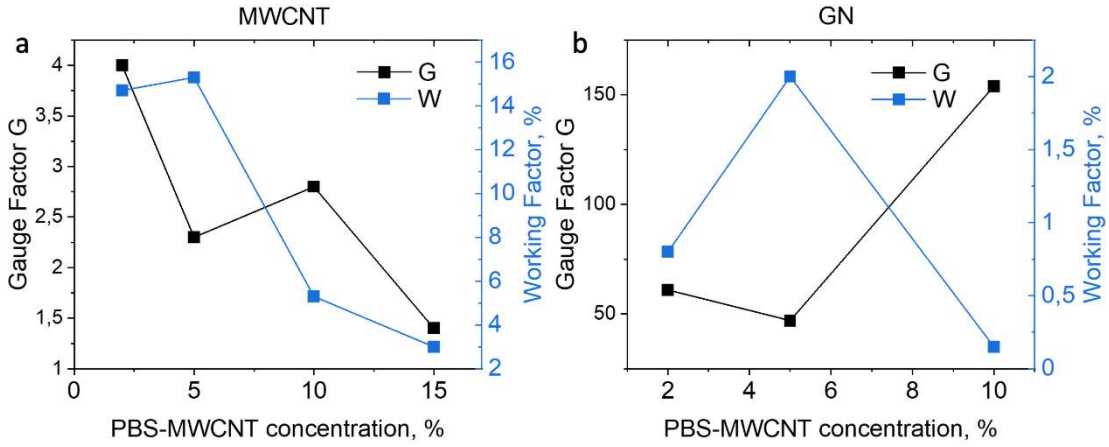

Figure S8. Gauge and Working factors of strain sensors with different concentration of PBS-carbon filler: a) MWCNT; b) GN

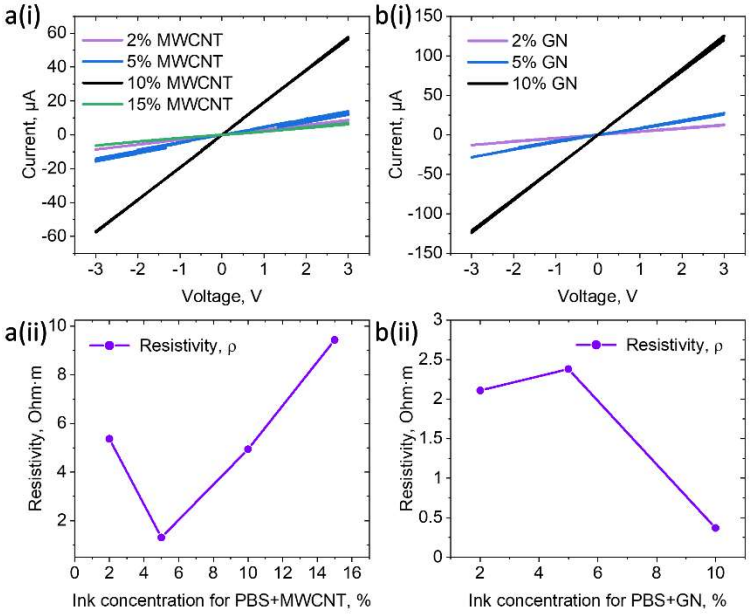

Figure S9. Volt-Ampere characteristic (i) and resistivity (ii) of 1%MWCNT/PBS (a) and 5%GN/PBS (b) mats with different concentration of used ink.

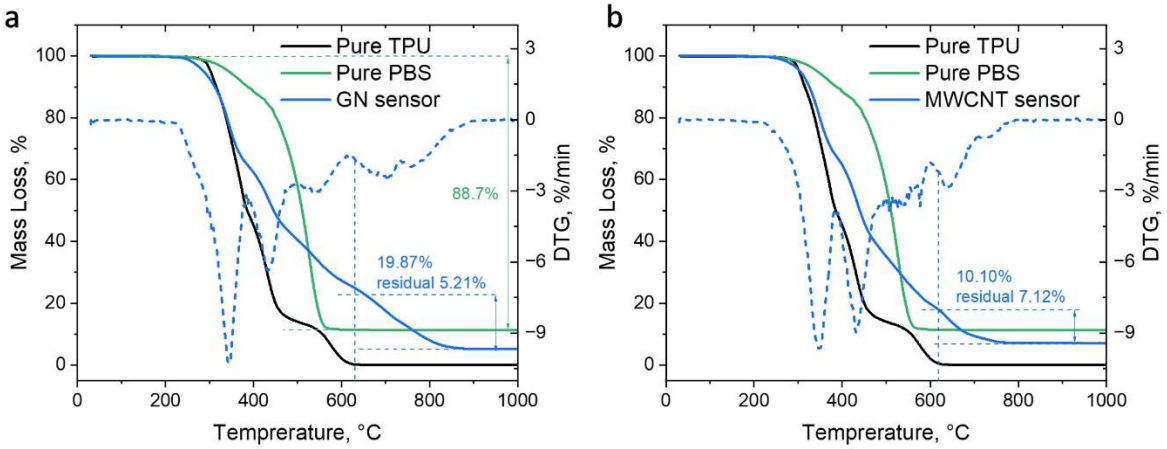

Figure S10. TGA data for Pure TPU, Pure PBS and a) GN and b) MWCNT based strain sensor. The measurements are performed in Air atmosphere at heating rate 20 K/min. The volume fraction φ was calculated according to the formula (as example, for GN)

$$\varphi = \frac{\frac{\omega_{GN}}{\rho_{GN}}}{\frac{\omega_{GN}}{\rho_{GN}}+\frac{(1-\omega_{GN})}{\rho_{PBS}}};\ \omega_{GN} = \frac{\gamma_{GN\ in\ sensor}}{\gamma_{GN\ in\ sensor}+\frac{\gamma_{residual}}{0.113}},$$

where ω_{GN} – weight fraction of filler in PBS, $\rho_{GN} = 2.2$ g/cm^3 – density of GN, $\rho_{MWCNT} = 2.0$ g/cm^3 – density of MWCNT, $\rho_{PBS} = 1$ g/cm^3 – density of PBS, γ_{GN} in sensor – weight fraction of filler in

sensor, $\gamma_{residual}$ – weight fraction of unburned part of PBS, 0.113 – mass fraction of unburned part of PBS for pure PBS.

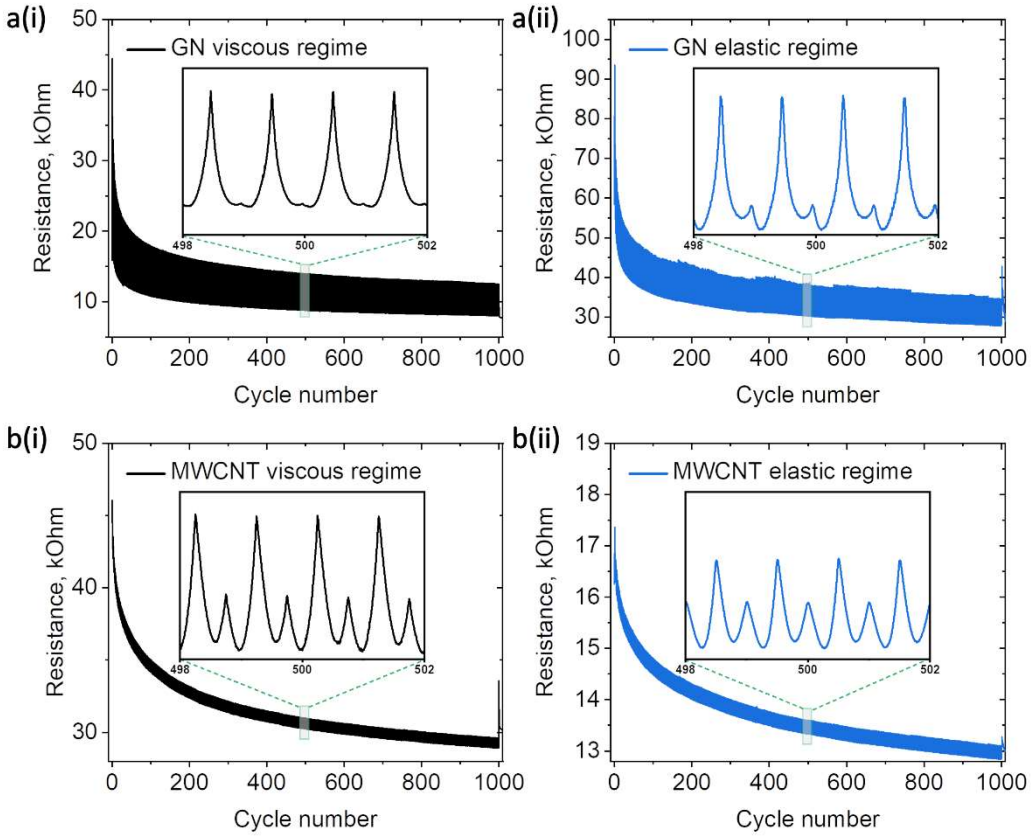

Figure S11. Piezoresistive response of a) GN and b) MWCNT based sensors at strain rate corresponding to (i) viscous and (ii) elastic regimes.

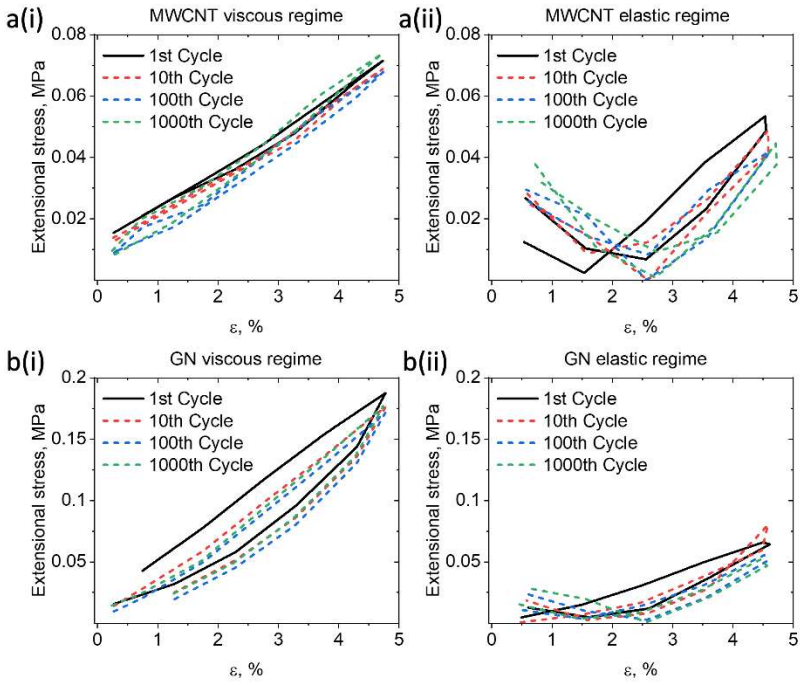

Figure S12. Stress-strain curve of 1st, 10th, 100th, 1000th cycles during fatigue test of MWCNT mats in a(i) viscous and a(ii) elastic regimes; of GN mats in b(i) viscous and b(ii) elastic regimes.

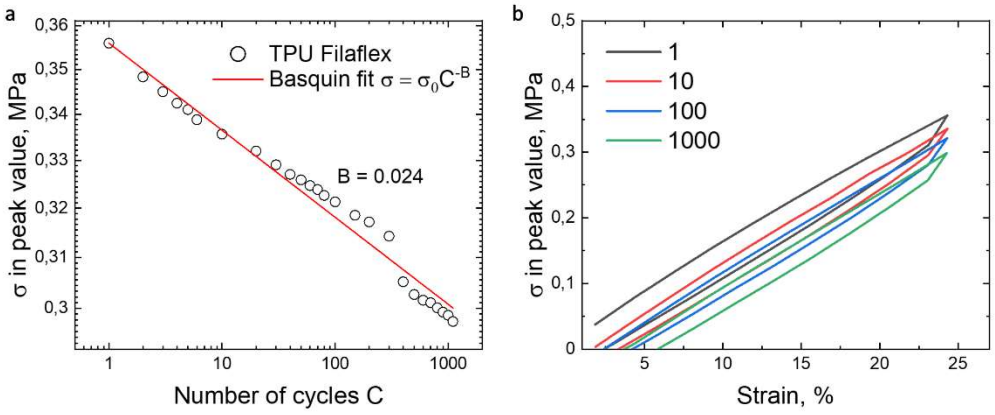

Figure S13. Fatigue results of pristine electrospun TPU mat made at 5% of strain amplitude at 1%/s strain rate: a) fatigue of maximum stress as the function of cycle numbers; b) stress strain curve for 1st, 10th, 100th, 1000th cycles

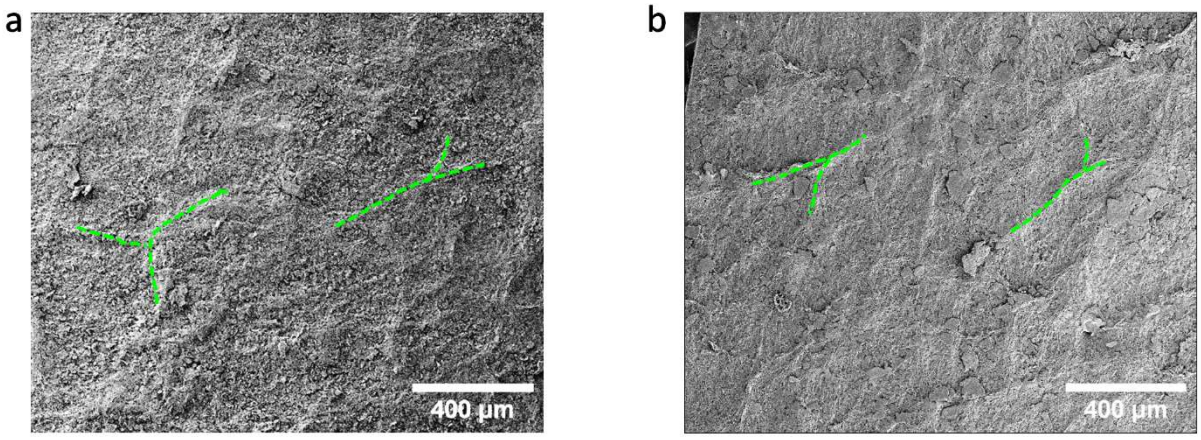

Figure S14. GN based sensor as well as wrinkles after cycling on top of GN based sensor after deformation in c(i) viscous and c(ii) regimes

Table S1. Values of exponent decay of resistivity curve after applied 5x 100% strain:

$R = R_0 + A_1 \cdot \exp(-(t-t_0)/t_1) + A_2 \cdot \exp(-(t-t_0)/t_2) + A_3 \cdot \exp(-(t-t_0)/t_3)$

	MWCNT (PBS)	MWCNT (NO PBS)	GN (PBS)	GN (NO PBS)
R_0, kOhm	0.51	0.88	0.23	0.45
A_1, Ohm	0.18	0.03	0.26	0.2
t_1, s	5.9	10	5	8.7
A_2, Ohm	0.14	0.04	0.25	0.16
t_2,s	48	67	33	68
A_3, Ohm	0.15	0.04	0.21	0.17
t_3, s	425	496	275	452
Coeff. of determination	0.999	0.999	0.999	0.999

Table S2. Basquin law fit for Figure S13 b(i) and c(i) for cycles >3

	MWCNT (PBS)	MWCNT (NO PBS)	GN (PBS)	GN (NO PBS)

α_0	0.069	0.022	1.07	0.30
α	0.21	0.018	0.87	0.13
B_0	0.059	0.074	0.119	0.095
B	0.051	0.040	0.118	0.009

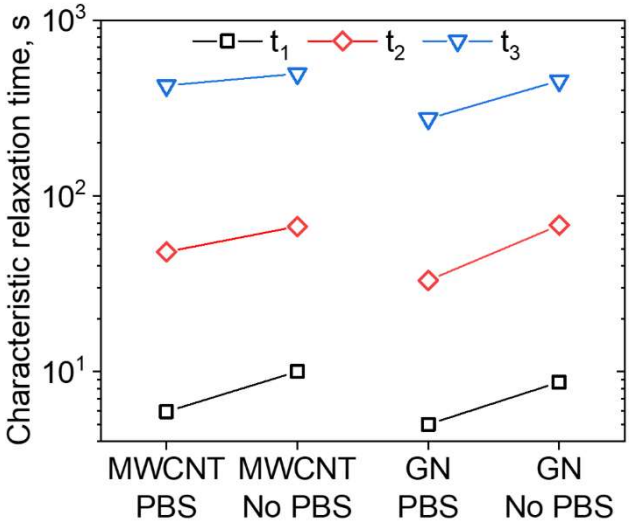

Figure S15. Characteristics time of resistance recovery after cyclic large strain (100%) was applied for MWCNT and GN based sensor with and without PBS. The data is taken from fitting parameters in Table S1

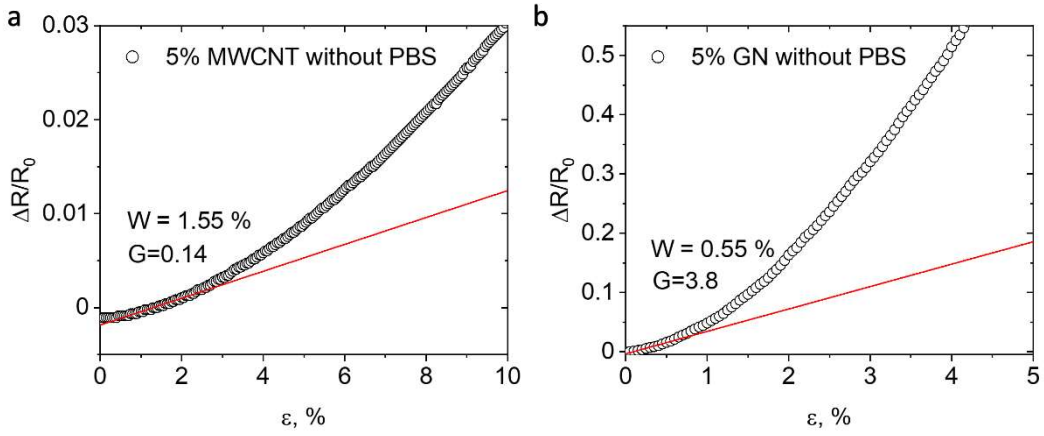

Figure S16. Fractional resistance vs strain plot with linear fit of linear region to determine working and Gauge factors: a) MWCNT and b) GN on TPU mat without PBS (particles concentration is remained the same)

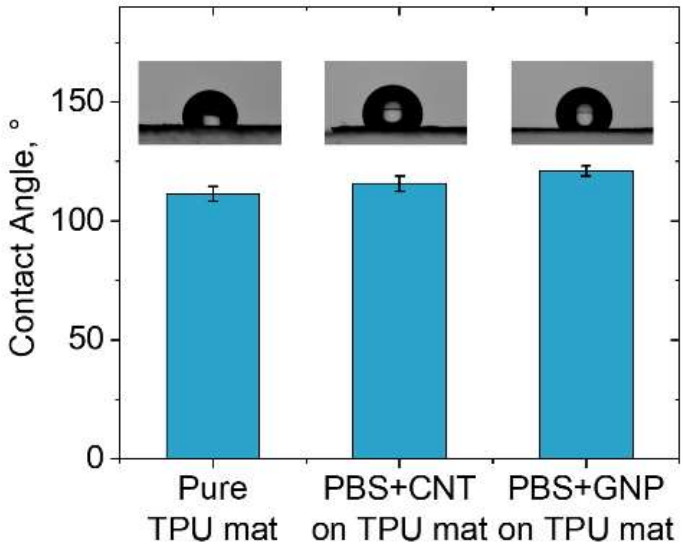

Figure S17. Contact angle measurements of pristine TPU mats and covered with carbon/PBS inks. The surface hydrophobicity of the TPU-based strain sensor coated with PBS/carbon composite was measured using the contact angle meter (Drop Shape Analyzer DSA25E, KRÜSS, Germany). The contact angle measurements were performed using the sessile drop method. A small water droplet (5 µl of Milli-Q H2O) was prepared on the tip of a syringe. It was carefully placed onto the surface of the strain sensor, taking care not to touch the surface with the syringe needle. The droplet was allowed to equilibrate for a few seconds until its shape became stable. The video of the droplet was captured using a high-resolution camera. The contact angle between the droplet and the sensor surface was measured using video analysis software

Acknowledgments

First and foremost, I would like to thank Prof. Leonid Ionov for the opportunity to work in his group. His invaluable advice, supervision, foresight, patience, and hours-long discussions have been crucial throughout my PhD marathon and are greatly appreciated.

I also would like to thank Dr. habill. Alla Synytska for valuable scientific discussions as well as involvement in Biovature GmbH and other side projects, which have broadened my scientific horizons and expertise.

I thank Dr. Indra Apsite-Vinzio and Ilia Sadilov for always finding the time for both scientific discussions and friendly support outside the lab.

I also would like to thank my colleagues, as well as the current and former members of the Ionov and Synytska groups, for their help with experiments and for fostering a supportive and collaborative atmosphere in the group: Gissela Constante, Waseem Kitana, Zhander Soreno, Dr. Neha Tiwari, Saskia Roth, Katharina Bauer, Shubham Pavale, Ainur Zhanbassynova, Dr. Chiara Pasini, Hongtao Cai, Anila Antony, Dr. Sarah Lentz, Dr. Anne Linhardt, Dr. Andres Posada, Antonia Debevc.

Thanks to all collaborators who helped me with conducting experiments or providing the equipment necessary for publications: Prof. Michael Danzer, Dr. Hendrik Bargel, Prof. Thomas Scheibel.

Special thanks to my family and friends, especially the Aslandukov family (Alëna, Arina, and Andrey), Fariia Albar, and Maxime Vinzio, for supporting me during difficult moments and celebrating small victories with me.

In addition, I thank the US embassy for not giving me a visa and Prof. Sergiy Minko and Dr. Vladimir Reukov for connecting me with Prof. Ionov.

Last, but not least, I want to thank me for believing in me and for doing all this hard work.

(Eidesstattliche) Versicherungen und Erklärungen

(§ 9 Satz 2 Nr. 3 PromO BayNAT)

Hiermit versichere ich eidesstattlich, dass ich die Arbeit selbstständig verfasst und keine anderen als die von mir angegebenen Quellen und Hilfsmittel benutzt habe (vgl. Art. 97 Abs. 1 Satz 8 BayHIG).

(§ 9 Satz 2 Nr. 3 PromO BayNAT)

Hiermit erkläre ich, dass ich die Dissertation nicht bereits zur Erlangung eines akademischen Grades eingereicht habe und dass ich nicht bereits diese oder eine gleichartige Doktorprüfung endgültig nicht bestanden habe.

(9 Satz 2 Nr. 4 PromO BayNAT)

Hiermit erkläre ich, dass ich Hilfe von gewerblichen Promotionsberatern bzw. -vermittlern oder ähnlichen Dienstleistern weder bisher in Anspruch genommen habe noch künftig in Anspruch nehmen werde.

(§ 9 Satz 2 Nr. 7 PromO BayNAT)

Hiermit erkläre ich mein Einverständnis, dass die elektronische Fassung meiner Dissertation unter Wahrung meiner Urheberrechte und des Datenschutzes einer gesonderten Überprüfung unterzogen werden kann.

(§ 9 Satz 2 Nr. 8 PromO BayNAT)

Hiermit erkläre ich mein Einverständnis, dass bei Verdacht wissenschaftlichen Fehlverhaltens Ermittlungen durch universitätsinterne Organe der wissenschaftlichen Selbstkontrolle stattfinden können.

…….

Ort, Datum, Unterschrift